INSTITUTE
FOR
AEROSPACE STUDIES

UNIVERSITY OF TORONTO

NUMERICAL PREDICTION OF BLAST-WAVE FLOWS OUTSIDE AND INSIDE A POWER HOUSE OF A NUCLEAR-POWER GENERATING STATION

by

J. J. Gottlieb, T. Saito, and K. Y. Zhang

April 1985

UTIAS Technical Note No. 239
CN ISSN 0082-5263

NUMERICAL PREDICTION OF BLAST-WAVE FLOWS OUTSIDE AND INSIDE A POWER HOUSE OF A NUCLEAR-POWER GENERATING STATION

by

J. J. Gottlieb, T. Saito, and K. Y. Zhang

Submitted November 1984

April 1985

UTIAS Technical Note No. 239
CN ISSN 0082-5263

Acknowledgements

The modelling of the blow-out panels and most of the associated computational were done by Mr. P. M. Ostaff, a research engineer at UTIAS, under the guidance of Professor J. S. Hansen of UTIAS. Their contributions are gratefully acknowledged with many thanks.

The help received from Mr. H. S. I. Sadek, a research engineer at UTIAS, for compiling most of the graphical results and completing the calculations of the differential pressures on the power house walls and roof are also gratefully acknowledged and appreciated.

The assistance of Ms. H.S. Murty, a M.A.Sc. graduate student, in writing up different parts of the nonstationary gas-flow analysis for this report was very helpful and much appreciated.

The help received from Ontario Hydro personnel, especially Mr. J. Skears, Mr. R. Pauls, Mr. R. Wong, and Mr. K. K. Lam, in freely giving relevant modelling data and many constructive comments is also gratefully acknowledged with many thanks.

Summary

The blast-wave flows both outside and inside a power house of a nuclear-power generating station, from an accidental explosion of an explosive like TNT or its equivalent during transportation past the power house by a train, are studied numerically and assessed with an appropriate model. Detailed descriptions of both the prediction model and numerical method of solution are given, as well as an interpretation of numerical results. The blast-wave flow into the power house through blow-out panels in the front wall is investigated, including the resulting flow inside the power house that travels through the turbine hall, through the turbine auxiliary bay, over the reactivity deck, through the reactor building, and, in some cases, down through a hoistway to three small rooms on the next lower level. Breaking blow-out panels in the rear wall of the power house and their effects on the internal blast-wave flow is also investigated. Two different flow paths are considered, one through an upper level of the power house and another through a lower level. Finally, the blast-wave flow over the outside of the power house is studied, with an approximate model, so that the pressure differences from the blast wave between the inside and outside of the roof, side walls, front wall, and rear wall can be determined and the resultant blast-wave loading on the building walls thereby obtained.

Table of Contents

Table of Contents (continued)

Notation

a	speed of sound of a gas
$a(t)$	acceleration of a part or all of the blow-out panel
a_o	constant used in the calculation of the dynamic viscosity μ (1.47×10^{-6} kg/m-s-$K^{1/2}$)
b_i	inside length of the base of the triangular part of the corrugations of the blow-out panel
b_o	outside length of the base of the triangular part of the corrugations of the blow-out panel
A	surface area of one-half of a blow-out panel
$A(x)$	local cross-sectional area of an area transition section
A_d	cross-sectional area of the channel downstream of an area change
A_u	cross-sectional area of the channel upstream of an area change
$c(t)$	time-dependent variable used as a coefficient for the mode shape of a beam or blow-out panel
$c'(t)$	time derivative of the variable c
C_f	skin-friction coefficient
C_p	specific heat at constant pressure
C_v	specific heat at constant volume
d	local diameter of a duct
d_h	local hydraulic diameter of a duct
e	total energy of a gas per unit volume $[p/(\gamma-1) + \rho u^2/2]$
E	Young's modulus of elasticity
f	Darcy-Weisbach friction factor
$f(x)$	mode shape for a blow-out panel
$f(t)$	time dependent force per unit length acting on a blow-out panel

Notation (continued)

$F(t)$	force on the blow-out panel
F_f	body force per unit volume due to friction
F_{hl}	body force per unit volume due to head loss
h_i	inside height of the triangular part of corrugations of a blow-out panel
h_o	outside height of the triangular part of corrugations on a blow-out panel
H	film coefficient for heat transfer
I	moment of inertia of a beam or blow-out panel
k	thermal conductivity of a gas
k_o	head-loss factor or coefficient
L	total length of a specific area transition section
L	length of one-half of the blow-out panel (3.75 m)
L	length of a building
m	mass per unit length of a beam or blow-out panel
M	local flow Mach number (u/a)
M_c	mass of corrugated sheet of blow-out panel
M_L	mass of a lumped system of a blow-out panel
M_p	moment due to the plastic hinge
M_t	total mass of the blow-out panel
n	free parameter for a blow-out panel loading expression
N	number of corrugations in the blow-out panel
Nu	Nusselt number (Hd/k or Hd_h/k)
p	static pressure of a gas flow
Δp	overpressure of a blast-wave flow

Notation (continued)

Δp_f	pressure change in a duct due to friction
Δp_{hl}	pressure change in a duct due to head loss
Pr	Prandtl number ($\mu C_p/k$)
q	heat transfer per unit surface area
q	uniform beam loading for a blow-out panel
Q	rate of heat transfer per unit volume into the gas flow
r_c	radius of one-half of the blow-out panel
R	gas constant for a perfect gas (air)
R	recovery factor ($Pr^{1/3}$) in equation 2.24
Re	Reynolds number ($\rho ud/\mu$ or $\rho ud_h/\mu$)
S	constant used in the calculation of the dynamic viscosity μ (113 K)
S_r	explosion scaling factor for distance
S_t	explosion scaling factor for time
St	Stanton number [Nu/(Pr Re)]
t	time
Δt	full time step used in numerical computations of the blast-wave flow field
Δt^*	half time step used in numerical computations of the blast-wave flow field
T	static temperature of a gas flow
T	time constant of the positive-overpressure part of the blast-wave signature
T_w	wall temperature
T_{aw}	adiabatic wall temperature
u	flow or particle velocity of a gas flow
u_u	flow velocity upstream of an area change
v	velocity of corrugated sheet of blow-out panel

Notation (continued)

V	translational velocity of a blow-out panel
$V(x)$	volume of the flow in a duct over which the head losses are distributed
$w(x,t)$	local beam displacement
W	weight or mass of an explosive
W_o	reference weight or mass of an explosive (1 kg TNT)
x	distance along a duct, displacement of the blow-out panel
Δx	distance over which head losses are distributed in a duct
y	distance measured from the centroid of the cross section of a beam or blow-out panel
γ	ratio of the specific heats for a perfect gas (C_p/C_v)
ε	absolute roughness of a shock-tube or duct wall
δ	length associated with a blow-out panel opening
θ	angular displacement of the rigid, rotating beam or blow-out panel
λ	wave length of a blast wave
μ	coefficient of viscosity or dynamic viscosity (equation 2.19)
ρ	density of a gas
ρ_u	density of a gas upstream of an area change
σ	porosity ratio of a porous plate (ratio of the total area of all orifices to the total flow area upstream of the perforated plate)
σ_y	yield stress of the mild steel plates of the blow-out panel
ω	natural frequency of vibration of the blow-out panel
Ω	reduction factor for the plastic moment

1. INTRODUCTION

1.1 Background Information

The Darlington Nuclear Power Generating Station that is now being built by Ontario Hydro in the township of Newcastle (80 km directly east of Toronto, Ontario, Canada) is located about 495 m away from a major train transportation line of Canadian National Railroads (CNR). Because a train may legally transport explosives in a combined quantity having a maximum yield equivalent to 61,500 kg of trinitrotoluene (TNT), there exists a very remote but nonetheless finite possibility of an accidental chemical explosion occurring at the CNR railroad tracks near the Darlington Generating Station. In order to provide the necessary blast protection to the nuclear power plant buildings, as well as equipment and personnel located inside the buildings, from the very remote event of such an explosion, these buildings with their many components must be designed to be resistant to air blast. In other words, they must be designed adequately to withstand some reasonable maximum blast-wave loading with relatively little or no substantial damage. Criteria for the maximum blast-wave loading and permissible damage that can be tolerated are generally specified by some government body or safety committee, such as the Atomic Energy Control Board of Canada, and these government guidelines or regulations are followed by Ontario Hydro in the design of the nuclear power plant.

An illustration of the Darlington Generating Station appears in Fig. 1, where a spherical blast-wave front from a hypothetical explosion at the tracks of the Canadian National Railroad (not shown) is depicted just prior to its impending interaction with the Station. The direction of the incident blast wave is indicated. Furthermore, an illustration of the blast wave interaction with the Darlington Generating Station power house is presented in Fig. 2. Outside the power house the incident blast-wave front and its reflection from the walls of the building are depicted, whereas inside the building the interior blast wave is sketched, which enters the building through the blow-out panel openings in the front wall facing the explosion.

The problem of predicting the characteristics of the incident blast wave at the site of the Darlington Generating Station power house has already been studied by Ontario Hydro [1-2], and this work has been reviewed recently [3]. Since these studies, however, new and relevant data of the characteristics of blast waves at various distances from the explosion of TNT and other explosives like mixed ammonium nitrate and fuel oil (ANFO) and a stoichiometric mixture of the gases propane and oxygen (PO) have become available [4-5], which are used in the present study. Finally, the problem of the prediction of the blast-wave loading on the front, roof, sides, and rear of the power house has also been undertaken at Ontario Hydro [1-2] and also reviewed [3], based on previous work involving the blast-wave loading from nuclear and chemical weapons explosions on different types of civilian and military buildings and equipment [e.g., see reference 6].

Most of the previous Ontario Hydro work [1-3] was directed at obtaining the pressure loading from the blast wave on the outside of nuclear power-plant buildings; that is, on the building front, roof, sides, and rear. From information of this type the crushing and rocking forces on the building can then be determined. In these analyses, no provision is made to include the effects of the blast wave on pressurizing the building interior from its entrance through open or smashed doors, through partly collapsed walls or the roof, and through

large broken blow-out panels in the side walls. Including pressurization of the building interior can be fairly important. For example, it can partly or even totally counter the blast-wave overpressure applied to the outside of the building, thereby reducing the resultant loading on some or all parts of the building, as well as reducing the crushing and rocking forces. Furthermore, equipment, instrumentation, and personnel that are located or working inside the building may actually be exposed to the blast wave, an important effect that might otherwise have been simply ignored or overlooked.

The power house of the Darlington Generating Station has many blow-out panels located in the front wall of the turbine hall which faces the railroad tracks where the accidental explosion might occur. Blow-out panels are located also in the rear wall of the power house - in the exterior wall of the reactor auxiliary bay. These blow-out panels are included in the design of the power house to minimize effects of a possible explosion occurring inside the power house, from a steam pipeline rupture for example. However, in the extremely remote event of an accidental explosion of the equivalent of 61,500 kg of TNT occurring at the railroad tracks, 495 m away, the blow-out panels in the front wall facing the explosion would undoubtedly be broken by the blast wave and blown into the turbine hall. The blow-out panels in the rear wall may also be broken by the blast wave and blown into the reactor auxiliary bay. This would result in the transient pressurization of the interior of the power house by the portion of the blast wave that travels into the power house through these blow-out panel openings. The rate of pressurization of the power house would, of course, be dependent on a number of different factors, such as the strength, shape, and duration of the incident blast wave, the degree of reflection at the front wall, the time for the blow-out panels in the front and rear walls to break and open, as well as the total area of the blow-out openings relative to the cross sectional area of the adjacent room.

1.2 Project Objectives

The major objectives of the present investigation are summarized briefly as follows:

a) predict the nonstationary blast-wave flow inside the Darlington Generating Station power house with an appropriate one-dimensional nonstationary flow analysis developed for this particular purpose, to obtain the blast-wave pressure loading inside the power house,

b) predict the transient blast-wave pressure loading on the outside of the power house, by using an approximate analysis like that presented in Refs. 1, 2 and 6,

c) determine the resultant blast-wave loading on the building front, roof, sides, and rear of the power house, from the difference in transient blast-wave pressures between the outside and inside of the power house.

In order to meet these major objectives, some important supporting tasks have to be undertaken and completed first. These are listed briefly as follows:

a) develop an appropriate numerical analysis for the one-dimensional nonstationary blast-wave flow inside the Darlington Generating Station power house, which includes the flow through area changes

with associated head losses, as well as the effects of friction from the flow at the power-house walls and heat transfer from the flow to the power-house walls,

b) develop an appropriate geometrical model of the interior of the power house, through which the blast wave travels inside the building, which is the flow area variation with distance required for the numerical analysis of the blast-wave flow inside of the power house,

c) define all of the properties of the blast wave incident on the power house from the explosion of a 61,500-kg hemispherical charge of TNT at the railroad tracks, 495 m away from the power house, which is the major part of the initial conditions required for the numerical analysis to commence the blast-wave flow computations inside the power house,

d) apply a suitable analysis to obtain the dynamic response and breaking of the blow-out panels, when subjected to the initial blast-wave loading on the power-house front, in order to obtain a good estimation of the characteristic time for the blow-out panels to completely break and open, which is required for the numerical analysis of the blast-wave flow inside the power house,

e) select suitable coefficients or factors for head losses resulting from area changes (both area reductions and area enlargements), head losses due to friction, and heat transfer due to temperature differences existing between the blast-wave flow and the interior walls of the power house,

f) develop a suitable approximate analysis - like that presented in Refs. 1, 2 and 6 - to predict the blast-wave loading on the outside walls and roof of the power house, in order to determine the blast-wave pressure loading on the exterior walls and roof of the power house,

g) develop appropriate computer programs based on the analysis and then produce numerical results required as part of the solution to the problem under consideration,

h) provide a discussion with an interpretation of the final numerical results, in regard to the problem under consideration.

Details of these tasks and the final numerical results, discussion and interpretation are presented in the following chapters. An introduction to most of these chapters is also given for readers who want only an overview, without having to read through all of the details.

2. NUMERICAL ANALYSIS OF THE BLAST-WAVE FLOW INSIDE THE POWER HOUSE

2.1 Introduction

The partial differential equations of motion (continuity, momentum and energy) along with the thermally perfect equation of state for one-dimensional, nonstationary, compressible gas flows in pipes or ducts with area changes, head

losses due to area changes, head losses from friction between the gas flow and duct walls, and heat transfer from the gas flow to the duct walls are presented and discussed in this chapter. It is worth mentioning here at the start which numerical method is employed to solve the present problem of the blast-wave flow inside the Darlington Generating Station power house. The solution method incorporated in this study is now fairly well known as the random-choice method (RCM), and it is of recent origin and unique, and it has important advantages over other finite-difference and finite-element methods. The RCM was invented formally in about 1965 by Glimm [7], who published it in a very mathematical format unfamiliar to most engineers and physicists, and it was not employed to solve engineering and other problems until much later, mostly because of the format but also partly because the numerical results from the method contained unacceptable levels of numerical noise. Chorin [8] overcame this latter difficulty in about 1976, by recognizing that it was best to choose only one random number for all calculations between grid zones at one time level instead of one new random number for each calculation. Also, he selected a better random-number algorithm to help reduce numerical noise [9-10]. Such improvements made the method practicable for solving engineering and other problems. He was also the first to apply the method to obtaining meaningful solutions to engineering gas flow problems in ducts of constant area. Shortly thereafter in about 1977, Sod [11] extended the RCM for solving only planar flow problems such that other complex cylindrical and spherical flow problems could also be solved, as well as flow problems with gradual area changes in pipes and ducts, by introducing the relatively new but fairly well-known operator-splitting technique to the RCM. Sod's technique is also employed in the present study.

The RCM is a first-order, explicit, numerical scheme that repeatedly solves a Riemann or shock-tube problem between adjacent grid points, in order to get the solution at the next time level. This method is highly suitable for solving systems of hyperbolic equations, if the Riemann problem can be defined simply, such as for the gasdynamics equations of motion. The numerical results show that shock-wave fronts and contact surfaces are well defined with sharp fronts, because the method does not employ any explicit or implicit artificial viscosity and does not have implicit or explicit numerical viscosity. These are definite advantages over other finite-difference and finite-element methods that smear out discontinuities, if sharp or discontinuous shock and contact-surface fronts are needed or even desired. Also, the RCM is relatively simple, relatively easy to learn and program, and not terribly inefficient in terms of computational costs. A detailed explanation of this method and its specific characteristics can be found in previously noted references [7-9, 11] and also especially in a UTIAS report by Saito and Glass [12]. Finally, it is worth mentioning that the RCM has been employed successfully in solving a number of unsteady flow problems at UTIAS since 1979 [5, 10, 12-23]. A number of these past studies are relevant to the present problem of the blast-wave flow inside the Darlington Generating Station power house [5, 10, 12-13, 16-19]. The RCM is well established, therefore, and it can now be applied successfully and with much confidence in the present study.

In this study the blast-wave flow inside the Darlington Generating Station power house is assumed to be both time dependent and one-dimensional; that is, the flow is firstly nonstationary and secondly depends on only one spatial dimension. This does not mean that the unsteady flow is assumed to be planar. The flow is assumed to be one-dimensional only in that it travels through both constant-area ducts and nonuniform-area ducts for which the area is a function of only linear distance. For this assumption to be realistic for actual flows, the area changes would have to be both smooth and gradual, which

is assumed for the current study. The effects of head losses from actual area changes will, of course, be employed in the numerical prediction of the actual nonstationary blast-wave flow.

It is worth mentioning here that the actual blast-wave flow inside the power house would, of course, be three-dimensional; that is, it would depend on three spatial dimensions. However, the flow is modelled in the present study as one-dimensional for the following reasons. Firstly, the numerical solution for three-dimensional nonstationary flows, as well as that for two-dimensional flows, requires large-storage and high-speed computers, which are generally not available. Secondly, the computational times and costs that are required to solve such complex flow fields are normally prohibitive. Thirdly, and very importantly, the assumption that the blast-wave flow inside the power house is one-dimensional is sufficiently good to provide a realistic solution to the problem under consideration.

2.2 Differential Equations of Nonstationary Gas Motion

The continuity, momentum and energy equations for one-dimensional, nonstationary, compressible gas flows in channels, pipes or ducts with area transitions or changes, including the effects of head losses from area changes, head losses from friction, and heat transfer from the flow to the tube walls are [13, and 24-25]

$$\frac{\partial}{\partial t}(\rho) + \frac{\partial}{\partial x}(\rho u) = -\frac{1}{A}\frac{dA}{dx}(\rho u) , \tag{2.1}$$

$$\frac{\partial}{\partial t}(\rho u) + \frac{\partial}{\partial x}(\rho u^2 + p) = -\frac{1}{A}\frac{dA}{dx}(\rho u^2) - F_{hl} - F_f , \tag{2.2}$$

$$\frac{\partial}{\partial t}(e) + \frac{\partial}{\partial x}(ue + up) = -\frac{1}{A}\frac{dA}{dx}(ue + up) + Q , \tag{2.3}$$

where p, ρ, u, e, x, and t denote the static pressure, density, flow velocity, total energy per unit volume, distance, and time, respectively. Also, A, F_f, F_{hl}, and Q denote the local flow or duct area, body force from friction per unit volume, body force from head loss per unit volume, and heat transfer per unit volume, respectively.

The total energy e is the sum of both the internal energy $\rho C_v T$ and the kinetic energy $\rho u^2/2$, where C_v and T are the specific heat at constant volume and the temperature. This sum is conveniently re-expressed as

$$e = \frac{p}{(\gamma - 1)} + \frac{1}{2}\rho u^2, \tag{2.4}$$

where γ is the gas specific-heat ratio. Equations 2.1 to 2.4 are completed by the thermal equation of state for a perfect gas; that is, $p = \rho RT$.

Although the basic, governing equations of the nonstationary flow are given by Eqs. 2.1 to 2.4, supplementary expressions are also required for the specification of the area change with distance, head losses from area changes, head losses due to friction, and heat transfer from the gas flow to the duct walls. These supplementary equations are presented in the following sections, where the basic details of their origin and meaning are illustrated. In some cases, additional or alternate expressions that are not used in the numerical analysis are also presented for completeness of the subject matter.

2.3 Supplementary Equations for Area Changes

To numerically solve the governing flow equations (Eqs. 2.1 to 2.4) the specific variation of area with distance A(x) is required. For this purpose the following function for an area change,

$$A(x) = A_u \exp[\ln(A_d/A_u)^{1/2} (1 - \cos\{\pi x/L\})] , \qquad (2.5)$$

which was selected by previous authors [10 and 16-19], is also used here. In this expression, A_u and A_d are the upstream and downstream areas, respectively, and L is the length of a particular area change section. From this equation, note that at x = 0 we have $A = A_u$, whereas at x = L we have $A = A_d$. This type of function is used because

$$\frac{1}{A}\frac{dA}{dx} = (\pi/2L) \ln(A_d/A_u) \sin(\pi x/L) \qquad (2.6)$$

is both symmetric and smooth, and it results in a reduction in numerical noise in the computed flow properties as compared to other variations of area that were tried previously.

In the present investigation the blow-out panels in the front wall of the power house are assumed to open linearly with time, and the characteristic opening time is determined in chapter 5. A linearly increasing area A(x,t) in time is easily incorporated in the numerical solution of Eqs. 2.1 to 2.4, by simply resetting this opening area at the location of the blow-out panels to that desired at each new time step. Because the area opening of the blow-out panels is a function of time, this would normally mean that the time-dependent term $(-\rho/A)dA/dt$ should be included in the continuity equation given previously by Eq. 2.1 [24-25]. This term is not included in the continuity equation in this study for the following reasons. Although the area opening for the blow-out panels is taken to increase linearly with time in the analysis, the actual duct area and duct volume do not increase with time in the actual case of the blast-wave flow in the power house. Although the blow-out panels do bend and break, they do not disappear and generate any additional volume for the blast-wave flow to move into and thereby occupy. Consequently, the additional term given by $(-\rho/A)dA/dt$, which accounts for duct area and volume changes, is not and should not be included in the present analysis.

2.4 Supplementary Equations for Head Losses due to Area Changes

In order to solve Eqs. 2.1 to 2.4, expressions for head losses due to area changes are required. Head-loss expressions are needed for area changes which consist of monotonic area reductions only, monotonic area enlargements only, and the combination of an equal contraction and expansion that essentially forms a perforated plate. These expressions are presented and discussed in the next three subsections.

Monotonic Reductions in Duct Area

Monotonic area reductions are encountered by the blast-wave flow inside the power house, as it propagates from one room or space of a certain cross-sectional area to another room or channel with a smaller cross-sectional area. Of course, if the convergence in area from one room to the next is relatively

smooth and gradual in practice, then the head loss is negligible, for all practical purposes, and the head loss for this area reduction need not be included or considered. However, for the blast-wave flow inside the power house this is generally not the case, and head losses at most area reductions need to be included in order to get realistic predictions of the flow inside the building.

Head losses for area reductions can be expressed in general terms as an equivalent body force per unit volume F_{hl} [24-28], which appears in the momentum equation presented earlier (Eq. 2.2). The body force per unit volume F_{hl} or $F_{hl}(x)$ is assumed to act over a finite distance Δx just downstream of this reduction [16]. This body force per unit volume can now be expressed in terms of an associated or corresponding pressure drop or head loss Δp_{hl} as

$$F_{hl} = \Delta p_{hl} \frac{A(x)}{V(x)} = \frac{\Delta p_{hl}}{\Delta x} , \qquad (2.7)$$

where Δx is the total duct length of distributed area $A(x)$ and volume $V(x)$ over which the head loss is distributed just downstream of the area reduction.

From experimental data for steady flows the head loss can be expressed as [26-27]

$$\Delta p_{hl} = k_o \frac{1}{2} \rho_u u_u^2 , \qquad (2.8)$$

where k_o is the head-loss factor or coefficient and $\rho_u u_u^2/2$, ρ_u, and u_u are the dynamic pressure, density, and flow velocity of the flow upstream of the area reduction, respectively. The head-loss factor for an area contraction depends on the downstream-to-upstream area ratio A_d/A_u, and values of this factor for a sudden area contraction are given in the following table [27].

A_d/A_u	0.00	0.01	0.09	0.25	0.49	0.81	1.00
k_o	0.50	0.47	0.42	0.33	0.22	0.03	0.00

If the area contraction is not sudden but is rather slightly rounded, then the values in this table should be reduced by a factor of two. For other degrees of roundedness other appropriate factors can, of course, be used. Note that a curve fit can be readily applied to the head-loss factor as a function of the downstream-to-upstream area ratio, such that head-loss factors can be obtained easily for any area ratio. The use of a cubic spline is one efficient means of achieving this curve fit, and the highly suitable cubic-spline method given in Ref. 29 is employed in this study.

It is worth mentioning here that the head loss for an area reduction that is quite short is the dominant head loss, and that due to friction is not significant [26]. For all of the area reductions encountered by the blast-wave flow in the power house, the area reductions are more than sufficiently short that the additional negligible effects from friction need not be considered.

Monotonic Enlargements in Duct Area

Monotonic area enlargements are encountered by the blast-wave flow inside the power house, as it propagates from one room or space of a certain

cross-sectional area to another room or channel with a larger cross-sectional area. Even for smooth and gradual area enlargements these head losses have to be taken into account, in order to get realistic predictions of the flow inside the building.

Head losses for area enlargements can again be expressed quite generally in terms of an equivalent body force per unit volume F_{hl} [24-28], which is in the momentum equation presented earlier (Eq. 2.2). The body force per unit volume F_{hl} or $F_{hl}(x)$ is assumed to act over a finite length Δx just downstream of this enlargement [16]. This body force per unit volume can once again be expressed in terms of a corresponding pressure drop or head loss Δp_{hl} as

$$F_{hl} = \Delta p_{hl} \frac{A(x)}{V(x)} = \frac{\Delta p_{hl}}{\Delta x} , \qquad (2.9)$$

where Δx is the total duct length of distributed area $A(x)$ and volume $V(x)$ over which the head loss is distributed just downstream of the area enlargement.

From experimental data for steady flows the head loss can once again be expressed as [26-27]

$$\Delta p_{hl} = k_o \frac{1}{2} \rho_u u_u^2 , \qquad (2.10)$$

where k_o is the head-loss factor or coefficient and $\rho_u u_u^2/2$, ρ_u, and u_u are the dynamic pressure, density, and flow velocity of the flow upstream of the area enlargement, respectively. The head-loss factor for an area increase depends generally on the upstream-to-downstream area ratio A_u/A_d and the divergence angle of the area enlargement [26-27]. For a relatively short enlargement the head-loss factor is independent of the divergence angle and given simply by

$$k_o = [1 - A_u/A_d]^2 . \qquad (2.11)$$

This expression is used in the numerical analysis because the area enlargements that the blast-wave flow encounters in the power house are typically short. If this were not true the divergence angle would then become another parameter of importance. Tabulated head-loss factors versus area ratio and divergence angle can be found in Ref. 26.

It is worth mentioning here that the head loss for an area enlargement that is quite short is the dominant head loss, and that due to friction is not significant [26]. For all of the area enlargements encountered by the blast-wave flow in the power house, the area enlargements are sufficiently short that the additional negligible effects from friction need not be considered.

Openings due to Broken Blow-Out Panels

After the blast wave that is incident on the power house breaks open the blow-out panels in the front wall, part of the blast-wave flow enters the power house through these openings, which are increasing in area with time until they are fully open. The wall with these openings acts much like a perforated plate to the entering blast-wave flow, for which the porosity is increasing in time to its maximum value. Head losses associated with the blast-wave flow through this 'perforated plate' can be highly significant, and they must, therefore, be included in the numerical analysis to get realistic predictions of the flow inside the power house.

Head losses for perforated plates can again be expressed quite generally in terms of an equivalent body force per unit volume F_{hl} [24-28], which are in the momentum equation presented earlier (Eq. 2.2). The body force per unit volume F_{hl} or $F_{hl}(x)$ is assumed to act over a finite length Δx just downstream of this perforated plate [16]. This body force per unit volume can again be expressed in terms of an associated or corresponding pressure drop or head loss Δp_{hl} as

$$F_{hl} = \Delta p_{hl} \frac{A(x)}{V(x)} = \frac{\Delta p_{hl}}{\Delta x} , \qquad (2.12)$$

where Δx is the total duct length of distributed area $A(x)$ and volume $V(x)$ over which the head loss is distributed just downstream of the perforated plate.

From experimental data for steady flows the head loss for a perforated plate can again be expressed as [26]

$$\Delta p_{hl} = k_o \frac{1}{2} \rho_u u_u^2 , \qquad (2.13)$$

where k_o is the head-loss factor or coefficient and $\rho_u u_u^2/2$, ρ_u, and u_u are the dynamic pressure, density, and flow velocity of the flow upstream of the perforated plate, respectively. The head-loss factor for a perforated plate is generally dependent on a number of factors:

a) porosity ratio σ, defined as the ratio of the total area of all of the holes or orifices in the plate to the total duct area upsteam or downstream of the perforated plate,

b) entrance corners of the orifices, whether they are sharp-edged, rounded, or bevelled,

c) thickness ratio, defined as the plate thickness divided by the orifice diameter,

d) Reynolds number, based on both the flow velocity in the orifice and the orifice diameter, and

e) upstream Mach number of the approaching flow.

The relative importance of these various effects on the value of the head-loss coefficient is illustrated in Ref. 26.

In the present study the expression for the head-loss coefficient k_o is taken to be

$$k_o = [(\{1 - \sigma\}/2)^{1/2} + \{1 - \sigma\}]^2/\sigma^2 , \qquad (2.14)$$

where σ is the porosity ratio defined earlier. This particular expression is selected because it is assumed that the breaking of the blow-out panels will lead to a high level of turbulence and rough flow, and the Reynolds number of the blast-wave flow through initially small cracks or openings will be quite large. Hence, the above expression is chosen because it corresponds to sharp-edged orifices in the plate, which leads to the highest head loss. This seems to be the most appropriate expression that represents experimental data given in Ref. 26. Finally, because the blast-wave flow velocities that are expected inside the power house are relatively small, no correction is needed or applied for high Mach number effects.

2.5 Supplementary Equations for Head Losses due to Friction

Friction from the blast-wave flow over the interior walls of the power house and over internal objects is not expected to play a dominant role and be an important effect, because the hydraulic diameters of the rooms in the power house are extremely large and the propagation distances are relatively short. However, friction is included in the numerical analysis, such that its effects can be assessed.

In order to solve Eqs. 2.1 to 2.4, the frictional body force per unit volume must be known, and its determination will now be discussed. The effects of friction are averaged across the duct flow, or included in a one-dimensional sense. In the momentum equation (Eq. 2.2), F_f is the frictional body force per unit volume. For friction the pressure drop along a constant-area duct, over a finite length Δx, is defined as [24-28]

$$\Delta p_f = \frac{f\,\Delta x}{d_h} \frac{1}{2} \rho u^2 , \tag{2.15}$$

where f is the Darcy-Weisbach friction factor, d_h is the hydraulic diameter of the pipe or duct, and $\rho u^2/2$ is the local dynamic pressure. The pressure drop in the flow direction is related to the body force per unit volume for friction according to the following expression

$$F_f = \Delta p_f \frac{A(x)}{V(x)} = \frac{\Delta p_f}{\Delta x} = \frac{f}{d_h} \frac{1}{2} \rho u^2 , \tag{2.16}$$

where A(x) is the cross-sectional area of the duct and V(x) is the volume of the duct contained in the distance Δx.

For laminar pipe flows it is known that the friction factor f depends on the Reynolds number Re only and is given by [25-28]

$$f = 64/Re , \tag{2.17}$$

where $Re = \rho u d_h/\mu$ is based on the hydraulic diameter d_h, gas density ρ, flow velocity u, and dynamic viscosity μ (or the coefficient of dynamic viscosity). For turbulent flows the friction factor f depends on the Reynolds number Re and the relative roughness ε/d_h of the pipe or duct wall, where ε is the absolute wall roughness [26-28]. A semi-empirical correlation

$$f^{-1/2} = -2 \log \left[\frac{2.51}{Re\ f^{1/2}} + \frac{\varepsilon/d_h}{3.70} \right] \tag{2.18}$$

of Colebrook [27] is used in the present study.

The dynamic viscosity μ that is required for the calculation of the Reynolds number Re is a function of temperature T only, and a simple empirical correlation for air is employed [30],

$$\mu = \frac{a_o T^{3/2}}{T + S} \left[1.0 + 1.53 \times 10^{-4} [T/S - 1.0]^2 \right] , \tag{2.19}$$

where the constants $a_o = 1.47 \times 10^{-6}$ kg/m-s-$K^{1/2}$ and S = 113 K and T denotes the temperature in degrees Kelvin. This expression is valid for air temperatures between 78 K and 2500 K [30].

The Reynolds number of the blast-wave flow inside the power house is relatively large, much larger than 100,000, because the hydraulic diameter is normally very large and the flow velocities are generally greater than a few meters per second. In this case, the friction factor is virtually constant for a given relative roughness ratio ε/d_h. This is obvious from the Moody diagram taken from Ref. 27 and reproduced for interest in Fig. 3. For the blast-wave flow in the power house the absolute roughness of the interior walls is assumed to be 0.022, corresponding to a fairly rough surface with deep grooves and protuberances. A constant value of 0.05 for the friction factor f is, therefore, obtained from the Moody diagram (Fig. 3) at high Reynolds numbers. This value of the friction factor is used in numerical analysis of the blast-wave flow inside the power house.

In many nonstationary flow computations the Reynolds number covers a very wide range of values, and the friction factor can no longer be considered to be constant. In order to illustrate how the friction factor can be handled in such a case, one approach is presented in the following two paragraphs. For this method it will be assumed that the relative roughness ratio ε/d_h is simply constant at 0.0001.

In the critical region between laminar and turbulent pipe flows, for Reynolds numbers between 1000 and 3000, the value of the friction factor f can lie somewhere between the laminar and fully turbulent values, as shown in the Moody diagram in Fig. 3. The laminar and turbulent correlations given earlier by Eqs. 2.17 and 2.18 are joined smoothly by simply extrapolating Colebrook's correlation curve back to lower Reynolds numbers until it finally intersects the laminar curve. This is indicated clearly in Fig. 3 by the dark, dashed line, for the specific case of $\varepsilon/d_h = 0.0001$.

Colebrook's correlation for f in terms of ε/d_h and Re is implicit in f. Hence, an iteration process is necessary to determine a specific value of f for specified values of ε/d_h and Re. This iterative scheme is avoided by fixing the value of ε/d_h at 0.0001 and using the following correlations for f as a function of Re only.

$$
\begin{aligned}
f &= 64/\mathrm{Re} && \text{if } 0 < \mathrm{Re} < 1033.65 \\
f &= [1.6798 \log(\mathrm{Re}) - 1.0501]^{-2} && \text{if } 1033.65 < \mathrm{Re} < 10^5 \\
f &= [7.349 + 1.825[1.0 \\
&\quad - \exp\{-1.2(\log(\mathrm{Re}) - 5.0)^{1.17}\}]]^{-2} && \text{if } \mathrm{Re} > 10^5
\end{aligned}
\qquad (2.20)
$$

The first correlation in Eqs. 2.20 is exactly Eq. 2.17, and the last two curve fits are suitable approximations which give values within 1% of those obtained from Colebrook's correlation (Eq. 2.18) with $\varepsilon/d_h = 0.0001$. Note that compressibility effects on the friction factor are usually negligible [28 and 31-32], and this is true especially for low-speed blast-wave flows in the power house.

2.6 Supplementary Equations for Heat Transfer

Heat transfer from the blast-wave flow inside the power house to the interior power-house walls is not expected to play a dominant role and be an important effect, because temperature differences are not unduly large and the heat-transfer coefficient is not appreciably high. However, heat transfer is still included in the numerical analysis, so that its effects can be assessed.

An expression is required for the heat transfer per unit volume from the wall into the flow, in order to solve Eqs. 2.1 to 2.4. The heat transfer per unit surface area is given by the following general expression [28 and 33]

$$q = H [T_w - T_{aw}] , \tag{2.21}$$

where H denotes the film coefficient for heat transfer, T_w is the power-house wall temperature, and T_{aw} is the bulk, recovery, or adiabatic wall temperature of the flowing gas [28 and 33]. The heat transfer per unit volume Q is then

$$Q = (4H/d_h) [T_w - T_{aw}] , \tag{2.22}$$

which can be obtained from Eq. 2.21. Because the Nusselt number Nu equals Hd_h/k, where k is the thermal conductivity, and because the Prandtl number Pr equals $\mu C_p/k$, where C_p is the specific heat at constant pressure, Eq. 2.22 can then be rewritten as

$$Q = (4\rho C_p u/d_h)[T_w - T_{aw}](Nu/(Pr\ Re)] = (4\rho C_p u/d_h)[T_w - T_{aw}]St , \tag{2.23}$$

where St = Nu/(Pr Re) is the Stanton number. (This nondimensional number is commonly encountered in heat-transfer problems involving flowing fluids in pipes and ducts.)

For the present study, the temperature T_w of the power-house walls is assumed to be constant at 288 K. This is well justified because these walls are massive, have a much higher heat capacity than air, and the blast-wave flow is transient and over in a relatively short time of less than one-half of a second. Finally, the initial temperature of the air in the power house is also assumed to be 288 K.

The adiabatic wall temperature T_{aw} for a compressible gas flow is given by the expression [28 and 33],

$$T_{aw} = T [1 + R(\gamma-1)M^2/2] , \tag{2.24}$$

where R is the so-called recovery factor and M = u/a is the flow Mach number. For laminar and turbulent compressible gas flows a reasonable approximation for the recovery factor is $R = Pr^{1/3}$ [28 and 33], which is based on theoretical derivations and experimental correlations.

An expression for the Stanton number St, which is a measure of the heat transfer, can be derived in an analogous manner to that for the skin friction, and this derivation is called the Reynolds analogy [28]. This analogy was initially developed for laminar, incompressible flows having a Prandtl number Pr equal to unity. However, this analogy can be extended to turbulent and compressible flows to calculate the heat transfer from the flow to the duct wall, or vice versa. The results of the Reynolds analogy give fairly simple relationships among the Stanton number St, the skin-friction coefficient C_f, and friction factor f [28], which are

$$St = Nu/(Pr\ Re) = C_f/(2Pr) = f/8 , \tag{2.25}$$

if the Prandtl number is unity. However, this is still a good approximation for air flows having a Prandtl number of 0.72 [28], and this result is used herein. The friction factor f that defines the skin-friction coefficient C_f and Stanton number St has been given previously, and it is used here as well.

2.7 Method of Solution

In order to illustrate certain aspects of the method of solution by the random-choice method (RCM), Eqs. 2.1 to 2.3 are rewritten in vector notation as

$$\frac{\partial}{\partial t}[G] + \frac{\partial}{\partial x}[F(G)] = H(G) + I(G) + J(G), \qquad (2.26)$$

where

$$G = \begin{bmatrix} \rho \\ \rho u \\ e \end{bmatrix}, \quad F(G) = \begin{bmatrix} \rho u \\ \rho u^2 + p \\ u(e + p) \end{bmatrix}, \quad H(G) = -\frac{1}{A}\frac{dA}{dx}\begin{bmatrix} \rho u \\ \rho u^2 \\ u(e + p) \end{bmatrix},$$

$$I(G) = \begin{bmatrix} 0 \\ -F_f \\ Q \end{bmatrix}, \quad \text{and} \quad J(G) = \begin{bmatrix} 0 \\ -F_{h1} \\ 0 \end{bmatrix}.$$

The symbols have their usual meaning defined earlier.

This set of partial differential equations (Eq. 2.26) along with initial and boundary conditions can be solved by using the method of characteristics, finite-difference or finite-element methods and the relatively new and unique random-choice method. The RCM is used in this study because it is particularly well suited for solving one-dimensional nonstationary flow problems involving shock-wave and contact-surface discontinuities. In the RCM, shock waves and contact surfaces are well defined with sharp changes or fronts (not smeared out over many mesh points), unlike the results from either finite-difference or finite-element methods in which they are smeared over many grid zones, because of the use of artificial viscosity terms added explicitly to the governing equations and/or the implicit presence of numerical viscosity. Solutions by means of the method of characteristics with additional implicit or explicit shock capturing or other techniques are too tedious to be seriously considered for this study.

The RCM was originally invented and developed for solving nonstationary planar flow problems by Glimm [7] and first made practical and used practically for solving such problems by Chorin [8], as mentioned in the introduction to this chapter. Sod [11] introduced the operating-splitting technique to the RCM, so that this method for solving planar flow problems could be extended to solve cylindrical and spherical flow problems, as well as problems involving gradual area changes. Note that the RCM is a first-order, explicit numerical scheme that repeatedly solves a Riemann or shock-tube problem between adjacent grid points, to get the solution at the next time level. Although most details of this method can be found in Refs. 7 to 9 and 12, a brief description is included herein.

The mesh or grid layout in the time-distance or physical plane for the RCM solution procedure is shown in Fig. 4a. At each time level the grid points are distributed uniformly along the distance axis, with a regular spacing of Δx or Δr between adjacent grid points. However, the grid points do alternate in location from one time level to the next, being at the midpoints between successive grid points of the previous time level. As a result of this alternating grid system, computations made from one time level to the next are done in a so-called half time step, and computations made for two consecutive half time

steps are said to be done for a full time step. The full time step has a time interval of Δt. Each half time step Δt^* should be controlled by the so-called Courant-Fredrichs-Lewy stability criterion [7-9, 12], which restricts the half time step such that any type of wave cannot travel more than one-half of a grid zone ($\Delta x/2$) in the time Δt^*, in order to guarantee numerical stability in the computations. However, sometimes for simplicity and mostly for a savings in computational cost from not always checking at every grid location the Courant-Fredrichs-Lewy criterion, the time interval for the second half time step is normally set equal to that for the first time step. Because this 'shortcut' does not result in any apparent stability difficulties with the numerical calculations, it is also used in the present numerical computations. Finally, note that the time interval Δt from one full time step to the next will, of course, generally be different, because of the application of the stability criterion.

When a complete set of initial conditions are specified at each of two grid points, on time level t (see Fig. 4a), a Riemann or shock-tube problem can be established and solved analytically for a planar flow [7-9]. Initial conditions for the RCM solution normally consist of knowing the pressure, density and flow velocity at each grid point for the first time level. The particular solution and its details are not repeated here, but they can be found in Refs. 7 to 9, as well at Ref. 12. However, one shock-tube wave pattern consisting of a rightward moving shock wave, contact surface and leftward moving rarefaction wave are depicted in Fig. 4b for interest. These waves and the contact surface separate growing quasi-steady or steady flow regions (i.e., 1, 2, 3 and 5 in Fig. 4b). Region 4 is a simple nonstationary region within the rarefaction-wave fan. There are three other patterns as well, consisting of a leftward moving shock wave and rightward moving rarefaction wave separated by a contact surface, leftward and rightward moving shock waves separated by a contact surface, and leftward and rightward moving rarefaction waves without a contact surface.

When the flow properties are evaluated from the Riemann solution for each of the five states, the flow properties can then be assigned to the intermediary grid point at the next time level. This assignment of flow properties to the intermediary grid point involves a fairly simple random sampling procedure [7-9], giving the random-choice method its name. By choosing a random number between -1/2 and +1/2 from a uniform distribution, the flow properties from one of the five states is then selected for assignment to the intermediary grid point at the next time level [7-9]. Because the random-number algorithm can affect the smoothness or quality of numerical results [9-10], sometimes in a drastic manner, the van der Corput algorithm which is recommended in Refs. 9 and 10 is used here.

For the case of computations involving nonstationary flows with area changes, the planar solution is always completed first. This initial solution is approximate, and it must be corrected for the change in area, by using the operator-splitting technique [11]. Note that this correction should be made at each half time step, not just over a full time step. Otherwise, the computed results will normally be inaccurate and not meaningful. The general solution procedure involves the solution of the Riemann problem between successive grid points at one time level, in an ordered sequence from left to right (or vice versa) across the entire flow field. When this is done and the flow properties have all been computed at the next time level, the process can then be repeated from one time level to the next, in order to compute the entire flow field of interest.

Equation 2.26 for nonstationary flows has three inhomogeneous terms on the right-hand side denoted by H(G), I(G), and J(G). If these three terms were missing, then a simple, closed-form, analytical solution for the Riemann or shock-tube problem can be obtained [6-9]. The inhomogeneous terms, resulting from including the effects of area changes, head losses from friction, heat transfer, and head losses due to area changes, prevent one from obtaining such a simple analytical solution for the complete Riemann or shock-tube problem. For this reason, the operator-splitting technique is employed to correct the planar flow solution and thereby give the complete numerical solution for the nonstationary flow with the effects of area changes, head losses, and heat transfer.

The first step in the RCM is to simply remove all inhomogeneous terms and then simply obtain in the first step an approximate solution from the homogeneous equation. This approximate solution we will call G_1, which is obtained from

$$\frac{\partial}{\partial t}[G] + \frac{\partial}{\partial x}[F(G)] = 0 , \tag{2.27}$$

which can be solved analytically in closed form, as mentioned previously. The solution technique and the exact expressions for the four elemental patterns of the Riemann problem, consisting of a combination of shock waves, contact surface, and rarefaction waves, are not presented here, but they can be found in Refs. 7 to 9 and 11. This is the general solution of the planar shock-tube problem.

The second step is to use this intermediate, approximate solution to get the next intermediate, approximate solution that includes the effects of the area changes from the inhomogeneous term H(G). This next approximate solution that is denoted as G_2 is obtained by making use of the following first-order, finite-difference correction

$$G_2 = G_1 - \Delta t^* H(G_1) , \tag{2.28}$$

where Δt^* is the half time step for the numerical computations.

The third step is to use this new, approximate solution to obtain the next intermediate, approximate solution that includes the effects of friction and heat transfer from the inhomogeneous term I(G). Hence, the corrected solution is determined from

$$G_3 = G_2 - \Delta t^* I(G_2) , \tag{2.29}$$

where G_3 is the new approximation.

The final step is to use this new, approximate solution to get the final solution G, which then includes the effects of head losses due to area changes from the inhomogeneous term J(G). The result is

$$G = G_3 - \Delta t^* J(G_3) . \tag{2.30}$$

The final solution G will now have all of the corrections for the area changes, head losses from area changes, head losses due to friction, and the effects of heat transfer. Note that one or more of the intermediate steps can be skipped if such corrections are not needed or desired, thereby removing the effects that are not required.

3. GEOMETRICAL MODELS OF THE POWER HOUSE FOR THE NUMERICAL ANALYSIS

3.1 Introduction

The judicious selection of a suitable but simple one-dimensional flow path or paths having an appropriate changing cross-sectional area with distance through the Darlington Generating Station power house is a rather difficult and subjective task, because the interior of the power house is not just a simple straight duct. As a good example of this, see the side view of the power house shown in Fig. 5. The flow path is not always straight but sometimes tortuous when it bends around obstacles like equipment and turns from one direction to another from one room or space to the next. The flow area along this flow path changes also because of obstacles like equipment, area constrictions like doorways or passageways between rooms, area enlargements from room size increases, and changes in ceiling or floor height from one space to another. However, by making use of realistic assumptions and approximations, appropriate flow paths having suitable area variations along the path can be selected, in order to get practical results.

Two different and separate flow paths are considered for the blast-wave flow in the power house. The upper flow path labelled 1 in Fig. 5 is for the case of the blast wave entering through blow-out panels in the upper part of the front wall of the power house and travelling in sequence through the upper parts of the turbine hall, turbine auxiliary bay and reactor building, as well as into three small rooms below the hoistway. Because it is possible for the blast wave inside the reactor building to break blow-out panels in the rear wall of the power house and thereby leave the building, the possibility of this scenario is also considered. In this scenario the blast-wave flow is branched; that is, it not only enters the three small rooms but it also simultaneously leaves the reactor building through the openings in the broken blow-out panels. Branched flows cannot be handled directly in the present RCM computer code. As a consequence, a few different, approximate, blast-wave flow paths are devised, such that realistic predictions of the branched flows can be obtained. These special considerations lead to modifications to the upper flow path (1) and its corresponding cross-sectional area with distance in both the reactor building and the three small rooms, resulting in the unfortunate increase in the numbers of geometric models for the power house, computer runs, and numerical results.

The lower flow path labelled 2 in Fig. 5 is for the final case of the blast wave entering through blow-out panels located in the lower part of the front wall of the power house and moving in sequence through the lower parts of the turbine hall, turbine auxiliary bay, and reactor building. However, owing to the small opening in the blast wall between the turbine auxiliary bay and reactor building, it is anticipated that only a very weak blast wave will enter the lower part of the reactor building. The modelling for this lower flow path (2) is essentially straightforward, and this time it does not lead to an unfortunate proliferation of geometric models, computer runs, and numerical results.

It is worth mentioning here that flow paths number 1 and 2 are taken to be different and separate blast-wave flow paths, notwithstanding the fact that there are small interconnecting openings. Ignoring these interconnecting openings is reasonable because they are rather small and essentially unimportant. Furthermore, for a blast wave propagating in each flow path at about the same time and at approximately the same strength, the resulting small leaks or flows through the interconnecting openings between one flow path and the other would generally be small and insignificant.

Additional details of the blast-wave flow paths, their cross-sectional areas with distance through the power house, the maximum openings of the blow-out panels, and the rational behind their selection are now presented briefly in the following sections of this chapter.

3.2 Geometrical Configuration A

The geometrical model of the power house called configuration A, for flow path number 1 for the blast wave in the upper part of the power house, is depicted at the top of Fig. 6. The room numbers, descriptions, lengths, and cross-sectional areas are summarized just below the top diagram. Additional information on the areas of the blow-out panels in the upper part of the front wall of the turbine hall, the interconnecting openings between rooms 6 to 9, as well as the area of the front wall of the power house associated with flow path number 1, are given just below the previously mentioned data. The lengths and cross-sectional areas of the various rooms and the area of the blow-out panels were obtained from Ontario Hydro drawings of the power house.

For configuration A, the blast wave that is incident on the power house breaks the blow-out panels in the front wall, and part of this blast wave then enters the power house, moving sequentially through the turbine hall, turbine auxiliary bay, reactor building, and the three small rooms below the hoistway. The blow-out panels in the rear wall of the power house are assumed to remain intact (i.e., not break), for the case of configuration A. Consequently, there is only one unbranched flow path of interest for this case, and this flow path starts at the blow-out panels in the front wall of the power house and ends in the three small rooms. For the numerical computations of the blast-wave flow inside the power house, the three small rooms with their original lengths and cross-sectional areas are then connected directly to the reactor building. It does not matter for the numerical computations as to whether these rooms are actually located below, behind, or to the side of the reactor building, as long as the correct length for the blast-wave propagation path is maintained.

The blast wave incident on the power house is depicted on the right of the top diagram in Fig. 6, moving toward the power house in a duct indicated by dashed lines. In any one-dimensional model of nonstationary flows, a duct must be specified for containing the incident blast wave, as well as its reflection from the front wall of the power house. Note that the cross-sectional area of this additional channel is not necessarily equal to that of the first room inside the power house, because the frontal area of the power house may be larger.

The geometrical model designated configuration A is an important one in helping to establish whether the blast-wave pressure inside the reactor building is sufficiently high to break the blow-out panels in the rear wall of the reactor building or power house. The pressure difference from the blast waves on the inside and outside these blow-out panels would, of course, have to be considered to get a realistic answer.

3.3 Geometrical Configuration B

The geometrical model of the power house called configuration B, for flow path number 1 for the blast wave in the upper part of the power house, is depicted at the top of Fig. 7. The room numbers, descriptions, lengths, and

cross-sectional areas are summarized just below the top diagram. Additional information on the area of the blow-out panels in the upper part of the front wall in the turbine hall, the area of the blow-out panels in the rear wall of the reactor building, as well as the areas of the front and rear walls of the power house associated with flow path number 1, are also given. The lengths and cross-sectional areas of the various rooms and the areas of front and rear walls were taken from Ontario Hydro drawings of the power house.

For configuration B, the blast wave that is incident on the power house breaks the blow-out panels in the front wall, and part of this blast wave then enters the power house, moving sequentially through the turbine hall, turbine auxiliary bay, and reactor building. The blast-wave flow inside the reactor building is assumed to break the blow-out panels located in the rear wall of the reactor building and then move outside the power house. For configuration B, therefore, there is only one unbranched flow path from the front wall of the power house to the rear wall. The three small rooms are not included in this configuration for flow path number 1, because their addition would produce a branched flow path. That is, the blast-wave flow path would eventually split into two separate flow paths, one that leaves the reactor building through the openings in the broken blow-out panels and the other that moves into the three small rooms. This type of branched blast-wave flow cannot be handled directly in the present computer program using the RCM, as mentioned earlier; however, the blast-wave flow in the three small rooms can be obtained in an approximate but still realistic manner (see configurations C and D).

The blast-wave pressures and effects predicted with the geometrical model for configuration B will be slightly high for the reactor building. This happens because no allowance for losses in mass, momentum, and energy from the blast-wave flow in the reactor building, due to the loss of flow to the three small rooms, have been accounted for in the numerical prediction. Because the reactor-building volume is fairly large relative to the combined volume of the three small rooms, these effects should not be large. However, they will not be negligible either, because the ratio the volumes of the reactor building and three small rooms is only about six.

3.4 Geometrical Configuration C

The geometrical model of the three small rooms below the hoistway in the reactor building is called configuration C, and it is sketched in Fig. 8. This configuration is associated with flow path number 1 for the blast wave in the upper part of the power house. The room numbers, descriptions, lengths and cross-sectional areas are summarized below this diagram, and this geometrical data was also obtained from Ontario Hydro drawings of the power house.

If the blast-wave flow that enters the first of the three small rooms is known, then the flow in these rooms can be predicted by the present RCM computer code. As an approximation for the present study, the blast-wave flow in the reactor building from configuration B is employed almost directly as input to predict the nonstationary flow in the three small rooms. Only one of the input conditions is modified; that is, the flow velocity is set equal to zero, because the flow velocity in the reactor building is basically perpendicular to that in the three small rooms. Hence, the blast-wave flow in the three small rooms originates as a flow resulting from an infinitely large reservoir with changing initial conditions corresponding to the blast-wave flow properties in the reactor building.

The predicted blast-wave pressures and effects in the three small rooms by such a flow model will be slightly high, for the following reason. The flow that leaves the reactor building and enters the three small rooms involves, in effect, losses of mass, momentum, and energy from the main blast-wave flow in the reactor building. As a result, the blast-wave flow in the reactor building will be reduced, which in turn will lead to a reduction in the flow into the three small rooms. This effect should be rather small, however, because the volume of the reactor building is much larger than the combined volumes of the three small rooms. However, it will not be negligible, because the ratio of the volumes of the reactor building to the three small rooms is only about six.

3.5 Geometrical Configuration D

The geometrical model of the power house called configuration D, for flow path number 1 for the blast wave in the upper part of the power house, is depicted at the top of Fig. 9. The room numbers, descriptions, lengths, and cross-sectional areas are summarized just below the top diagram. Additional information on the areas of the blow-out panels in the upper part of the front wall of the power house, as well as the interconnecting openings between rooms 6 to 9, are again given just below. Most of these lengths and cross-sectional areas of the various rooms were obtained from Ontario Hydro drawings of the power house.

For configuration D, the blast wave that is incident on the power house breaks the blow-out panels in the front wall, and part of this blast wave then enters the power house, moving sequentially through the turbine hall, turbine auxiliary bay, reactor building, and the three small rooms below the hoistway. These three small rooms have been increased in cross-sectional area by a factor of 23.5 and connected directly to the rear of the reactor building. Furthermore, the mimimum areas between two adjacent rooms have been suitably increased also, as indicated in Fig. 9. The reasons for these modifications to the three small rooms are brought out in the following paragraph.

Configuration D corresponds to the case for which the blast-wave flow in the reactor building breaks instantly the blow-out panels in the rear wall of this building, and the blast-wave flow thereby leaves the reactor building via the blow-out panel openings. See the illustration of this in Fig. 10a. In order to include the three small rooms directly in the configuration for the numerical computations of the blast-wave flow, without a branched flow path, a new combined geometry of the three small rooms and blow-out panel openings had to be developed, as illustrated in Fig. 10b. The new geometry is based on the behavior of steady, incompressible flows through branched ducts, which is only approximate. The method of obtaining the magnification factor for the cross-sectional areas of the small rooms and the simple additional increase in inlet areas for the small rooms are indicated directly in Fig. 10b. When these new enlarged rooms are connected directly to the rear of the reactor building, they then cover the entire blow-out panels openings. However, these rooms have been increased appropriately in size such that the combined flow from both the reactor building and the three small rooms should be indicative of that occurring in the original, unmagnified, three small rooms. Hence, the blast-wave pressures should also be indicative of the those experienced in the actual smaller rooms.

The primary goal for geometrical configuration D is to obtain a second prediction of the blast-wave flow in the three smaller rooms, when the blow-out

panels in the rear power-house wall break, because the previous prediction from the combined configurations B and C is known to be slightly high.

3.6 Geometrical Configuration E

The geometrical model of the power house called configuration E, for flow path number 2 for the blast wave in the lower part of the power house, is depicted at the top of Fig. 11. The room numbers, descriptions, lengths, and cross-sectional areas are summarized just below the top diagram. Additional information on the area of the blow-out panels in the lower part of the front wall in the turbine hall, the minimum area of the small opening in the blast wall, as well as the areas of the front wall of the power house associated with flow path number 2, are also given. The lengths and cross-sectional areas of the various rooms and the areas of front and rear walls were again taken from Ontario Hydro drawings of the power house.

For configuration E, the blast wave that is incident on the power house breaks the blow-out panels in the front wall, and part of this blast wave then enters the power house, moving sequentially through the lower parts of the turbine hall, turbine auxiliary bay, and reactor building. For configuration E, therefore, there is only one unbranched flow path from the front wall of the power house to the rear wall, and this particular geometry and flow path are easily handled.

The primary purpose of this geometrical configuration is to determine numerically the blast-wave pressures for the lower flow path in the turbine hall, the turbine auxiliary bay, and especially the reactor building behind the blast wall.

4. PROPERTIES OF THE BLAST WAVE INCIDENT ON THE POWER HOUSE

4.1 Introduction

All of the basic flow properties of the blast wave that is incident on the Darlington Generating Station power house are needed as initial conditions to start the RCM computations of the blast-wave flow which enters and travels through the power house. These basic properties that are required are the flow velocity, pressure, and density. All of the other flow properties such as the sound speed, temperature, energy, enthalpy, flow Mach number, dynamic pressure, and Reynolds number per unit length can be obtained from the first three flow properties.

The blast-wave flow properties that are generally required for most numerical analyses can be given in one of two equivalent forms. The variation of the flow properties can be specified as a function of time, at a fixed distance from the explosion, corresponding to that for the power plant. Alternatively, the variation of the flow properties can be given as a function of distance, at a fixed time after the origin of the explosion. In either case the subsequent propagation of the blast wave with time and distance can be predicted by some appropriate numerical method.

In the present work, the blast-wave flow properties are obtained at the power house, 495 m away from the railroad tracks where a hypothetical explosion of 61,500 kg of TNT occurs, by using the most recent numerical and experimental

data for TNT explosions [4-5]. Tabulated temporal and spatial distributions of the basic blast-wave flow properties at the power house are presented in tables 1 and 2, and this data was obtained by employing the analyses in Refs. 4 and 5. The spatial distributions of the flow properties of the blast wave, just before it interacts with the power house, is the form used for the initial conditions for most of the present work. Note that additional information on the method of obtaining the blast-wave flow properties at the power house, which are given in tables 1 and 2, are presented in the following sections of this chapter.

4.2 Flow Properties at the Blast-Wave Front

Much of the past work dealing with chemical and nuclear explosions was concerned mainly with the flow properties of the blast- or shock-wave front; that is, the peak values of the flow properties at the nearly discontinuous shock front. The decay of the amplitude, especially the peak overpressure, as a function of distance from the explosion is normally investigated numerically and experimentally. The variations of the flow properties behind this front, with time and also distance, were not ignored, but they were not documented for convenient usage. Over the past thirty years the properties of the blast-wave front have become better known, but the information is still normally scattered in many different laboratory reports.

The open literature on the flow properties of the blast-wave front was reviewed recently, and the knowledge of such flow properties has been extended [see 4]. A new form of the equation for the shock-front trajectory, in terms of distance versus time, has been proposed and also carefully checked against data from many TNT explosion trials. This shock-trajectory equation is very successful in giving all of the flow properties of the blast-wave front as a function of distance from the explosion center, including the initial decay or derivatives of the flow properties with time and distance. The means by which it can be used cannot be given here, but the details are explained in Ref. 4.

For the present example of a hypothetical explosion of 61,500 kg at a distance of 495 m from the power house, the analytical results given in Ref. 4 predict that the peak overpressure of the blast wave at the front of the power house is 11.45 kPa, and the arrival time after the detonation of the explosives is 1.108 s. Furthermore, at the blast-wave front, the peak value of the flow velocity is 26.2 m/s, and the peak temperature increase is 8.70 K.

Because all of the expressions in Ref. 4 are given in scaled form for a 1 kg TNT surface charge, Sachs's scaling factors $S_r = [(W/W_o)\ (p_0/p_1)]^{1/3}$ for distance and $S_t = (a_0/a_1)S_r$ for time need to be used to get the above stated results. In the preceding expressions, $W = 61{,}500$ kg of TNT for the present example, $W_o = 1$ kg of TNT is the reference charge mass, and $p_1 = 101.33$ kPa and $a_1 = 340.29$ m/s are the assumed ambient or atmospheric conditions, which are taken in this example to equal the reference conditions (i.e., $p_0 = 101.33$ kPa and $a_0 = 340.3$ m/s). Hence, $S_r = S_t = 39.47$. Note that these peak values of the blast-wave front properties occur at a distance of 495 m from the 61,500 kg charge or at a closer distance of 12.54 m ($495/S_r$) from a 1 kg TNT charge.

Although peak values of the blast-wave flow properties are important indicators of the damage of the blast to a building, they are for the most part insufficient for an extensive and accurate assessment. All of the blast-wave flow properties are generally required, especially if flows around and inside the building need to be considered, as mentioned previously.

4.3 Flow Properties of the Blast Wave

A few different methods are presently available for constructing blast-wave flow properties as a function of time and distance for a particular region of the flow field, without using large computer programs that are not only time consuming but also costly [e.g., see 5 and 34-40]. Of these available methods, the most recent and versatile one by Lau and Gottlieb [5] is chosen for determining the blast-wave flow properties at the power house.

This method involves, essentially, a tedious trial-and-error process of constructing the best possible path of a fluid particle or equivalent piston motion at the upstream side of the flow field of interest (containing the power house), such that the resulting flow field constructed numerically in front of the moving piston (where the power house is located) agrees as well as possible with all available although limited experimental data from many past explosion trials. An illustration of the spherical blast-wave flow field and the flow-field region being constructed numerically appears in Fig. 12, showing that the flow fields in front of a fluid particle and piston exhibiting the same motion are equivalent.

The solution procedure is now outlined briefly. The first step is to simply guess a piston path that is located between the explosion center and the power house, on the upstream side of the flow field. This initial guess of the piston path includes the initial distance-time coordinates, initial slope or piston velocity, and initial profile or shape, as illustrated in Fig. 13a. In the present study, the path guessed is initially specified with only fourteen discrete distance-time coordinates. These coordinate points are usually spaced closer together where the piston path is believed to have a higher curvature or velocity. Furthermore, the coordinate points are distributed fairly smoothly without jaggedness along the piston path (see Fig. 13a), based on a quick subjective assessment, unless the piston path is expected to have an abrupt kink or change in slope resulting from a sudden change in piston velocity. In the present work the piston path found in Ref. 5 is used as the starting point.

The second step is to spline a continuous curve through the coordinate points (Fig. 13a) to get an analytical function for the piston path, which will in turn easily yield the path velocity and acceleration by differentiation. In the present study, a cubic spline based on a piecewise continuous third-order polynomial is employed, and its logic and computer-program listing are given in Ref. 29.

Two boundary conditions are required at each end of the cubic spline. These are the coordinate position and slope of the curve at both ends. At the initial end of the splined curve (see Fig. 13a), both the coordinate point and the slope are chosen to agree with experimental or other data. The slope or piston velocity is normally set equal to the measured flow velocity. (For an experimentally or other known shock trajectory, the particle velocity would normally be obtained by using the Rankine-Hugoniot relations.) At the other end the coordinate point is initially guessed, and the slope or velocity is set equal to an initially undetermined constant, by specifying that the second time derivative or acceleration is zero.

The third step consists of computing as much of the flow field in front of the specified or guessed piston path as desired (Fig. 13b). This is done in the manner described in Ref. 5, by using the random-choice method (RCM) with an appropriate piston boundary condition also described in that reference.

The fourth step is to compare some of the computed flow-field properties to all available experimental or other useful information. The various types of disagreement and the magnitudes of the differences are noted at this stage. A qualitative or subjective assessment of the disagreement is utilized. This generally involved looking at many differences between the computed and all available information, which were displayed conveniently in graphical form. Such a form is easier to digest than a table of numbers.

The final step is to modify the initial piston path and repeat all of the steps after the first one (Fig. 13c). The piston path should be modified in such a manner that the disagreement between computed flow properties and all available comparison information is reduced, as compared to the previous case. This step is then repeated as many times as desired, until the best possible agreement is obtained. In this manner the available experimental or other information can be simulated numerically.

This flow field is reconstructed to agree as well as possible with different types of scaled experimental information from a number of different sized explosions of TNT. The types of experimental information that are used from different sized explosions are itemized as follows:

a) a shock trajectory in equational form from Ref. 4, which was obtained from an empirical curve fit to measured arrival times of the shock- or blast-wave front at various different radii from the center of a 20-ton TNT surface explosion [41] and two 500-ton TNT surface explosions named SNOWBALL and SAILOR HAT [37],

b) thirty-five particle paths or trajectories measured by means of high-speed photography of smoke trails or tracers at various different radii from the center of a 500-ton surface explosion named SNOWBALL [37],

c) twenty particle paths or trajectories measured by means of high-speed photography of smoke trails or tracers at various different radii from the center of a 500-ton surface explosion named SAILOR HAT [37],

d) twenty time histories of overpressure measured with piezoelectric pressure transducers at various different radii from the center of a 20-ton TNT surface explosion that were made by American researchers [41],

e) twenty-one time histories of overpressure measured with piezoelectric pressure gages at various different radii from the center of a 20-ton TNT surface explosion that were made by British researchers [41],

f) eigthteen time histories of overpressure measured with piezoelectric pressure gages at various different radii from the center of a 20-ton TNT surface explosion that were made by Canadian researchers [41],

g) six time histories of density measured with specially designed beta-ray density gages at various different radii from the center of a 100-ton TNT surface explosion [35].

Additional information on the method of reconstruction of the blast-wave flow properties to agree with experimental measurements, as well as the various types of experimental measurements and how they were obtained in field trials, can be found in Refs. 4 and 5, respectively. Note that Ref. 5 contains many references to laboratory reports that contain experimental data.

The previously described method was used to generate the temporal and spatial distributions that are presented in tabular form in tables 1 and 2, for the blast wave that is incident on the power house. These two sets of data can now be employed as the starting point or initial conditions for the numerical computations for the blast-wave flow inside the power house and also over or around the power house.

4.4 Specification of the Initial Conditions for the Numerical Computations

For the numerical computations of the blast-wave flow field inside and outside of the power house, the initial conditions can be specified in two different but equivalent ways. The initial conditions can be given in the form of spatial distributions at a fixed time or, alternately, in the form of temporal distributions at a fixed distance. This is aptly illustrated in Fig. 14, for the case of a wave moving from right to left and eventually interacting with an area change. With each method, however, certain precautions have to be taken to ensure that the specification of the initial conditions is done correctly for the numerical computations.

Specification of the initial conditions (e.g., pressure, flow velocity, temperature and density) in the form of spatial distributions at a some fixed initial time (e.g., $t = 0$) is the simplest and most straigthforward approach. This approach is the one that is always utilized in the present investigation. These initial conditions are simply inserted in the numerical computations at the appropriate spatial node locations (in computer array storage) at the first or initial time level, just prior to beginning the computations. In order to do this properly, an appropriate length of duct where these spatial conditions are specified must be included as part of the flow-field width. This additional length must be sufficiently long such that it includes the entire spatial range over which the initial conditions are required (or are important to the problem in question). For the present problem of the blast-wave flow inside the power house, a duct with a length of about 80 m was appropriate to contain the blast wave incident on the power house, because the length of the blast wave is approximately 75 m (see table 2). The additional length of duct is depicted by the dashed lines in Figs. 6, 7, 9, and 11, at the right side of the sketches of the power-house geometry.

It is worth mentioning here that the boundary condition specified at the right side of the flow field should be that the additional channel continues indefinitely to the right. This type of boundary condition is not difficult to program into the computer code. Such a boundary condition permits reflected waves or any waves arriving from the left part of the flow field to leave this right part without reflecting at this right boundary.

Specification of the initial conditions (e.g., pressure, flow velocity, temperature and density) in the form of temporal distributions at a some fixed distance in the flow field (e.g., ahead of the power house) is more complex and less straightforward than that for the spatial distributions at a fixed time. This approach is not used in the present investigation, but is discussed here only for interest. In this case, the initial or actually boundary conditions have to now be inserted in the numerical computations at only one spatial grid point, but this has to be done at each individual time level of the numerical computations, or at least until the entire temporal distributions that are required (or are of interest) for the problem in question have been completely entered.

The location at which the temporal distributions are inserted in the flow field for the numerical computations must be the right-most boundary of this flow field being computed, as illustrated in Fig. 14. Furthermore, this location must be sufficiently far to the right or upstream of any area change or power house that reflected waves or any other waves from this area change or power house do not arrive at the right-most boundary during the time that the initial or boundary conditions are being specified. If a reflected wave does arrive during the time of the specification of these conditions, its effect or modification to the specification is generally unknown and, therefore, cannot be taken into account. If the effect of the reflected wave is simply ignored, then the computed flow field will be in error, and the degree of error will no doubt depend on the particular circumstances of the nonstationary flow and the initial and boundary conditions.

In order to avoid the problem of reflected waves arriving at the right-most boundary during the time the flow properties are being specified at this boundary, the flow field length must be increased appropriately such that this right-most boundary is sufficiently far to the right. The additional length has to be estimated in advance of doing the numerical computations, based on the generation and arrival of reflected disturbances. However, the additional length will be nearly the same as that required if the initial conditions were specified as spatial distributions. Hence, for the present problem involving a blast-wave flow inside of the power house, this additional length would again be about 80 m.

Once the flow conditions have been fully specified over the required time period, the boundary conditions at the right-most edge of the flow field should then be changed. The new boundary condition that should be inserted is that which makes the additional length of duct appear to be infinitely long to the right. Consequently, any reflected waves that arrive at the right-most boundary will then continue on out of the flow field that is being computed, as required.

5. ANALYSIS OF THE BREAKING AND OPENING TIME OF THE BLOW-OUT PANELS

5.1 Introduction

The amplitude and shape of the blast wave moving inside the Darlington Generating Station power house, as well as its destructive effects, depends rather strongly on the manner in which the blow-out panels in the front wall of the power house break and open with time, from the incident blast wave striking and reflecting from this wall. It is by means of these openings, which are increasing in area with time, that part of the incident blast wave makes its way into the power house. For this reason, a good estimate of the opening area of the blow-out panels, as a function of time, is required for obtaining realistic numerical computations of the blast-wave flow inside of the power house. This means that a fairly realistic model and analysis of the breaking and opening process of the blow-out panels from the incident blast-wave loading has to be devised.

In the model of the breaking and opening of the blow-out panels it is envisaged that the panel breaking and opening process occurs in four separate but linked phases, because of the shape, construction, and materials properties of the panels (see Figs. 15 to 18). The first phase is assumed to consist of a wall collapsing mode, because each blow-out panel is constructed in the form of

a two-sheet, hollow wall, with some light insulation in one part of the gap between the two steel sheets, and the two sheets are held apart only flimsily. In this mode the outer corrugated steel sheet is assumed to be accelerated and then eventually jammed against the inner steel sheet, from the initial part of the impact of the incident blast wave. The insulation between the outer and inner steel sheets is assumed to have no rigidity or no resistance to compression, and that it also compacts to a negligible thickness. This phase will eventually end just as the outer corrugated sheet compresses the insulation fully and finally strikes the inner steel sheet.

The second phase is assumed to consist of a sharing of momentum among the initially moving corrugated sheet, the initially stationary inner steel sheet, and the initially stationary insulation between these two sheets. This sharing is assumed to take place in a negligibly short time, and in two separate stages, just as the outer corrugated sheet strikes the stationary, inner, steel sheet. In the first stage, the translational momentum of the outer corrugated sheet, from its collapsing motion, is assumed to be shared instantly by both steel sheets and this insulation. During this stage the velocities of the various parts are uniform and unidirectional everywhere on the blow-out panel. The collapsed blow-out panel is assumed to undergo translation only. In the second stage, this translational momentum from the motion must be redistributed instantly in the collapsed blow-out panel such that its various parts can now respond as a cantilever beam, bending in unison as a sandwich about the I-beam, along its centerline. The I-beams are taken to be perfectly rigid, restraining supports. This redistribution of momentum will lead to a variation in the velocity of the beam from its centerline support to its edges. This second phase will end just when beam bending begins.

The third phase is assumed to consist of each collapsed blow-out panel or wall bending elastically as a cantilever beam, with an initial distributed velocity along the beam, from the loading of the blast wave that acts on the outside surface. In this phase, the outer edges of each collapsed panel are assumed to have slipped off their outer I-beam supports and the two identical halves of the panel then bend elastically and symmetrically about the remaining I-beam support along the centerline. Each half thus bends identically like a cantilever beam. Eventually, if the blast-wave loading is sufficiently strong, the bending of the cantilever beam will become large and cease being elastic, and this phase will thus end.

The fourth and final phase consists of each collapsed blow-out panel rotating as a rigid beam with a plastic hinge about its I-beam support, along the centerline. The resisting torque of the plastic hinge is estimated for the case of plastic bending beavior of the combined outer corrugated steel sheet and inner flat sheet about the I-beam. This final phase will end eventually, when the two halves of the blow-out panels finally rotate to their fully open positions.

As the blow-out panels open and the blast wave enters the power house, the pressure on the front of the opening blow-out panels will drop with time. One reason for this is that the reflected blast-wave pressure on the front wall of the power house is decaying with time, and this effect is taken into account in the analysis of the motion of the blow-out panels. Another reason is that the pressure of the flow moving over the blow-out panels is slightly less than the reflected pressure on the front of the building. However, this effect is very small for the present work and can be neglected. Finally, the loading on the outside surface of the blow-out panels from the flow into the power house

will eventually be partially countered by the pressure increase on the rear of these panels, which results from the eventual pressurization of the interior of the power house. This resulting reduction in the differential loading across the blow-out panels, which would result in a longer opening time, is also taken into account in an approximate manner in the analysis, so that a more realistic approximation of the opening time of the blow-out panels can be obtained.

From the analysis of the breaking and opening of the blow-out panels, it was discovered that the panels took a time of 10 ms just to begin to open after the incident blast wave arrived, after which the opening area to the blast-wave flow that enters the power house was approximately linear with time. The additional time for the panels to open completely was found to be 75 ms. This is why the blow-out panels were said to open linearly earlier in this report, which is now shown to be a good approximation. Additional details concerning the analysis of the blow-out panels and numerical results are now given in the following sections of this chapter.

5.2 Characteristics of the Blow-Out Panels

A sketch of one blow-out panel appears in Fig. 15, showing the basic shape, dimensions, and rear I-beam supports. The side view given in Fig. 16 provides some additional information. The sketch of the blow-out panel cross section shown in Fig. 17 depicts various parts of these panels and their dimensions. Furthermore, tables of relevant data are presented for the masses and materials properties of the outer corrugated steel sheet, fiberglass insulation and inner flat steel sheet. The upper set of tabulated data is presented for one-half of a blow-out panel having one-half of the height or 3.75 m and the entire length of 37.5 m. One-half of the panel therefore spans two adjacent, horizontal I-beams, from the one along the centerline to another at the upper or lower edge. This data was obtained from Ontario Hydro drawings of the blow-out panels. Finally, the lower set of data can be found in most handbooks containing the materials properties of metals.

5.3 Collapse Phase of the Blow-Out Panels

The interaction of the blast wave incident on the power house with the front wall of this building produces a reflected wave. The resulting reflected overpressure on the front face is slightly more than double that of the incident wave, because the incident wave is relatively weak [6]. The overpressure signature of the incident blast wave and the resulting pressure loading on the front face of the power house are depicted in Fig. 18a, as if the front wall is of infinite extent. The reduction in overpressure that occurs when the rarefaction or relief waves arrive from the sides and top of the power house is not indicated here. However, in the center of the front wall the first relief wave from the sides would not arrive until about 45 ms after the incident blast wave strikes the power house. Hence, for the collapse phase, which will be found to be relatively short (approximately 7 ms), these relief waves do not need to be considered.

The pressure on the blow-out panels can be assumed, for all practical purposes, to be linearly decreasing with time from the maximum overpressure, for this part of the analysis. By considering the initial, temporal variation of the overpressure signature given in table 1, and doubling these values to get the reflected overpressure, the expression for the reflected overpressure

loading $\Delta p = \Delta p(t)$ on the blow-out panels during the collapse phase can be obtained simply as $\Delta p(t) = \Delta p_0(1 - t/T_0)$, where the peak or maximum reflected overpressure at time $t = 0$ is $\Delta p_0 = 22.0$ kPa and the initial time decay constant for the overpressure is $T_0 = 151.0$ ms.

The initial blast-wave loading on the blow-out panel is assumed first to accelerate the outer corrugated steel sheet toward the stationary fiberglass insulation and inner steel sheet, until it eventually compresses the insulation to a negligible thickness and finally comes into contact with the inner steel sheet. A diagram of the final collapsed blow-out panel is shown in Fig. 18b. The collapsing motion of the corrugated sheet can be obtained by using Newton's second law of motion in the form of $F = M_c a = M_c dv/dt = M_c d^2x/dt^2$, where the time-dependent force $F = F(t) = \Delta p(t)A$ from the time-dependent pressure loading $\Delta p(t)$ on the corrugated sheet having a total mass M_c (1880 kg) and a total surface area A (281.2 m), which produces an acceleration a(t), a velocity v(t) and a displacement x(t), which are all functions of time t. Hence, the resulting expressions for the corrugated panel displacement, velocity, and acceleration are given as $x(t) = (\Delta p_0 A/M_c)[1 - t/3T_0]t^2/2$, $v(t) = (\Delta p_0 A/M_c)[1 - t/2T_0]t$, and $a(t) = (\Delta p_0 A/M_c)[1 - t/T_0]$, respectively. They apply only during the collapse phase. For the total displacement of 7.62 cm at the end of the collapse, the time t can be found iteratively from the previous equation given for x(t) to be 6.85 ms. Then, the impact velocity and acceleration at the end of the collapse phase follow directly from the other two expressions as 22.0 m/s and 3142 m/s^2, respectively. Hence, the first phase consisting of the collapsing of the blow-out panels takes 7 ms, roughly, and the blow-out panels do not allow any blast-wave flow into the power house during this time. Note that this collapse phase takes a relatively short time, and the linear drop in the overpressure loading during this short time is only about 4.5%, which is relatively small.

5.4 Momentum Sharing Phase

This phase occurs just at the time when the outer corrugated sheet has fully compressed the fiberglass insulation and has finally made initial contact with the inner flat sheet (Fig. 18b). The momentum sharing is assumed to occur almost instantaneously, before the inner sheet begins to move appreciably and before the rear I-beam supports begin to restrain the motion of the inner sheet or the blow-out panels. The momentum sharing from the inelastic collision is assumed to take place in two separate but linked stages. In the first stage the translational momentum of the outer corrugated sheet is shared with the insulation and inner sheet, and the resulting combined motion at this moment is still considered to be in translation. The application of the conservation of translational momentum for this case results in a new translational velocity, the same translational momentum, and a new translational energy of the combined corrugated sheet, insulation, and inner sheet. The new translational velocity obtained from the calculation of (22.0 m/s)(1880 kg)/(3280 kg) for the combined motion is then V = 12.6 m/s.

The second stage consists of redistributing this translational momentum in a bending cantilever beam that is taken to represent the collapsed blow-out panel, such that it reappears as an initial bending momentum. The total translational momentum is simply the total mass M_t of the blow-out panel times the velocity V; that is, $M_t V$. The total bending momentum in a cantilever beam with a uniform mass distribution per unit length M_t/L is simply the integral, over the entire beam length L, of this mass loading times the local beam velocity w'; that is, $\int_0^L (M_t/L)w'dx$. For this expression, $w = w(x,t)$ denotes the local

beam displacement at time t and w' = w'(x,t) is the local beam velocity [42].

For simple bending motions of a cantilever beam, the bending mode shape can be assumed in such a way that the displacement w = w(x,t) is given by the product of a time dependent coefficient c(t) and a specified distance dependent mode shape function f(x). Hence, w(x,t) = c(t)f(x). The local beam velocity w'(x,t) is then given by c'(t)f(x), and the local beam acceleration w''(x,t) is c''(t)f(x). For a simple cantilever beam the mode shape f(x) can be taken, for all practical purposes, to be equal to $1 - (4/3)(x/L) + (1/3)(x/L)^4$ [42], which is equal to 0, 17/48, and 1 at the root (x = L), midpoint (x = L/2), and free end (x = 0), respectively.

By employing these past developments, and by equating the translational momentum to the beam bending momentum, the initial value of c'(t=0) or simply c'(0) can be found, which is the value at the end of the momentum sharing phase or at the start of the beam bending phase. The corresponding initial velocity of the beam in the beam bending phase follows as w'(x,0) = c'(0)f(x). Now, the initial value of c'(0) for the present problem can be shown to be equal to 5V/2 or 31.5 m/s, which is needed in the next section. The initial displacement of the beam c(t=0) or c(0) that is also needed in the next section is, of course, given by c(0) = 0, because the beam is assumed to be flat initially, before the beam bending starts.

It is of interest to determine the initial velocity of the bending beam or blow-out panel at the midpoint of the half span (x = L/2) and also at the free end (x = 0). From c'(0)f(x), the initial velocity w'(x,0) at the midpoint (x = L/2) is 11.2 m/s and that at the free end (x = 0) is 31.5 m/s. The initial velocity of the beam at the centerline support is obviously zero. It is interesting to observe that the initial velocity at the midpoint of the beam is about the same as the initial translational velocity of the collapsed blow-out panel, whereas the free-end velocity is more than twice as large, as might be expected from the process of redistributing the same amount of momentum from a translating beam to a bending cantilever beam.

5.5 Elastic Beam Bending Phase

Before investigating the dynamic response in the elastic bending regime for a cantilever beam that is taken to represent a collapsed blow-out panel, it is necessary to first determine the limiting conditions for which elastic beam bending occurs. These conditions (maximum beam deflection and stress) signify the end of the elastic beam bending phase and also the start of the inelastic beam bending phase. These limiting conditions can be obtained from static beam bending theory [42] and a good understanding or experimental knowledge of the minimum pressure difference across the blow-out panel that just causes failure.

From experimental evidence provided by Ontario Hydro, it is known that the blow-out panels fail under a differential pressure loading Δp_f of 2.4 kPa. For this loading the maximum deflection and stress in the cantilever beam that is taken to represent the blow-out panels will now be calculated. The general expression for the maximum free-end deflection of a uniformly loaded cantilever beam is $qL^4/(8EI)$, where $q = \Delta p_f A/L$ is the uniform loading per unit length over the total area A and length L, E is Young's modulus of elasticity, and I is the moment of inertia of the collapsed blow-out panel. The latter two properties have been tabulated for quick reference in Fig. 17. The free-end deflection resulting from the loading that causes failure can be calculated to be 16.4 cm,

which seems to be a very reasonable deflection considering the the magnitude of the loading and the geometry of the blow-out panel.

The maximum stress will occur at the centerline of the blow-out panel, where it is being supported by a central I-beam, or at the root of the assumed cantilever beam. This maximum stress is given by the general expression Mc/I, where M is the moment, c is the distance from the neutral axis to the outside edge of the beam (4.67 cm), and I is again the moment of inertia. The resulting maximum stress is found to be 458 MPa, which is almost exactly equal to the tensile strength of mild steel (460 MPa). Hence, the maximum failure stress for the blow-out panel is of the right magnitude for the material properties under consideration, which is very satisfying. However, this a bit fortuitous that it worked out so closely, considering that a relatively simple cantilever beam has been used to represent a fairly complex blow-out panel.

The elastic beam bending phase occurs, therefore, for beam deflections at the free end ranging from 0 to 16.4 cm, with the corresponding stress at the beam centerline ranging from 0 to 458 MPa. Whenever the beam tip deflects more than 16.4 cm, or has a corresponding stress at the centerline that is greater than 458 MPa, it will then be assumed that this additional beam deflection is inelastic. The dynamic response of the elastic bending beam is now considered, whereas the additional dynamic response of the inelastic bending beam is considered in the following section.

The general partial differential equation governing the dynamic motion of a beam that has mass and applied forces is

$$m\,w'' \;+\; (EI)\,\partial^2 w/\partial x^2 \;=\; f(t) \qquad (5.1)$$

where $m = M_t/L$ is the beam mass per unit length, $w = w(x,t)$ is the local beam displacement, E is Young's modulus of elasticity, I is the beam's moment of inertia, f(t) is the input force on the beam per unit length, x is the distance along the beam, and t is time. The beam velocity is again denoted by $w'(x,t)$ and the corresponding beam acceleration is $w''(x,t)$. Now let the solution to this differential equation again have the form $w(x,t) = c(t)[1 - (4/3)(x/L) + (1/3)(x/L)^4]$, where c(t) is the time dependent coefficient, the latter part in square brackets is the assumed distance dependent mode shape, and L is the total length of the beam.

The solution for w(x,t) is now sought by making a simple substitution of the assumed solution into the differential equation. This step is expected to give an ordinary differential equation for c(t), which is a function of time t only. However, it can be easily shown that the resulting equation will also contain some terms having a dependence on distance x. In order to circumvent this problem, created by employing an assumed mode shape for beam bending, an approximate solution for c(t) is sought, which is independent of the distance. This is achieved by employing an averaging or weighting process. The equation obtained from the substitution, with the unwanted distance dependence, is first multiplied by a weighting function, which is taken here to be the bending mode shape, and then integrated over the entire length of the beam, thereby removing the dependence on distance. This procedure yields the desired ordinary differential equation for c(t), having dependence on time only. The final result is

$$c''(t) \;+\; (162/13)(EI/mL^4)\,c(t) \;=\; (81/52)(1/m)\,f(t) \qquad (5.2)$$

which can be solved for c(t) once the initial conditions c(0) and c'(0) are

specified and the forcing function f(t) is known. From the previous work on both the collapse phase and momentum sharing phase, we already know that the initial conditions for time-dependent function c(t) are simply c(0) = 0 and c'(0) = 31.5 m/s.

Although the collapse phase and momentum sharing phase were quite short (6.85 ms), the reflected pressure loading on the blow-out panels did decrease slightly during this time (by 4.5%). This drop in the loading is taken into account, even though it is fairly small. The pressure loading for the elastic beam bending phase can now be specified as $\Delta p = \Delta p_1[1 - (t - t_0)/T_1]$, where the peak reflected pressure Δp_1 = 21.0 kPa at the time $t = t_0$ = 6.85 ms, when the elastic beam bending phase begins, and the re-adjusted duration T_1 = 144.2 ms. The loading f(t) per unit length of beam can now be expressed in the following manner as $f(t) = (\Delta p_1 A/L)[1 - (t - t_0)/T_1] = f_1[1 - (t - t_0)/T_1]$, where A is the area of one-half of the panel (140.6 m^2), L is one-half of the panel length (3.75 m), and $f_1 = \Delta p_1 A/L$.

The final solution to Eq. 5.2, after the forcing function is inserted and the initial conditions are applied, is

$$c(t) = [\Delta p_1 AL^3/8EI]\,[1 - (t - t_0)/T_1 - \cos(\omega\{t - t_0\}/T_1) + (1/\omega T_1)\sin(\omega\{t - t_0\}/T_1)] + [c'(0)/\omega]\cos(\omega\{t - t_0\}/T_1) \qquad (5.3)$$

where the natural frequency of the beam in the bending mode is

$$\omega = [(162/13)\,(EI/M_t L^3)]^{1/2} \qquad (5.4)$$

For the present study with E = 210 GPa, $I = 6.45 \times 10^{-5}$ m^4, $f_1 = \Delta p_1 A/L$, Δp_1 = 21 kPa, A = 140.6 m^2, L = 3.75 m, M_t = 1640 kg, t_0 = 6.85 ms, T_1 = 144.15 ms and c'(0) = 31.5 m/s, one can obtain $\Delta p_1 AL^3/(8EI)$ = 1.438 m and ω = 44.18 rad/s or 7.0 Hz. This natural frequency for the blow-out panel seems quite reasonable, considering its geometry, construction, and materials properties.

Results from Eqs. 5.3 and 5.4 will now be presented and discussed. From the deflection equation, $w(x,t) = c(t)[1 - (4/3)(x/L) + (1/3)(x/L)^4]$, the free-end deflection and velocity at x = 0 are simply equal to c(t) and c'(t). These results are shown graphically in Fig. 19, as a function of time $t - t_0$, from the time when elastic beam bending just begins to when it just ends. The free-end deflection increases almost linearly with time until it reaches 16.4 cm and the elastic beam bending phase ends. The free-end velocity also increases almost linearly from its initial value of 31.5 m/s to the value of 43.0 m/s when elastic bending ceases. However, the beam is slowing down slightly from the retarding elastic forces of the beam. Note that the deflection and velocity at the midpoint of the beam (where x = L/2) are 17/48 of the values just quoted, or 5.80 cm and 15.2 m/s.

From the solution, the time duration from the beginning to the end of the elastic beam bending phase is 4.39 ms, which is rather short. The reasons for this can be attributed to the following: the beam has a relatively high initial velocity, the maximum bending stress occurs after only a small displacement, and the pressure loading that produces the motion is relatively high.

5.6 Plastic Beam Bending Phase

In this phase the blow-out panel is taken to be a rigid, rotating beam with a plastic hinge at the centerline support. The retarding torque or moment from this plastic hinge, which opposes the moment from the pressure loading, is taken into account, as is the time dependence of the blast-wave reflected pressure loading on the blow-out panel. In order to obtain an approximate solution for the dynamic motion of the blow-out panel in the plastic beam bending phase, a number of steps are required to establish the initial conditions for the beam motion, plastic retarding moment, and applied pressure loading. These will not be set out before the final solution and results are presented.

When the analysis is switched from that for the elastic bending beam to that for the rigid, rotating beam, the momentum of the two beams must be equal at this time. This conservation of momentum leads to the new initial condition for the angular velocity of the rigid, rotating beam with the retarding plastic hinge. The momentum in the blow-out panel or bending beam in the elastic bending phase is $\int_0^L (M_t/L)w'dx = (M_t/L)c'(t)\int_0^L [1 - (4/3)(x/L) + (1/3)(x/L)^4]dx = (M_t/L)c'(t)[2L/5] = 2M_t c'(t)/5$. The momentum in the rigid and rotating beam is simply $\int_0^L (M_t/L)w'dx = (M_t L)c_p'(t)\int_0^L [1 - x/L]dx = (M_t/L)c_p'(t)[L/2] = M_t c_p'(t)/2$, where $w_p = w(x,t)$ is the displacement of the rigid, rotating beam, $c_p(t)$ is the corresponding time dependent coefficient, and $[1 - x/L]$ is the mode shape for rigid rotation. The conservation of momentum then leads to $c_p'(t) = (4/5)c'(t)$, or the free-end velocity of the rigid rotating beam is four-fifths that of the elastic bending beam with the same momentum. At the very end of the elastic beam bending phase for the present problem, the free-end velocity was found to be 43.0 m/s. Consequently, the initial velocity of the free end of the rigid, rotating beam is now taken as 34.4 m/s for the plastic beam bending analysis. Note that the velocity at its midpoint will now be one-half of the free-end velocity, or 17.2 m/s.

From the free-end velocity of 34.4 m/s and the blow-out panel length of 3.75 m, the angular velocity of the rigid, rotating beam can be calculated to be 9.17 rad/s. Because the beam displacement at the end of the elastic beam bending phase is 16.4 cm, its initial rotational displacement is approximately 0.044 rad. These are the initial conditions needed later for the analysis of the dynamic motion of the rotating beam with a plastic hinge.

In order to get the retarding moment M_p of the plastic hinge, one must perform the integration for $Mp = \int_0^A \sigma_y\, y\, dA$, where A is the cross-sectional area of the blow-out panel, σ_y is the material yield stress, and y denotes the distance from the centroid of the cross-sectional area. For a sequence of hollow triangular sections, the plastic moment $M_p = (8/81)N\sigma_y[b_o h_o - b_i h_i]\Omega$, where N = 268 is the number of triangles along the 37.5-m width of the blow-out panel, σ_y = 300 MPa denotes the yield stress of the mild steel sheets of the blow-out panels, b_o = 14.0 cm and b_i = 13.88 cm are the outer and inner bases of the hollow triangular sections, h_o = 7.00 cm and h_i = 6.88 cm are the outer and inner heights of the hollow triangular sections, and Ω = 1/3 has been inserted as a reduction factor on the plastic moment, in order to account for the straightening out of the triangles that would occur under severe bending conditions. The resulting plastic moment M_p = 77 kNm. Note that an accurate calculation of the plastic moment is not important, because this moment can be shown to play an insignificant role in the blow-out panel opening time. It is only a small percentage (less than 5%) of the moment produced by the blast-wave pressure loading. For example, a pressure loading of 20 kPa will produce a moment of about 5 MNm.

Although the total time for the collapse, momentum sharing, and elastic beam bending phases to be completed is relatively short (about 11.24 ms), the reflected blast-wave overpressure loading has dropped a small but noticeable amount from the original value of 22 kPa. The reflected overpressure at the beginning of the plastic beam bending phase is now $\Delta p_2 = 20.4$ kPa. Also, the new duration of the remaining part of the reflected blast-wave overpressure is $T_2 = 139.8$ ms. Hence, the reflected blast-wave overpressure on the front wall of the power house can be given as $\Delta p = \Delta p_2[1 - (t - t_1)/T_2]$, where the time $t_1 = 11.24$ ms is the time when the plastic beam bending phase begins. Although this expression gives the reflected overpressure on the front wall of the power house, it is not necessarily the overpressure loading that produces the motion of the blow-out panels in the plastic beam bending phase. As soon as the blow-out panels move and open a flow area for the blast wave to move into the building, the loading will change. The change in overpressure loading is the result of the blow-out panel motion that produces some additional space for the flow to expand into, the flow pressure over the blow-out panels being somewhat less than the reflected pressure, and resulting counter loading on the backside of the blow-out panels due to the pressurization of the building interior or backside space by the blast-wave flow that enters the building.

All of these effects just mentioned are not understood quantitatively in sufficient detail to model each one individually in any rigorous manner and thereby include these effects in the present analysis. Consequently, the best approach that is available at the present time is to use a simple model with a free parameter to take into account all of the effects in an approximate yet practical manner. With this in mind, the net differential overpressure loading on the blow-out panels is taken to have the form $\Delta p_n = \Delta p_2[1 - \{(t-t_1)/T_2\}^n]$, in which n is the free parameter just mentioned. If n equals unity, the full effects of the reflected overpressure loading are then imposed on the blow-out panels, and all of the reductions in the overpressure loading from the panel motion is therefore neglected. This is the worst panel loading case. If n is less than unity, the effects of a reduction in overpressure loading is taken into account approximately. The reduction in the panel overpressure loading increases as n decreases, allowing the effects of increasing degrees of reduction to be investigated. (Note that if n equals zero, there is no overpressure loading on the blow-out panels.)

An appropriate value of n is required for the present analysis. If the blow-out panel opening time is very short as compared to the fill time of the building interior behind the blow-out panels or the buildup of a significant counterpressure on the backside of the panels, then n will have a value quite close to unity. On the other hand, if the panel opening time is very long in comparison to the time to pressurize the backside of the panels, the value of n will be near zero to reflect this effect. For the present case of the blast-wave flow into the Darlington Generating Station power house, it is expected that the value of n will be in the range from 1/4 to 1/10. However, a final value need not be chosen at this time. It can and will be selected later in the analysis, after its effect on the dynamic motion of the blow-out panels is investigated, when additional information is available on which a more reasonable choice can be based.

The motion of the rigid, rotating beam representing the blow-out panel in the plastic bending phase, having an applied overpressure loading from the blast wave and a resisting torque from the plastic hinge, can be considered as an equivalent lumped mass system with applied and retarding moments. In this case, the total beam mass M_t can be located at the center of the rotating beam,

or at a radius r_c of one-half the beam length (1.875 m). The ordinary differential equation that governs the angular motion of this lumped mass system or beam is simply $M_t r_c \theta''(t) = M_L(t) - M_p$, in which θ'', θ', and θ are the angular acceleration, velocity, and displacement of the lumped mass (beam), respectively. Also, M_p is the plastic retarding torque or moment, and $M_L = \Delta p_n A r_c$ is the moment resulting from the net differential overpressure loading $\Delta p_n = \Delta p_n(t)$ on the blow-out panel having a total area A. After the previous equation for the loading, that is, $\Delta p_n = \Delta p_2[1 - \{(t-t_1)/T_2\}^n]$, is substituted into the governing differential equation, the integration can be performed fairly readily to give the closed-form solution

$$\theta = \theta_i + \theta_i' [t - t_1] - \frac{M_p}{2 r_c M_t} [t - t_1]^2 + \frac{\Delta p_2 A T_2^2}{2 M_t} \left[1 - \frac{2}{(n+1)(n+2)} \left[\frac{t - t_1}{T_2} \right]^n \right] \left[\frac{t - t_1}{T_2} \right]^2 . \quad (5.5)$$

In this solution, the initial angular displacement $\theta_i = 0.044$ radians, initial angular velocity $\theta_i' = 9.17$ radians/s, time t_1 for the plastic beam bending to begin is 11.24 ms, plastic hinge retarding moment Mp equals 77 kNm, half panel length $r_c = 1.875$ m, overpressure amplitude $\Delta p_2 = 20.4$ kPa, half panel area A is 140.6 m^2, overpressure duration T_2 equals 139.8 ms, total half panel mass M is 1610 kg, and free parameter n is to be chosen later.

Results from Eq. 5.5 are now presented graphically in Fig. 20, in terms of the angular position of the blow-out panel or rotating beam and its free-end velocity as a function of the time $t - t_1$ from when the plastic beam bending begins. These results are also given in terms of the free parameter n, having values of 1, 1/2, 1/4, 1/8, 1/16 and 1/32, to illustrate the effect on the solution for the blow-out panel motion. This effect is quite significant, as can be observed. For example, if n equals 1 for the worst loading case when the full reflected overpressure loading acts on the blow-out panel with no type of loading reduction, the panel rotates to its fully open position of 90 degrees in a short time $t - t_1 = 38$ ms, and free-end velocity would then be fairly high at about 240 m/s. If n = 1/8 for the more realistic case when a substantial reduction in reflected overpressure loading occurs, then the blow-out panels would become fully open after a longer time of 68 ms and the free-end velocity would be a lot lower at 110 m/s.

Based on the graphical results presented for the free-end velocity of the blow-out panel, it is felt that a reasonable value for the free parameter n is about 1/16. One of the main reasons for this choice is that the free-end velocity of the blow-out panel is in this case less than 75 m/s. Higher free-end velocities are not expected in practice, which suggests that the value of n for the present model must be 1/16 or even less. Free-end velocities higher than 75 m/s are not expected to occur in practice because the flow velocity associated with the blast wave incident on the power house and that inside of the power house do not have velocities that are even this high. Therefore, they could not follow the free-end motion of the panel, let alone drive this motion. It is worthy to note that typical flow velocities associated with the blast wave are less than 50 m/s. For the case of n = 1/16, the time $t - t_1$ for the blow-out panels to open fully to 90 degrees is about 91 ms, or the time t is about 112 ms after the incident blast-wave first strikes the front wall of the power house, and the free-end velocity at the end of the opening stage is approximately 75 m/s. These values were obtained from results given in Fig. 20.

5.7 Flow Area Due to the Breaking Blow-Out Panels

After a detailed consideration of the approximate solution for the motion of the blow-out panels from the blast-wave loading, the flow area through which the blast wave enters the Darlington Generating Station power house can now be determined from this solution. The blast-wave flow area is not simply the area from the free end of the blow-out panel to the remaining wall support that the free end originally rested on. Rather, it is the area obtained by means of the minimum distance between this remaining wall support and the blow-out panel, and this is illustrated in Fig. 21. This distance is perpendicular to the blow-out panel, as shown in the figure. Furthermore, this area opening to the flow only begins to open after the free end of the blow-out panel moves completely free of the remaining wall support, which is taken to have a width x of 10 cm, as indicated. The angular rotation of the beam at the point when the free end of the blow-out panel just clears this wall support is therefore 0.027 radians, as given in the figure.

Based on this angle of rotation of the blow-out panel (0.027 radians), the time t at which the flow area starts to open is 10.0 ms after the incident blast-wave strikes the front wall of the power house. This time occurs during the elastic beam bending phase, which ends when the free-end displacement is 16.4 cm (or at a time t of 11.24 ms). However, the blast-wave flow area opens only slightly during the elastic beam bending phase, because this phase is soon over (at 11.24 ms).

The area opening for the blast-wave flow is directly proportional to the length δ shown in Fig. 21. Also, the total area opening to the flow will be directly proportional to the half panel length L = 3.75 m. Hence, the ratio of the flow opening to the total flow opening, or the normalized area opening, is simply equal to the length ratio δ/L. This ratio is given from the geometry in Fig. 21 as $\sin(\theta - \Delta\theta)$, where $\Delta\theta$ is 0.027 radians and θ is obtained from the previous solution for the motion of the breaking blow-out panel from the blast-wave loading.

The final results for the flow area of the blow-out panels through which the blast wave enters the power house are given in Fig. 22. The percentage of the total open flow area is shown as a function of of the free parameter n and the time t after the incident blast wave strikes the front wall of the power house. Immediately obvious are the following: the opening of the blow-out panels produce a blast-wave flow area only after 10 ms, the subsequent flow area opening occurs almost entirely in the plastic beam bending phase, the increase in the flow area opening is slower for smaller values of n for which the reduction in loading is greater, and for all values of n the main part of the flow area opens almost linearly with time.

For the specific case when the free parameter n equals 1/16, which was chosen previously to dictate the net differential overpressure loading on the blow-out panels, one could approximate accurately the blast-wave flow area opening as a simply linear change with time. If this is done, in fact, then the flow area would open linearly with time over a period of approximately 75 ms.

In order to simplify the numerical analysis of the nonstationary blast-wave flow inside the power house, it was found convenient not to include the entire blow-out panel analysis in the present form in the nonstationary computations. Instead, the results of the blow-out panel analysis are included in the computations in a much simplified form, as a linear area opening with time.

6. BLAST-WAVE OVERPRESSURE ON THE OUTSIDE OF THE POWER HOUSE

6.1 Introduction

Obtaining a solution for the overpressure on the outside wall surfaces of the Darlington Generating Station power house from its interaction with the incident blast wave is a three-dimensional nonstationary flow problem. In view of the fact that a three- or even two-dimensional nonstationary flow analysis will not be undertaken here, a simplified analysis or a well-developed method is required to obtain an approximate yet realistic solution for the blast-wave overpressure on the exterior walls and roof of the power house. Most of the simplified methods of getting the blast-wave overpressure loading at a position of interest on the outside walls of a structure or building, including the one used herein, require as an input condition a knowledge of the incident blast wave at the location of interest. This means that the flow properties of the incident or free-field blast wave are required, without the presence of the structure or power house. By means of some appropriate method, the incident blast-wave flow properties are warped or altered to obtain the overpressure loading on the building exterior. Consequently, the method for obtaining all of the flow properties of the incident blast wave at various locations along the length of the power house, without any interference by the power house, is presented in the next section, and the results are given for later use. This is then followed by the method that is employed to obtain the blast-wave overpressure loading on the outside walls of the power house, from the incident flow properties.

6.2 Flow Properties of the Free-Field Blast Wave

In order to obtain the flow properties of the free-field blast wave at various distances along the length of the power house, the initial spatial distributions of the incident blast wave that are tabulated in table 2 are used as input data for computer computations by means of the random-choice method which was described previously (Chaps. 2 and 4). The computations of the blast-wave flow are carried out step-by-step to larger radial distances and longer times, to get all of the flow properties. For these computations, the blast-wave flow area that is used was not one of the geometrical configurations for the power house, but it is a solid angle of a sphere. In this manner the flow properties of a free-field, spherical blast wave are obtained, as temporal distributions at any radius of interest, or as spatial distributions at any time of interest.

Spatial distributions of the pressure ratio p/p_1, density ratio ρ/ρ_1, flow-velocity ratio u/a_1, and temperature ratio T/T_1 are given in Fig. 23, for which p_1, ρ_1, a_1, and T_1 are atmospheric values corresponding to a pressure of 1 atm and a temperature of 288 K. In each set of distributions shown, each successive distribution is displaced upward slightly from the previous one, both for clarity and to produce the effect of a time-distance diagram. The time between successive distributions is always 60 ms, in these results and also ones to be given later. Furthermore, the number of grid zones used for the entire flow-field is 750, which will always be used for the entire flow field in later results.

In the first distribution at the bottom of each set, one can see the initial profile of the incident blast wave, just before the location of the front wall of the power house at distance zero. In successive distributions the free-running blast wave propagates to the left. Its amplitude decreases a

little with distance because of the spherical geometry, and its shape changes slightly, but this latter effect is not noticeable in the graphical results.

Note that the vertical lines appearing in Fig. 23 are dividing lines between the various rooms in the geometrical configuration of the power house. In this case the lines correspond directly to configuration A, as depicted in Fig. 6. The first vertical line on the right is the location of the front wall of the power house (at which the distance is zero). The next line over to the left is the end of the turbine hall and the start of the turbine auxiliary bay, and so forth.

Seven sets of temporal distributions or time histories of the pressure, density, flow velocity and temperature are also given in Fig. 24 (a to g) for the free-field running blast wave, at different distances along the power house corresponding to the location of the incident wave ahead of the power house and the centers of rooms one to six in Fig. 6. Because the time is measured from time zero corresponding to when the blast wave first arrives at the front wall of the power house, the relative time delay in the blast-wave arrival at the various locations is apparent in the graphical results.

6.3 Overpressure on the Power House from the Free-Field Blast Wave

Originally, the simplified method presented in Ref. 6 and also given in Ref. 2, was going to be employed to alter or warp the free-field blast-wave flow properties to get the overpressure loading on the outside surfaces of the power house. However, in the interim, this particular method was found to be inadequate and judged to be inappopriate for the present problem. The reasons are brought out in the following few paragraphs. They have also been presented and discussed in more detail in Ref. 3.

There is a conceptual and an actual difference between the blast-wave overpressure acting at a specific point on a surface and the average blast-wave overpressure loading on the entire surface. The difference is brought out most clearly by using a simple example. Let a flat-topped wave having an amplitude A and a length L move at a constant velocity V of unity over a flat surface of length 6L in the direction of motion and width W transverse to this motion, as illustrated in Fig. 25a. The resulting overpressure as a function of time at the surface center is sketched in Fig. 25b. The overpressure experienced at this point has an amplitude of A and lasts for a short period of time given by L/V. The average overpressure loading on the entire surface is the integral of the overpressure acting on the surface, taken over the entire surface at each new instant in time, and divided by the total area (LW). By doing this, the resulting overpressure loading for the example can be obtained as depicted in Fig. 25c. It first increases linearly from zero to A/6 in a period of time of L/V, then remains constant at A/6 for a time period of 5L/V, after which it falls linearly back to zero in a time period of L/V. Because of the averaging process over the entire surface of the overpressure acting on a part or all of the surface, the resulting overpressure loading for the entire surface is quite different than the overpressure experienced at any specific point on such a surface. The overpressure at a particular point and the average loading are nearly the same only if the length of the incident wave is much longer than that of the surface of interest.

The previous example brings out clearly the difference existing between the overpressure acting at a specific point on a surface and the average over-

pressure loading over the entire surface. In seeking the detrimental effects of blast-wave loading on a structure, therefore, it is obvious that the use of the average overpressure loading as defined in the previous paragraph could result in substantial misinterpretation or error, especially if the length of the incident wave is smaller than the length of the structure. This does not mean to say that the average loading as defined in the previous paragraph is always used as previously defined in obtaining the overpressure loading on structures subjected to blast waves from nuclear and chemical explosions, as can be found in Refs. 2 and 6. However, in determining the complete overpressure loading profile with time for one wall of a structure, a similar averaging process is used to obtain part of the profile. In such work this is reasonable, provided that the length of the incident wave is much greater than the length of the object or structure. In dealing with blast waves from nuclear explosions, it is always assumed that the building or structure is totally engulfed or immersed in the blast wave, that is, the length of the structure is much smaller than the length of the blast wave. This is quite reasonable for such work because the yield of most nuclear weapons is relatively large, resulting in extremely long duration blast waves. Then, the approximate analysis and methods given in Ref. 6 are valid for application. However, this is not true in the present case, and this is illustrated in the next few paragraphs.

Consider the interaction of a blast wave having a wave length λ with a building having some typical length L. If the length of the wave is much smaller than that of the building, or the length ratio λ/L is much less than unity, then, as the blast wave interacts with the building, it continuously diffracts around the building, moving first over the front face, then over the mid portion, and finally over the rear part. The interaction continuously produces a reflected wave that move away from the building, and the blast-wave flow consisting of the diffracted and reflected waves is always unsteady. At any particular location on the building surface the loading will be varying relatively rapidly with time as the blast wave passes, because the wave length is relatively short, and the loading cannot be obtained on the basis of using simple steady or quasi-steady analyses. Nonstationary flow analyses are, of course, required to get a meaningful loading prediction. The overpressure loading on the building from this type of blast wave and building interaction is most properly called diffraction loading or the diffraction loading phase.

Now consider the opposite case, when the length of the blast wave is much larger than that of the building, or the length ratio λ/L is much larger than unity. Then, as the blast wave interacts with the building, its wave front (not the entire wave) initially diffracts around the building and moves on, and a reflected wave front also move away from the building and decays. This diffraction phase ends relatively quickly. However, because the wave is so much longer than the building, and the flow totally engulfs the entire building, the flow in the latter part of the blast wave is still moving over the building. Because the blast-wave flow properties are changing relatively slowly with time, a virtually steady flow, or so-called quasi-steady flow, is produced around the building. In this later phase, the flow properties are changing relatively slowly with time and the loading on the building at any point can be calculated from the theory for steady flows over objects, or from experimental data of steady flows over models, provided one uses the local flow conditions at each new time. This phase in the interaction of a blast wave with a building is the so-called drag phase, and the overpressure loading is properly called the drag loading.

The previous two paragraphs set out the limits of diffraction and drag

loading for a blast wave interacting with a structure. When the blast wave is much longer than the length of the building, the initial interaction is mainly unsteady diffraction, but because this phase does not last very long, it can most often simply be ignored, in spite of the fact that it normally results in a very high loading for a very short time, and then only the more extensive steady drag loading phase need be handled. However, even in this case, both stages of diffraction and drag exist, not just one or the other, although they more or less are distinct phases. When the dimensions of the blast wave and building are nearly equal, then the blast-wave interaction with the building is a more or less an equal combination of diffraction and drag loading, and the two stages are no longer readily separable. Finally, when the blast wave is much shorter than the building, the diffraction stage is all important and the drag stage really ceases to exist. However, the unsteady flow over each part of the building must be computed before one can obtain the overpressure loading on each part of the building.

Although the length ratio λ/L is a good conceptual guide for indicating which type of blast loading is important (diffraction and/or drag), there is little data available that helps specify the limits of each different loading phase in terms of precise values of λ/L. The present opinion is that for λ/L values greater than two the dominant loading mechanism is the drag loading and the diffraction loads can be safely neglected. However, as the value of λ/L becomes smaller, the diffraction loading becomes a more and more important part of the combined diffraction and drag loading, and, therefore, it cannot be neglected.

In the present problem of the blast-wave flow over the power house, the length of the incident blast wave is approximately 70 m, whereas the length of the power house in the direction of the blast-wave motion is almost twice as long at about 125 m. This means the ratio λ/L is about 0.6. As a consequence, many parts of the analysis and method of obtaining the blast-wave loading on structures as set out in Refs. 2 and 6 are simply not valid for the present problem. The blind application of such methods could lead to erroneous results and misinterpretations. In fact, the initial, straighforward application of the method presented in Ref. 6 lead to quite unreasonable overpressure profiles for the loading on the walls and roof of the power house. Hence, this method is abandoned in this study.

The present procedure of obtaining good estimates of the overpressure loading on the front, side, top, and rear walls of the power house, as well as the final results, are now presented. In the case of the front wall of the power house, in which the blow-out panels are located, the reflected overpressure of the incident blast wave is simply taken as double that of the incident wave, because the wave is quite weak. The pressure relief resulting from rarefaction waves coming from the sides and top of the building are simply ignored, because their shape is not known. For a point in the center of this wall, the relief wave from the top would arrive after a time t of about 70 ms, and those from the two side walls would arrive a lot later, after about 150 ms. The former would have some influence on reducing the overpressure loading on the front wall, whereas the latter would effectively have none, due to its late arrival time. The resulting overpressure loading on the power-house front wall is shown in Fig. 26a.

For the overpressure loading on the side walls and roof, it is assumed that the blast wave incident on the power house negotiates the front wall of this building and then has a sufficient distance to readjust to essentially the

free-field condition. Because the power house is long compared to the blast-wave length, this is a reasonable assumption. As the incident blast wave moves farther along the outside of the building the reflected wave from the front of the building and the relief waves from the sides will continuously get weaker, leaving a more-or-less free-field blast wave. Under such simplifying assumptions, the blast-wave overpressure loading on the side walls and roof, at the same distance from the explosion center, will be the same. The three overpressure loading signatures for the side walls and roof are presented graphically in Fig. 26 (b, c, and d), one for the center of the turbine hall (location 1 in room 1 in Fig. 6), one for the latter part of the turbine auxiliary bay (location 3 in room 3), and the last one for the midpoint of the reactor building (location 5 in room 5).

The overpressure loading on the outside of the rear wall of the power house is finally sketched in Fig. 26e. This overpressure loading is lower than the overpressure of the incident wave at the same radial location, and it also starts at a later time, all because of the nature of the assumed flow over the rear of the power house or building. To estimate this overpressure loading, some of the shock-wave loading data obtained experimentally from simple models placed in shock tubes were employed as a guide (see Refs. 43 to 45). The loading on this rear wall starts later than the arrival at this radial location of the free-field blast wave, because the incident wave must also propagate down the rear wall to its center, where the overpressure loading is estimated. This delays the start of the overpressure loading at the center of the rear wall by approximately 70 ms.

7. BLAST-WAVE OVERPRESSURE INSIDE THE POWER HOUSE

7.1 Introduction

The numerical results for the nonstationary blast-wave flow inside the power house, for geometrical configurations A to E described in chapter 3, and obtained with the numerical analysis outlined in chapter 2, are given in this chapter. These results are presented along with discussion, but most of the conclusions are reserved for a later chapter. Pertinent observations that make the numerical results understandable are, of course, required.

Numerical results are given for three different blow-out panel opening times of 0, 100, and 500 ms, in order to illustrate the effects of different opening times on the results. No results are given for the specific opening time of 75 ms, that was determined from the blow-out panel analysis presented in chapter 5, for the following reasons. Firstly, the original blow-out panel analysis, which was much cruder than the one given in chapter 5, gave a value of just over 100 ms. This subsequent work was then guided by this original result. Secondly, in spite of the better analysis for the blow-out panels, it is believed that an even more refined analysis would give a somewhat longer blow-out panel opening time. Finally, results for 75 ms are not very different than those for 100 ms. Hence, it was deemed not worthwhile to redo all of the costly computer runs to get new but only slightly different results.

Although the three sets of spatial distributions for pressure, density, flow velocity and temperature for the three different opening times are shown as separate sets of graphical results (e.g., see Fig. 27a, 27b and 27c), the sets of temporal distributions of pressure, flow velocity, density and temperature at each location of interest for the three different opening times are

condensed onto corresponding graphs, so that the results for different opening times can be compared readily (e.g., see Fig. 27d to 271).

7.2 Results for Configuration A

For configuration A, the three small rooms under the hoistway are included in the blast-wave flow path (number 1) at the end of the reactor building (see Fig. 6 and section 3.2), mainly to get a good estimate of the overpressures in these small rooms. The spatial and temporal distributions of the pressure, density, flow velocity, and temperature for this configuration are shown in Fig. 27 (a to 1).

The spatial distributions are excellent for showing the nonstationary wave motion. For example, as the blast wave that moves to the left enters the power house through the blow-out panels, a reflected wave forms and moves off to the right. At other area changes within the power house, reflected waves are also produced, and these also move off to the right. Some of these are reflected again and these re-reflected waves then follow the primary wave to the left. The spatial distributions contain some numerical noise, which is typical of the random-choice method. It can be reduced by using a finer computational grid, or more grid points to represent the flow field. However, the increased cost of using a finer grid was not judged worthwhile to reduce the numerical noise any further.

When the opening time of the blow-out panels is very short (e.g., 0 ms), the blast wave incident on the power house enters the power house through the openings almost unhampered or unchanged, except for the initially double peaked front (see Fig. 27a). In this case the reflected wave from the contraction in area of 75% at the blow-out panels is N shaped, rather short, and not highly significant. When the blow-out panel opening time is long (e.g., 500 ms), the blast wave inside the power house is altered more substantially. Its front is no longer steep but rather smooth and spread out, although it steepens from a compression front into a shock front with increasing distance (see Fig. 27c). The reflected wave is no longer a short N-shaped wave but is one of substantial length, because the slow opening time of the blow-out panels makes the front wall of the power house more of a rigid reflecting wall (Fig. 27c).

The temporal distributions are excellent for illustrating how the transient flow changes with time at some particular spatial location or in some particular room of interest. Such signatures are important in the determination of the maximum pressures and flow velocities of interest. However, the particular signature shape does not indicate which direction the wave or waves are moving or how the maximum values are produced. Therefore, it is not always possible to distinguish the primary wave from the reflected and re-reflected waves, or if the maximum pressure or flow velocity is the result of one wave or a combination of waves.

From the graphical results for the time signatures of the flow properties, the following observations can be made. Firstly, the overpressure and other flow properties in each room are lower for increasing opening times of the blow-out panels, especially for an long opening time of 500 ms. From an opening time in the range of 0 to 100 ms, the reduction is not highly significant. Secondly, for short opening times, the peak amplitude of the blast wave that travells inside the turbine hall (room 1) is approximately the same as that of the incident wave, because the effects of the area reduction of the

blow-out panels are not very significant if they open rapidly. Thirdly, owing to the convergence in flow area from the turbine hall to the reactor building (rooms 1 through 5) and the resulting reflected waves, the blast wave inside these rooms actually increases in strength or amplitude as it travels through them. Fourthly, the overpressure in the reactor building increases further from the reflection of the primary blast wave at the end wall of the reactor building, or at the severe area convergence existing at the first of the three small rooms. This overpressure increase is particularly noticeable in room 5. Finally, the peak overpressure in the three small rooms is rather higher than expected, being almost equal in amplitude to that of the incident blast wave. This is partly due to the focussing of the blast wave as it propagates through the power house, and partly due to the high reflected overpressure that occurs at the entrance to the first of the three small rooms.

One might ask why the reflected wave from the front wall of the power house with instantly or rapidly breaking blow-out panels is N-shaped. This can be explained easily on the basis of previous research given in Ref. 13. When a shock wave with subsonic flow behind its front interacts with an area change, the reflected wave is a shock wave for an area reduction and a rarefaction wave for an area enlargement. Hence, for a convergent-divergent area change like that of the blow-out panels the reflected wave should consists of a shock wave followed by an expansion wave, giving rise to the N shape. After the initially transient flow from the blast-wave front interacting with the blow-out panel openings is over, and the N-shaped wave has left the vicinity of the blow-out panels, the flow finally decays into an approximately steady or quasisteady flow through these panel openings, and the blast wave continues to move through the openings without additional reflection effects. When the blow-out panels open more slowly than about 50 ms, the reflection process is altered from that just described and more extended in time. Then the reflected wave is no longer simply N shaped.

7.3 Results for Configuration B

For configuration B, the three small rooms under the hoistway are not included in the flow path (number 1), and the blow-out panels in the rear wall of the power house are allowed to open from the overpressure loading of the blast wave moving through the reactor building (see Fig. 7 and section 3.3). The spatial and temporal distributions of the pressure, density, flow velocity, and temperature for this configuration are shown in Fig. 28 (a to i).

Spatial and temporal distributions of pressure, flow velocity, density, and temperature for configuration B are similar to those for configuration A, especially for rooms 1 through 4, with the following exceptions. Because the flow path does not include the three small rooms at the end, but rather a rear wall with breaking blow-out panels, the reflected wave from this rear wall is now changed appreciably from configuration A to B, especially for the case of a short opening time of the blow-out panels. When the panels blow out instantly (0 ms), the reflected wave is again N shaped, rather short, and not highly significant (see Fig. 28a). On the other hand, when the opening time is long (500 ms), the reflected wave from the rear wall of the reactor building is much more substantial or longer, as one might expect (see Fig. 28c).

In the temporal distributions, the reflected overpressure of the blast wave which was sustained for some time for configuration A (Fig. 27i) is now only a short spike (N-shaped wave) for configuration B (Fig. 28i). This should

be expected because the breaking of the blow-out panels in the reactor-building rear wall will provide a pressure relief inside the building, especially when the blast-wave flow over the exterior of the power house is ignored.

7.4 Results for Configuration C

For configuration C, the blast-wave flow inside the three small rooms is considered separately (see Fig. 8 and section 3.4). The blast-wave flow into these rooms is computed on the basis of employing the blast-wave flow in room 6 from configuration B as the initial or input conditions, and by using a separate random-choice method computation for obtaining these unsteady-flow results, as mentioned earlier in section 3.4. The spatial and temporal distributions of the flow properties for this configuration are presented in Fig. 29 (a to f).

The overpressure, flow velocity, density, and temperature histories of the blast-wave flow inside the three small rooms have rather slowly rising or compression-wave fronts, rather than sudden rises or shock-wave fronts, mainly because of head losses suffered by the flow as it goes through the convergent-divergent area constriction into the first and subsequent rooms. The rate of rise at the begining of these signatures is lower for subsequent rooms, because of the increasing number of area constrictions and total head losses that the flow experiences. Furthermore, the rate of rise at the begining of these signatures is less for the case of longer blow-out panel opening times, but this is principally due the slower rises on the initial blast-wave flow in room 6, which were used as input data.

In the case of fairly rapid blow-out panel opening times of 0 and 100 ms, for which the input blast-wave flow has a steep or shock front, the flow surges into room 1 fairly rapidly and reflects at the area reduction to room 2. This reflected wave and others that follow from this room (and the other two rooms) set up flow oscillations or surges in room 1. This is readily evident in the flow-velocity signature in Fig. 29d, where flow-velocity surges even produce reverse direction flows. The same surges are not nearly so prominant in the overpressure, density, and temperature signatures, because single compressive waves and crossing compressive waves both increase the pressure, density, and temperature. Hence, these signatures do not have the same shape as those for the flow velocity. Flow surges are much less in room 2 and almost nonexistent in room 3, because of the additional convergent-divergent area constrictions and their associated head losses, which act as a good damping mechanism on the transmission of flow surges.

The flow-property signatures in rooms 1, 2, and 3 are approximately the same for the case of blow-out panel opening times of 0 and 100 ms, especially during early times, mainly because the initial or input conditions of the blast-wave flow in room 6 are quite similar. The signatures for the longer opening time of 500 ms increase more slowly and are substantially smaller in amplitude than those for opening times of 0 and 100 ms, especially during early times, because the input flow properties in room 6 rise more slowly. Furthermore, the peak amplitude of the overpressure signatures is essentially less for longer blow-out panel opening times, especially in rooms 2 and 3, because of the combination of the finite duration of the incident wave and the damping mechanism of the area constrictions with their associated head losses.

It is now worthwhile to compare the peak amplitudes of the overpressure and other signatures for rooms 1, 2, and 3 from geometrical configurations A

and C, in order to observe the effects of the two different models. Note that configuration A includes the three small rooms at the end of flow path number 1 and also excludes blow-out panels breaking at the rear of the power house (see section 3.2 and Fig. 6), whereas configuration C includes blow-out panels that break at the rear of the power house (section 3.3 and Fig. 7) and handles the three small rooms separately from flow path number 1 as a type of branched duct flow (section 3.4 and Fig. 8). Hence, overpressure and other signatures given earlier in Figs. 27j to 27l for configuration A should now be compared to those presented here in Figs. 29d to 29f for configuration C. Note that the vertical scales for the overpressure, density, and temperature signatures are different for configurations A and C.

The comparison will reveal the following observations. The basic shapes of the flow-property signatures for configurations A and C are similar, but the amplitudes for those of configuration A are approximately twice as high as those of configuration C. The reasons for this difference in amplitude is easily understood. For configuration A, the blast wave inside the power house largely reflects at the entrance to the three small rooms, because no breaking blow-out panels are included in this particular model, thereby providing a high reflected overpressure to drive the flow into the three small rooms. On the other hand, for configuration C with the breaking blow-out panels, only the normal blast-wave overpressure inside the power house, which is about one-half that of the reflected wave, forces the flow into the three small rooms. Consequently, it should be expected that the amplitude of the overpressure and most other flow properties for the case of configuration C would be only roughly one-half of that for the case of configuation A. Detailed differences in the signatures and their amplitudes of configurations A and C are, of course, due to detailed model differences.

7.5 Results for Configuration D

For configuration D, the three small rooms are included in the flow path (number 1) at the end of the reactor building (see Fig. 9 and section 3.5). For this configuration the three room volumes at the end of the flow path have been adjusted such that the artificial configuration geometry (Fig. 10) corresponds to the case when the blow-out panels in the rear wall of the reactor building break open instantly, yet the predicted blast-wave flow in each of the three small rooms should be typical of what actually happens in a real branched duct flow (see section 3.5).

Spatial and temporal distributions of pressure, flow velocity, density, and temperature for configuration D appear in Fig. 30 (a to l). They are given for all of the rooms (from 1 to 9), not just for the three small rooms (7 to 9) that have been enlarged.

A comparison of results for configurations A, B, C, and D is worthwhile. Only the main results are mentioned here. Note that results for rooms 1 to 6 are mentioned first, followed by those for the three small rooms. Spatial and temporal distributions for the pressure, flow velocity, density, and temperature for configuration D are most similar to those for configuration B, especially for rooms 1 to 6, as one might expect, because in both cases the blow-out panels in the rear wall of the reactor building break open. However, because the blow-out panels open instantly in the rear wall of the reactor building when the wave arrives for configuration D, and the extra three small rooms have been enlarged considerably, the reflected wave for configuration D is one of rarefaction only

instead of one of compression followed by one of rarefaction for configuration B. This makes the blast-wave flows in configurations B and D differ slightly, especially close to the end of the flow path in rooms 5 and 6 of the reactor building.

The flow-property signatures in the three small rooms for configurations A, C, and D have roughly similar shapes, but the amplitudes are different. The amplitudes for configuration D are most similar to those of configuration C, and both of these are about one-half those of configuration A, because the overpressure that drives the blast-wave flow into the three small rooms does not result from a reflected wave. One might expect that the amplitudes for configurations B and D should be similar, albeit the peak overpressures for the three small rooms in configuration D is somewhat smaller by approximately 35% than those for configuration C. Both sets of results are essentially for the same case of breaking blow-out panels in the rear wall of the reactor building and the three small rooms are included in different but supposedly equivalent ways.

7.6 Results for Configuration E

For configuration E, an alternate blast-wave flow path (number 2) in the power house is considered (see Fig. 11 and section 3.6). For this lower flow path a blast wall exists between rooms 5 and 6. The main aim is to investigate the blast-wave overpressure occurring in room 6, behind the blast wall with the small opening. The spatial and temporal distribution of the pressure, density, flow velocity, and temperature are given in Fig. 31 (a to h).

The spatial distributions of the pressure, flow velocity, density, and temperature are, for the most part, similar to those found for configurations A and B, especially in rooms 1 to 5, with the following exception. Owing to the blast wall with the small fixed-area opening through which the blast wave must travel to get into room 6, the peak overpressure in room 6 is quite small, as one might have expected.

8. PRESSURE DIFFERENCE ACROSS THE POWER-HOUSE WALLS

The pressure difference across the Darlington Generating Station power-house walls from the blast-wave overpressure loading on the outside and inside of the power house is presented in this chapter. This pressure difference is defined herein to be the blast-wave overpressure on the outside walls minus the overpressure on the inside walls. Consequently, a positive pressure difference corresponds to net inward pressure or crushing force on the building wall and a negative pressure difference corresponds to a net outward pressure or expanding force on the building wall. The net overpressure difference is obtained by employing information that was already presented in chapters 6 and 7, for blast-wave overpressures acting on the outside and inside walls of the power house. Most of the information can be used in a straightforward manner to get the net pressure loading, and no further details are given.

The final four sets of results for the pressure differences across the front wall; across the sides and roof at location and room numbers 1, 3 and 5; and across the rear wall are presented in Figs. 32, 33, 34, and 35, for geometrical configurations A, B, D, and E, respectively. For each set of results the opening time of the blow-out panels is 100 ms. Results for opening times that are shorter (e.g., 0 and 10 ms) are very nearly the same as those presented.

Results for longer opening times like 500 ms will, of course, be different; however, as these opening times are not typical for the blow-out panels, such results are not presented here.

In the case of the front wall, it first experiences the reflected overpressure loading of the blast wave from the outside. As the blast-wave flow enters the turbine hall, after an initial delay of 10 ms before the blow-out panels begin to open slowly, it then eventually counters this outside loading, and the net pressure difference on the front wall then decreases, as shown in Figs. 32 to 35. This is why the large spike with an amplitude of about 0.2 atm or 20 kPa occurs at the front of the signature. Reflected waves arriving in the turbine hall at later times eventually produce a larger overpressure inside the turbine hall than outside the front wall, resulting in a negative net pressure on the front wall.

In the cases of rooms 1, 3, and 5, the blast-wave overpressures on the outside and inside of the power house are nearly the same initially. Hence, they tend to counter or cancel each other, except at the leading edge of the wave or signature. Because the blast wave on the outside of the building arrives a bit sooner than that on the inside, because the blow-out panels take a finite time to open, the leading edge of the wave has a spike of about 0.1 atm or 10 kPa. At later times in the signatures, for the pressure difference for rooms 1, 3 and 5, the net pressure difference is either negative or positive depending on whether the reflected waves are compressions or rarefactions, respectively. The type of reflected wave depends on whether the blow-out panels in the rear wall of the power house remain closed or break open, as mentioned in the last chapter.

In the case of the rear wall of the power house, the blast-wave outside of the building always arrives later than that on the inside, because the wave outside takes additional time to move down the rear wall to its center point. Hence, the pressure difference on the rear wall is initially negative or outwards, before it is finally countered by the overpressure of the wave on the outside of the building. The initial spike can also be quite large, because the blast wave inside the reactor building reflects from the rear wall as a compression wave in configurations A and B. For configuration D, there is a reflected rarefaction wave and the initial spike is lower. Finally, for configuration E, the pressure in the last room is very low; hence, the pressure difference is also small.

9. CONCLUSIONS

It is important to first determine which scenario is the most likely one to occur, that is, which geometrical configuration should be employed for the numerical computations of the nonstationary blast-wave flow inside and outside the Darlington Generating Station power house. In order to make this selection for blast-wave flow path number 1 through the upper portion of the power house, the numerical results for the pressure difference across the rear wall of the power house that are presented in Figs. 32 to 35 need to be considered. From such a consideration, it should become readily apparent that the pressure difference across the blow-out panels in the rear wall is sufficiently high that they would break and open, for each geometrical configuration (A, B, and D). Hence, configuration A, for which the blow-out panels are assumed not to break, is not realistic, and it becomes more or less of tangential interest only. Configurations B and D then become of primary interest, as well as configuration C

for giving the blast-wave flow in the three small rooms from input conditions from configuration B. Note that numerical results for the case of the blow-out panels opening in 100 ms are the main ones of interest and the only ones that will be considered in this chapter.

Although both the spatial and temporal distributions for configurations B and D have been discussed previously in chapter 7, some final comments are worthwhile making here. In rooms 1 to 5 for configurations B and D, the peak overpressures of the blast wave are approximately the same, and they are quite similar to that of the incident blast wave (0.1 atm or 10 kPa). Furthermore, the overpressure signatures are also fairly similar. This is because the end condition for the blow-out panels in the rear wall of the reactor building is not markedly different for configurations B and D. For configuration B, the blow-out panels open over a period of 100 ms starting from when the blast wave first arrives there, whereas, for configuration D, the blow-out panels open instantly and the three small rooms with a much increased size are connected directly to the back of the reactor building. For the last case of the reactor building (room 6), the peak overpressures of the blast wave can, for a short period of time, be larger by 50% than that of the incident wave. This is due in part to the focussing of the blast wave as it moves through the power house and in part to reflections of the primary wave from the back wall of the power house. One can conclude, therefore, that geometrical configurations B and D both give practically the same numerical predictions for rooms 1 to 6, and especially rooms 1 to 5.

For the case of the three small rooms, predictions of the blast-wave flow in these rooms are given for configurations C and D. In both predictions the numerical results are very similar, with the amplitude of the blast wave being somewhat lower for case D than C (by 35%). The lower results for configuration D could well be due to an inaccurate specification of the enlargement factor for the three small rooms, because this factor is quite arbitrary. The prediction for configuration C is judged to be the most appropriate, because it is based on the most realistic physical model. This model would also result in somewhat of an overprediction of the blast-wave amplitudes in the rooms, or give conservative values, because the initial or forcing blast-wave flow in room 6 of configuration B is not reduced in strength by any loss of mass, momentum, and energy to the three small rooms, as mentioned previously. For configuration D, therefore, the peak overpressures in the three small rooms is typically less than about 0.06 atm or 6.0 kPa for the first small room, and correspondingly less for the second and third ones.

For the case of configuration E and flow path number 2, the blast wall is very effective in limiting the amplitude of the blast wave that finally enters the room behind it via the small opening. The peak overpressure in the last room is typically less than about 0.025 atm or 2.5 kPa.

10. CONCLUDING REMARKS

The present models of the blast-wave flows inside and outside the power house are one-dimensional, which are approximate for actual blast-wave flows and buildings. It would, of course, be very interesting to obtain numerical predictions with more realistic two- or even three-dimensional models, although it is realized that this not only would require additional human efforts but would also especially need increased computational costs. Although details of the blast-wave flow should be predicted more accurately and additional details

found, which would be quite interesting from a scientific and engineering point of view, it is not expected that significantly different and important results would be obtained in regard to the blast-wave pressure loading on the inside and outside walls of the power house.

11. REFERENCES

1. M. Brook, 'Darlington G.S. Structural Design Against Accidental Explosions (at CNR tracks)', Civil Section, Darlington Engineering Department, Design and Development Division, Ontario Hydro, Toronto, Ontario, Canada, 1980.

2. A. V. Singh, 'Procedures for the Blast Resistant Design of Nuclear Power Plant Structures', OH Report No. 83159, Civil Design Department, Design and Development Division, Ontario Hydro, Toronto, Ontario, Canada, January 1983.

3. J. J. Gottlieb, 'Blast-Wave Loading on Darlington Generating Station Power Plant Buildings in the Event of an Explosion at the Nearby Railroad Tracks', contract report prepared for the Nuclear Studies and Safety Department, Ontario Hydro, Toronto, Ontario, Canada, September 1984.

4. H. S. I. Sadek and J. J. Gottlieb, 'Initial Decay of Flow Properties of Planar, Cylindrical and Spherical Blast Waves', UTIAS Technical Note No. 244, University of Toronto Institute for Aerospace Studies, Downsview, Ontario, Canada, October 1983.

5. S. C. M. Lau and J. J. Gottlieb, 'Numerical Reconstruction of Part of an Actual Blast-Wave Flow Field to Agree with Available Experimental Data', UTIAS Technical Note No. 251, University of Toronto Institute for Aerospace Studies, Downsview, Ontario, Canada, August 1984.

6. S. Glasstone (Ed.), 'The Effects of Nuclear Weapons', U.S. Department of Defence and Atomic Energy Commission, Washington, D.C., 1957; revised in 1962; subsequent revision in 1977 with P.J. Dolan (Ed.) - last revision does not contain the list of past nuclear tests.

7. J. Glimm, 'Solution in the Large for Nonlinear Hyperbolic Systems of Equations', Communications in Pure and Applied Mathematics, Vol. 18, pp. 697-715, 1965.

8. A. J. Chorin, 'Random Choice Solution of Hyperbolic Systems', Journal of Computational Physics, Vol. 22, No. 4, pp. 517-533, 1976.

9. P. Colella, 'Glimm's Method for Gas Dynamics', Society for Industrial and Applied Mathematics, Journal of Scientific and Statistical Computing, Vol. 3, No. 1, March 1982.

10. O. Igra, J. J. Gottlieb, and T. Saito, 'An Analytical and Numerical Study of the Interaction of Rarefaction Waves with Area Changes in Ducts - Part 2: Area Enlargements', UTIAS Report No. 273, University of Toronto Institute for Aerospace Studies, Downsview, Ontario, Canada, December 1984.

11. G. A. Sod, 'A Numerical Study of a Converging Cylindrical Shock', Journal of Fluid Mechanics, Vol. 83, Part 4, pp. 785-794, 1977.

12. T. Saito and I. I. Glass, 'Application of Random Choice Method to Problems

in Gasdynamics', Prog. in Aerospace Sci., Vol. 21, pp. 201-247, 1984. Also, 'Applications of Random-Choice Method to Shock and Detonation-Wave Dynamics', UTIAS Report No. 240, University of Toronto Institute for Aerospace Studies, Downsview, Ontario, Canada, October 1979.

13. D. R. Greatrix and J. J. Gottlieb, 'An Analytical and Numerical Study of a Shock Wave Interaction with an Area Change', UTIAS Report No. 268, University of Toronto Institute for Aerospace Studies, Downsview, Ontario, Canada, November 1982.

14. T. Saito, 'An Experimental, Analytical and Numerical Study of Temperatures Near Hemispherical Implosion Foci', UTIAS Report No. 260, University of Toronto Institute for Aerospace Studies, Downsview, Ontario, Canada, December 1982.

15. T. Saito and I. I. Glass, 'Temperature Measurements at an Implosion Focus', Proceedings of the Royal Society of London, Vol. 384(A), pp. 217-231, 1982.

16. J. J. Gottlieb, O. Igra, and T. Saito, 'Simulation of a Blast Wave With a Constant-Area Shock Tube Containing Perforated Plates in the Driver', Proceedings of the Eighth International Symposium on Military Applications of Blast Simulation, Vol. 2, pp. 7-1 to 7-21, sponsored by the Gruppe for Rustangsdienste, AC-Laboratorium Spiez, Spiez, Switzerland, symposium held on the 20-24 June 1983 in Spiez, Switzerland.

17. J. J. Gottlieb and T. Saito, 'An Analytical and Numerical Study of the Interaction of Rarefaction Waves with Area Changes in Ducts - Part 1: Area Reductions', UTIAS Report No. 272, University of Toronto Institute for Aerospace Studies, Downsview, Ontario, Canada, November 1983.

18. J. J. Gottlieb and O. Igra, 'Interaction of Rarefaction Waves with Area Reductions in Ducts', Journal of Fluid Mechanics, Vol. 137, pp. 287-307, December 1983.

19. O. Igra and J. J. Gottlieb, 'Interaction of Rarefaction Waves with Area Enlargements in Ducts', submitted to the AIAA Journal in August 1983.

20. H. Miura and I. I. Glass, 'On a Dusty-Gas Shock Tube', UTIAS Report No. 250, University of Toronto Institute for Aerospace Studies, Downsview, Ontario, Canada, May 1981.

21. H. Miura and I. I. Glass, 'On a Dusty-Gas Shock Tube', Proceedings of the Royal Society of London, Vol. 382(A), pp. 373-388, 1982.

22. H. Miura and I. I. Glass, 'On the Passage of a Shock Wave Through a Dusty-Gas Layer', UTIAS Report No. 252, University of Toronto Institute for Aerospace Studies, Downsview, Ontario, Canada, January 1982.

23. H. Miura and I. I. Glass, 'On the Passage of a Shock Wave Through a Dusty-Gas Layer', Proceedings of the Royal Society of London, Vol. 385(A), pp. 85-105, 1983.

24. G. Rudinger, 'Wave Diagrams for Nonsteady Flow in Ducts', D. van Nostrand Company, New York, New York, U.S.A., 1955. Also, 'Nonsteady Duct Flow: Wave Diagram Analysis', Dover Publications, New York, New York, U.S.A., 1969.

25. J. A. Owczarek, 'Fundamentals of Gasdynamics', International Textbook Company, Scranton, Pennsylvania, U.S.A., 1964.

26. I. E. Idel'chik, 'Handbook of Hydraulic Resistance: Coefficients of Local Resistance and of Friction', originally in Russian in 1960, translated into English in 1966 by the Israel Program for Scientific Translations, available from the Clearinghouse for Federal Scientific and Technical Information, U. S. Department of Commerce, Springfield, Virginia, U.S.A., 22151.

27. T. Baumeister and L. S. Marks (Eds.), 'Standard Handbook for Mechanical Engineers', seventh edition, McGraw-Hill Book Company, New York, New York, U.S.A., 1966.

28. A. H. Shapiro, 'The Dynamics and Thermodynamics of Compressible Fluid Flow', Vol. I and II, The Ronald Press Company, New York, New York, U.S.A., 1954.

29. G. E. Forsythe, M. A. Malcolm, and C. B. Moler, 'Computer Methods for Mathematical Computation', Prentice-Hall, Englewood Cliffs, New Jersey, U.S.A., 1977.

30. J. J. Gottlieb and D. V. Ritzel, 'A Semi-Empirical Equation for the Viscosity of Air (U)', DRES Suffield Technical Note No. 454, Defence Research Establishment Suffield, Ralston, Alberta, Canada, July 1979.

31. R. G. Deissler, 'Analytical and Experimental Investigation of Adiabatic Turbulent Flow in Smooth Tubes', NACA Technical Note No. 2138, National Advisory Committee on Aeronautics, Washington, D.C., U.S.A., 1950.

32. V. L. Lelchuk, 'Heat Transfer and Hydraulic Flow Resistance for Streams of High Velocity', NACA Technical Note No. 1054, National Advisory Committee on Aeronautics, Washington, D.C., U.S.A., 1943.

33. F. Kreith, 'Principles of Heat Transfer', International Textbook Company, second edition, Scranton, Pennsylvania, U.S.A., 1967.

34. R. C. Makino and R. E. Shear, 'Unsteady Spherical Flow Behind a known Shock Line', BRL Report No. 1154, U.S. Army Ballistic Research Laboratory, Aberdeen Proving Ground, Maryland, U.S.A., November 1961.

35. John M. Dewey, 'The Air Velocity and Density in Blast Waves from TNT Explosions (U)', DRES Suffield Report No. 207, Defence Research Establishment Suffield, Ralston, Alberta, Canada, March 1964.

36. John M. Dewey, 'The Air Velocity in Blast Waves from TNT Explosions', Proceedings of the Royal Society, Series A, Vol. 279, pp. 366-385, 1964.

37. John M. Dewey, 'The Properties of a Blast Wave Obtained from an Analysis of the Particle Trajectories', Proceedings of the Royal Society, Series A, Vol. 324, pp. 275-299, 1971.

38. J. J. Gottlieb and D. V. Ritzel, 'Flow Properties of a Spherical Blast Wave', Proceedings of the Sixth Internation Symposium on Military Applications of Blast Simulation, Vol. 1, pp. 1.4-1 to 1.4-29, held on 25-29 June 1979 in Cahors, France, and sponsored by the Centre d'Etude de Gramat, Gramat, France.

39. J. M. Dewey and D. J. McMillin, 'The Properties of a Blast Wave Produced by a Large-Scale Detonable Gas Explosion', Proceedings of the Seventh International Symposium on Military Applications of Blast Simulation, Vol. 1, pp. 6.6-1 to 6.6-18, held on the 13-17 July 1981 in Medicine Hat, Alberta, sponsored by the Defence Research Establishment Suffield, Ralston, Alberta, Canada.

40. A. Celmins, 'Reconstruction of a Blast Field from Selected Pressure Observations,' Proceedings of the Seventh International Symposium on Military Applications of Blast Simulation, Vol. 1, pp. 2.5-1 to 2.5-17, held on the 13-17 July 1981 in Medicine Hat, Alberta, sponsored by the Defence Research Establishment Suffield, Ralston, Alberta, Canada.

41. Anon., 'Scientific Observations on the Explosion of a 20-ton TNT Charge (U)', DRES Suffield Report No. 203, Vol. 2, Defence Research Establishment Suffield, Ralston, Alberta, Canada, September 1961.

42. E. P. Popov, 'Mechanics of Materials', second edition, Prentice-Hall Inc., Englewood Cliffs, New Jersey, U.S.A., 1976.

43. W. Bleakney, D. K. White, and W. C. Griffith, 'Measurements of Diffraction of Shock Waves and Resulting Loading of Structures', Journal of Applied Mechanics, Vol. 7, pp. 439-445, 1950.

44. N. B. Brooks and N. M. Newmark, 'The Response of Simple Structures to Dynamic Loads', Structural Research Series No. 51, University of Illinois, U.S.A., 1953.

45. N. M. Newmark, 'An Engineering Approach to Blast Resistant Design', Transactions of the American Society of Civil Engineering, Vol. 121, pp. 45-55, 1956.

Table 1

Temporal variation of the flow properties of the blast wave incident on the power house, at a radius of 494.5 m.

Time (ms)	Overpressure $(p - p_1)/p_1$	Sound Speed a/a_1	Density ρ/ρ_1	Flow Velocity u/a_1
0.0000	0.1131	1.0154	1.0795	0.0772
1.0696	0.1129	1.0154	1.0794	0.0772
2.1590	0.1117	1.0153	1.0785	0.0763
3.2286	0.1115	1.0152	1.0784	0.0763
4.3180	0.1099	1.0150	1.0773	0.0753
5.3877	0.1097	1.0150	1.0772	0.0753
6.4770	0.1082	1.0148	1.0761	0.0742
7.5467	0.1070	1.0148	1.0753	0.0736
8.6360	0.1060	1.0145	1.0746	0.0730
9.7057	0.1059	1.0145	1.0745	0.0730
10.7950	0.1047	1.0143	1.0737	0.0722
11.8805	0.1046	1.0143	1.0736	0.0722
12.9541	0.1039	1.0142	1.0731	0.0718
14.0395	0.1037	1.0142	1.0730	0.0718
15.1131	0.1026	1.0141	1.0722	0.0712
16.1985	0.1021	1.0139	1.0719	0.0709
17.2721	0.1013	1.0139	1.0713	0.0704
18.3575	0.1011	1.0139	1.0712	0.0704
19.4271	0.1003	1.0138	1.0706	0.0699
20.5165	0.1003	1.0138	1.0706	0.0698
21.6059	0.0978	1.0134	1.0689	0.0683
22.6755	0.0977	1.0134	1.0688	0.0683
23.7649	0.0969	1.0133	1.0682	0.0677
24.8345	0.0949	1.0131	1.0668	0.0664
25.9239	0.0941	1.0130	1.0663	0.0660
26.9935	0.0940	1.0130	1.0662	0.0660
28.0829	0.0925	1.0127	1.0652	0.0650
29.1525	0.0924	1.0127	1.0651	0.0650
30.2419	0.0914	1.0126	1.0644	0.0643
31.3116	0.0912	1.0126	1.0643	0.0643
32.4009	0.0894	1.0123	1.0631	0.0631
33.4706	0.0882	1.0122	1.0622	0.0624
34.5599	0.0876	1.0121	1.0618	0.0620
35.6454	0.0874	1.0120	1.0617	0.0620
36.7189	0.0858	1.0119	1.0605	0.0609
37.8044	0.0857	1.0118	1.0605	0.0609
38.8740	0.0852	1.0118	1.0601	0.0605
39.9634	0.0850	1.0117	1.0600	0.0605
41.0330	0.0840	1.0116	1.0592	0.0598
42.1224	0.0835	1.0115	1.0590	0.0597
43.1920	0.0787	1.0109	1.0556	0.0565

Table 1 (continued)

Temporal variation of the flow properties of the blast wave incident on the power house, at a radius of 494.5 m.

Time (ms)	Overpressure $(p - p_1)/p_1$	Sound Speed a/a_1	Density ρ/ρ_1	Flow Velocity u/a_1
44.2814	0.0786	1.0109	1.0555	0.0565
45.3510	0.0778	1.0108	1.0549	0.0559
46.4404	0.0776	1.0107	1.0548	0.0559
47.5100	0.0765	1.0106	1.0541	0.0552
48.5994	0.0764	1.0106	1.0540	0.0552
49.6691	0.0757	1.0105	1.0535	0.0548
50.7584	0.0756	1.0105	1.0534	0.0548
51.8280	0.0737	1.0102	1.0521	0.0535
52.9174	0.0736	1.0102	1.0520	0.0535
53.9871	0.0727	1.0101	1.0514	0.0529
55.0764	0.0727	1.0101	1.0514	0.0528
56.1461	0.0705	1.0098	1.0498	0.0515
57.2354	0.0704	1.0098	1.0498	0.0515
58.3051	0.0699	1.0097	1.0494	0.0510
59.3945	0.0687	1.0095	1.0486	0.0503
60.4641	0.0683	1.0095	1.0483	0.0501
61.5535	0.0682	1.0095	1.0482	0.0501
62.6231	0.0672	1.0094	1.0475	0.0494
63.7125	0.0671	1.0093	1.0475	0.0494
64.7821	0.0648	1.0090	1.0458	0.0478
65.8715	0.0647	1.0090	1.0458	0.0478
66.9411	0.0633	1.0088	1.0448	0.0470
68.0266	0.0622	1.0087	1.0440	0.0462
69.1001	0.0621	1.0087	1.0439	0.0461
70.1856	0.0620	1.0087	1.0438	0.0461
71.2591	0.0609	1.0085	1.0431	0.0455
72.3446	0.0608	1.0085	1.0430	0.0455
73.4181	0.0602	1.0084	1.0426	0.0450
74.5036	0.0601	1.0084	1.0425	0.0450
75.5732	0.0586	1.0082	1.0415	0.0440
76.6626	0.0579	1.0081	1.0410	0.0436
77.7322	0.0564	1.0079	1.0400	0.0426
78.8216	0.0563	1.0079	1.0399	0.0426
79.8912	0.0559	1.0078	1.0396	0.0423
80.9806	0.0558	1.0078	1.0395	0.0423
82.0502	0.0533	1.0074	1.0378	0.0407
83.1396	0.0532	1.0074	1.0377	0.0407
84.2290	0.0530	1.0074	1.0375	0.0405
85.2986	0.0525	1.0073	1.0372	0.0402
86.3880	0.0521	1.0073	1.0369	0.0401

Table 1 (continued)

Temporal variation of the flow properties of the blast wave incident on the power house, at a radius of 494.5 m.

Time (ms)	Overpressure $(p - p_1)/p_1$	Sound Speed a/a_1	Density ρ/ρ_1	Flow Velocity u/a_1
87.4576	0.0521	1.0073	1.0369	0.0401
88.5470	0.0505	1.0071	1.0358	0.0390
89.6166	0.0504	1.0071	1.0357	0.0390
90.7060	0.0489	1.0069	1.0346	0.0379
91.7757	0.0488	1.0068	1.0346	0.0379
92.8650	0.0480	1.0067	1.0340	0.0373
93.9347	0.0472	1.0066	1.0335	0.0368
95.0240	0.0470	1.0066	1.0333	0.0367
96.0937	0.0469	1.0066	1.0332	0.0367
97.1791	0.0467	1.0066	1.0331	0.0364
98.2685	0.0466	1.0066	1.0330	0.0364
99.3381	0.0436	1.0061	1.0309	0.0344
100.4275	0.0435	1.0061	1.0309	0.0344
101.4971	0.0425	1.0060	1.0301	0.0336
102.5865	0.0423	1.0060	1.0300	0.0336
103.6561	0.0421	1.0060	1.0298	0.0335
104.7455	0.0420	1.0059	1.0298	0.0335
105.8151	0.0415	1.0059	1.0294	0.0330
106.9045	0.0414	1.0058	1.0294	0.0330
107.9741	0.0409	1.0058	1.0290	0.0326
109.0635	0.0408	1.0057	1.0290	0.0326
110.1332	0.0383	1.0054	1.0272	0.0309
111.2225	0.0369	1.0052	1.0262	0.0300
112.2922	0.0360	1.0051	1.0255	0.0294
113.3815	0.0359	1.0051	1.0255	0.0294
114.4709	0.0344	1.0049	1.0244	0.0286
115.5406	0.0344	1.0049	1.0244	0.0286
116.6259	0.0337	1.0048	1.0239	0.0281
117.6996	0.0337	1.0048	1.0239	0.0281
118.7850	0.0334	1.0047	1.0237	0.0281
119.8586	0.0334	1.0047	1.0237	0.0281
120.9440	0.0329	1.0046	1.0234	0.0279
122.0176	0.0329	1.0046	1.0233	0.0279
123.1030	0.0323	1.0046	1.0229	0.0276
124.1726	0.0322	1.0046	1.0228	0.0276
125.2620	0.0304	1.0043	1.0216	0.0265
126.3316	0.0304	1.0043	1.0216	0.0265
127.4210	0.0298	1.0042	1.0212	0.0262
128.4906	0.0293	1.0042	1.0208	0.0259
129.5800	0.0276	1.0039	1.0196	0.0248

Table 1 (continued)

Temporal variation of the flow properties of the blast wave incident on the power house, at a radius of 494.5 m.

Time (ms)	Overpressure $(p - p_1)/p_1$	Sound Speed a/a_1	Density ρ/ρ_1	Flow Velocity u/a_1
130.6694	0.0276	1.0039	1.0196	0.0248
131.7390	0.0265	1.0038	1.0188	0.0241
132.8087	0.0265	1.0038	1.0188	0.0241
133.8980	0.0252	1.0036	1.0179	0.0233
134.9677	0.0252	1.0036	1.0179	0.0233
136.0570	0.0247	1.0035	1.0175	0.0231
137.1464	0.0231	1.0033	1.0164	0.0221
138.2160	0.0228	1.0032	1.0162	0.0219
139.3054	0.0227	1.0032	1.0161	0.0219
140.3751	0.0221	1.0031	1.0157	0.0215
141.4644	0.0220	1.0031	1.0157	0.0216
142.5341	0.0207	1.0030	1.0147	0.0206
143.6195	0.0206	1.0029	1.0147	0.0206
144.6931	0.0188	1.0027	1.0134	0.0194
145.7785	0.0185	1.0027	1.0131	0.0193
146.8521	0.0181	1.0026	1.0129	0.0191
147.9375	0.0181	1.0026	1.0128	0.0191
149.0111	0.0174	1.0025	1.0124	0.0187
150.0965	0.0174	1.0025	1.0124	0.0187
151.1701	0.0169	1.0024	1.0120	0.0183
152.2555	0.0168	1.0024	1.0119	0.0183
153.3251	0.0163	1.0023	1.0116	0.0181
154.4145	0.0162	1.0023	1.0115	0.0181
155.4842	0.0151	1.0022	1.0107	0.0173
156.5735	0.0150	1.0021	1.0107	0.0173
157.6432	0.0137	1.0020	1.0097	0.0165
158.7325	0.0136	1.0019	1.0097	0.0165
159.8219	0.0129	1.0018	1.0092	0.0161
160.8916	0.0129	1.0018	1.0091	0.0161
161.9809	0.0114	1.0016	1.0081	0.0150
163.0506	0.0114	1.0016	1.0081	0.0150
164.1399	0.0100	1.0014	1.0071	0.0141
165.2096	0.0100	1.0014	1.0071	0.0141
166.2990	0.0093	1.0013	1.0066	0.0137
167.3686	0.0092	1.0013	1.0065	0.0137
168.4579	0.0088	1.0012	1.0063	0.0135
169.5276	0.0088	1.0012	1.0062	0.0135
170.6170	0.0080	1.0011	1.0057	0.0130
171.6866	0.0080	1.0011	1.0056	0.0130
172.7720	0.0069	1.0010	1.0049	0.0123

Table 1 (continued)

Temporal variation of the flow properties of the blast wave incident on the power house, at a radius of 494.5 m.

Time (ms)	Overpressure $(p - p_1)/p_1$	Sound Speed a/a_1	Density ρ/ρ_1	Flow Velocity u/a_1
173.8614	0.0069	1.0010	1.0049	0.0123
174.9310	0.0065	1.0009	1.0046	0.0121
176.0204	0.0064	1.0009	1.0045	0.0121
177.0901	0.0054	1.0008	1.0038	0.0114
178.1794	0.0054	1.0008	1.0038	0.0114
179.2491	0.0052	1.0007	1.0037	0.0114
180.3384	0.0039	1.0005	1.0028	0.0105
181.4081	0.0038	1.0005	1.0027	0.0104
182.4975	0.0038	1.0005	1.0026	0.0104
183.5671	0.0028	1.0004	1.0020	0.0098
184.6564	0.0027	1.0004	1.0019	0.0098
185.7261	0.0023	1.0003	1.0016	0.0096
186.8155	0.0023	1.0003	1.0016	0.0096
187.8851	0.0021	1.0003	1.0014	0.0095
188.9745	0.0021	1.0003	1.0014	0.0095
190.0441	0.0006	1.0001	1.0004	0.0085
191.1335	0.0006	1.0001	1.0004	0.0085
192.2031	-0.0002	1.0000	0.9998	0.0079
193.2925	-0.0003	0.9999	0.9998	0.0079
194.3621	-0.0017	0.9997	0.9988	0.0070
195.4515	-0.0017	0.9997	0.9988	0.0070
196.5211	-0.0020	0.9997	0.9985	0.0068
197.6105	-0.0031	0.9996	0.9977	0.0060
198.6801	-0.0047	0.9993	0.9966	0.0049
199.7656	-0.0047	0.9993	0.9966	0.0049
200.8392	-0.0057	0.9992	0.9959	0.0042
201.9246	-0.0058	0.9992	0.9958	0.0042
202.9982	-0.0066	0.9990	0.9953	0.0037
204.0836	-0.0066	0.9990	0.9953	0.0037
205.1572	-0.0072	0.9990	0.9948	0.0033
206.2426	-0.0077	0.9989	0.9945	0.0030
207.3320	-0.0078	0.9989	0.9944	0.0030
208.4016	-0.0078	0.9989	0.9944	0.0030

Table 2

Spatial variation of the flow properties of the blast wave incident on the power house.

Distance (m)	Overpressure $(p - p_1)/p_1$	Flow Velocity u/a_1	Density ρ/ρ_1
494.51	0.11315	0.07716	1.07954
493.87	0.11196	0.07643	1.07871
493.23	0.11036	0.07549	1.07760
492.59	0.10881	0.07455	1.07653
491.94	0.10774	0.07391	1.07579
491.30	0.10681	0.07346	1.07514
490.66	0.10567	0.07278	1.07435
490.02	0.10497	0.07248	1.07387
489.38	0.10393	0.07186	1.07314
488.74	0.10348	0.07172	1.07283
488.10	0.10264	0.07124	1.07224
487.45	0.10190	0.07085	1.07173
486.81	0.09948	0.06932	1.07005
486.17	0.09864	0.06882	1.06946
485.53	0.09666	0.06767	1.06809
484.89	0.09599	0.06729	1.06762
484.25	0.09446	0.06634	1.06656
483.61	0.09347	0.06578	1.06586
482.96	0.09166	0.06463	1.06460
482.32	0.09039	0.06394	1.06372
481.68	0.08984	0.06363	1.06333
481.04	0.08809	0.06263	1.06212
480.40	0.08757	0.06233	1.06175
479.76	0.08645	0.06174	1.06097
479.12	0.08613	0.06159	1.06075
478.47	0.08111	0.05839	1.05725
477.83	0.08028	0.05788	1.05666
477.19	0.07914	0.05727	1.05587
476.55	0.07846	0.05686	1.05539
475.91	0.07649	0.05563	1.05401
475.27	0.07566	0.05512	1.05343
474.63	0.07347	0.05368	1.05190
473.98	0.07285	0.05341	1.05147
473.34	0.07172	0.05270	1.05068
472.70	0.07128	0.05253	1.05037
472.06	0.07023	0.05188	1.04963
471.42	0.06783	0.05040	1.04795
470.78	0.06642	0.04949	1.04696
470.14	0.06530	0.04881	1.04618
469.49	0.06520	0.04878	1.04610

Table 2 (continued)

Spatial variation of the flow properties of the blast wave incident on the power house.

Distance (m)	Overpressure $(p - p_1)/p_1$	Flow Velocity u/a_1	Density ρ/ρ_1
468.85	0.06417	0.04811	1.04538
468.21	0.06337	0.04771	1.04482
467.57	0.06193	0.04677	1.04381
466.93	0.06114	0.04637	1.04325
466.29	0.05963	0.04538	1.04219
465.65	0.05914	0.04518	1.04185
465.00	0.05655	0.04346	1.04002
464.36	0.05626	0.04333	1.03982
463.72	0.05553	0.04287	1.03931
463.08	0.05390	0.04177	1.03816
462.44	0.05222	0.04075	1.03698
461.80	0.05130	0.04015	1.03633
461.16	0.05040	0.03955	1.03569
460.51	0.05008	0.03941	1.03547
459.87	0.04850	0.03834	1.03436
459.23	0.04692	0.03726	1.03325
458.59	0.04570	0.03655	1.03238
457.95	0.04559	0.03650	1.03231
457.31	0.04538	0.03642	1.03216
456.67	0.04481	0.03605	1.03175
456.02	0.04422	0.03565	1.03134
455.38	0.04147	0.03387	1.02940
454.74	0.04006	0.03293	1.02840
454.10	0.03904	0.03234	1.02768
453.46	0.03756	0.03134	1.02663
452.82	0.03698	0.03091	1.02622
452.18	0.03676	0.03087	1.02607
451.53	0.03638	0.03064	1.02580
450.89	0.03579	0.03028	1.02538
450.25	0.03396	0.02902	1.02409
449.61	0.03347	0.02868	1.02374
448.97	0.03292	0.02841	1.02335
448.33	0.03112	0.02719	1.02208
447.69	0.02999	0.02651	1.02127
447.04	0.02869	0.02563	1.02036
446.40	0.02819	0.02539	1.02000
445.76	0.02649	0.02421	1.01880
445.12	0.02619	0.02405	1.01858
444.48	0.02560	0.02365	1.01816
443.84	0.02419	0.02265	1.01716

Table 2 (continued)

Spatial variation of the flow properties of the blast wave incident on the power house.

Distance (m)	Overpressure $(p - p_1)/p_1$	Flow Velocity u/a_1	Density ρ/ρ_1
443.20	0.02219	0.02137	1.01574
442.55	0.02184	0.02112	1.01549
441.91	0.02079	0.02050	1.01475
441.27	0.02028	0.02015	1.01439
440.63	0.01971	0.01986	1.01398
439.99	0.01845	0.01897	1.01308
439.35	0.01701	0.01801	1.01206
438.71	0.01625	0.01747	1.01152
438.07	0.01467	0.01634	1.01040
437.42	0.01312	0.01536	1.00930
436.78	0.01241	0.01485	1.00879
436.14	0.01203	0.01457	1.00852
435.50	0.01117	0.01400	1.00791
434.86	0.01003	0.01317	1.00709
434.22	0.00956	0.01294	1.00676
433.58	0.00851	0.01219	1.00601
432.93	0.00831	0.01215	1.00587
432.29	0.00683	0.01109	1.00481
431.65	0.00666	0.01107	1.00469
431.01	0.00562	0.01032	1.00395
430.37	0.00512	0.01007	1.00359
429.73	0.00494	0.00992	1.00347
429.09	0.00327	0.00883	1.00227
428.44	0.00234	0.00816	1.00161
427.80	0.00078	0.00707	1.00050
427.16	0.00047	0.00684	1.00027
426.52	-0.00082	0.00588	0.99935
425.88	-0.00378	0.00385	0.99723
425.24	-0.00468	0.00318	0.99659
424.60	-0.00548	0.00270	0.99602
423.95	-0.00595	0.00235	0.99568
423.31	-0.00609	0.00233	0.99558
422.67	-0.00629	0.00216	0.99544
422.03	-0.00737	0.00139	0.99466
421.39	-0.00803	0.00090	0.99419
420.75	-0.00820	0.00067	0.99407
420.11	-0.00872	0.00025	0.99370
419.46	-0.00901	0.00013	0.99349
418.82	-0.00990	-0.00055	0.99285
418.18	-0.01059	-0.00095	0.99236

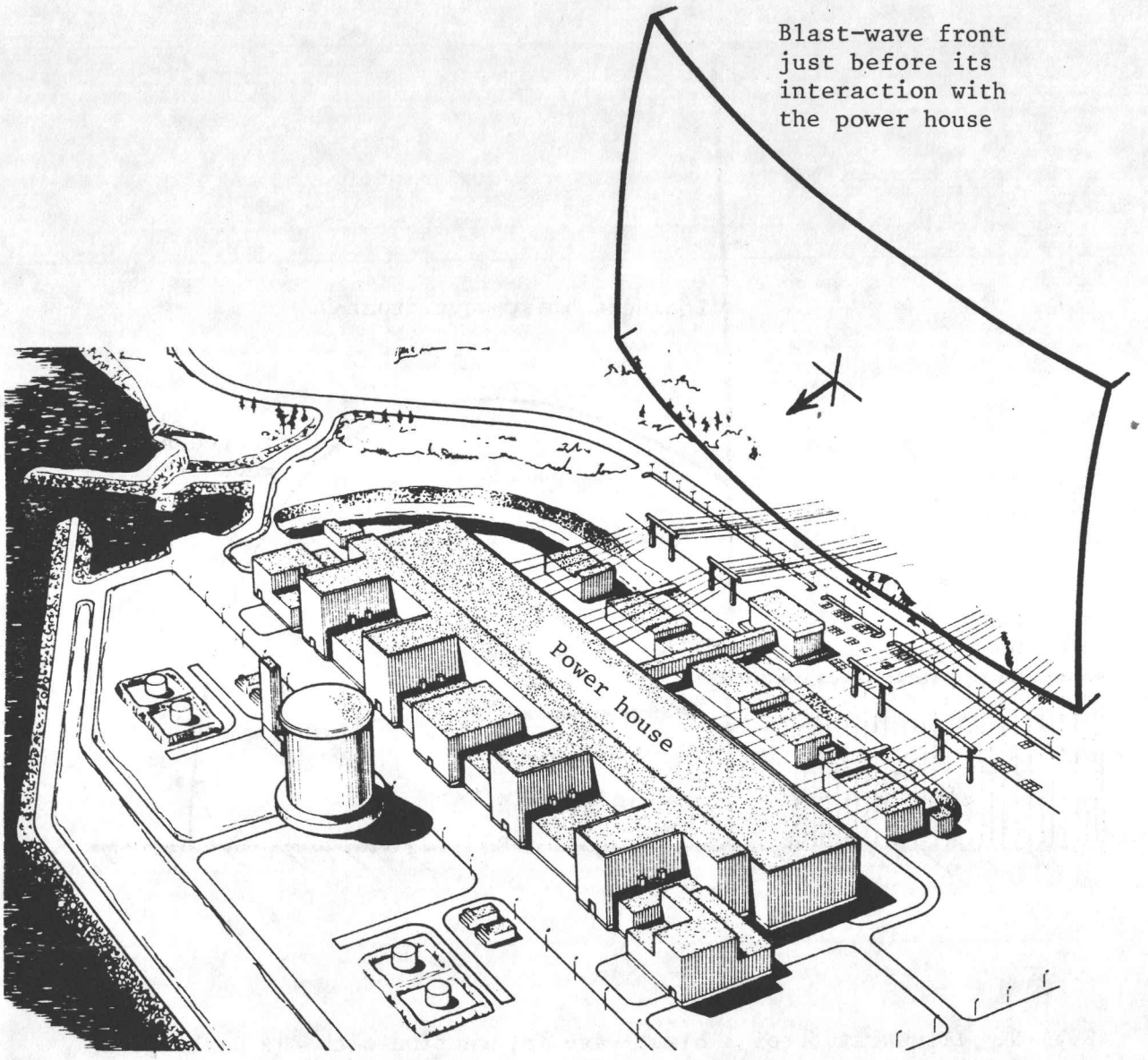

Fig. 1. Illustration of the Darlington Generating Station, showing an incident blast-wave front from a hypothetical explosion at the Canadian National Railroad tracks (not shown here).

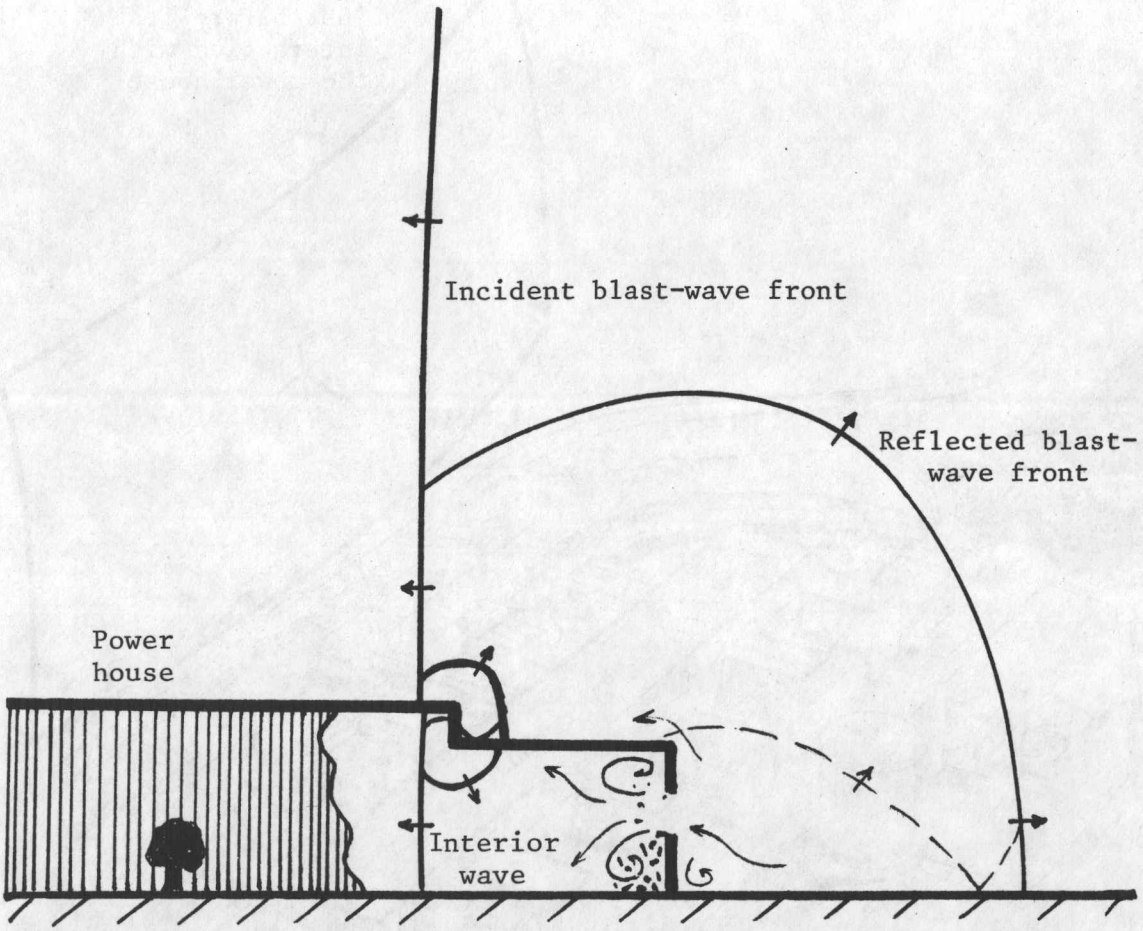

Fig. 2. Illustration of a blast wave interaction with the Darlington Generating Station power house, depicting the incident wave and reflected waves outside the power house, as well as the wave inside the building which entered through the blow-out panel openings.

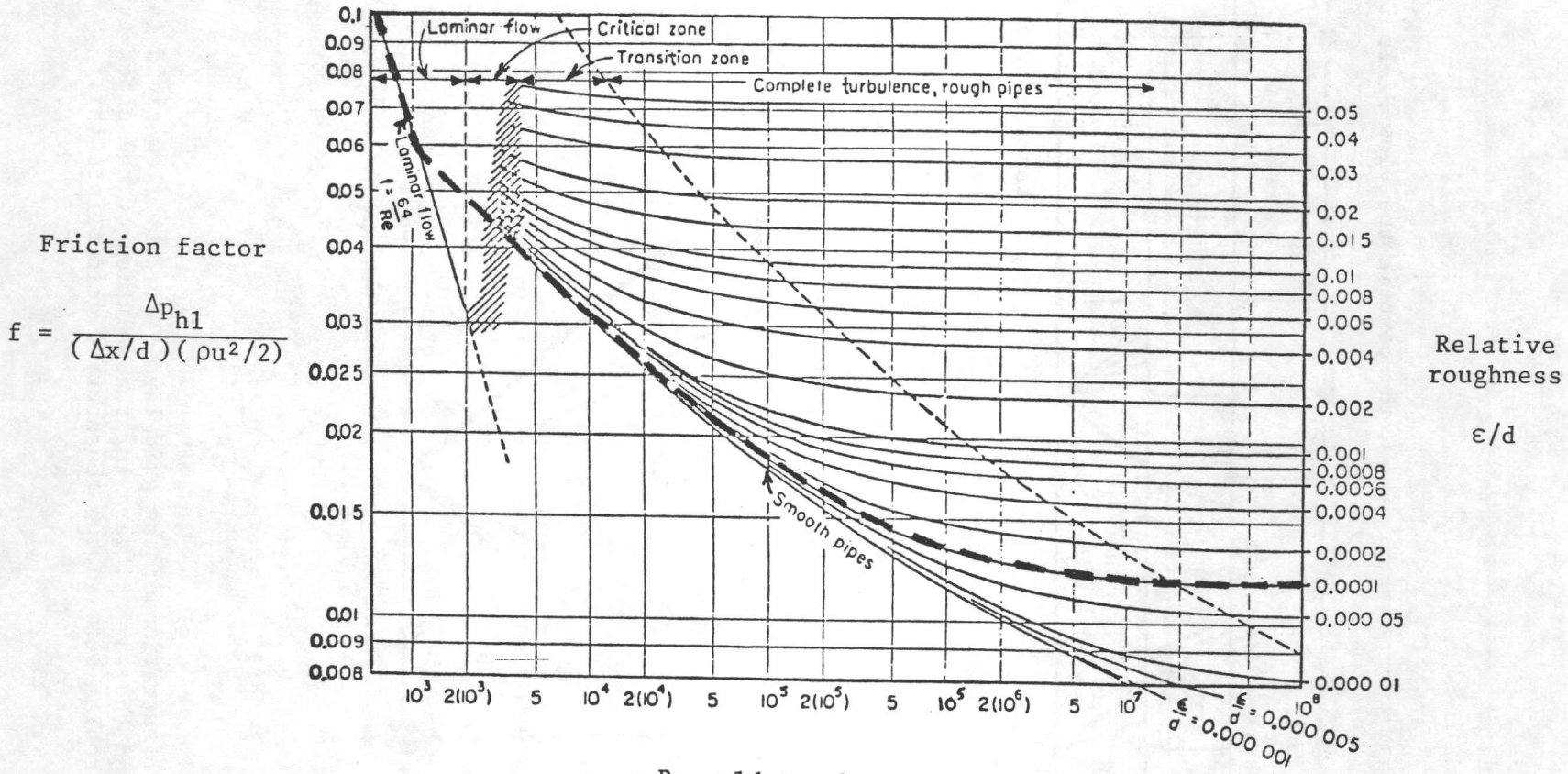

Fig. 3. Darcy-Weisbach friction factor for laminar and turbulent pipe flows [27]. Note that the solid lines in the turbulent-flow region are given by Colebrook's semi-empirical expression

$$\frac{1}{\sqrt{f}} = -2 \log \left(\frac{2.51}{Re \sqrt{f}} + \frac{\epsilon}{3.7d} \right)$$

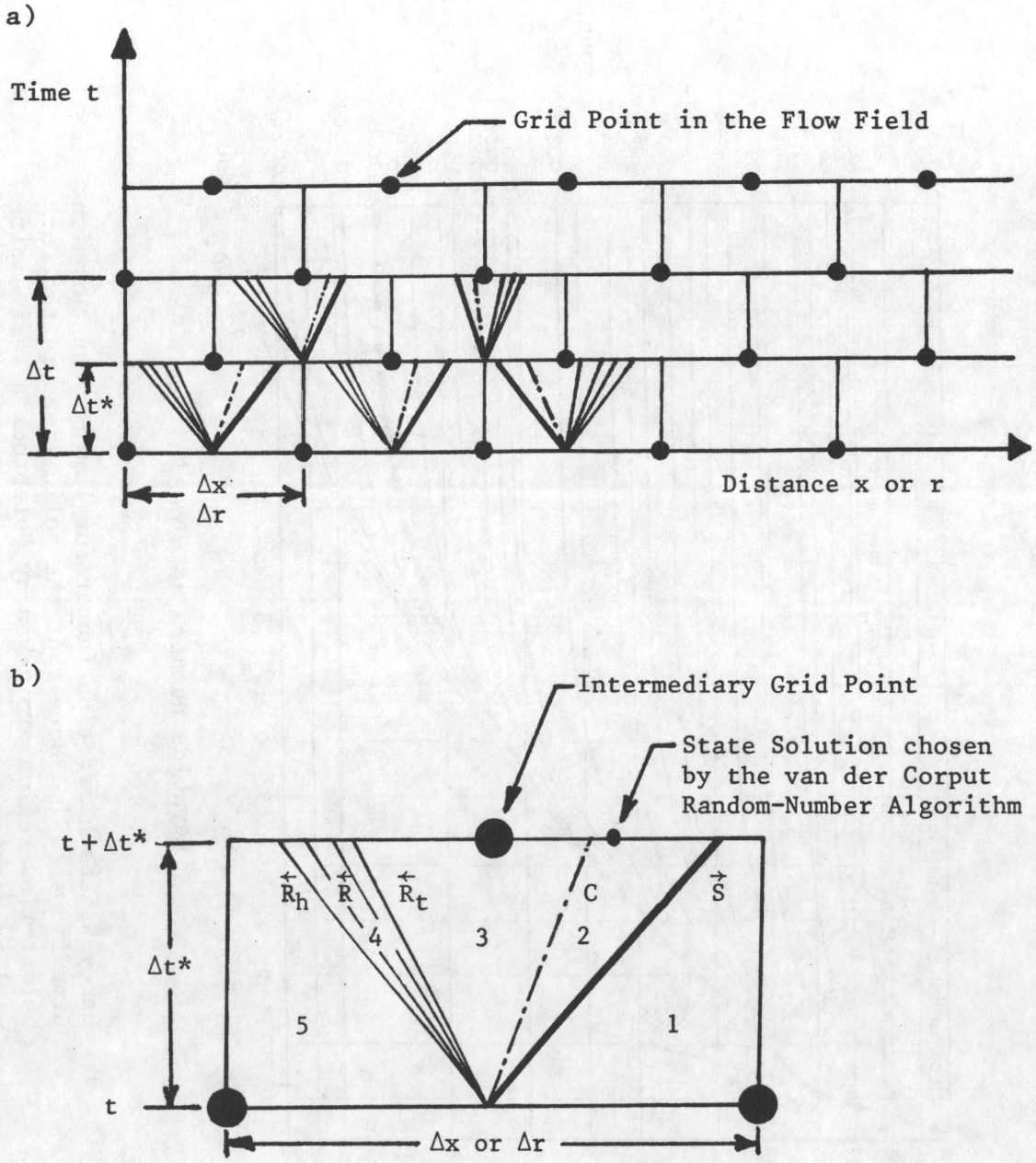

Fig. 4. Illustration of the grid layout for the flow field (a) and the wave pattern for the solution of the shock-tube problem between two consecutive grid points (b).

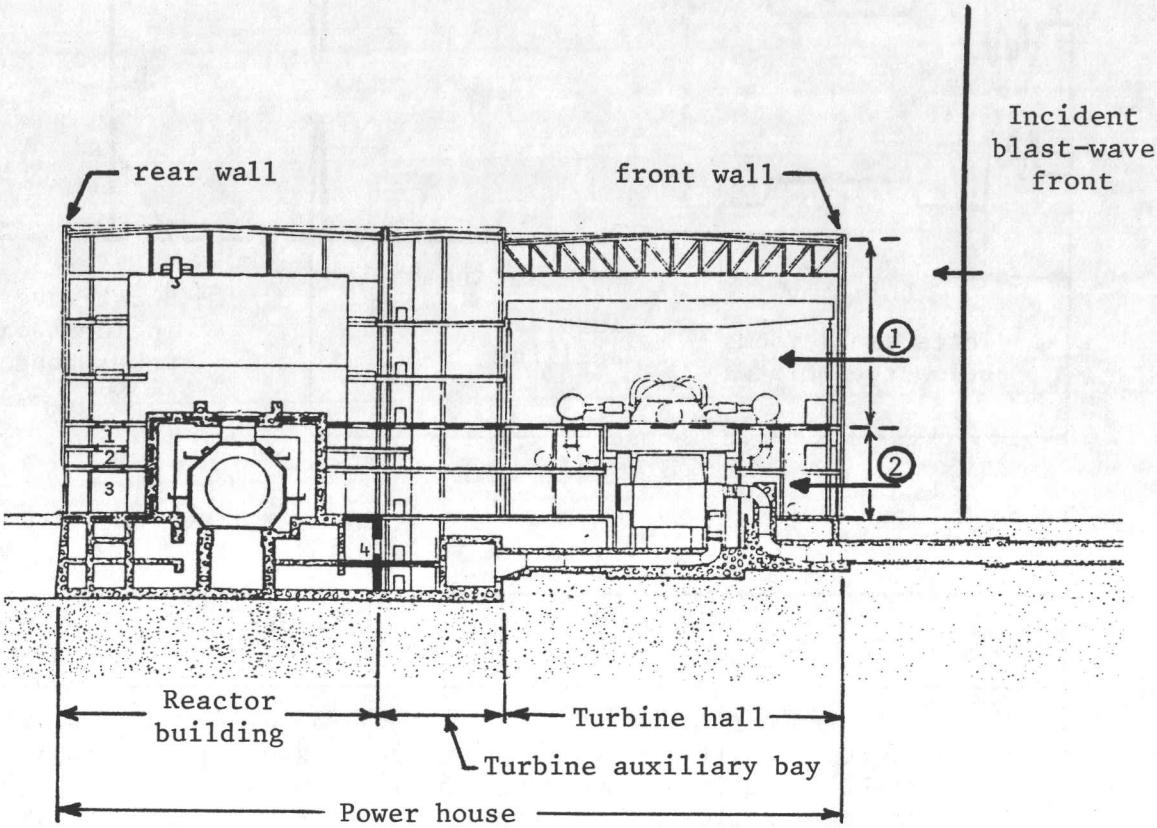

① Flow path 1 for the blast-wave flow inside the power house

② Flow path 2 for the blast-wave flow inside the power house

1, 2, 3 Three small rooms below the hoistway, at the left of the power house shown above

4 Opening in the blast wall between the turbine auxiliary bay and the reactor building, near the bottom of the power house

Fig. 5. Side view of the Darlington Generating Station power house.

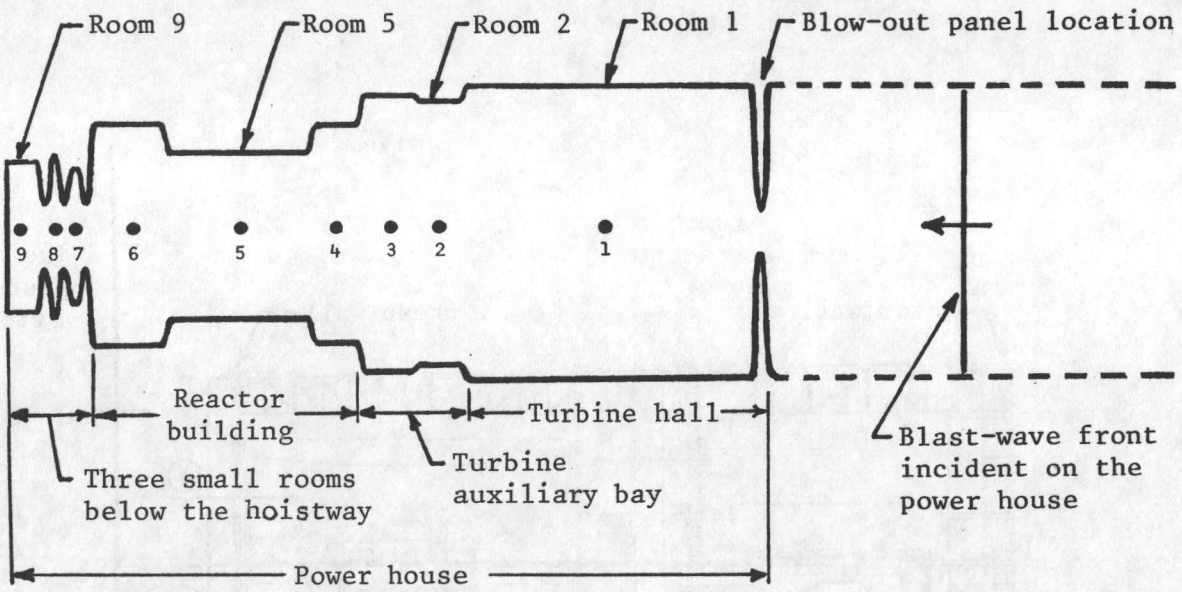

Room number	Room description	Length (m)	Cross-sectional area (m^2)
1	Turbine hall	54.0	2,597
2	Turbine auxiliary bay (region 1)	9.0	2,112
3	Turbine auxiliary bay (region 2)	10.5	2,244
4	Reactor building (region 1)	9.0	1,294
5	Reactor building (region 2)	27.0	697
6	Reactor building (region 3)	14.5	1,367
7	First room below hoistway	4.0	431
8	Second room below hoistway	3.5	670
9	Third room below hoistway	7.5	560

Minimum area between:	
outside and room 1 (blow-out panels)	linearly increasing with time from 0 to 2,016 m^2
rooms 6 and 7	40.6 m^2
rooms 7 and 8	40.6 m^2
rooms 8 and 9	40.6 m^2
Area of the front wall of the building associated with flow path number 1	2,691 m^2

Fig. 6. Geometrical configuration A for flow path number 1 in the upper part of the power house. The three small rooms below the hoistway are included at the end of the flow path, with their original lengths and cross-sectional areas.

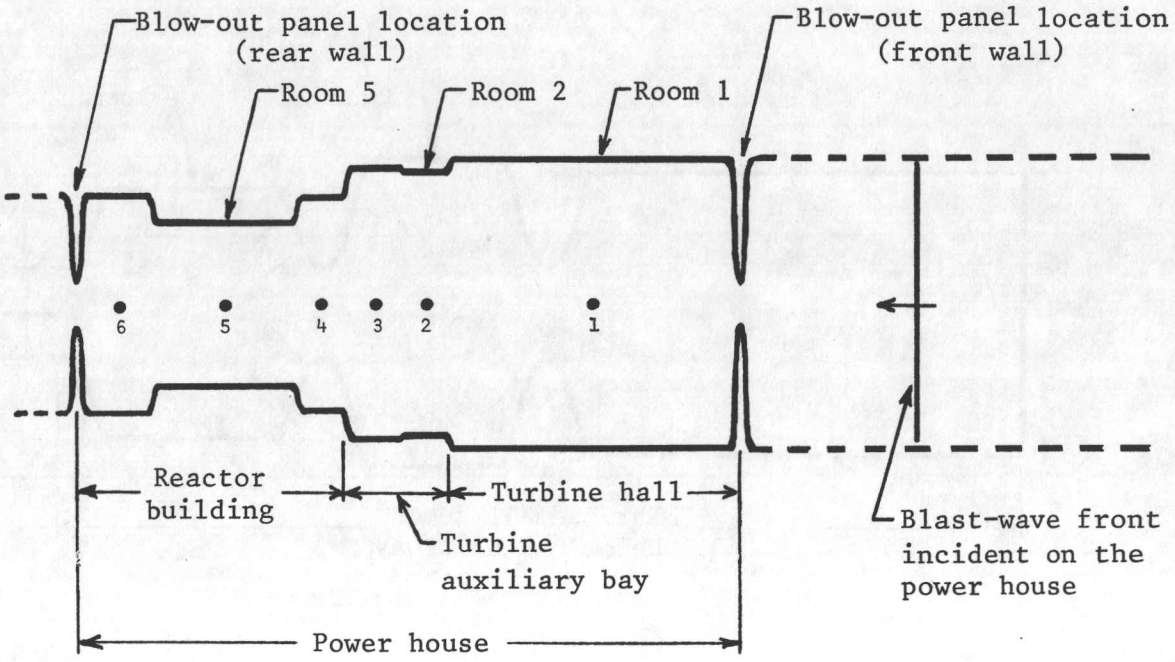

Room number	Room description	Length (m)	Cross-sectional area (m^2)
1	Turbine hall	54.0	2,597
2	Turbine auxiliary bay (region 1)	9.0	2,112
3	Turbine auxiliary bay (region 2)	10.5	2,244
4	Reactor building (region 1)	9.0	1,294
5	Reactor building (region 2)	27.0	697
6	Reactor building (region 3)	14.5	1,367

Minimum area of blow-out panels in the front wall	linearly increasing with time from 0 to 2,016 m^2
Minimum area of blow-out panels in the rear wall	linearly increasing with time from 0 to 915 m^2
Area of the front and rear walls of the power house associated with flow path number 1	2,691 m^2

Fig. 7. Geometrical configuration B for flow path number 1 in the upper part of the power house. The three small rooms are excluded from the flow path, and the blow-out panels in the rear wall of the power house are allowed to break and open.

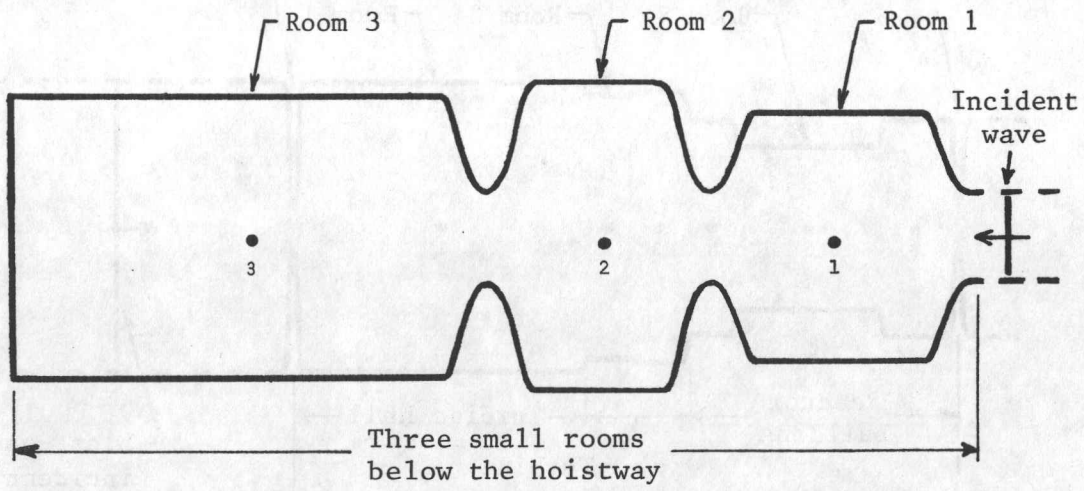

Room number	Room description	Length (m)	Cross-sectional area (m^2)
1	First room below hoistway	4.0	431
2	Second room below hoistway	3.5	670
3	Third room below hoistway	7.5	560

Minimum area between:	
outside and room 1 (entrance)	40.6 m^2
rooms 1 and 2	40.6 m^2
rooms 2 and 3	40.6 m^2

Fig. 8. Geometrical configuration C for the three small rooms below the hoistway.

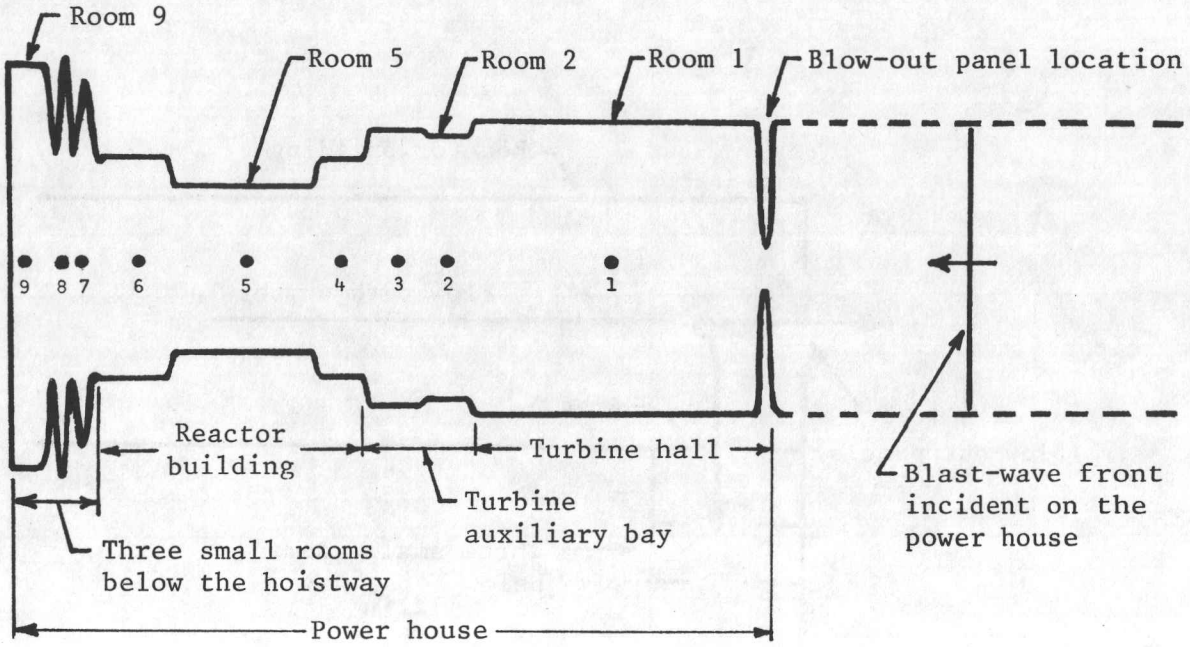

Room number	Room description	Length (m)	Cross-sectional area (m^2)
1	Turbine hall	54.0	2,597
2	Turbine auxiliary bay (region 1)	9.0	2,112
3	Turbine auxiliary bay (region 2)	10.5	2,244
4	Reactor building (region 1)	9.0	1,294
5	Reactor building (region 2)	27.0	697
6	Reactor building (region 3)	14.5	1,367
7	First room below hoistway	4.0	10,131
8	Second room below hoistway	3.5	15,767
9	Third room below hoistway	7.5	13,171

Minimum area between:	
outside and room 1 (blow-out panels)	linearly increasing with time from 0 to 2,016 m^2
rooms 6 and 7	950 m^2
rooms 7 and 8	950 m^2
rooms 8 and 9	950 m^2
Area of the front wall of the power house associated with flow path number 1	2,691 m^2

Fig. 9. Geometrical configuration D for flow path number 1 in the upper part of the power house. The three small rooms below the hoistway are included at the end of the flow path, with their original lengths but much larger cross-sectional areas.

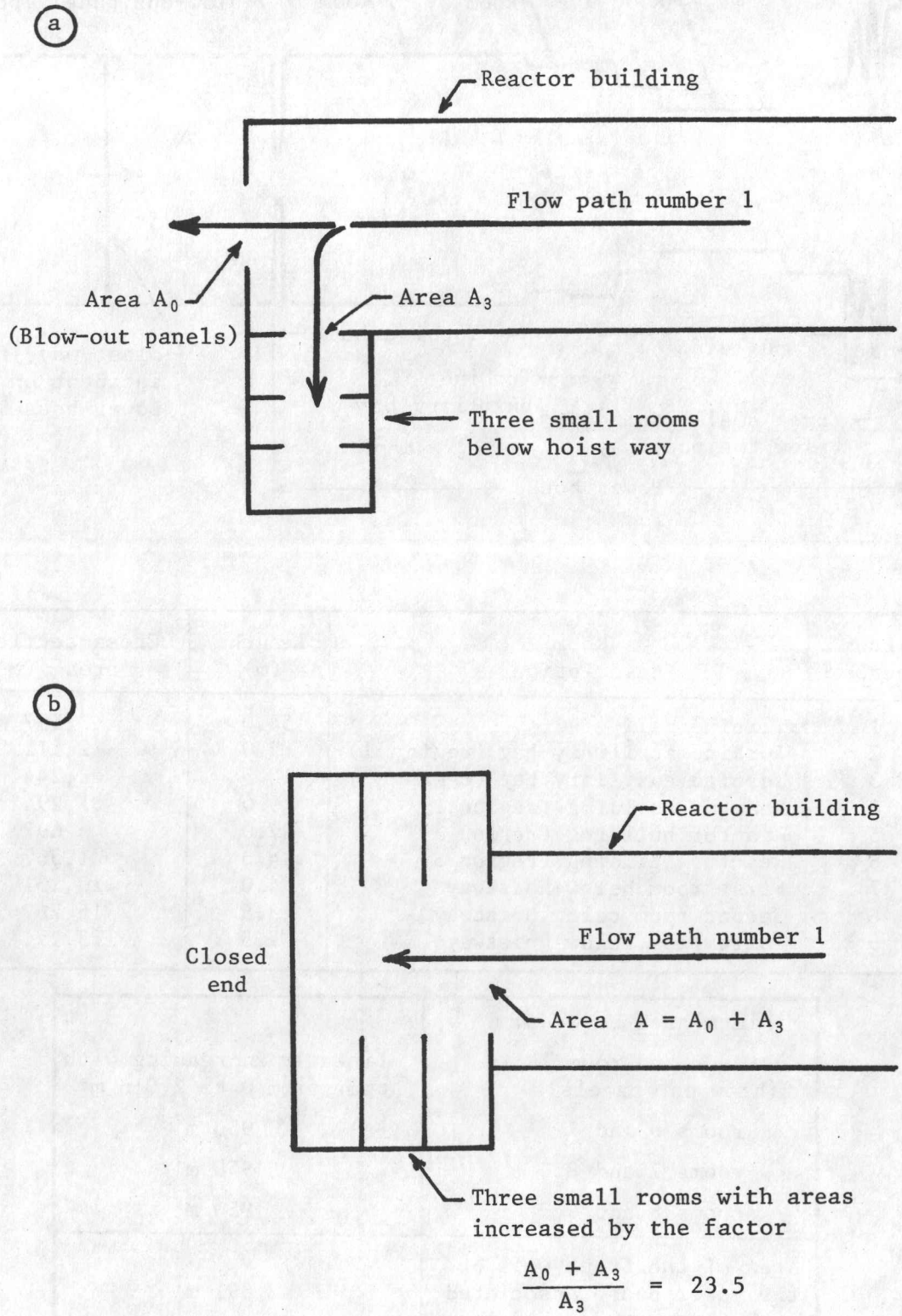

Fig. 10. Illustration of how the branched flow path to the outside of the reactor building and to the three small rooms (a) is changed to a single flow path to the three small rooms with modified cross-sectional areas (b) for the one-dimensional numerical analysis, in order to get a realistic estimate of the blast-wave flow in these three small rooms for geometrical configuration D.

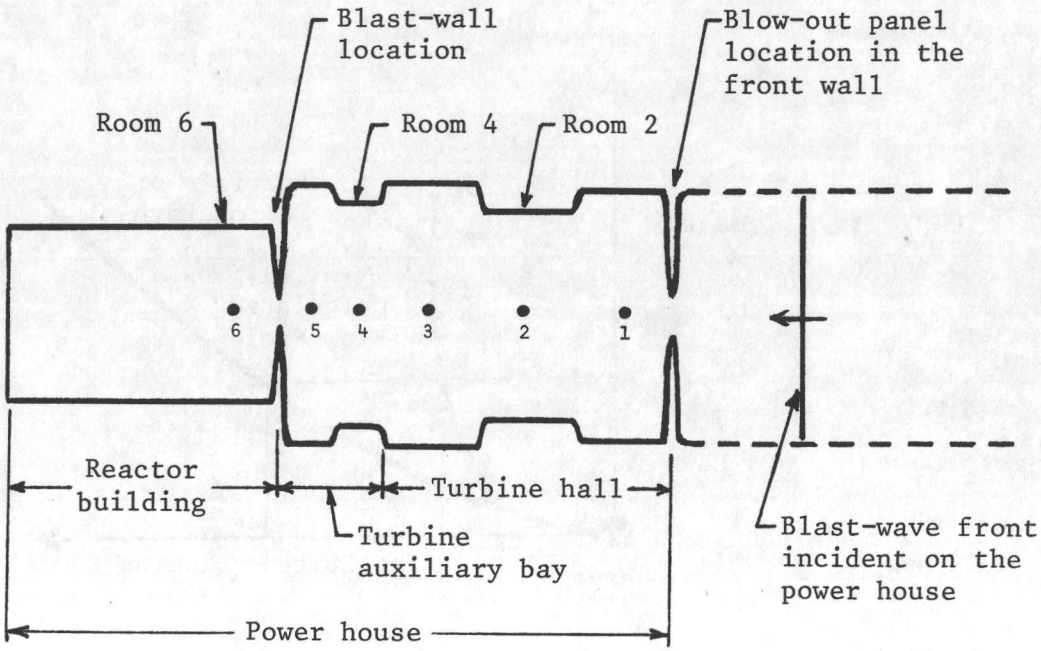

Room number	Room description	Length (m)	Cross-sectional area (m^2)
1	Turbine hall (region 1)	18.0	999
2	Turbine hall (region 2)	18.0	675
3	Turbine hall (region 3)	18.0	1,134
4	Turbine auxiliary bay (region 1)	9.0	783
5	Turbine auxiliary bay (region 2)	10.5	1,094
6	Reactor building	50.5	459

Minimum area of blow-out panels in the front wall	linearly increasing with time from 0 to 887 m^2
Minimum area in the blast wall between rooms 5 and 6	26 m^2
Area of the front wall of the power house associated with flow path number 2	1,350 m^2

Fig. 11. Geometrical configuration E for flow path 2 in the lower part of the power house, which contains a small opening in the blast wall between the turbine auxiliary bay and the reactor building.

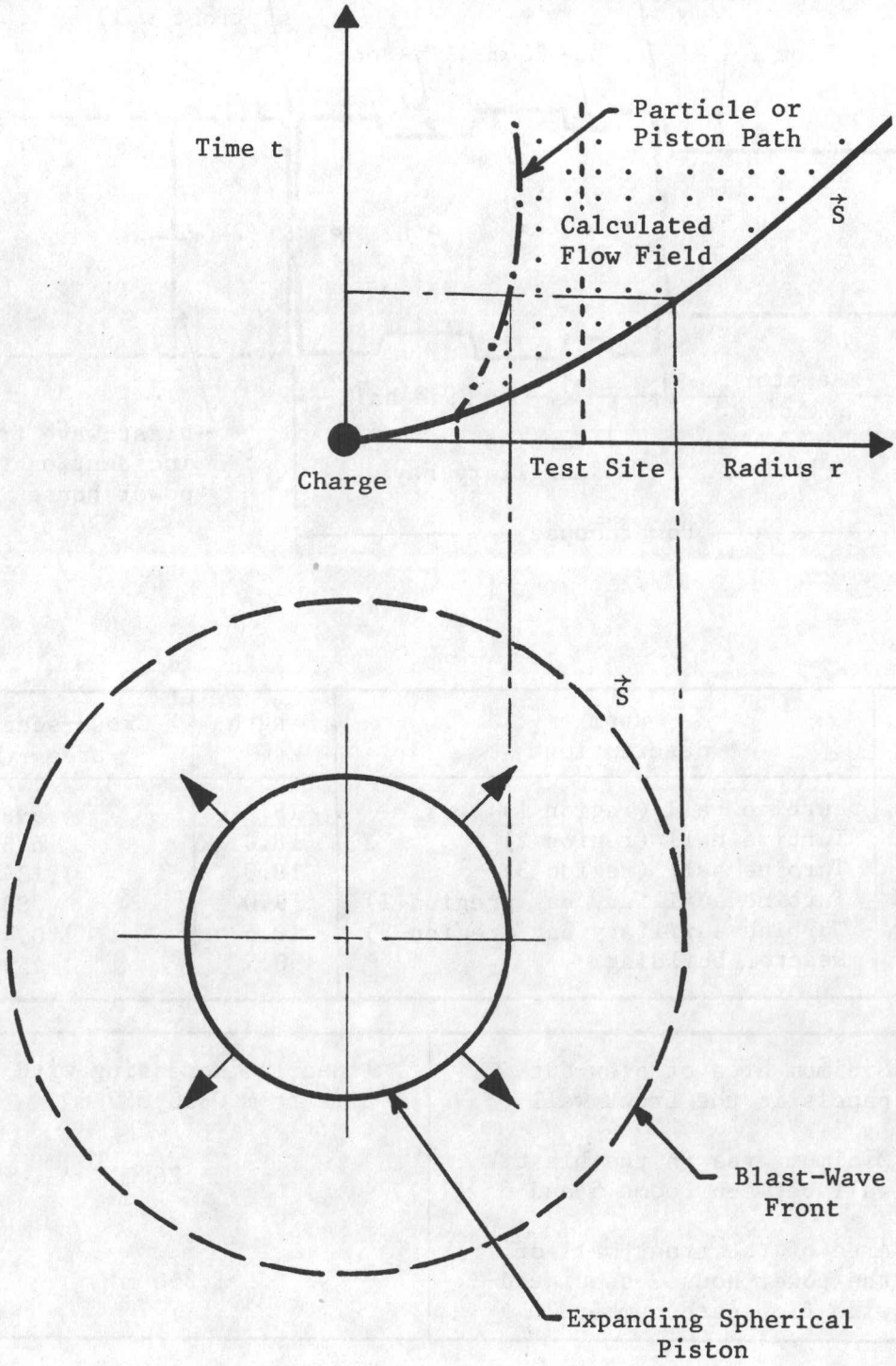

Fig. 12. Explosion flow field produced by an expanding spherical piston.

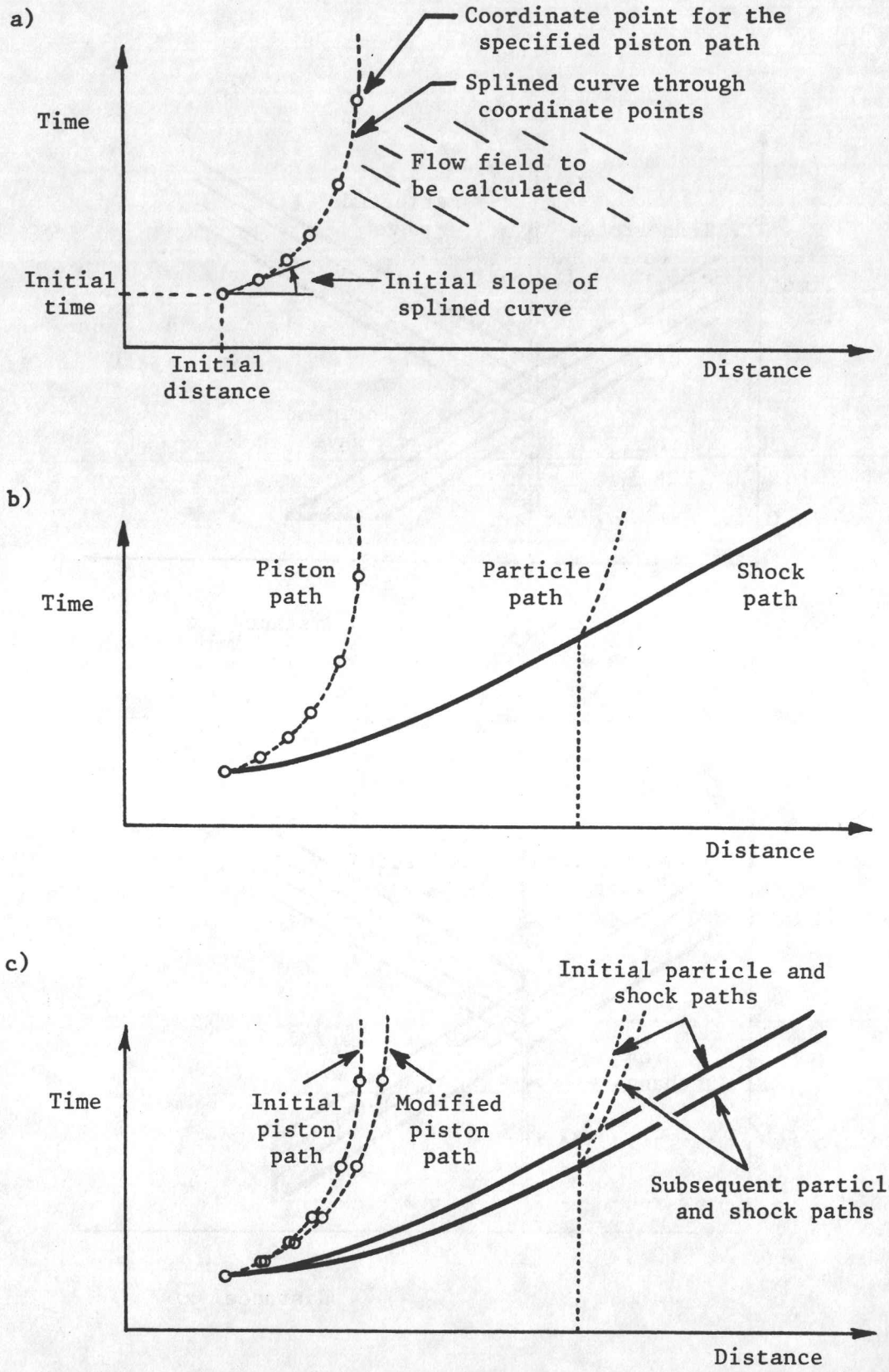

Fig. 13. Illustration of the initial guess of the coordinate points for the piston path and the splined curve (a), resulting prediction of the flow field in front of the moving piston (b), and the first modification to the piston path that gives the modified flow field.

a)

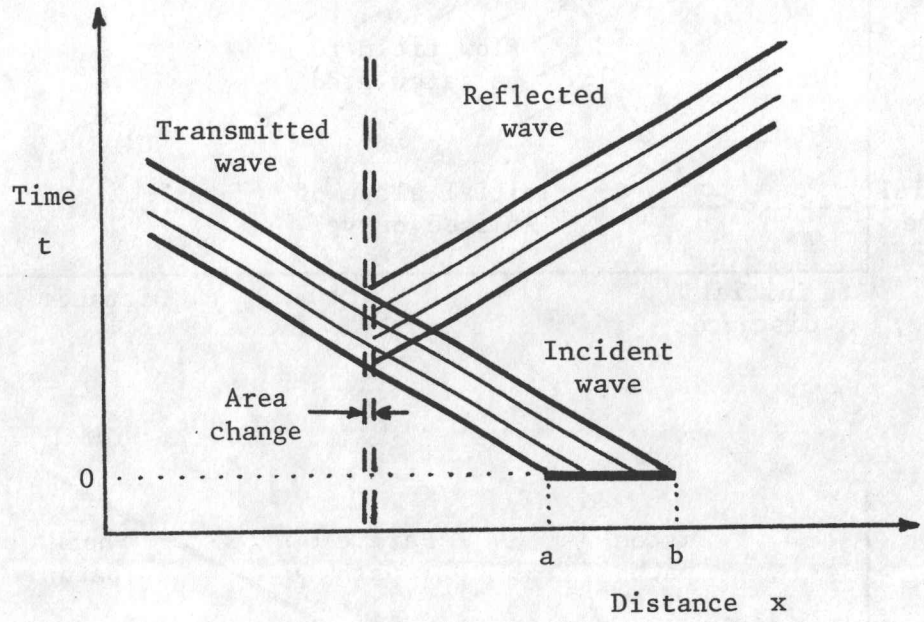

b)

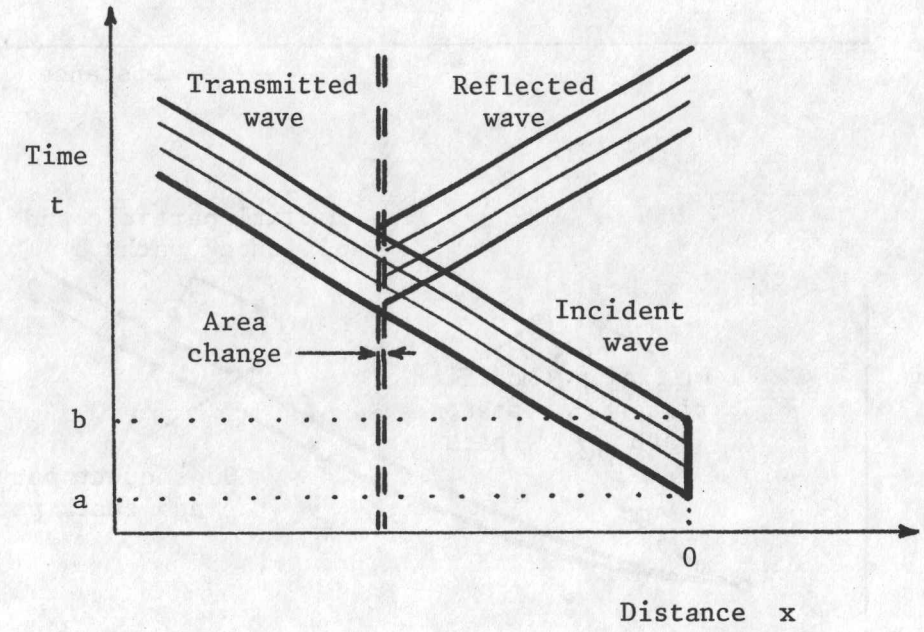

Fig. 14. Illustrations of alternate methods of specifying the initial conditions for the motion of a wave. These conditions can be specified in the form of a spatial distribution at a fixed time (a) or a temporal distribution at a fixed distance (b).

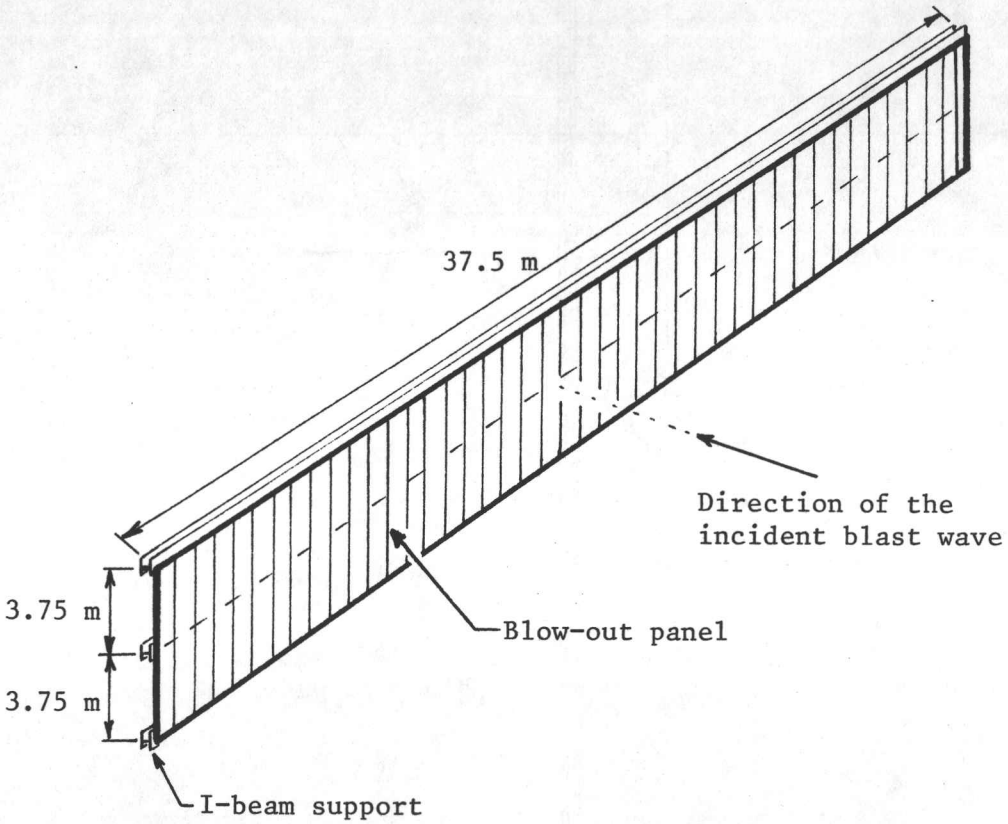

Fig. 15. A sketch of one blow-out panel, showing the basic shape, dimensions and I-beam supports.

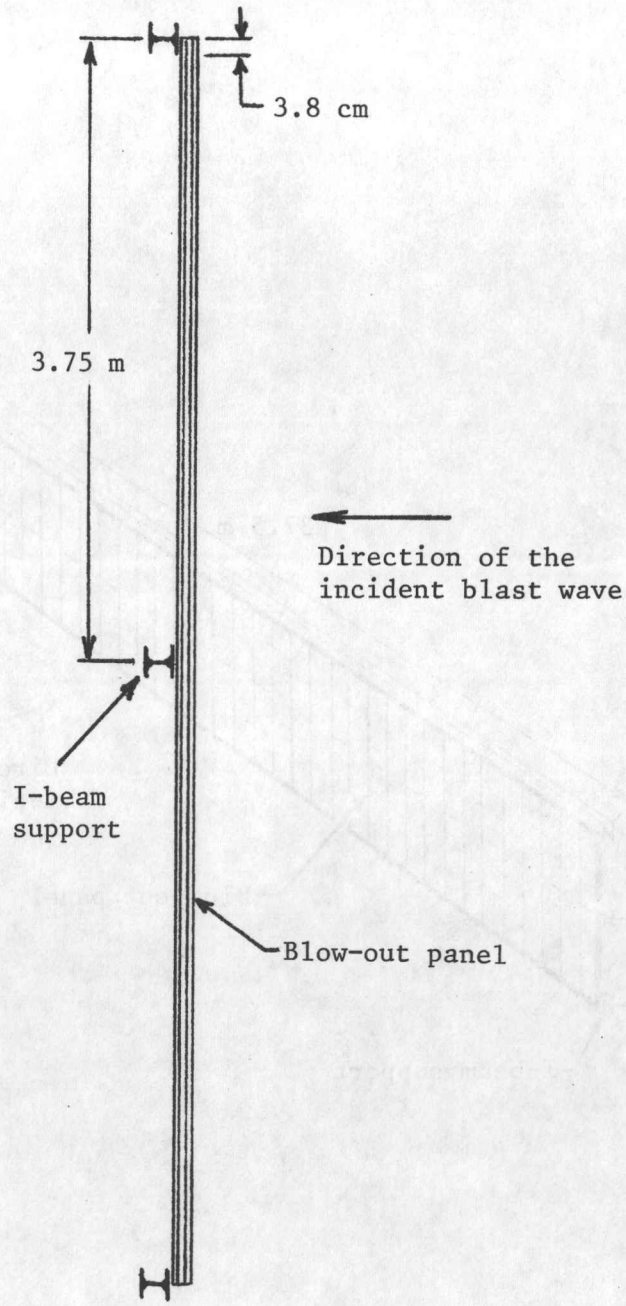

Fig. 16. Side view of the blow-out panel.

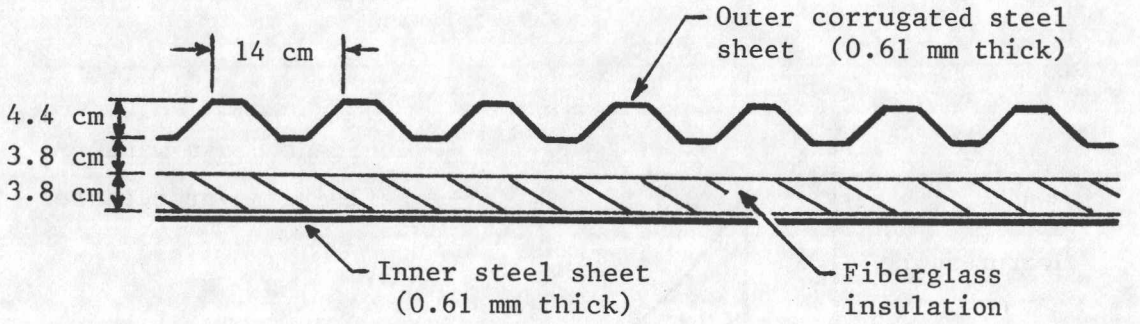

Data for one-half of the blow-out panel with an overall size of 3.75 m by 37.5 m	
Mass of the outer corrugated mild steel sheet	940 kg
Mass of the inner flat mild steel sheet	670 kg
Mass of the fiberglass insulation	30 kg
Total mass of the blow-out panel (one-half)	1,640 kg
Moment of inertia of the collapsed blow-out panel	6.45×10^{-5} m^4

Properties of the mild steel of the outer and inner steel sheets of the blow-out panels.	
Density	7,850 kg/m^3
Young's modulus of elasticity (E)	210 GPa
Yield strength	300 MPa
Tensile strength	460 MPa

Fig. 17. Sketch of the cross section of the blow-out panel and tables of relevant date of various parts of the blow-out panel.

a)

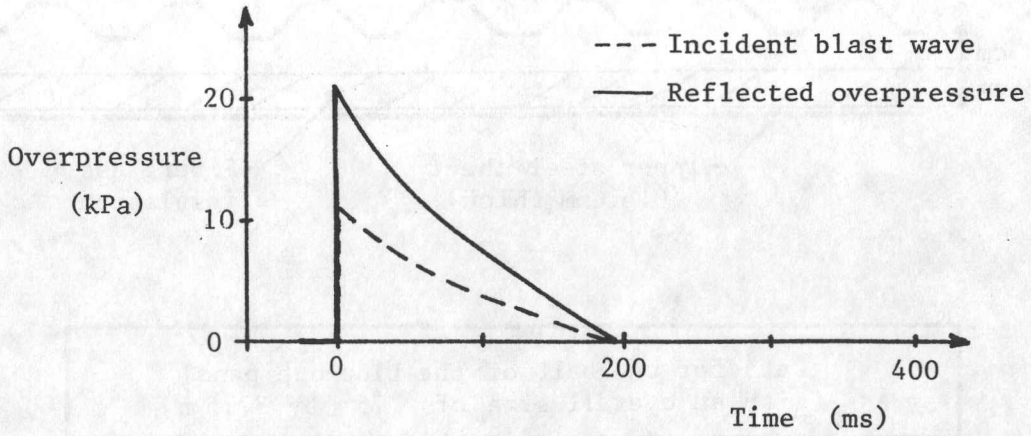

b)

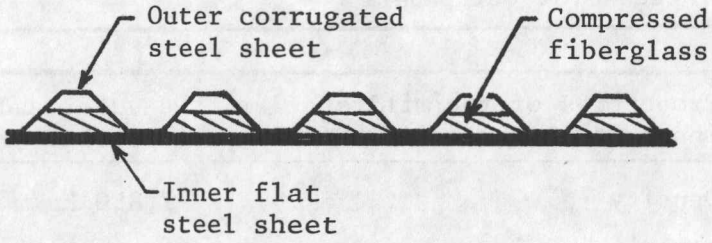

Fig. 18. Illustrations of the overpressure of the incident blast wave and the resulting reflected overpressure on the front wall of the power house (a), and the collapsed blow-out panel from the resulting blast-wave loading.

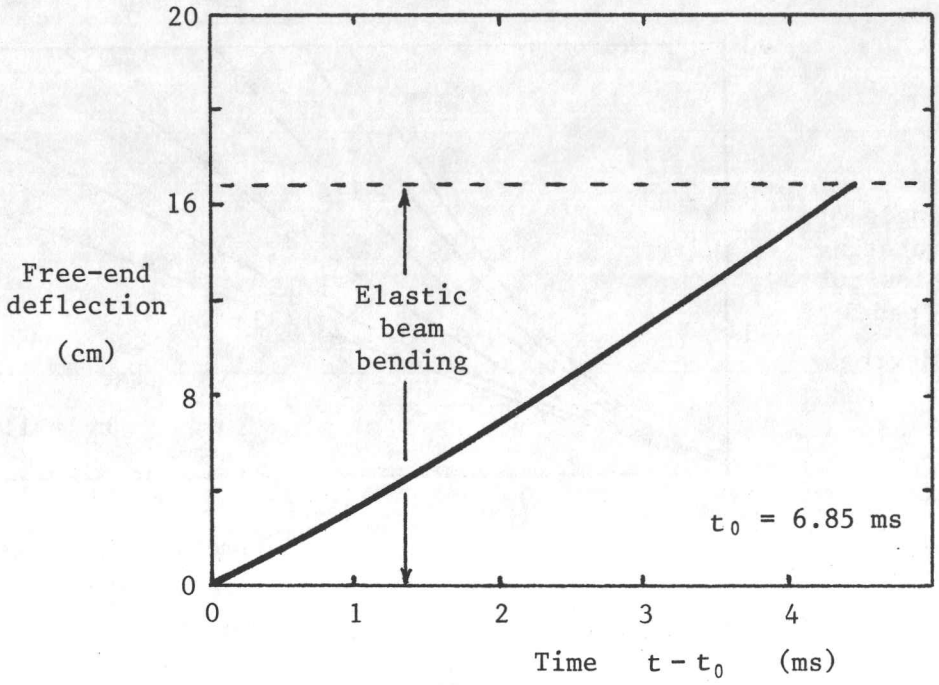

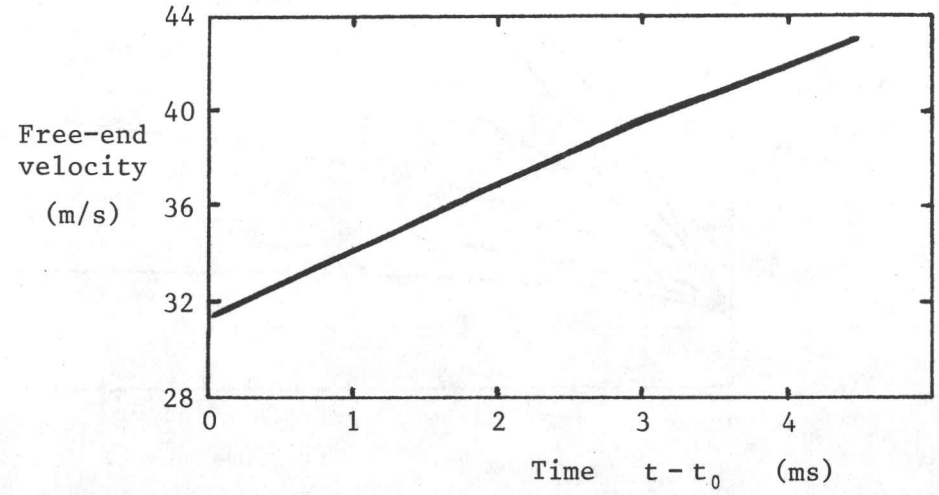

Fig. 19. Free-end deflection and velocity of the blow-out panel as a function of time, during the elastic beam bending phase.

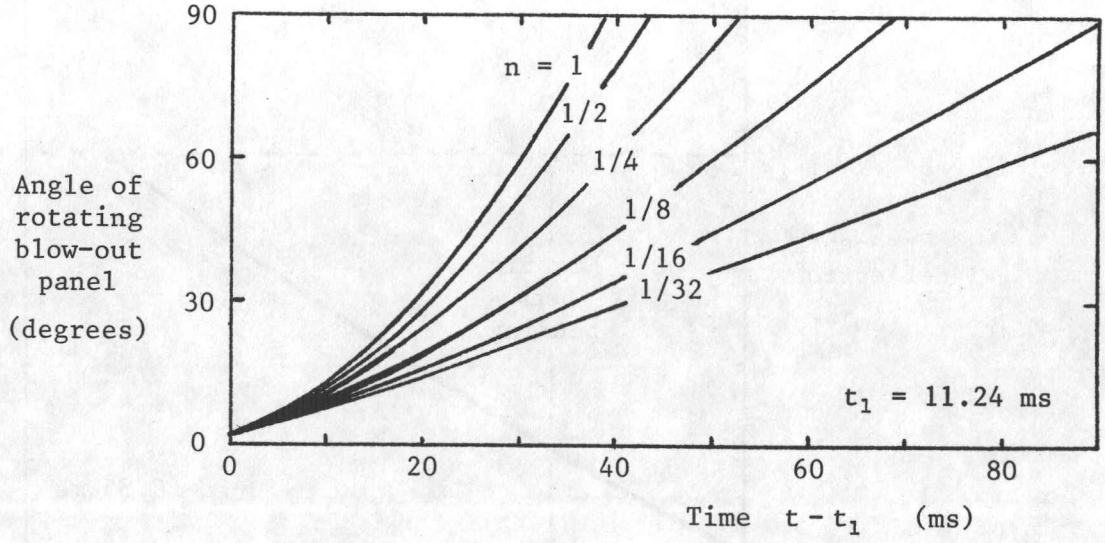

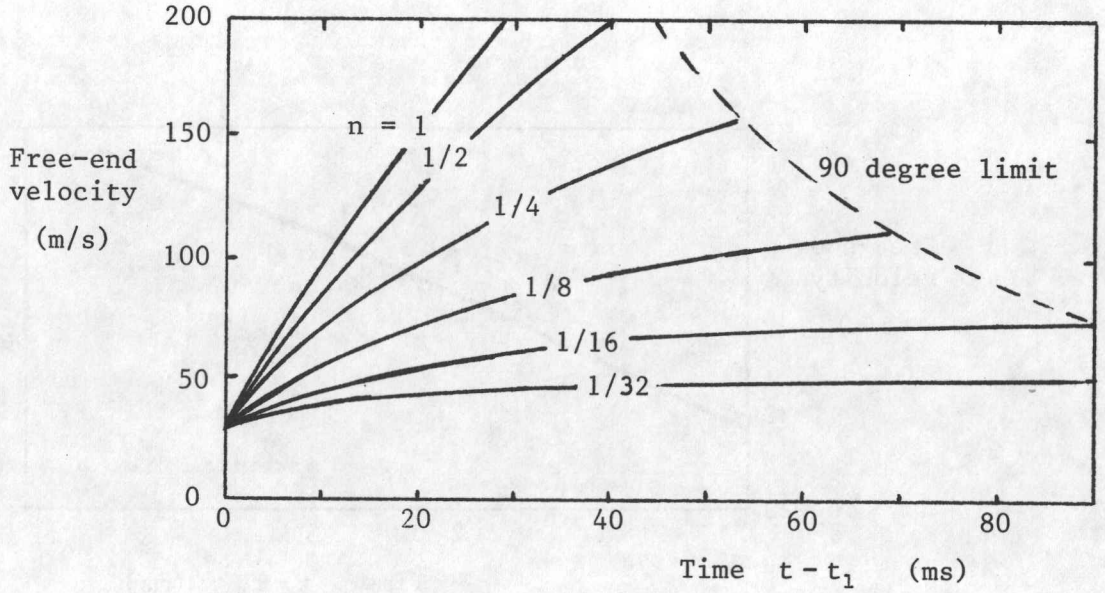

Fig. 20. Angular position and free-end velocity of the blow-out panel as a function of time, during the plastic beam bending phase.

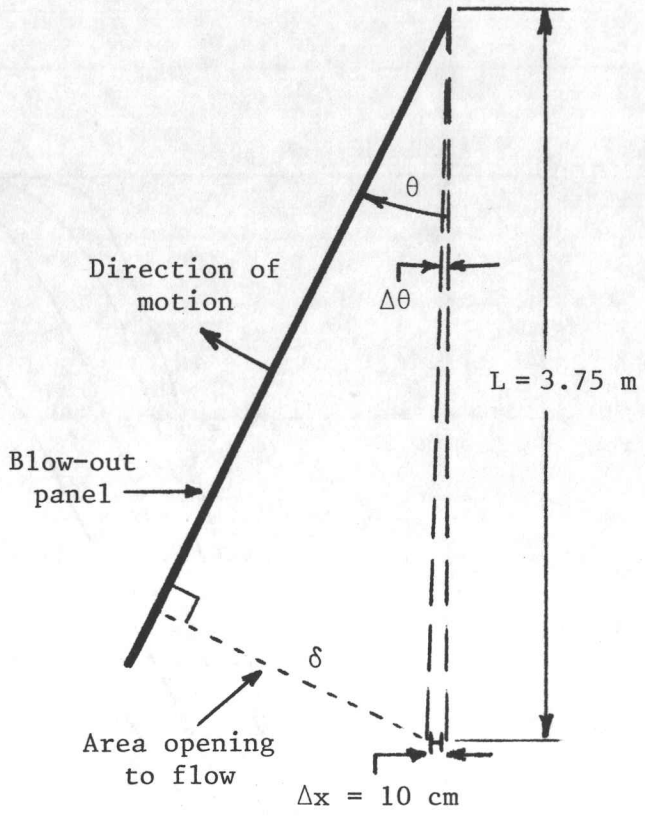

$$\Delta\theta = \Delta x/L = 0.027 \text{ radians}$$

$$\sin(\theta - \Delta\theta) = \delta/L$$

$$\frac{\text{flow area}}{\text{total flow area}} = \frac{\delta}{L} = \sin(\theta - \Delta\theta)$$

Fig. 21. Illustration of the area opening to the blast-wave flow from the breaking of the blow-out panels.

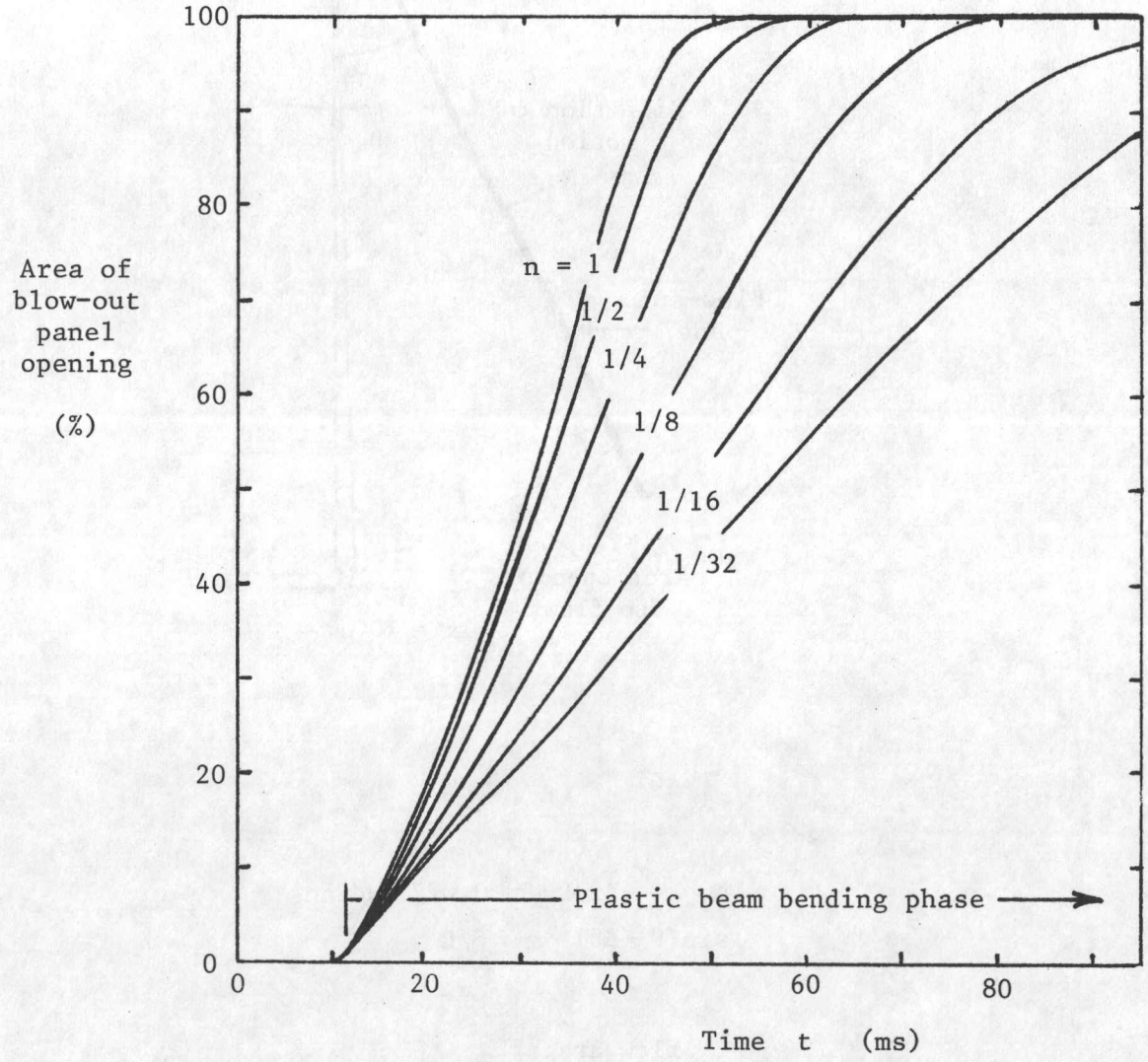

Fig. 22. Blast-wave flow opening as a percentage of the total area opening produced by the breaking of the blow-out panels.

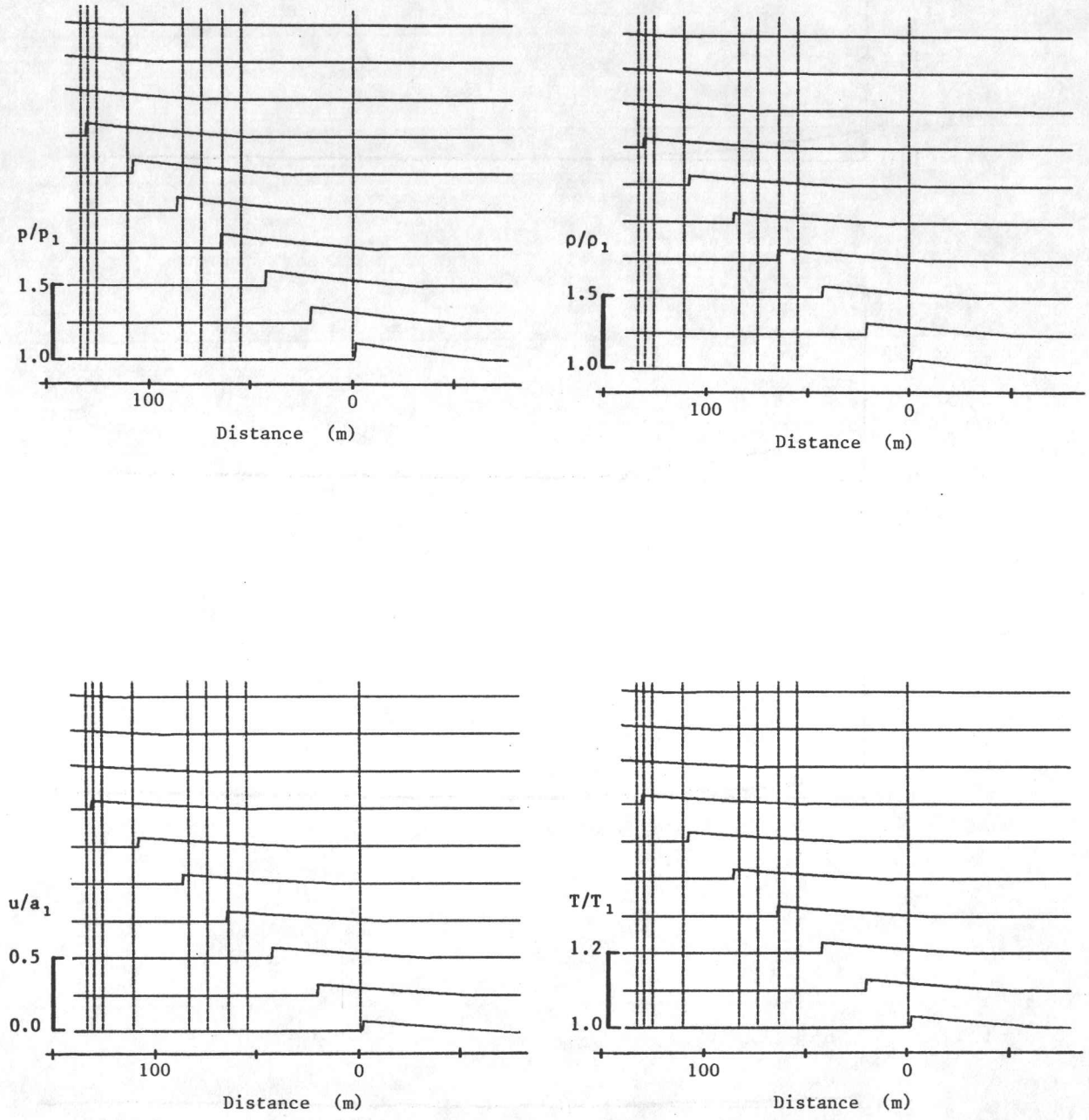

Fig. 23. Spatial distributions of pressure, density, flow velocity and temperature for the free-field blast wave, without the presence of the power house.

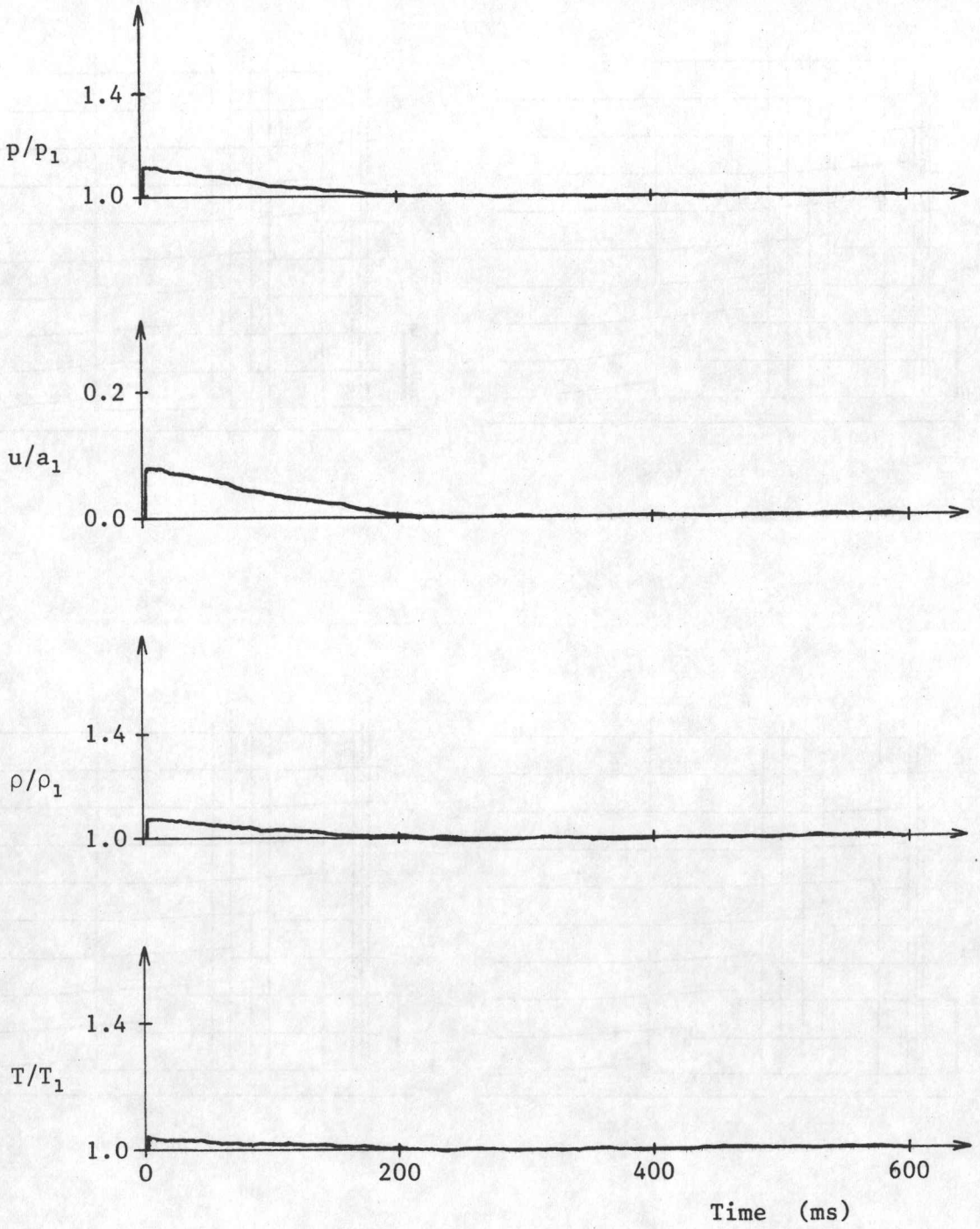

Fig. 24a. Free-field blast-wave signatures of pressure, flow velocity, density and temperature just ahead of the front wall of the power house.

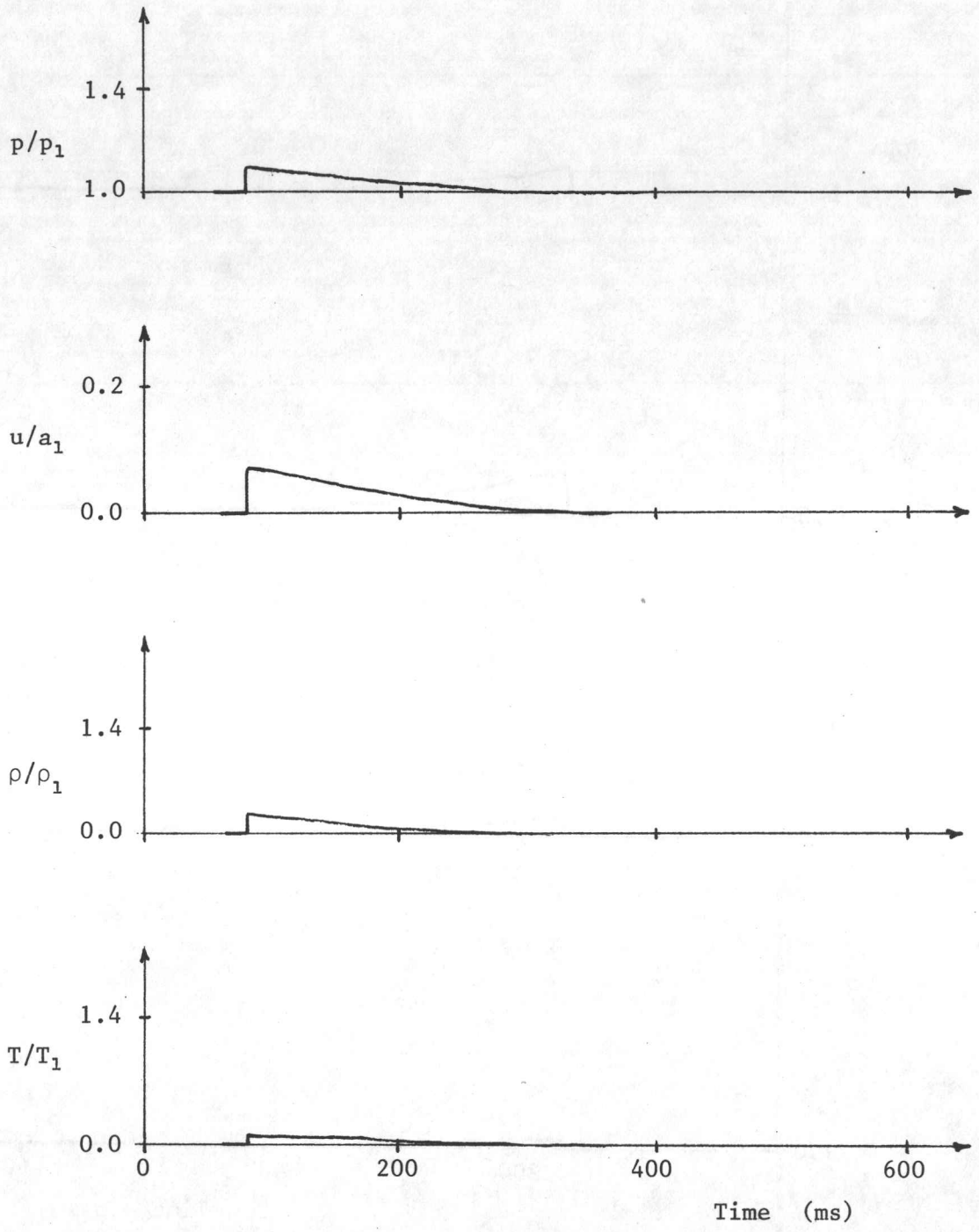

Fig. 24b. Free-field blast-wave signatures of pressure, flow velocity, density and temperature at location 1 in room 1 (of Fig. 6).

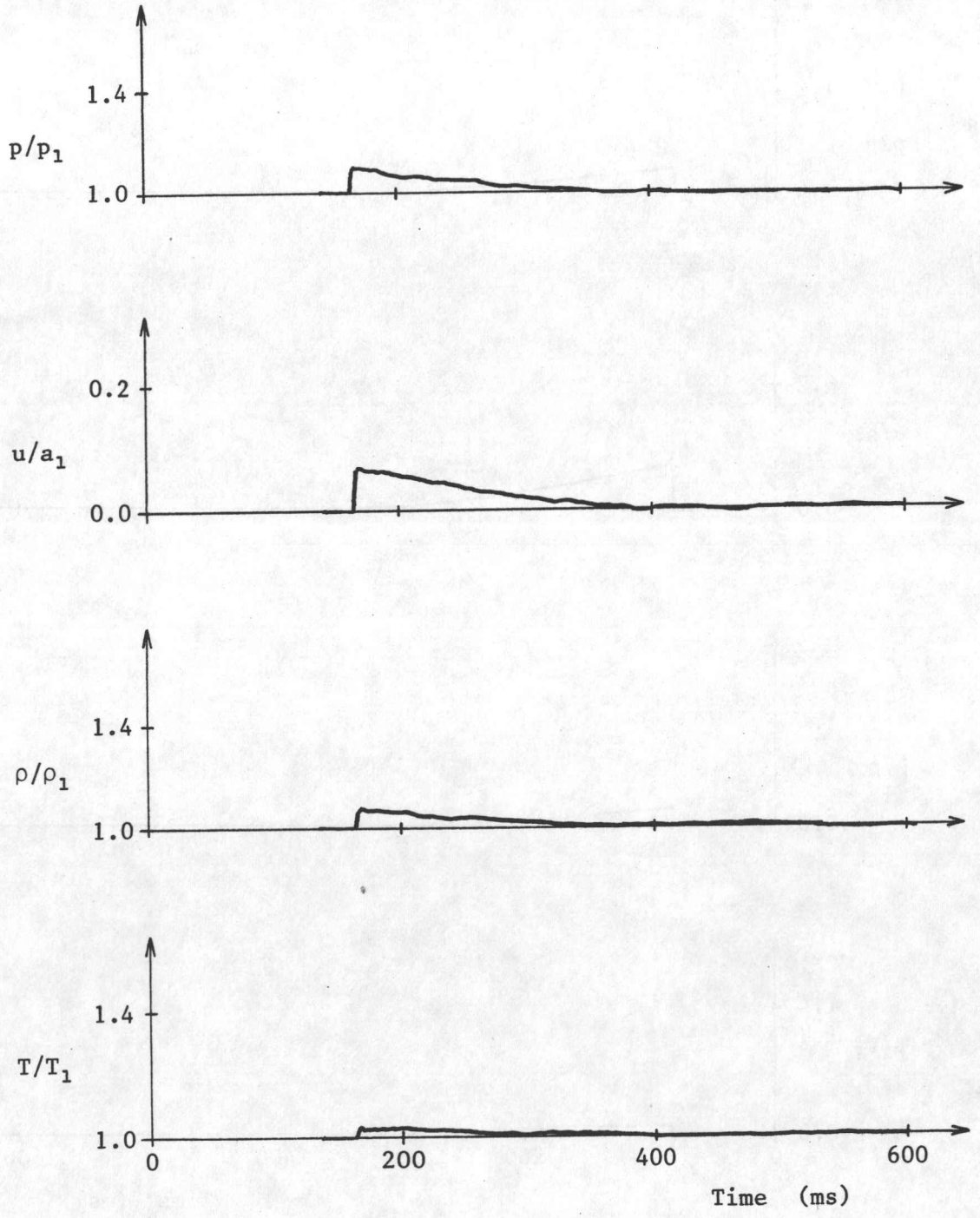

Fig. 24c. Free-field blast-wave signatures of pressure, flow velocity, density and temperature at location 2 in room 2 (of Fig. 6).

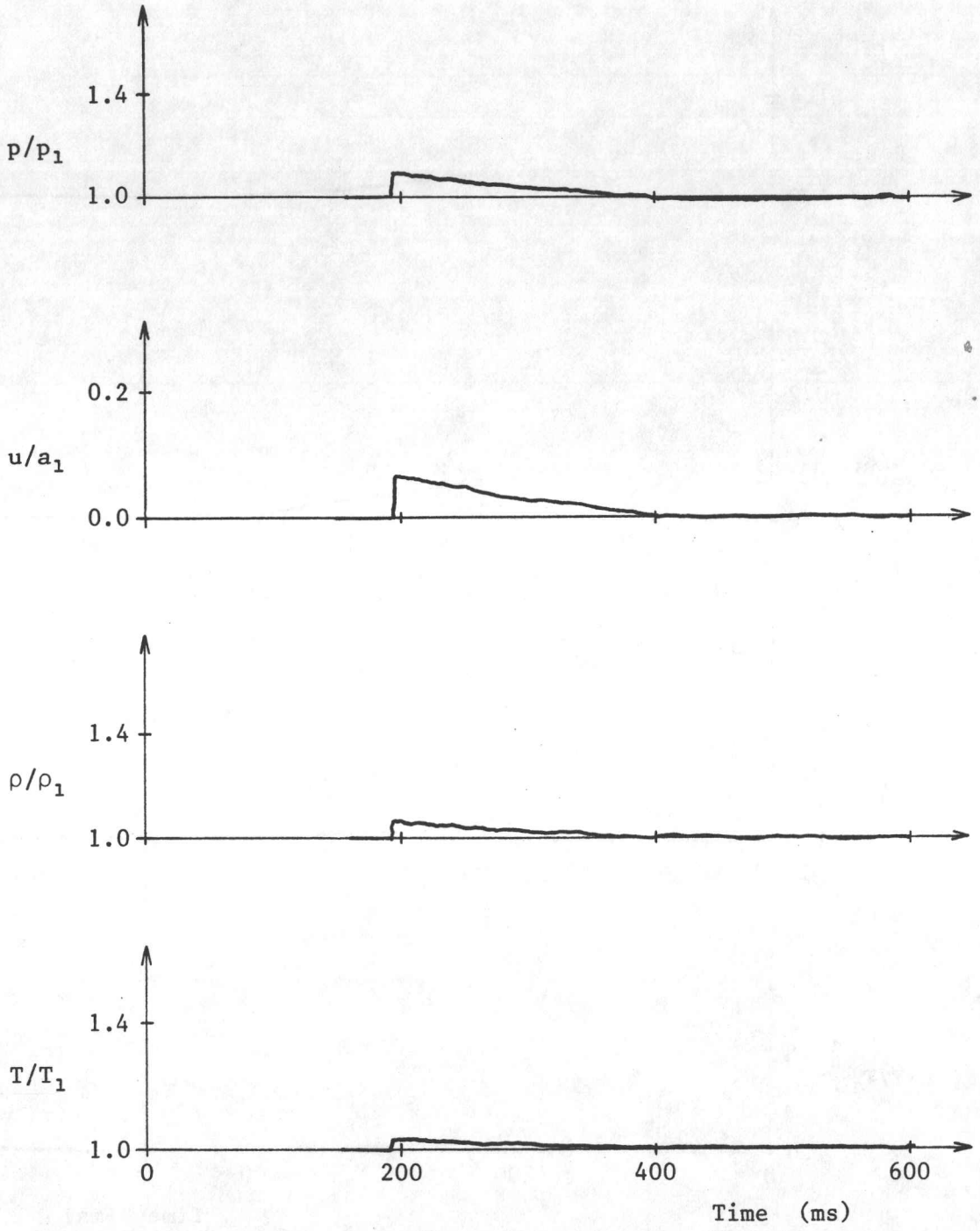

Fig. 24d. Free-field blast-wave signatures of pressure, flow velocity, density and temperature at location 3 in room 3 (of Fig. 6).

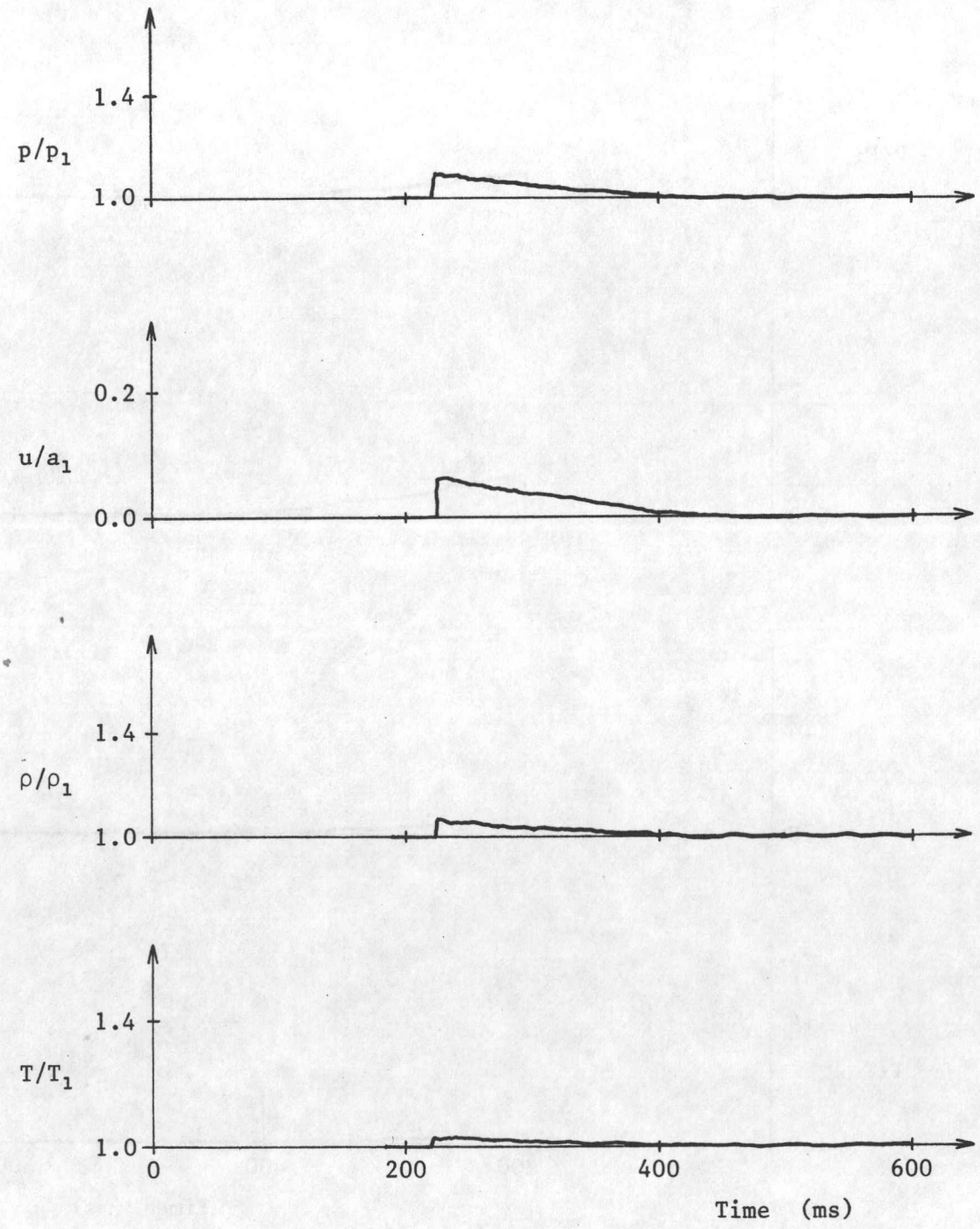

Fig. 24e. Free-field blast-wave signatures of pressure, flow velocity, density and temperature at location 4 in room 4 (of Fig. 6).

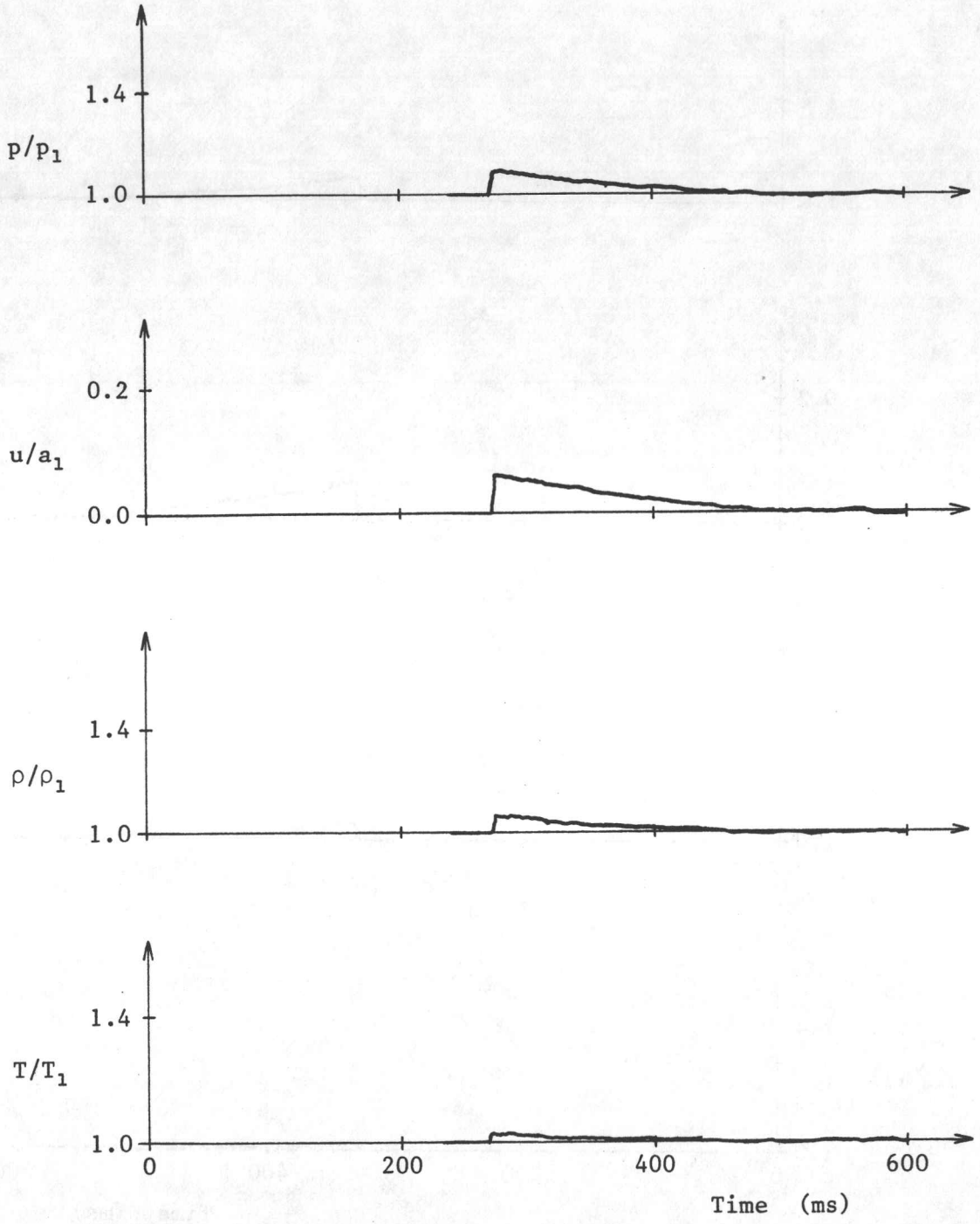

Fig. 24f. Free-field blast-wave signatures of pressure, flow velocity, density and temperature at location 5 in room 5 (of Fig. 6).

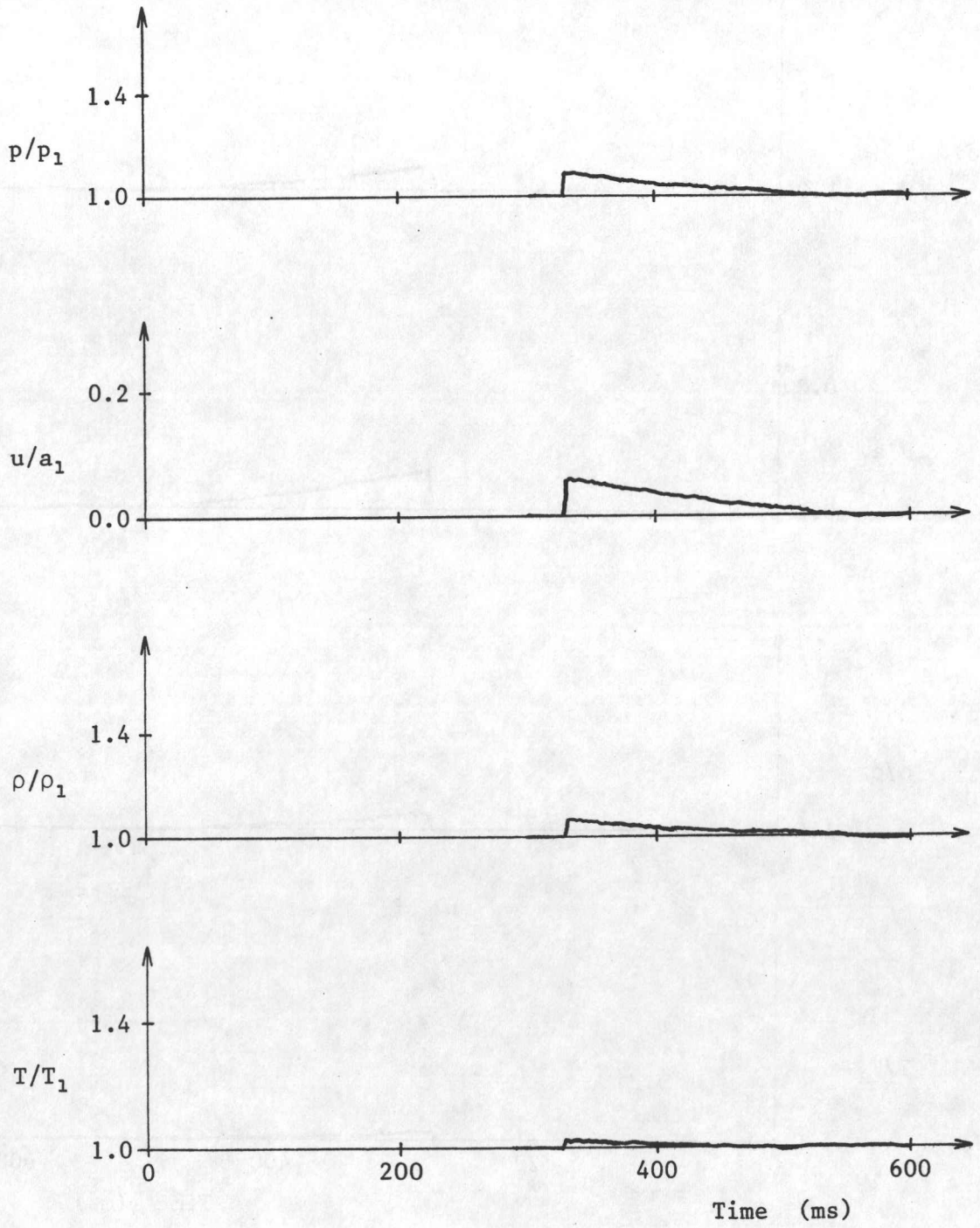

Fig. 24g. Free-field blast-wave signatures of pressure, flow velocity, density and temperature at location 6 in room 6 (of Fig. 6).

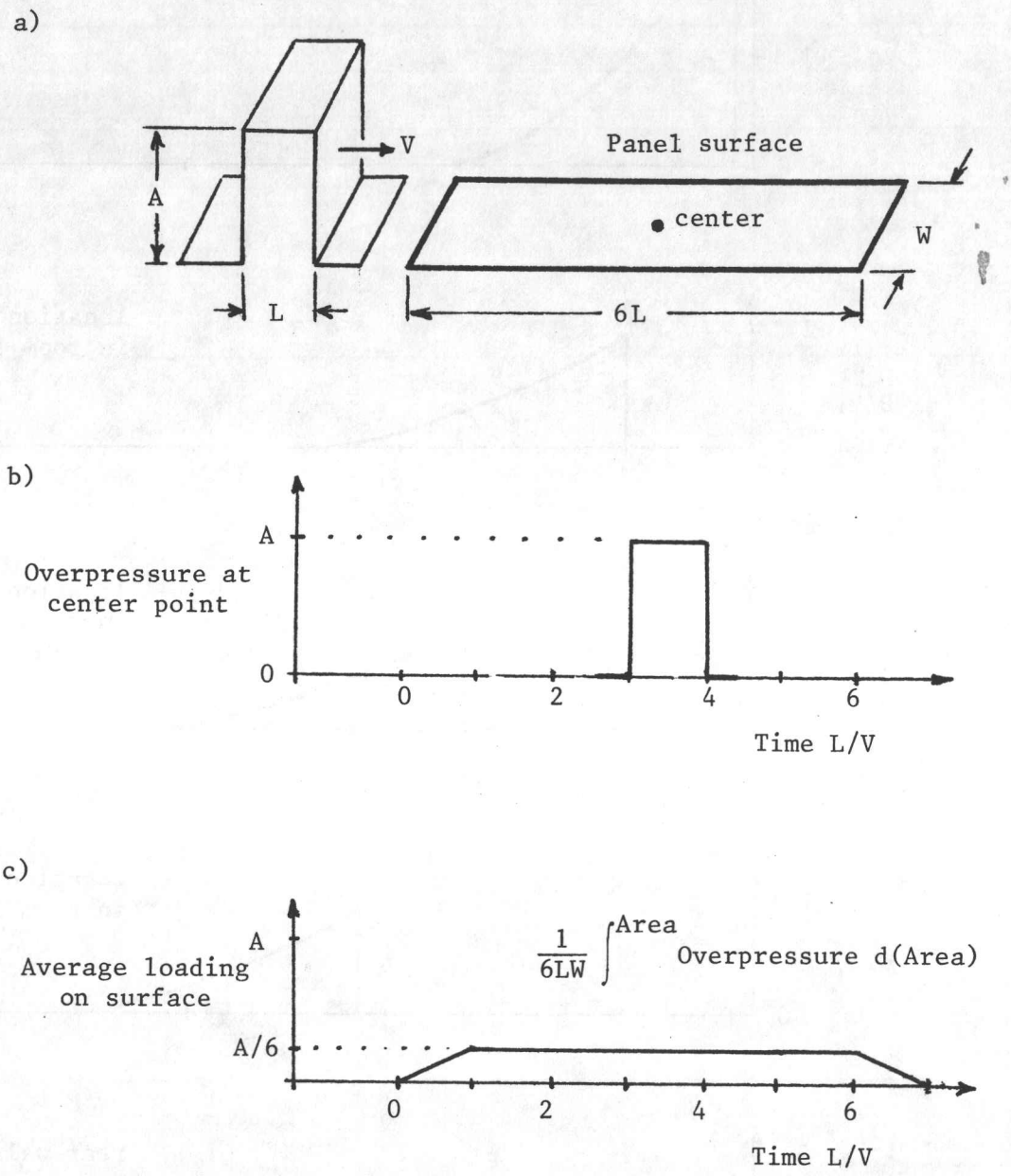

Fig. 25. Illustration of the difference between the overpressure at the panel center and the average overpressure loading on the entire panel surface.

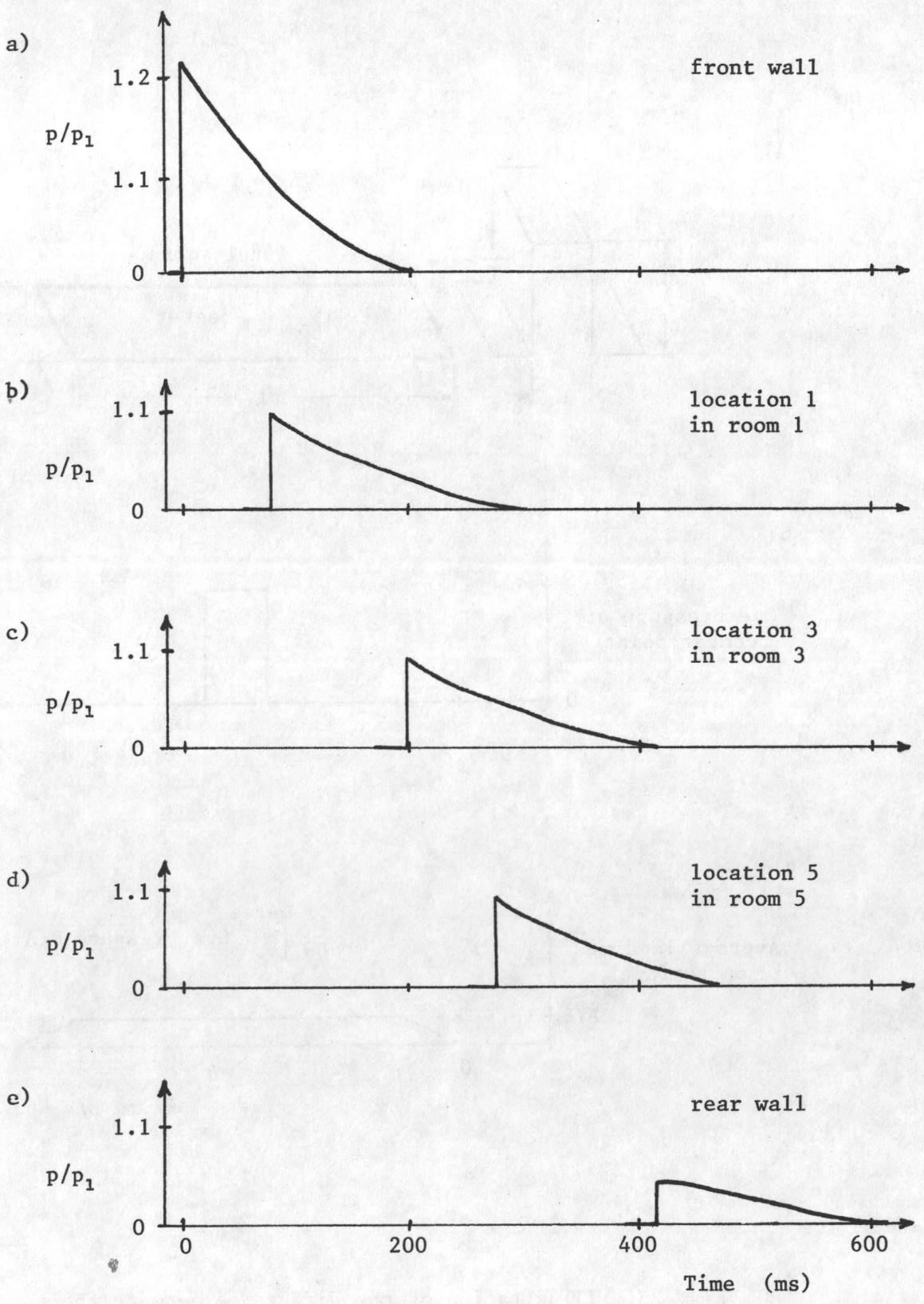

Fig. 26. Overpressure loading at various places indicated on the outside walls and roof of the power house.

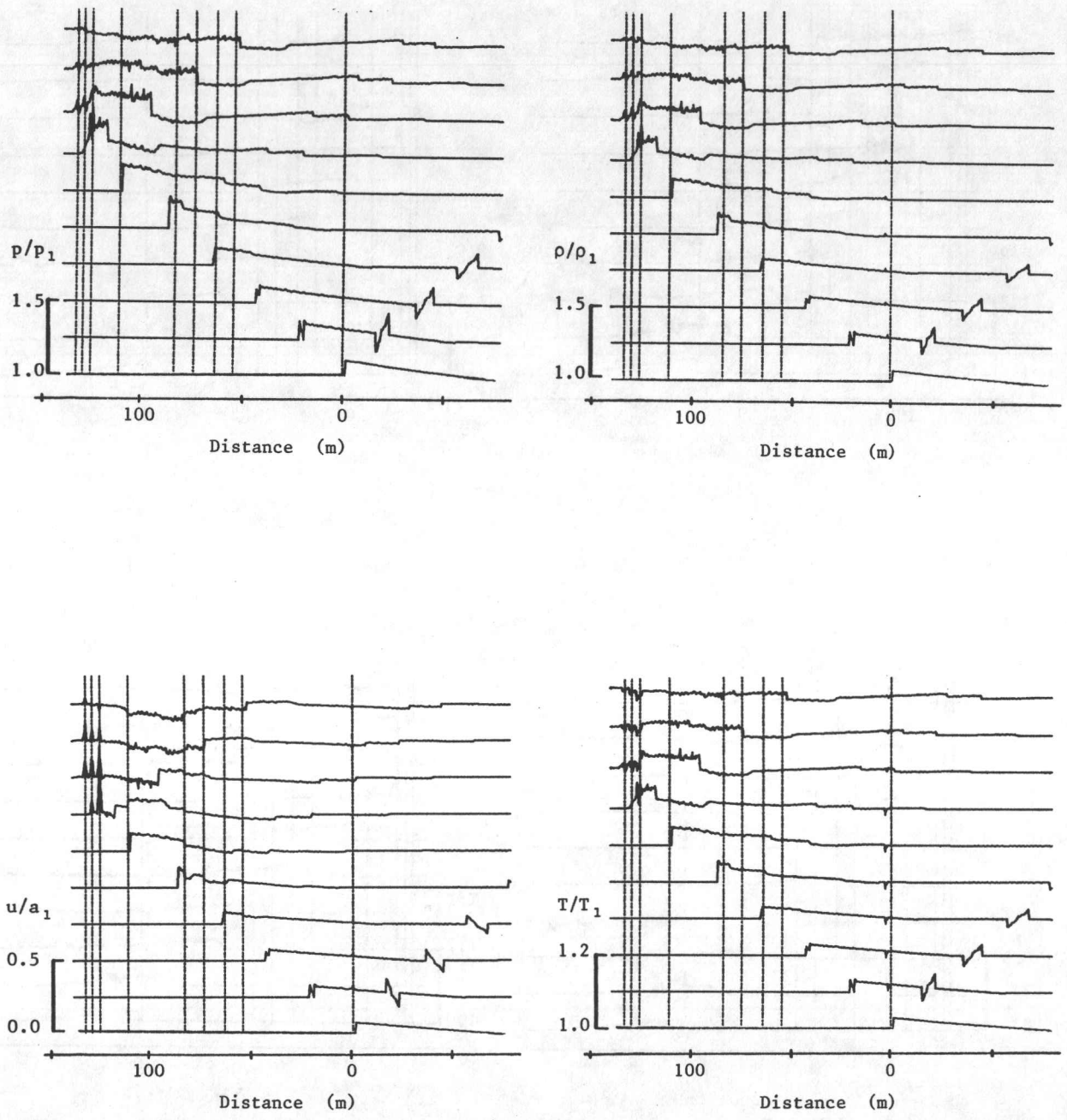

Fig. 27a. Spatial distributions of pressure, density, flow velocity and temperature for the blast-wave flow field inside the power house.

Geometrical configuration: A
Blow-out panel opening time: 0 ms

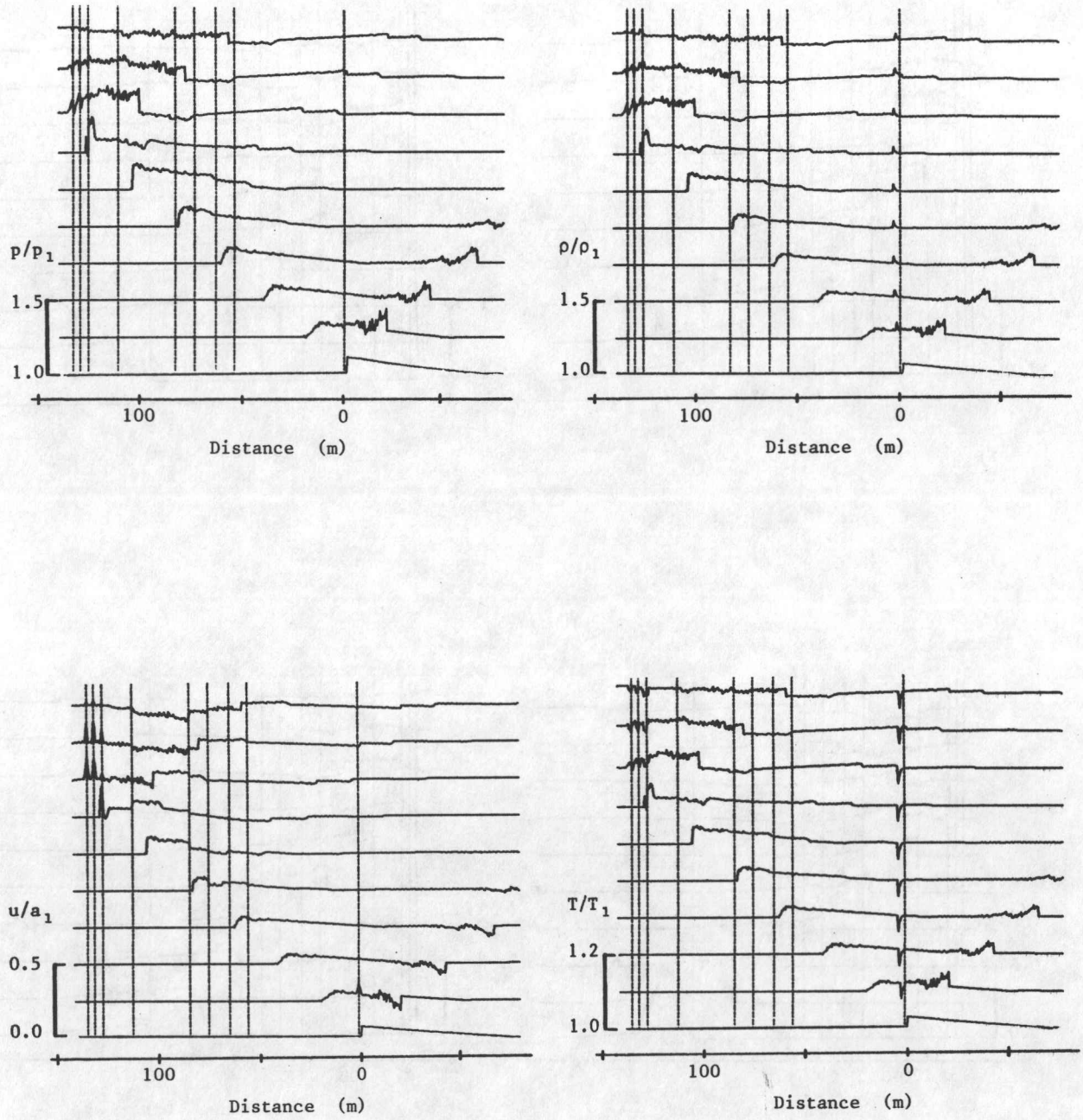

Fig. 27b. Spatial distributions of pressure, density, flow velocity and temperature for the blast-wave flow field inside the power house.

Geometrical configuration: A
Blow-out panel opening time: 100 ms

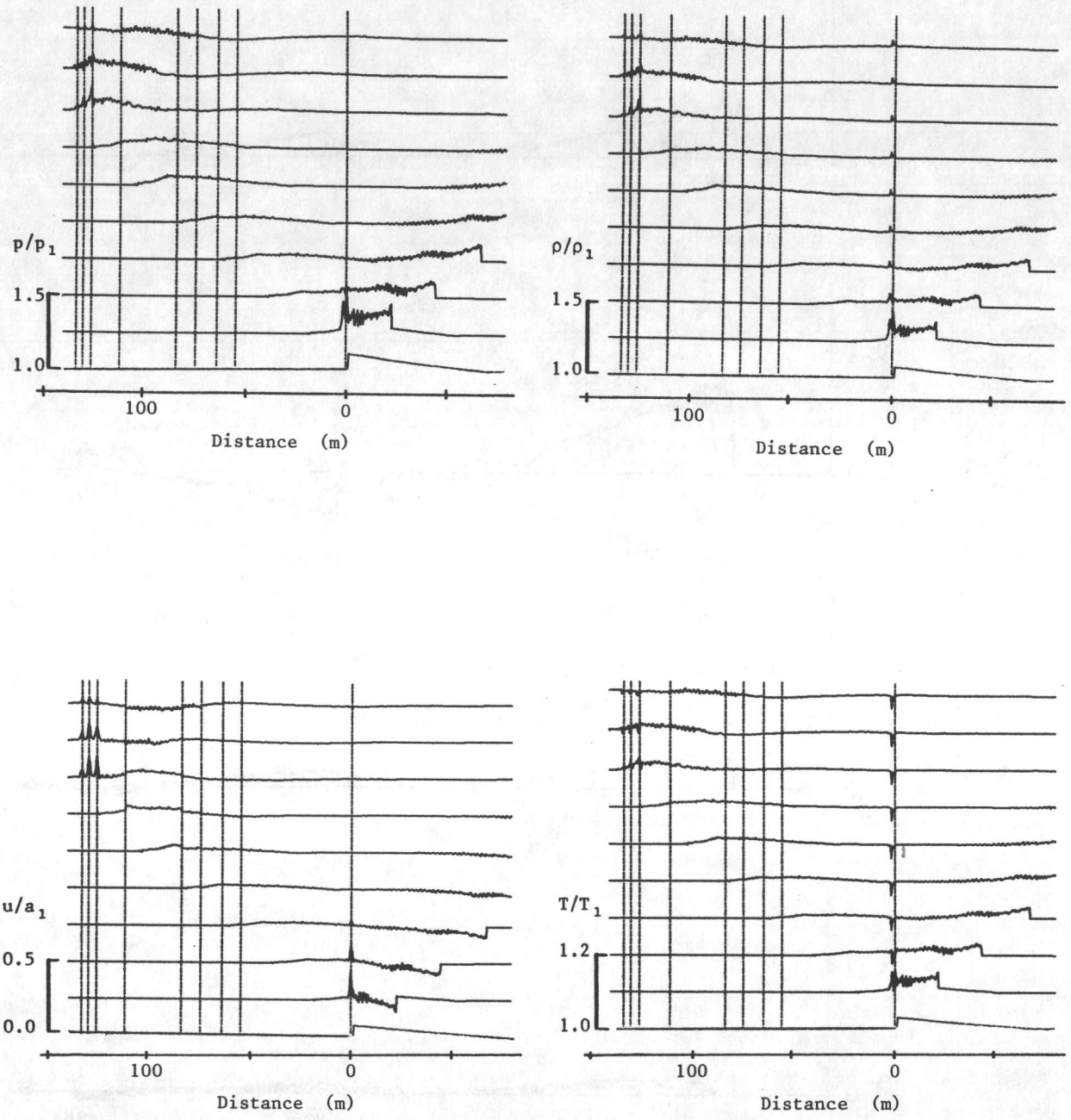

Fig. 27c. Spatial distributions of pressure, density, flow velocity and temperature for the blast-wave flow field inside the power house.

Geometrical configuration: A
Blow-out panel opening time: 500 ms

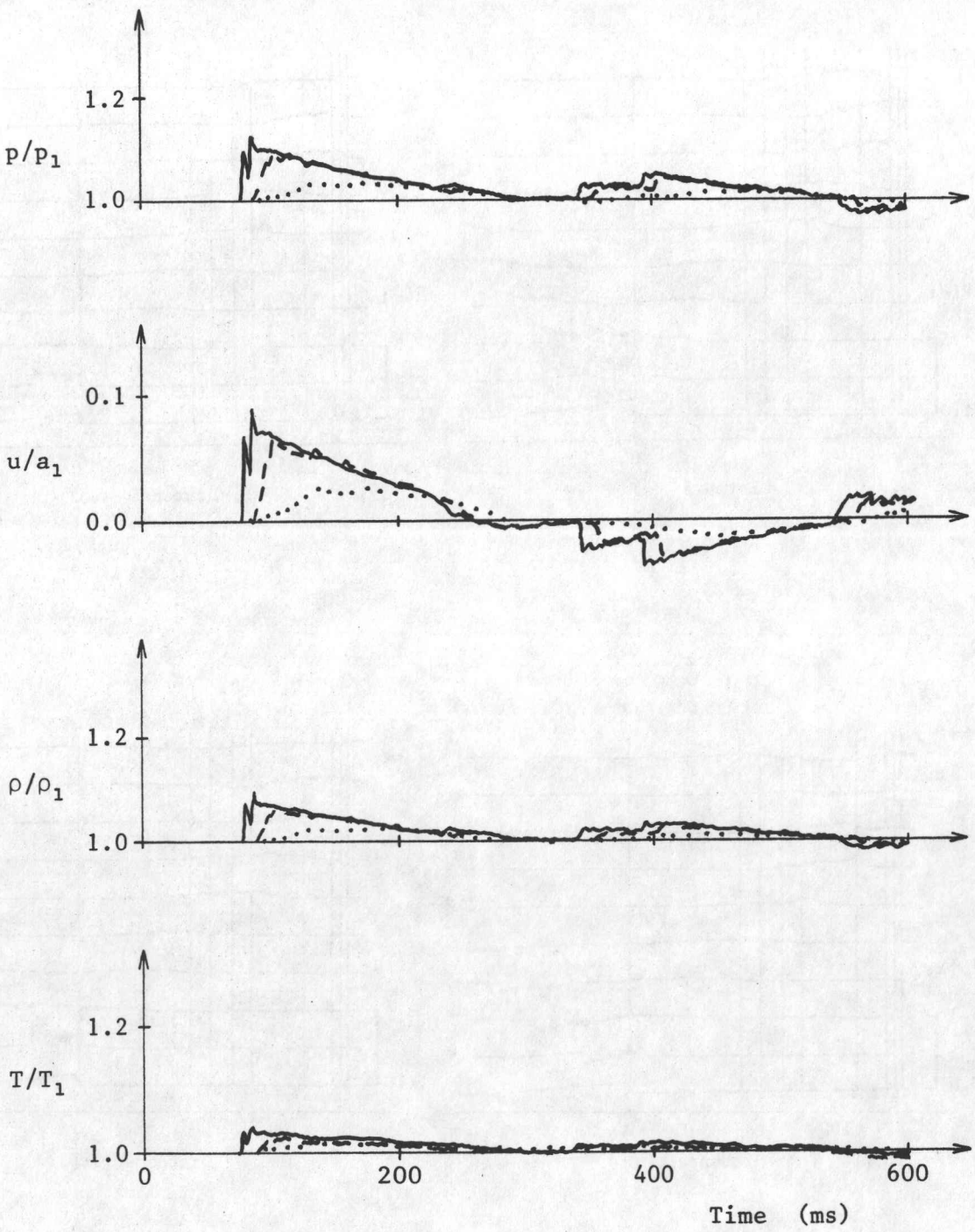

Fig. 27d. Temporal distributions of pressure, density, flow velocity and temperature for the blast-wave flow field inside the power house.

Geometrical configuration:	A
Blow-out panel opening time:	0 ms ———
	100 ms - - - -
	500 ms . . . . .
Location and room number:	1

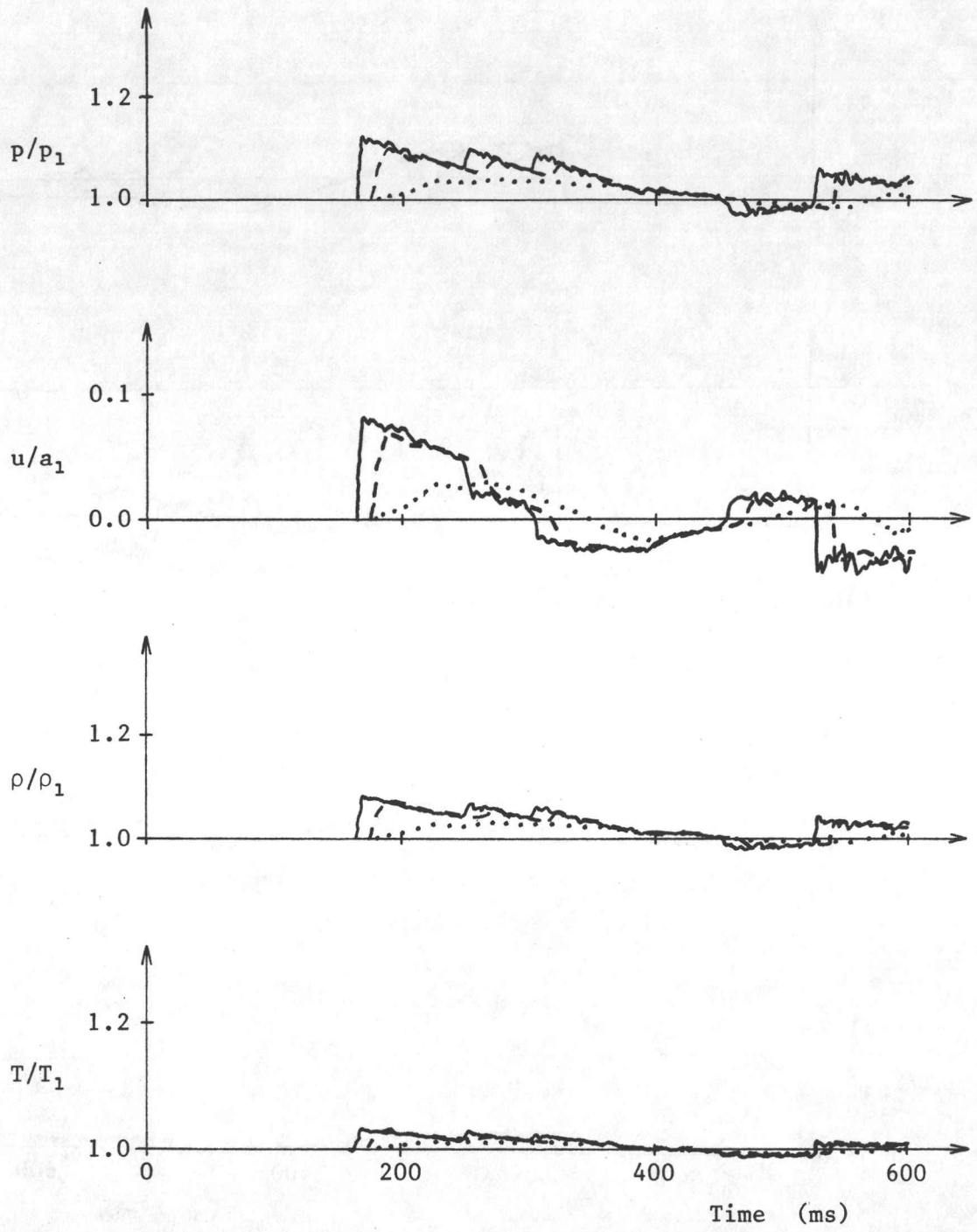

Fig. 27e. Temporal distributions of pressure, density, flow velocity and temperature for the blast-wave flow field inside the power house.

Geometrical configuration:	A
Blow-out panel opening time:	0 ms ———
	100 ms - - - -
	500 ms .....
Location and room number:	2

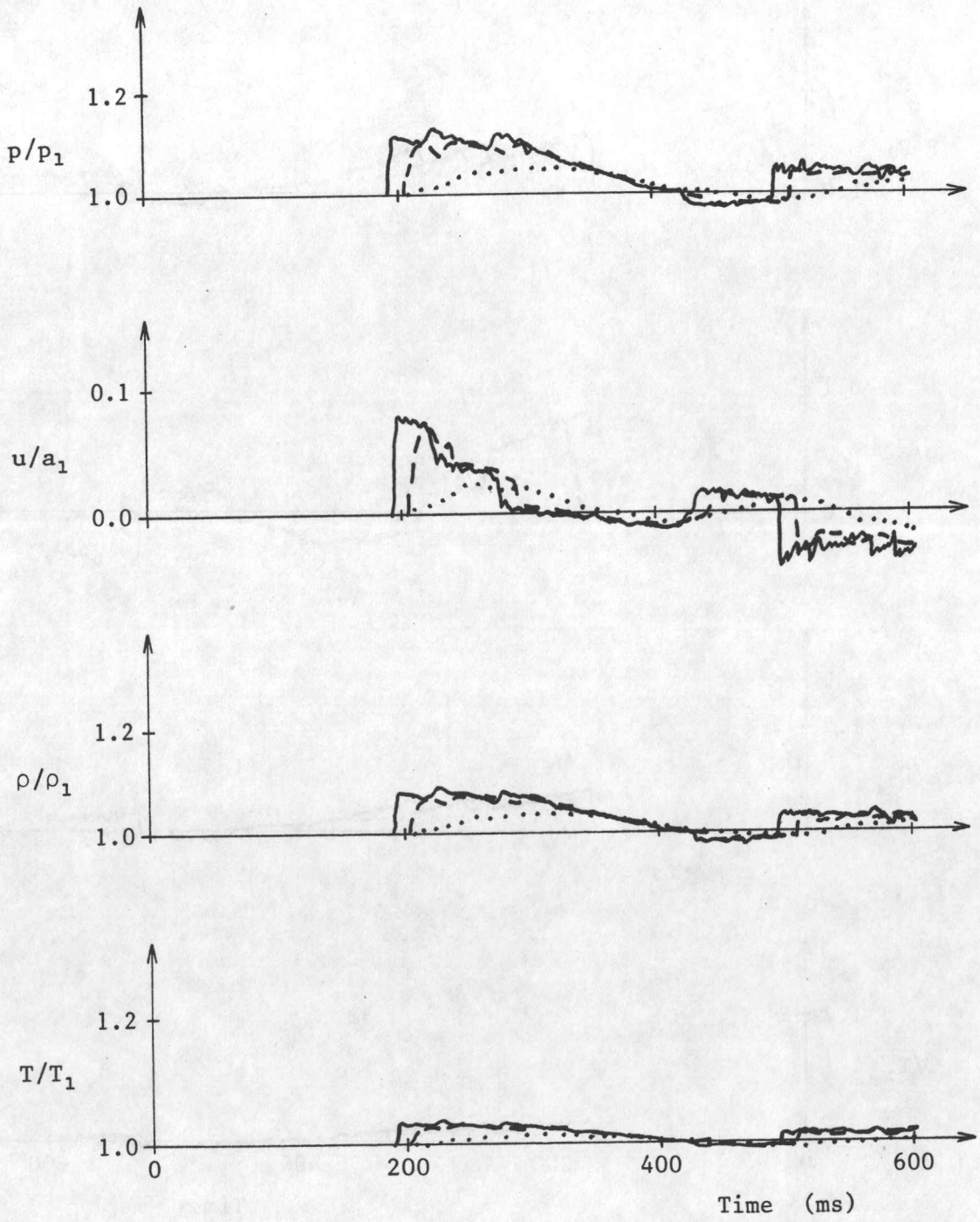

Fig. 27f. Temporal distributions of pressure, density, flow velocity and temperature for the blast-wave flow field inside the power house.

Geometrical configuration:	A
Blow-out panel opening time:	0 ms ———
	100 ms — — — —
	500 ms . . . . .
Location and room number:	3

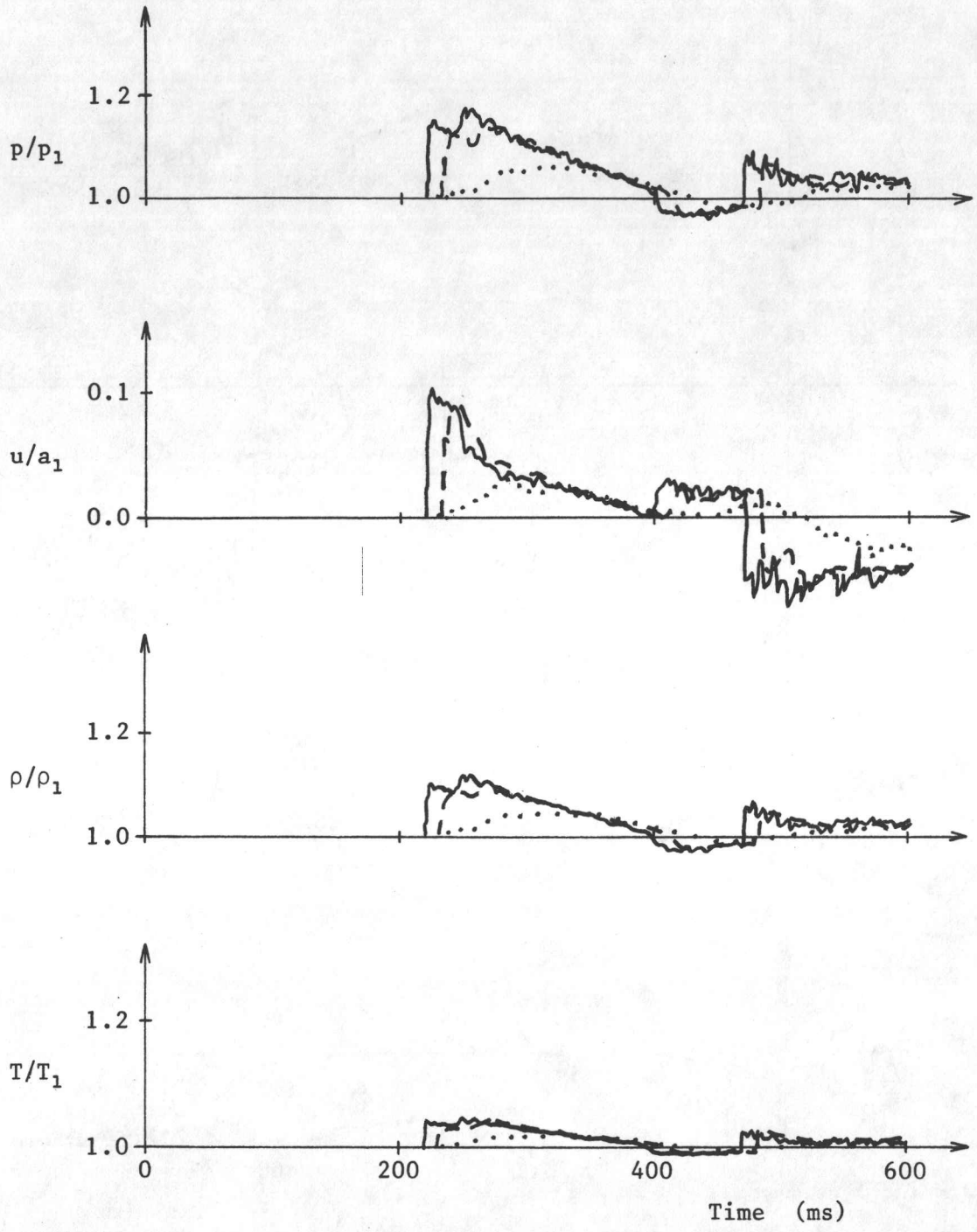

Fig. 27g. Temporal distributions of pressure, density, flow velocity and temperature for the blast-wave flow field inside the power house.

Geometrical configuration:	A
Blow-out panel opening time:	0 ms ———
	100 ms — — —
	500 ms . . . . .
Location and room number:	4

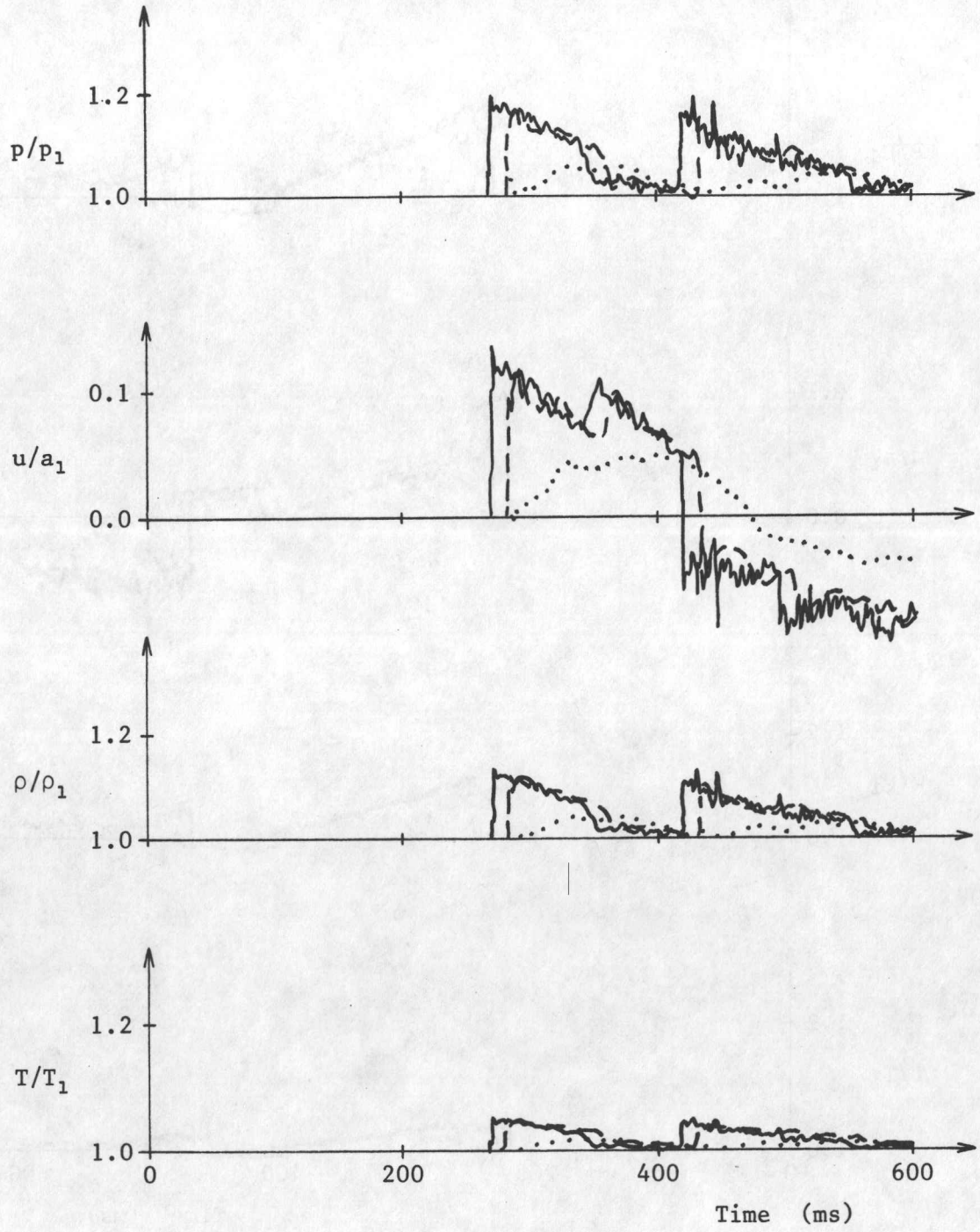

Fig. 27h. Temporal distributions of pressure, density, flow velocity and temperature for the blast-wave flow field inside the power house.

Geometrical configuration:	A
Blow-out panel opening time:	0 ms ———
	100 ms - - - -
	500 ms . . . . .
Location and room number:	5

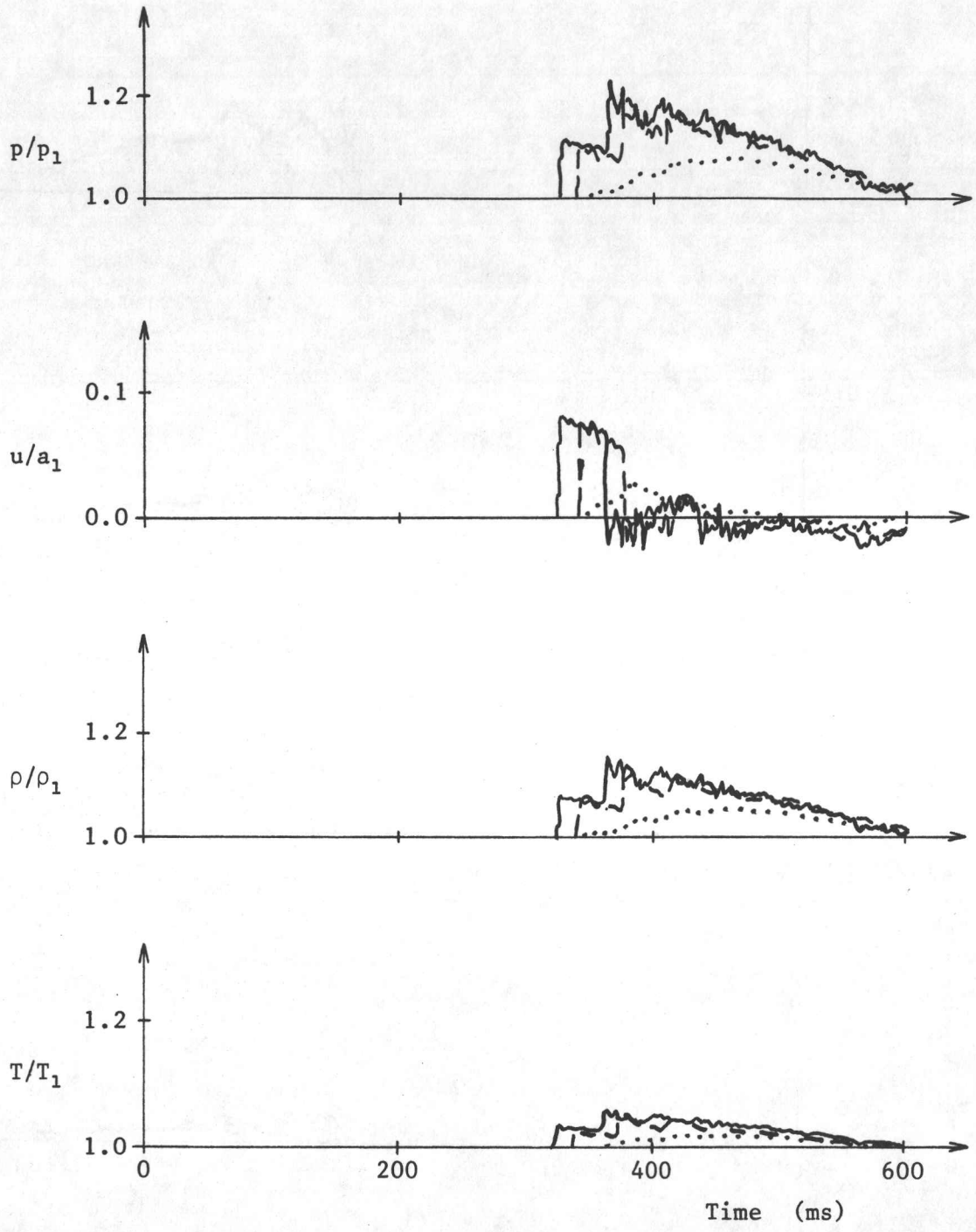

Fig. 27i. Temporal distributions of pressure, density, flow velocity and temperature for the blast-wave flow field inside the power house.

Geometrical configuration: A
Blow-out panel opening time: 0 ms ———
100 ms — — — —
500 ms · · · · ·
Location and room number: 6

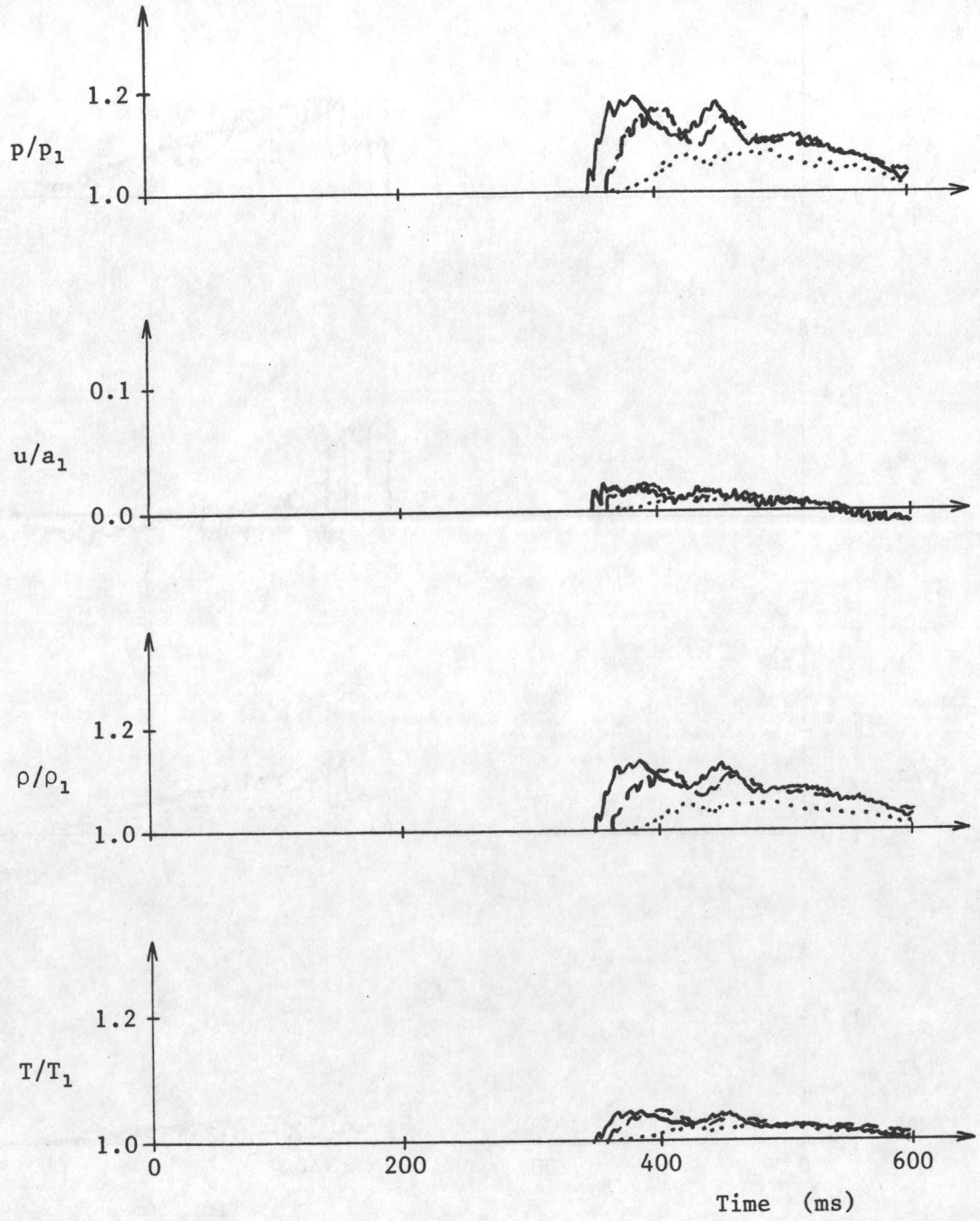

Fig. 27j. Temporal distributions of pressure, density, flow velocity and temperature for the blast-wave flow field inside the power house.

Geometrical configuration:	A
Blow-out panel opening time:	0 ms ———
	100 ms — - - -
	500 ms · · · · ·
Location and room number:	7

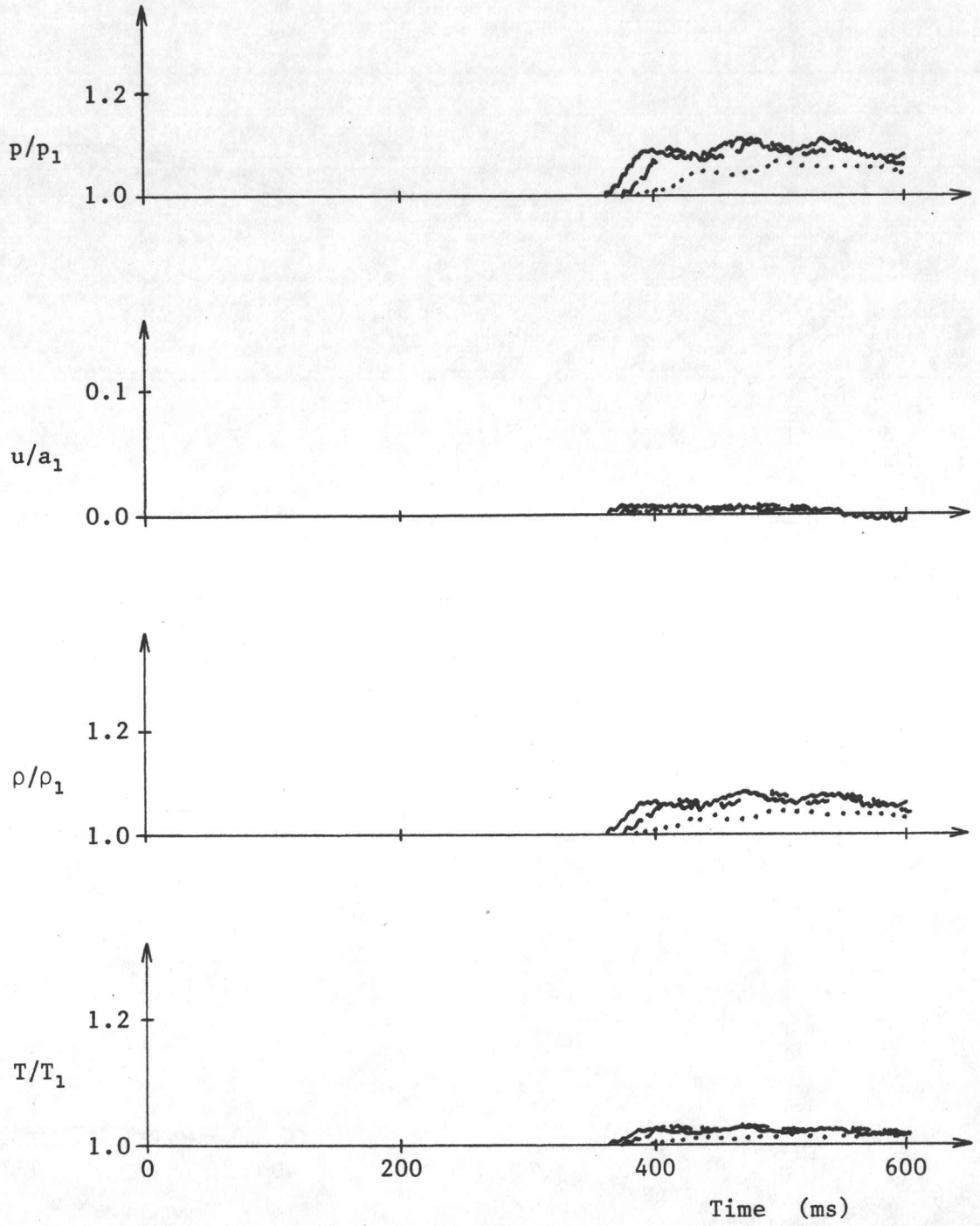

Fig. 27k. Temporal distributions of pressure, density, flow velocity and temperature for the blast-wave flow field inside the power house.

Geometrical configuration:	A
Blow-out panel opening time:	0 ms ———
	100 ms - - - -
	500 ms · · · · ·
Location and room number:	8

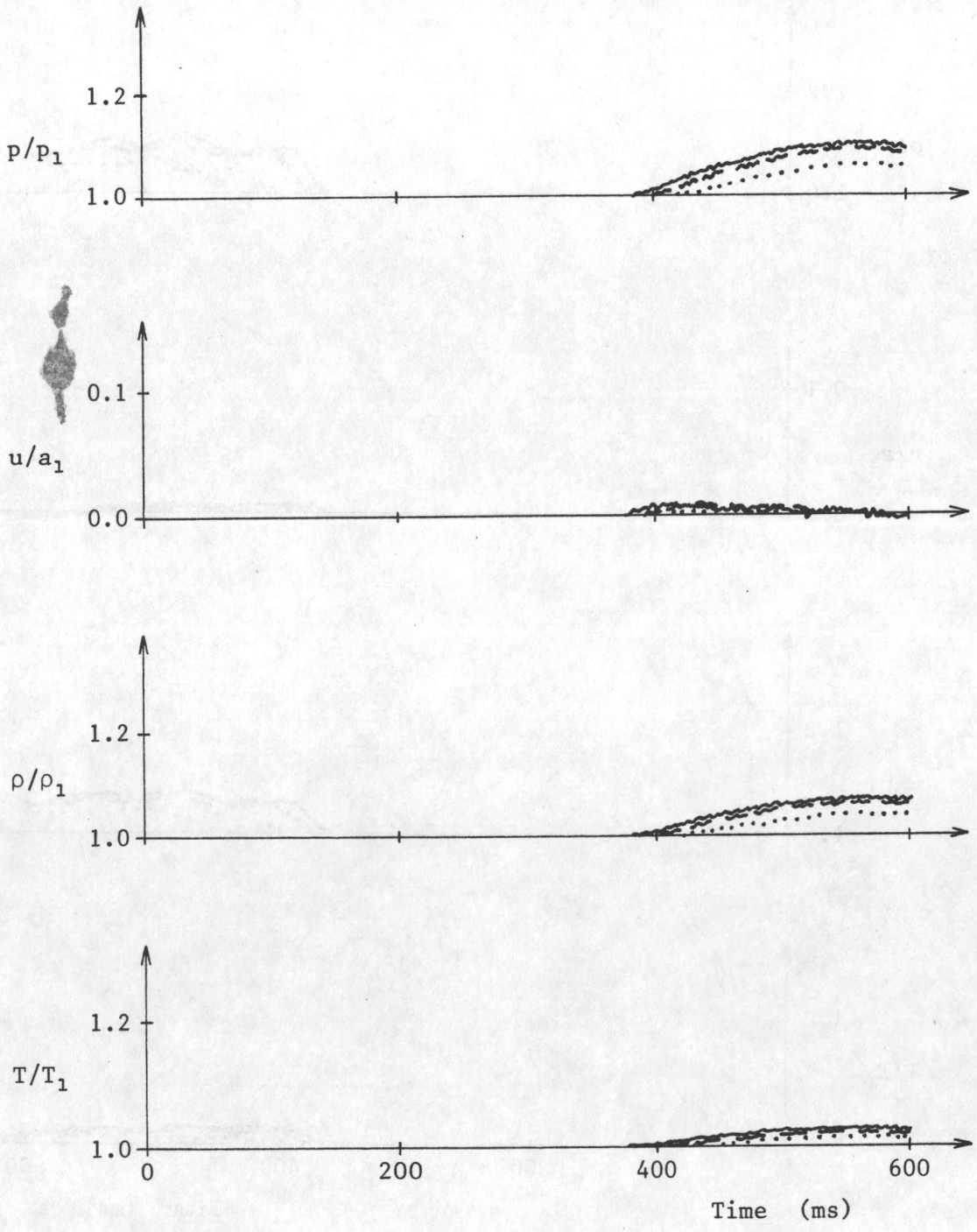

Fig. 271. Temporal distributions of pressure, density, flow velocity and temperature for the blast-wave flow field inside the power house.

Geometrical configuration:	A
Blow-out panel opening time:	0 ms ———
	100 ms – – – –
	500 ms · · · · · ·
Location and room number:	9

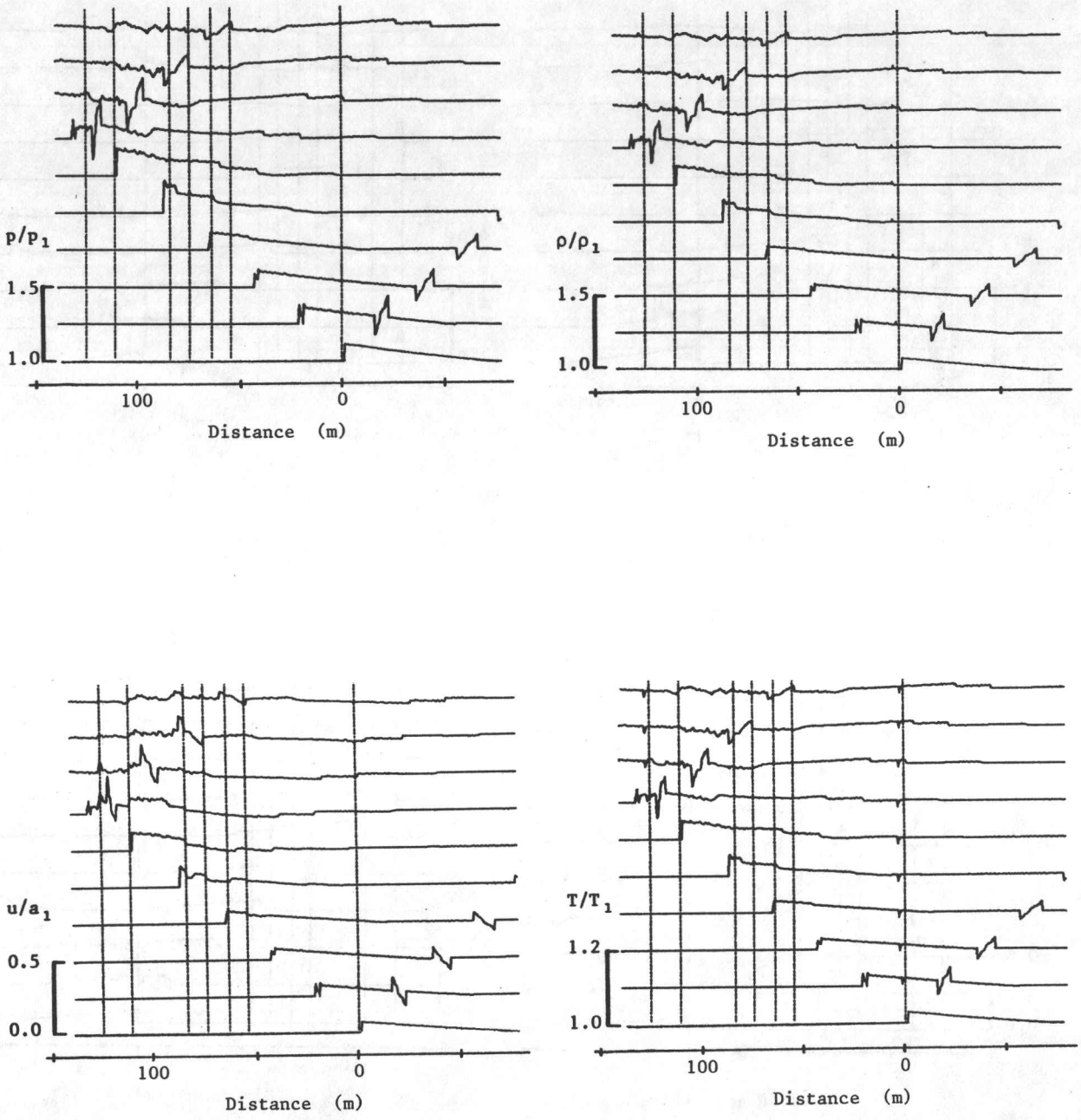

Fig. 28a. Spatial distributions of pressure, density, flow velocity and temperature for the blast-wave flow field inside the power house.

Geometrical configuration: B
Blow-out panel opening time: 0 ms

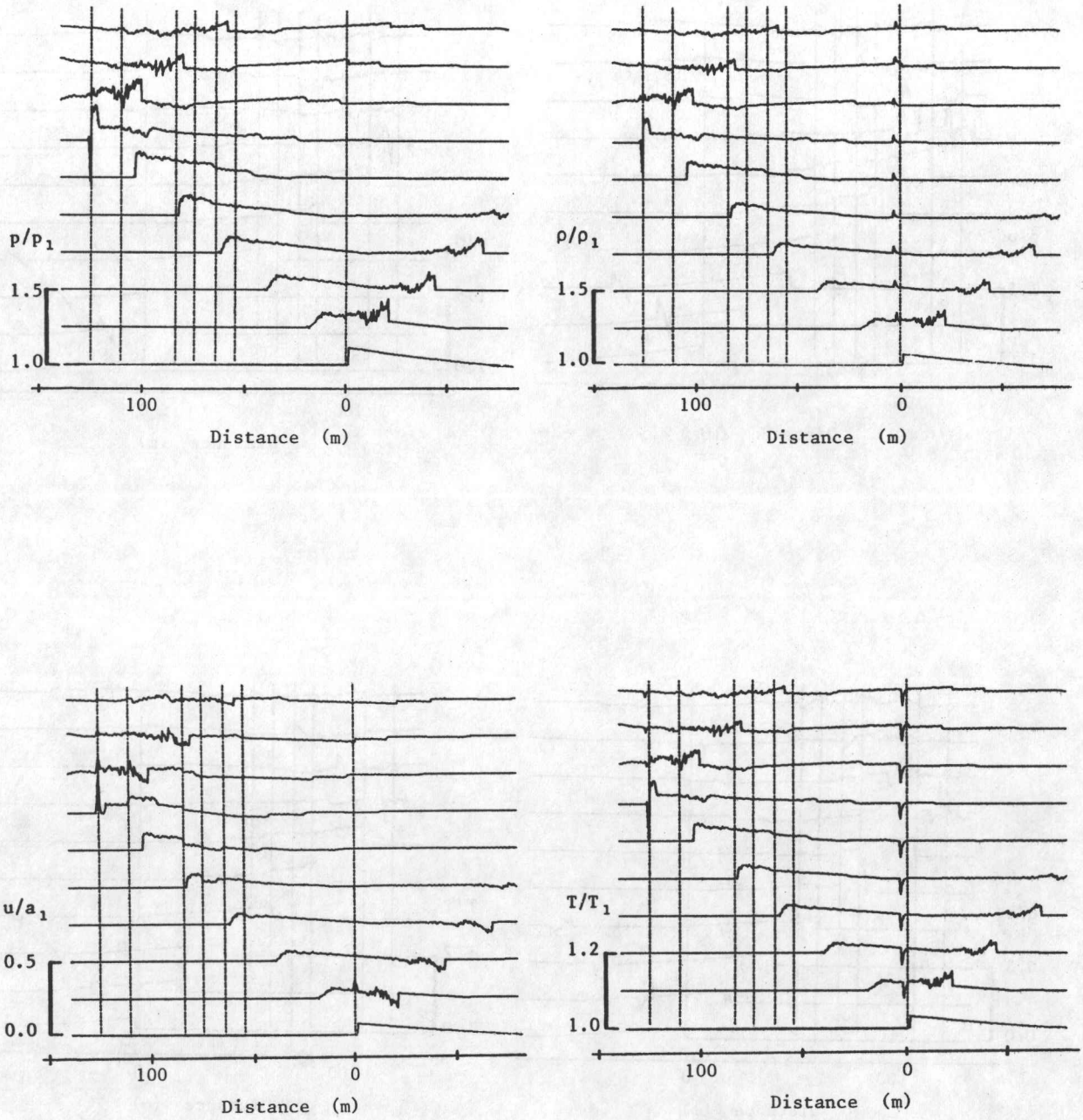

Fig. 28b. Spatial distributions of pressure, density, flow velocity and temperature for the blast-wave flow field inside the power house.

Geometrical configuration: B
Blow-out panel opening time: 100 ms

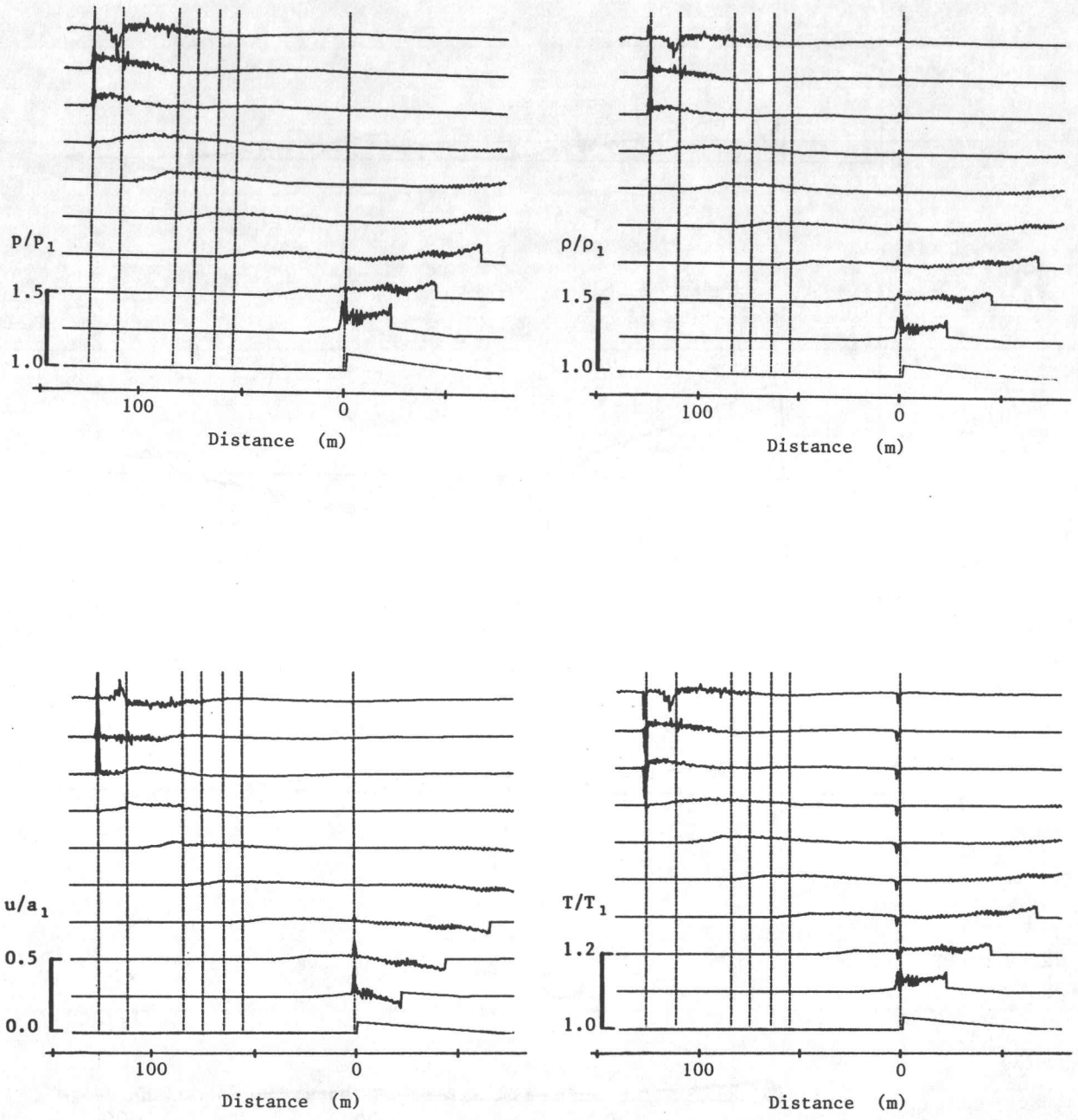

Fig. 28c. Spatial distributions of pressure, density, flow velocity and temperature for the blast-wave flow field inside the power house.

Geometrical configuration: B
Blow-out panel opening time: 500 ms

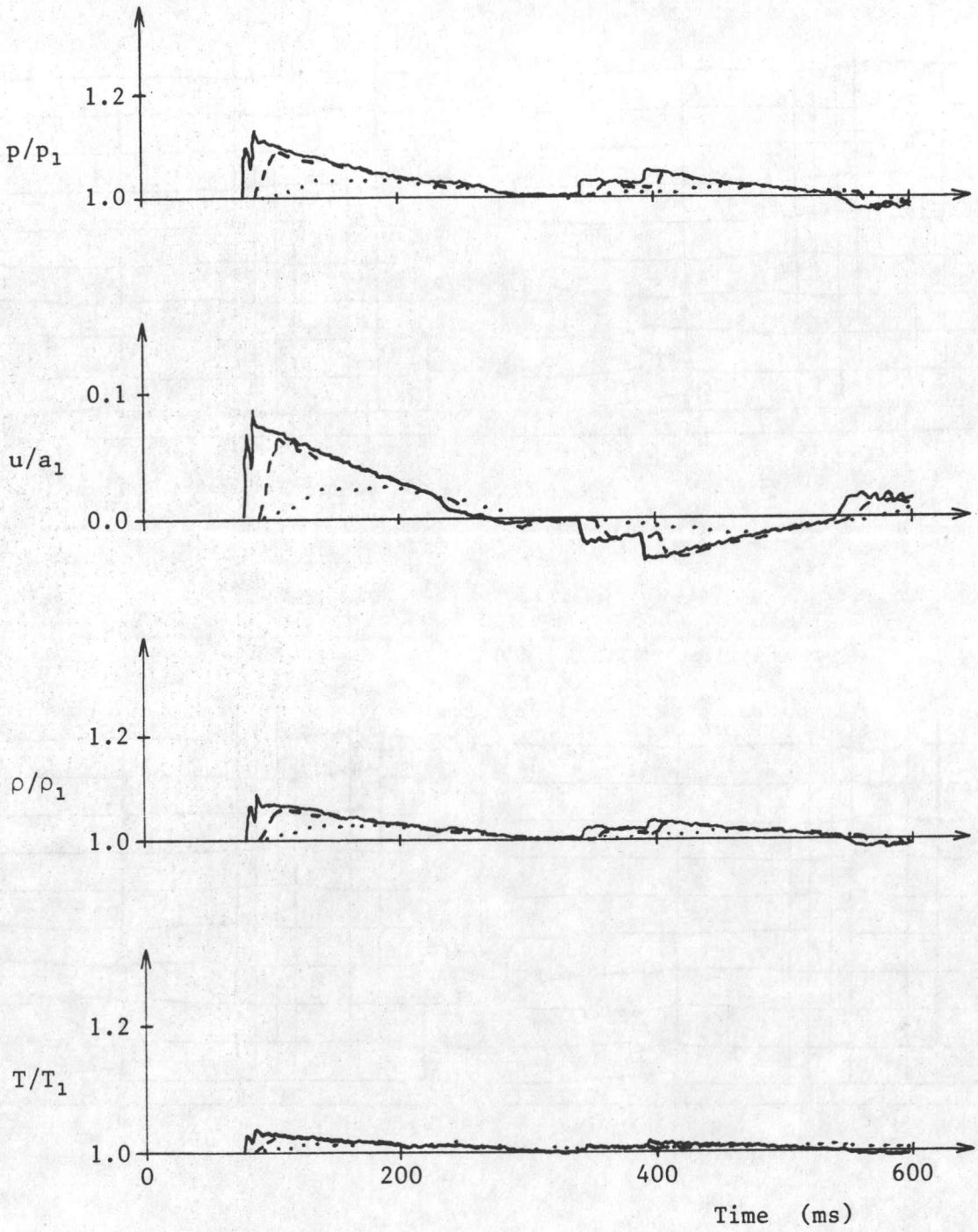

Fig. 28d. Temporal distributions of pressure, density, flow velocity and temperature for the blast-wave flow field inside the power house.

Geometrical configuration: B
Blow-out panel opening time: 0 ms ——————
100 ms - — — —
500 ms · · · · ·
Location and room number: 1

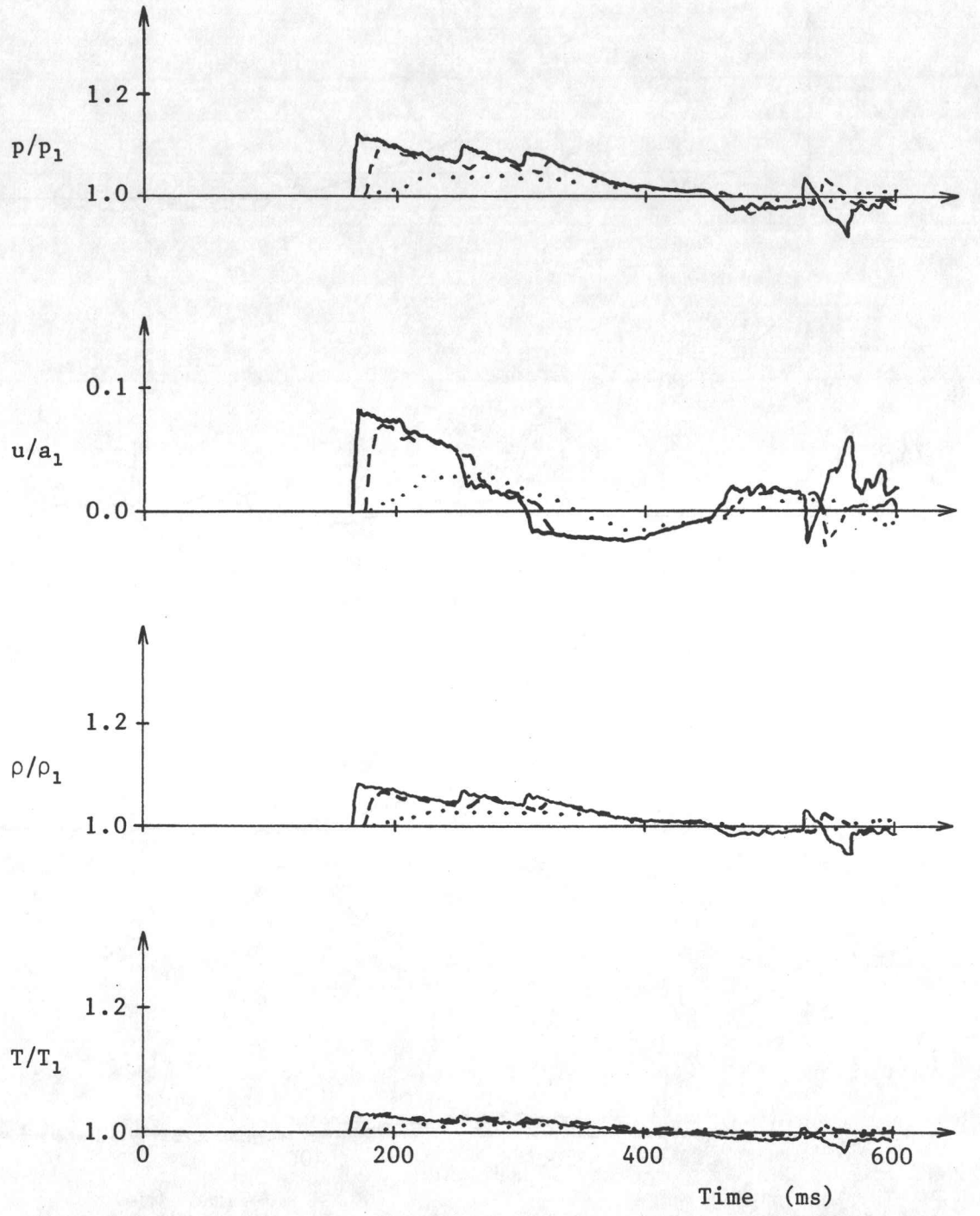

Fig. 28e. Temporal distributions of pressure, density, flow velocity and temperature for the blast-wave flow field inside the power house.

Geometrical configuration:	B
Blow-out panel opening time:	0 ms ———
	100 ms — — — —
	500 ms . . . . .
Location and room number:	2

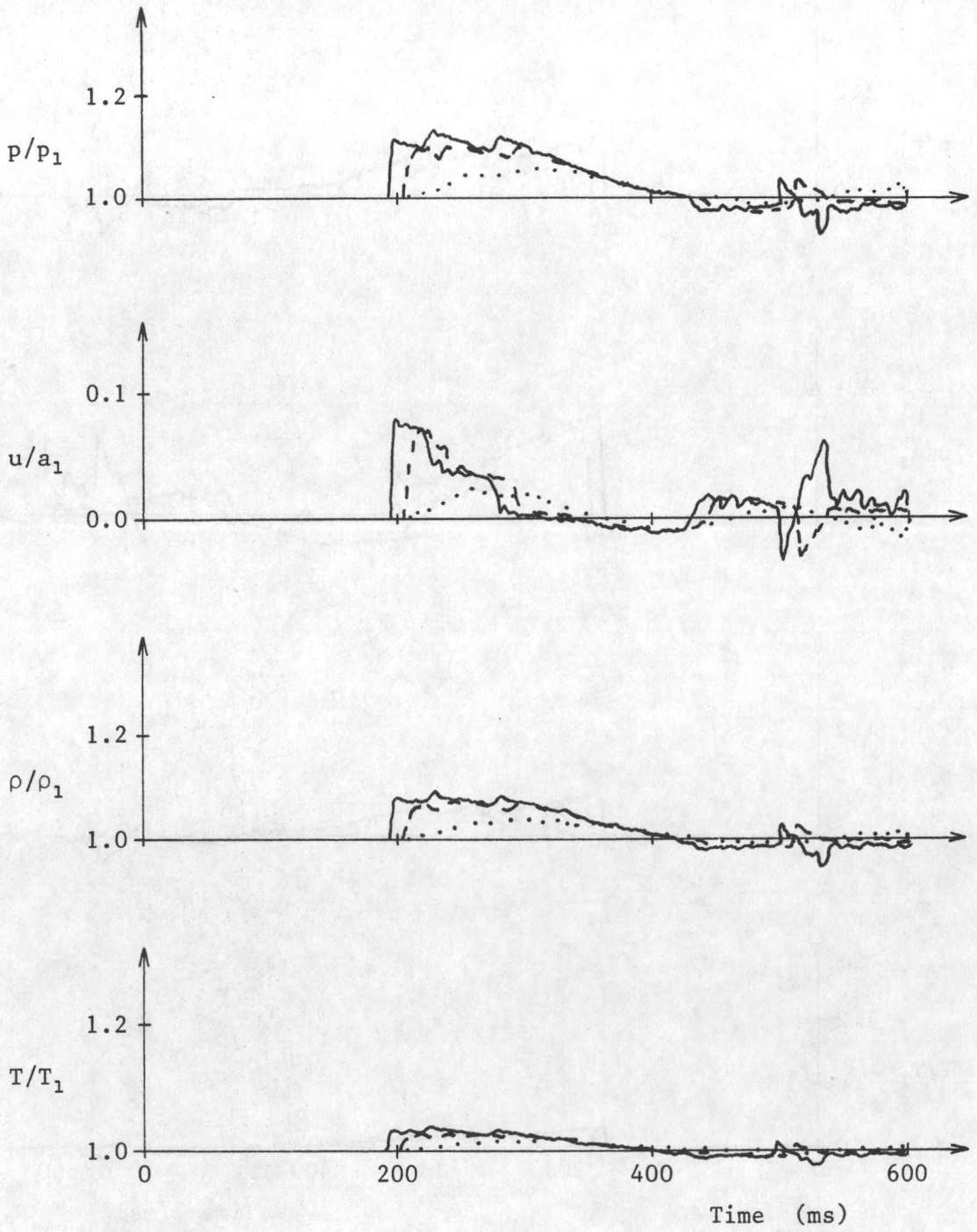

Fig. 28f. Temporal distributions of pressure, density, flow velocity and temperature for the blast-wave flow field inside the power house.

Geometrical configuration:	B
Blow-out panel opening time:	0 ms ———
	100 ms — — — —
	500 ms · · · · ·
Location and room number:	3

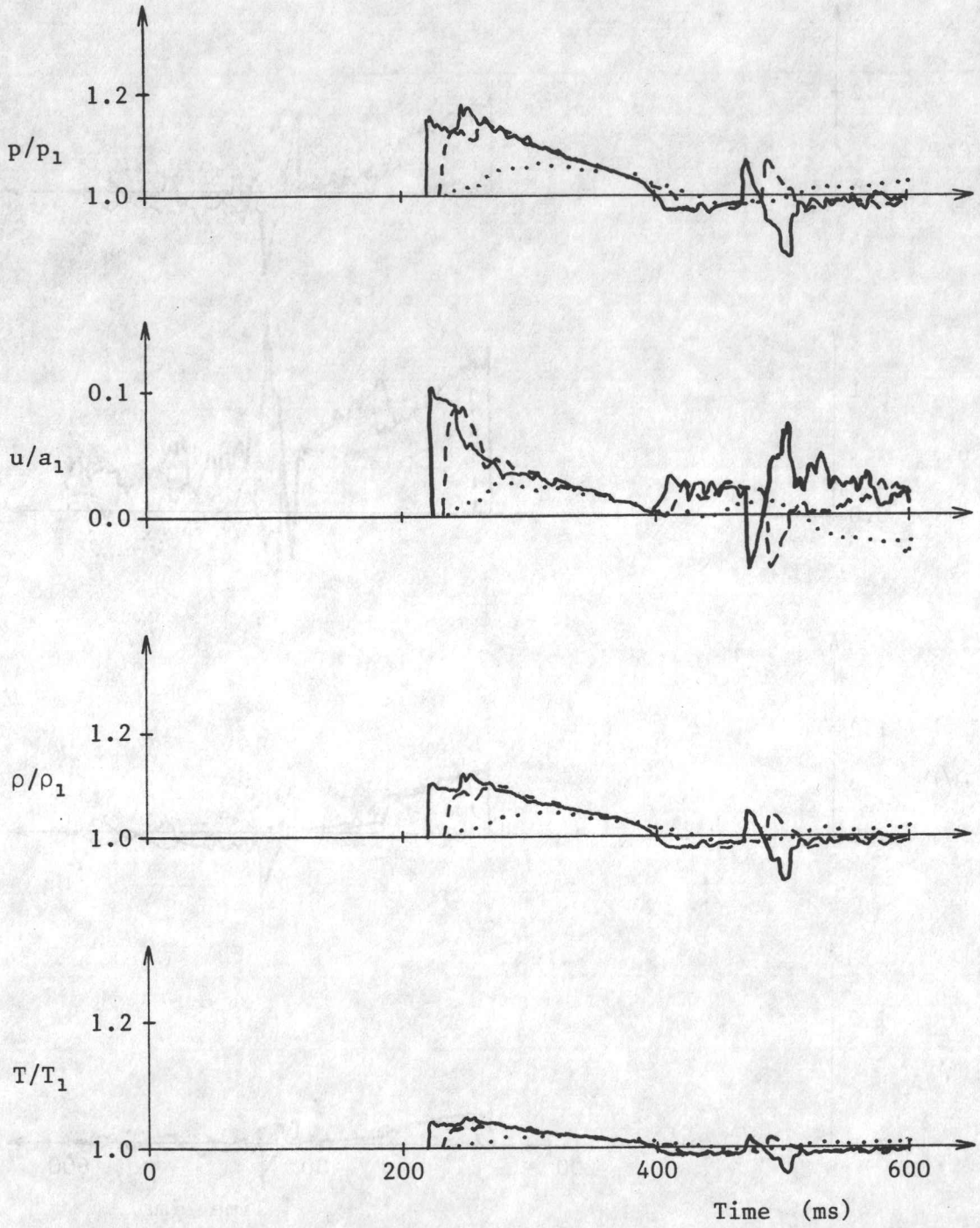

Fig. 28g. Temporal distributions of pressure, density, flow velocity and temperature for the blast-wave flow field inside the power house.

Geometrical configuration: B
Blow-out panel opening time: 0 ms ——————
100 ms — — — —
500 ms . . . . . .
Location and room number: 4

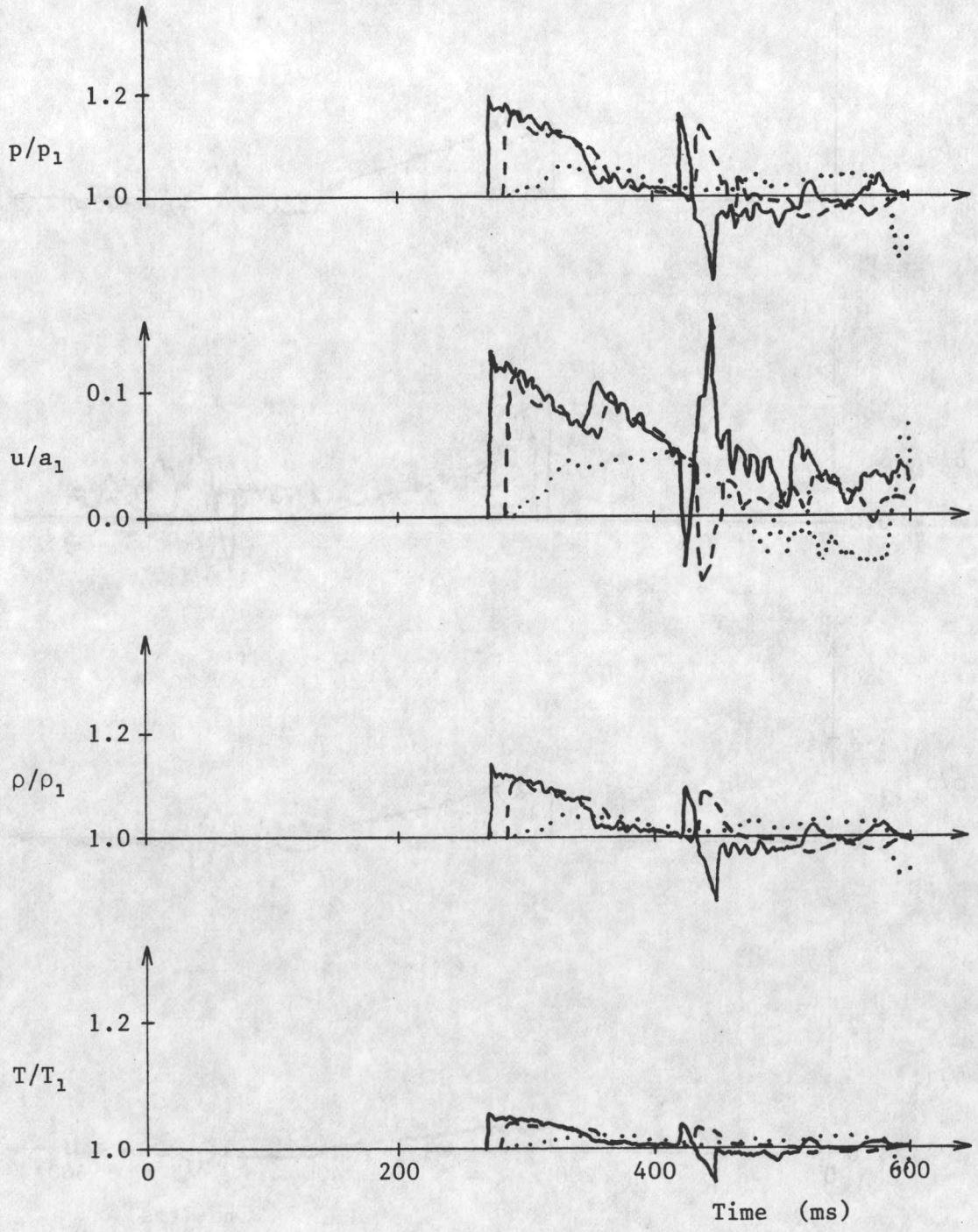

Fig. 28h. Temporal distributions of pressure, density, flow velocity and temperature for the blast-wave flow field inside the power house.

Geometrical configuration:	B
Blow-out panel opening time:	0 ms ———
	100 ms - - - -
	500 ms . . . . .
Location and room number:	5

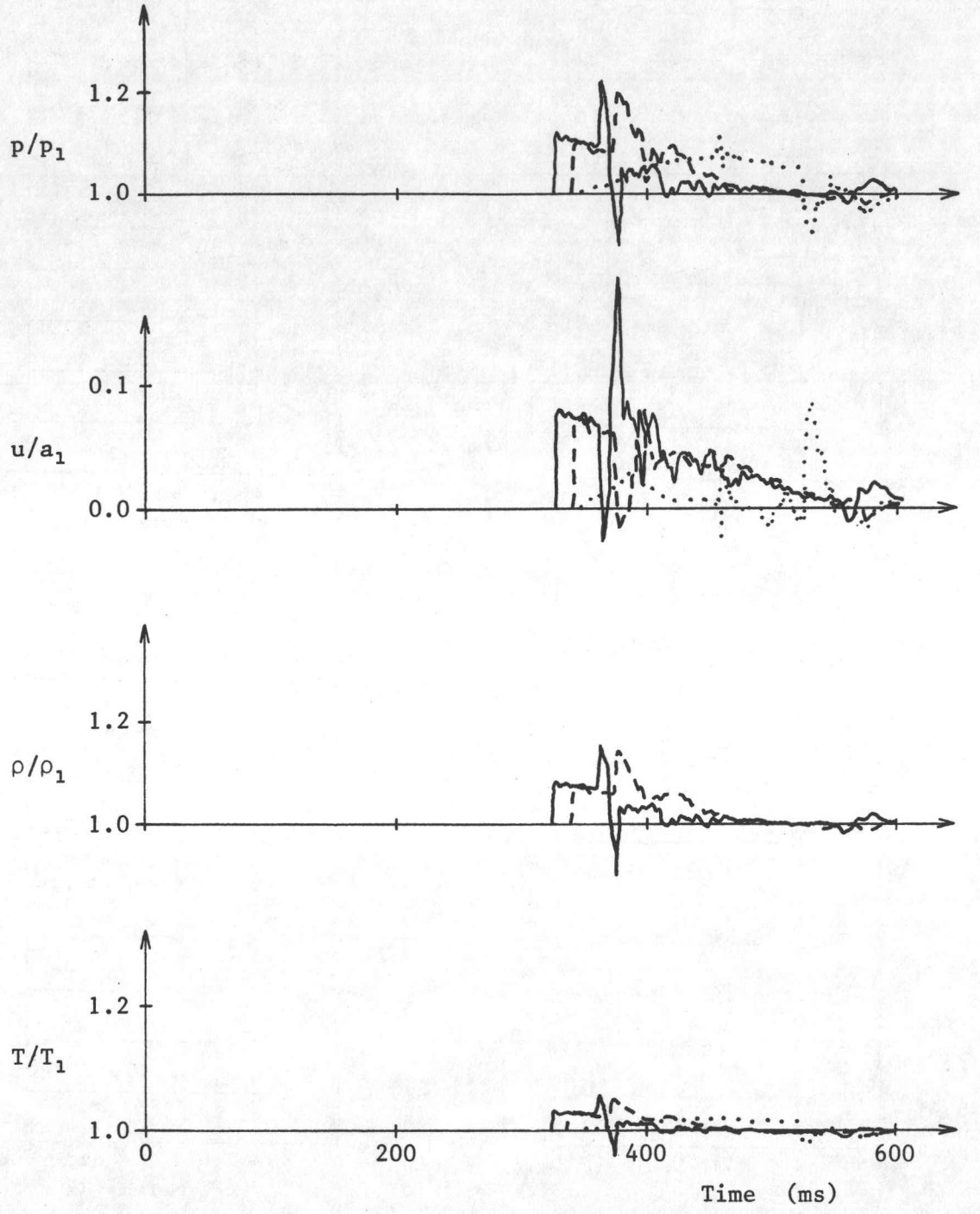

Fig. 28i. Temporal distributions of pressure, density, flow velocity and temperature for the blast-wave flow field inside the power house.

Geometrical configuration:	B
Blow-out panel opening time:	0 ms ———
	100 ms — — —
	500 ms . . . . .
Location and room number:	6

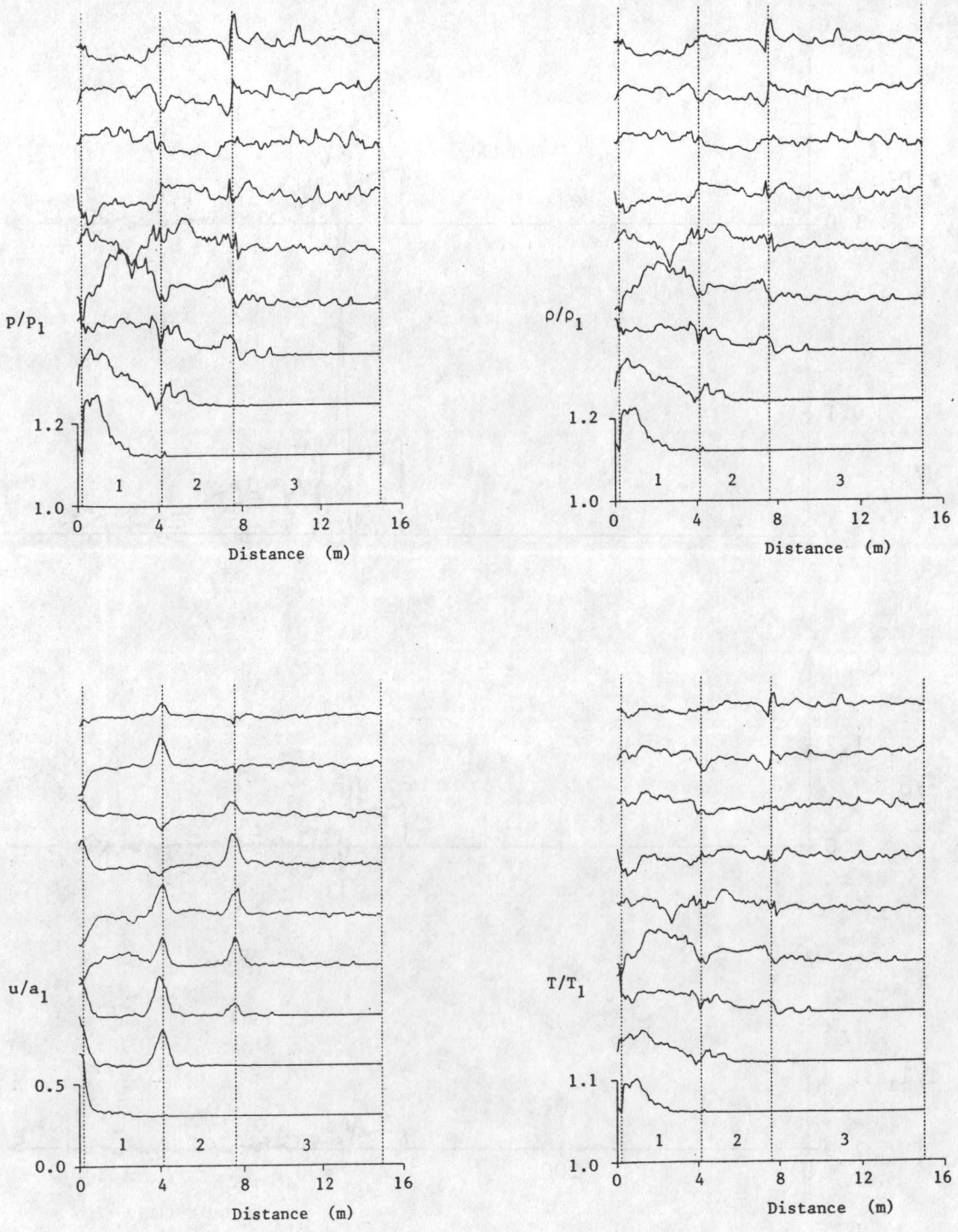

Fig. 29a. Spatial distributions of pressure, density, flow velocity and temperature for the blast-wave flow field inside the three small rooms below the hoistway.

Geometrical configuration: C
Blow-out panel opening time: 0 ms

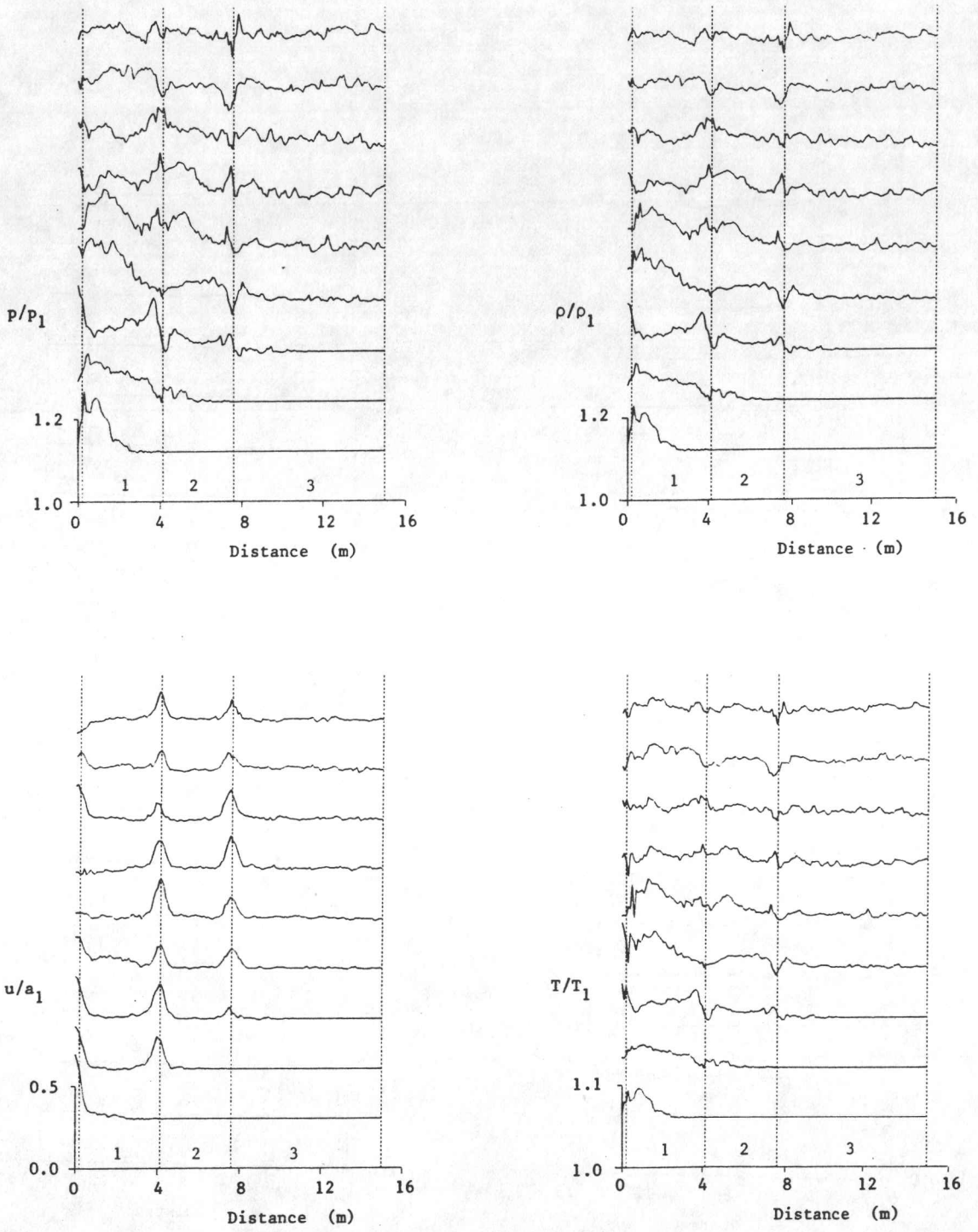

Fig. 29b. Spatial distributions of pressure, density, flow velocity and temperature for the blast-wave flow field inside the three small rooms below the hoistway.

Geometrical configuration: C
Blow-out panel opening time: 100 ms

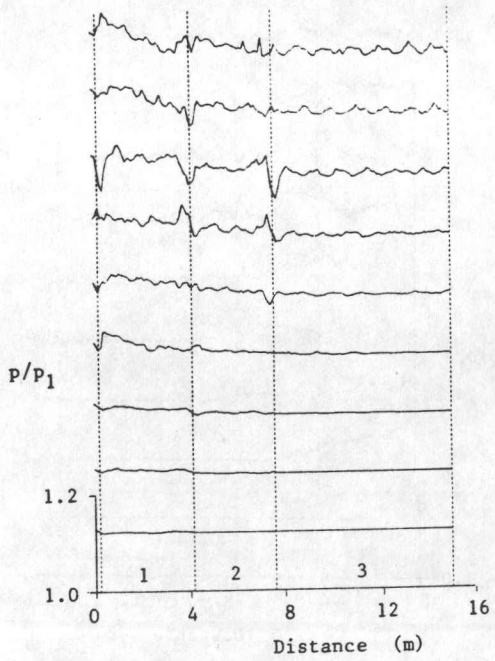

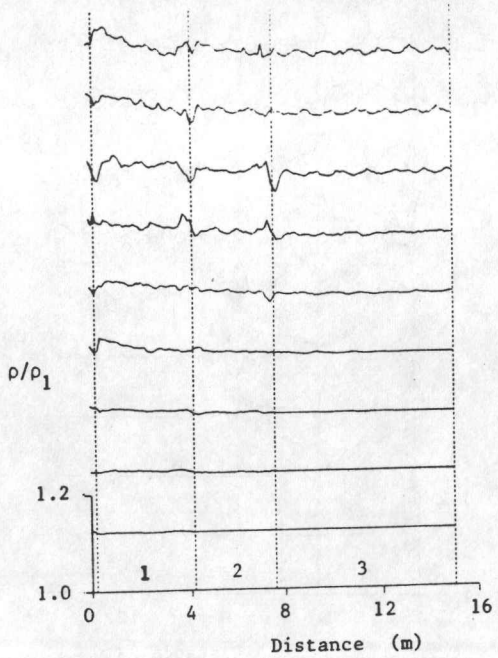

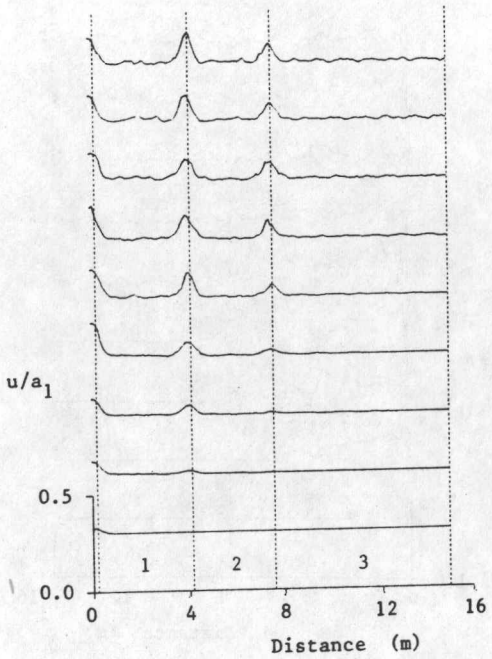

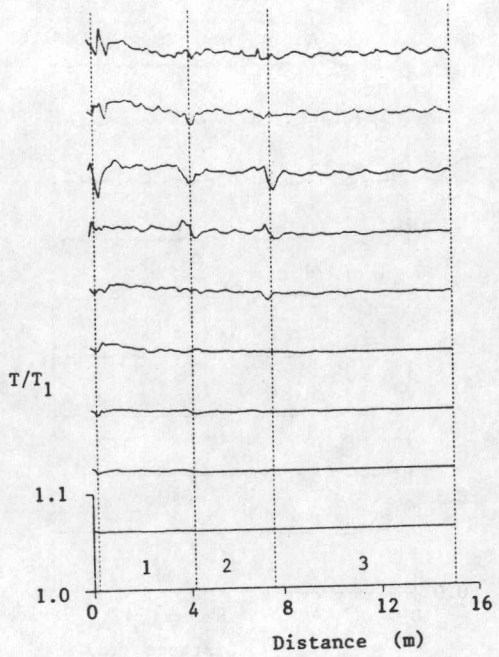

Fig. 29c. Spatial distributions of pressure, density, flow velocity and temperature for the blast-wave flow field inside the three small rooms below the hoistway.

Geometrical configuration: C
Blow-out panel opening time: 500 ms

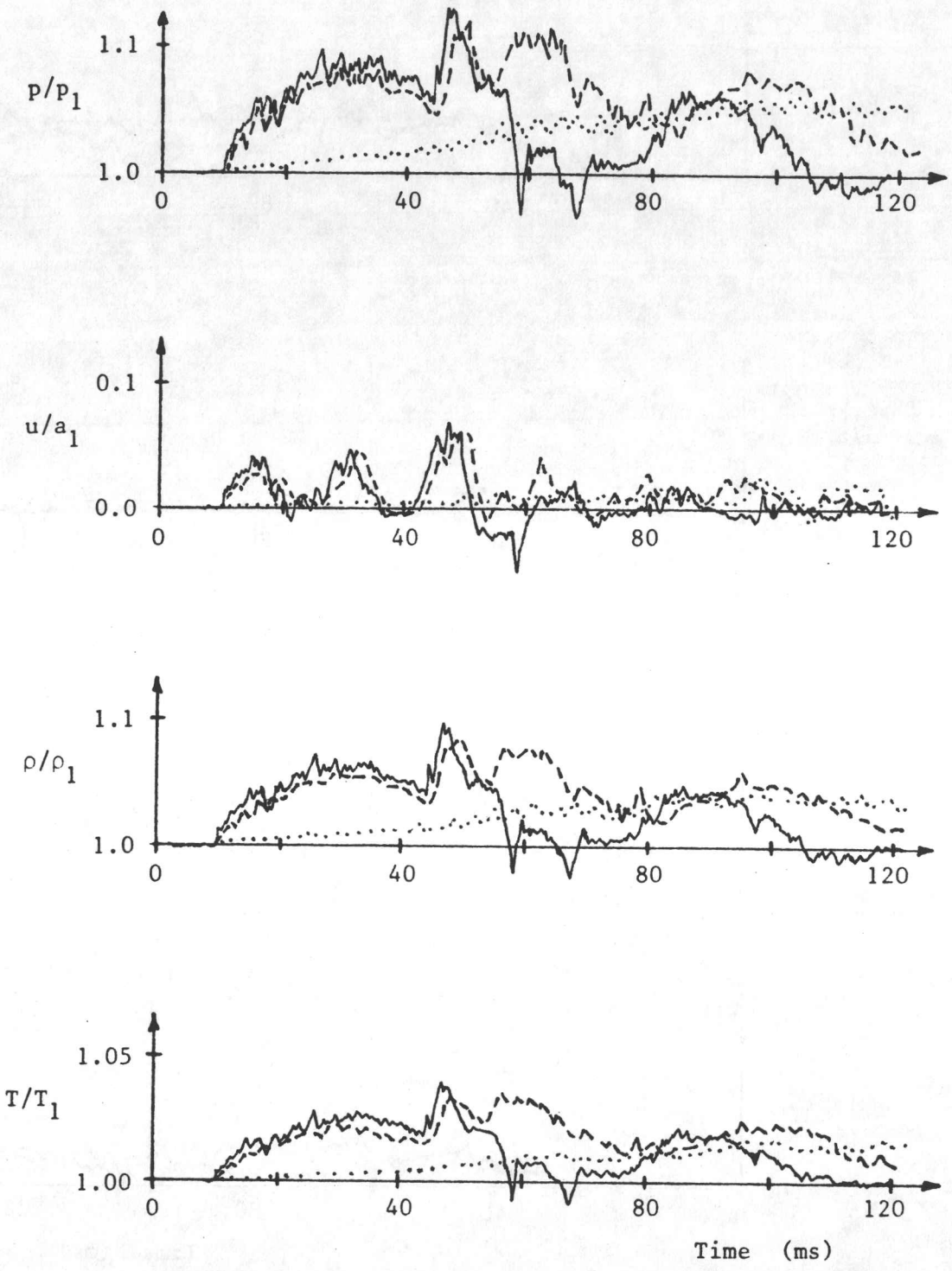

Fig. 29d. Temporal distributions of pressure, density, flow velocity and temperature for the blast-wave flow field inside the three small rooms below the hoistway.

Geometrical configuration: C
Blow-out panel opening time: 0 ms ———
100 ms - - - -
500 ms . . . . .
Location and room number: 1

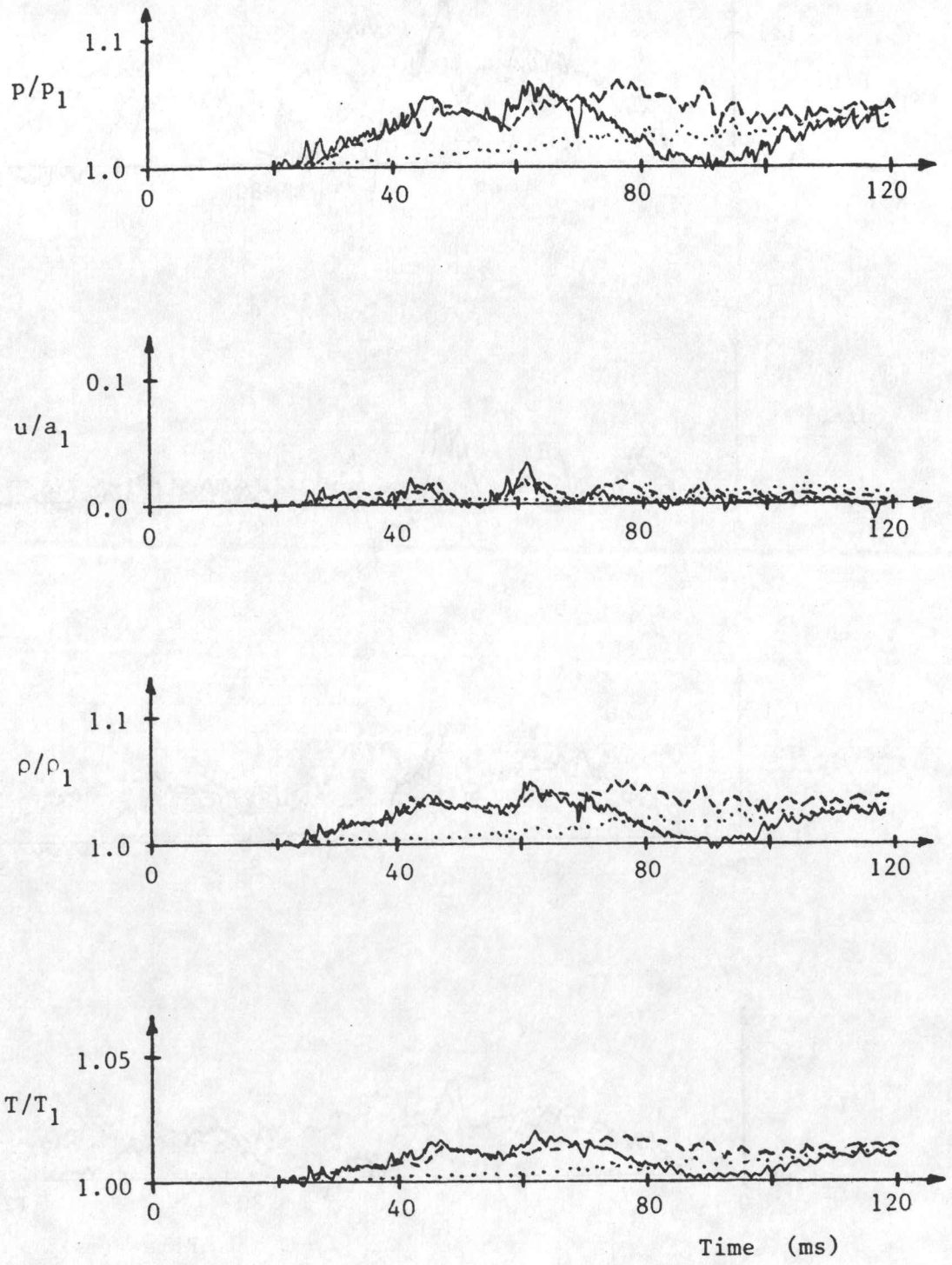

Fig. 29e. Temporal distributions of pressure, density, flow velocity an temperature for the blast-wave flow field inside the three small rooms below the hoistway.

Geometrical configuration: C
Blow-out panel opening time: 0 ms ——————
100 ms - - - -
500 ms . . . . .
Location and room number: 2

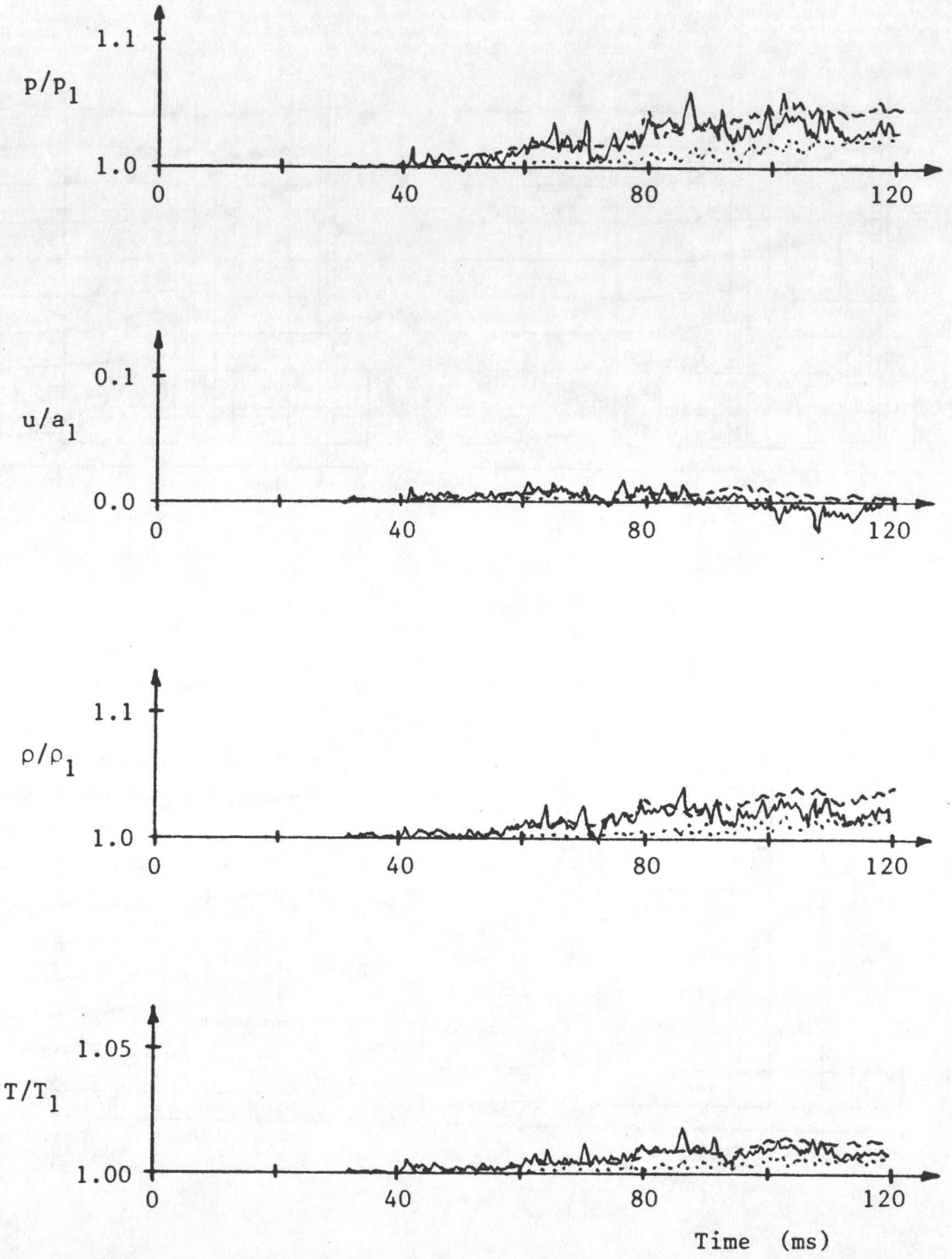

Fig. 29f. Temporal distributions of pressure, density, flow velocity and temperature for the blast-wave flow field inside the three small rooms below the hoistway.

Geometrical configuration: C
Blow-out panel opening time: 0 ms ——————
100 ms — — — —
500 ms . . . . .
Location and room number: 3

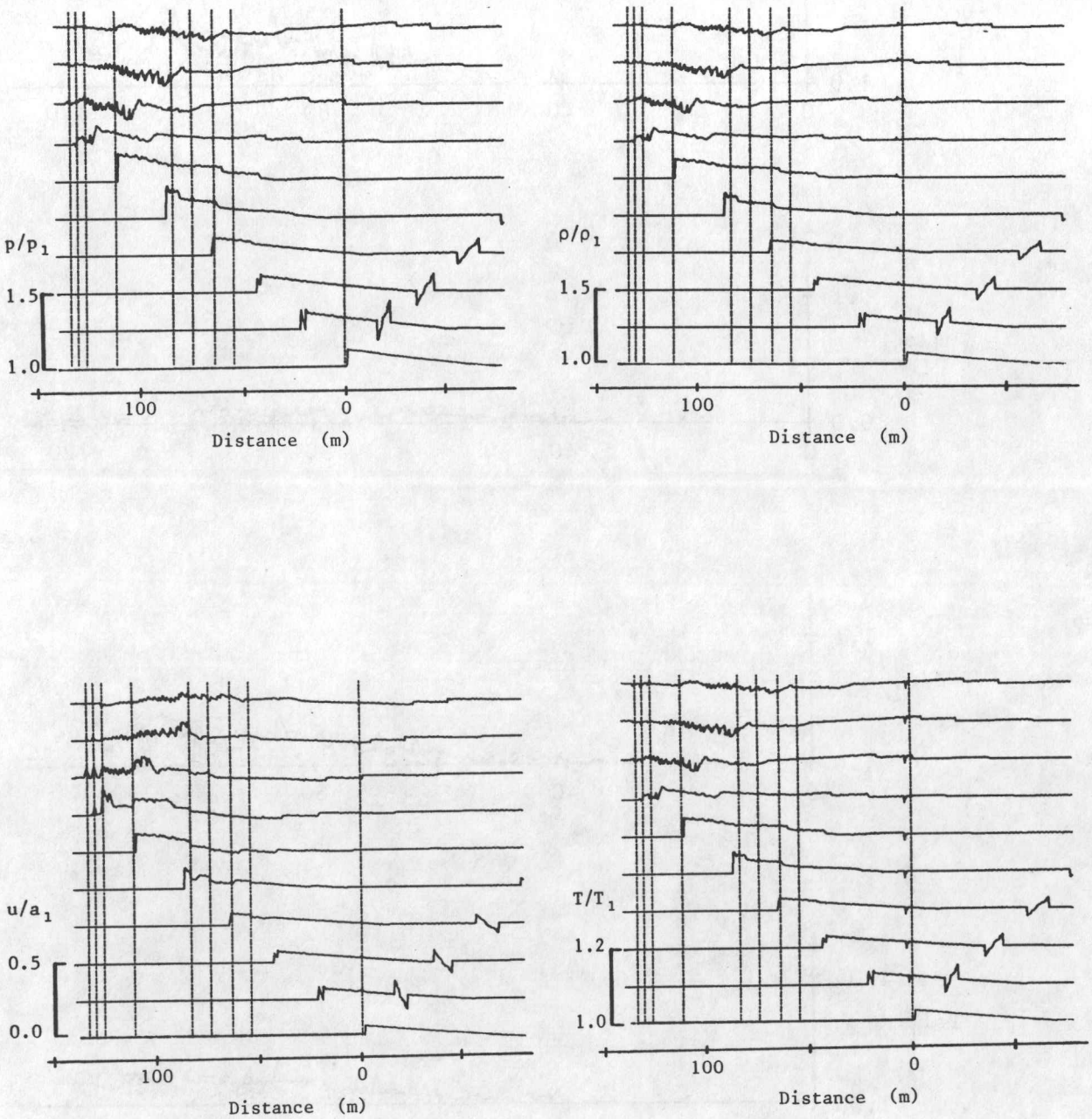

Fig. 30a. Spatial distributions of pressure, density, flow velocity and temperature for the blast-wave flow field inside the power house.

Geometrical configuration: D
Blow-out panel opening time: 0 ms

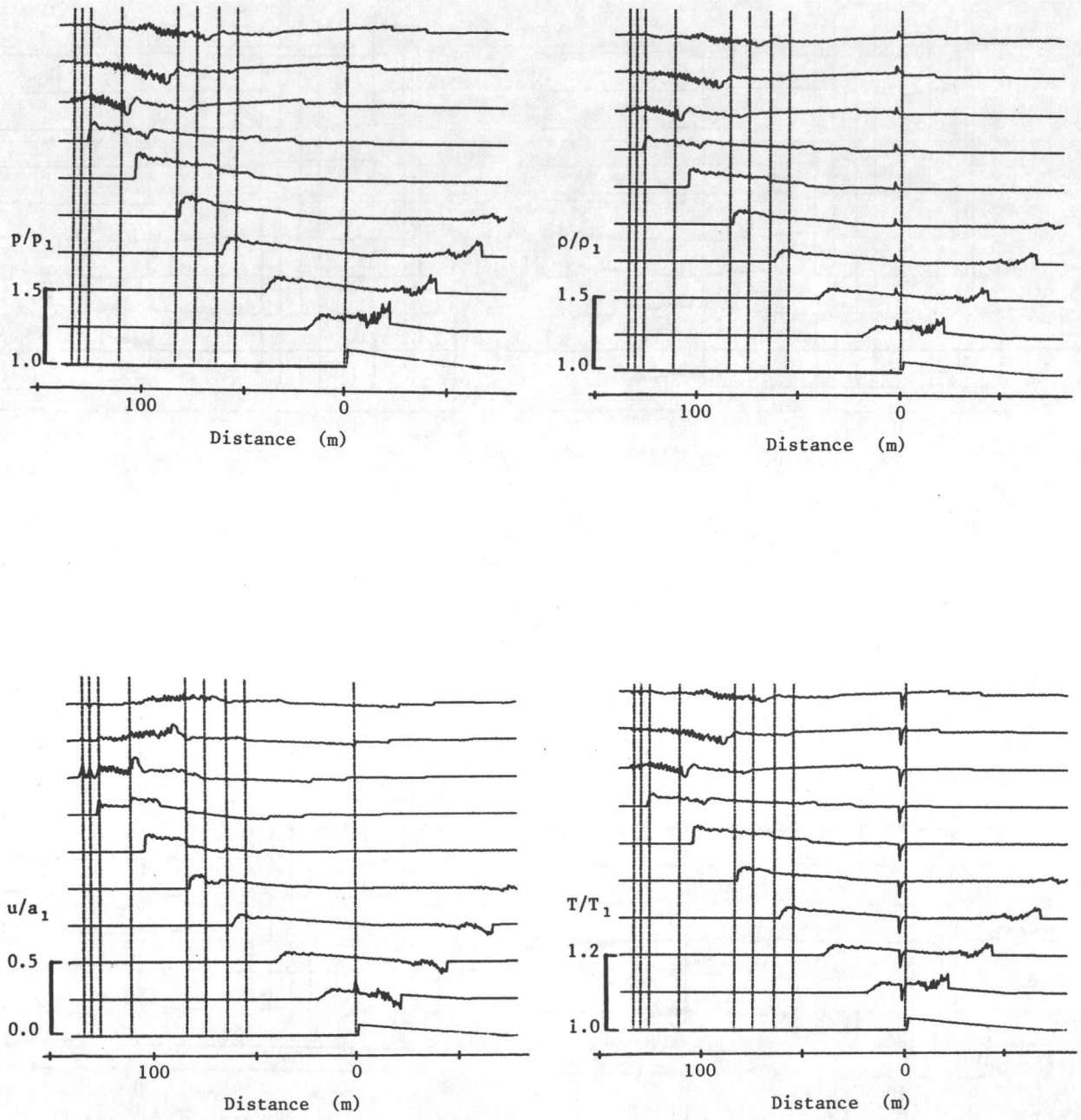

Fig. 30b. Spatial distributions of pressure, density, flow velocity and temperature for the blast-wave flow field inside the power house.

Geometrical configuration: D
Blow-out panel opening time: 100 ms

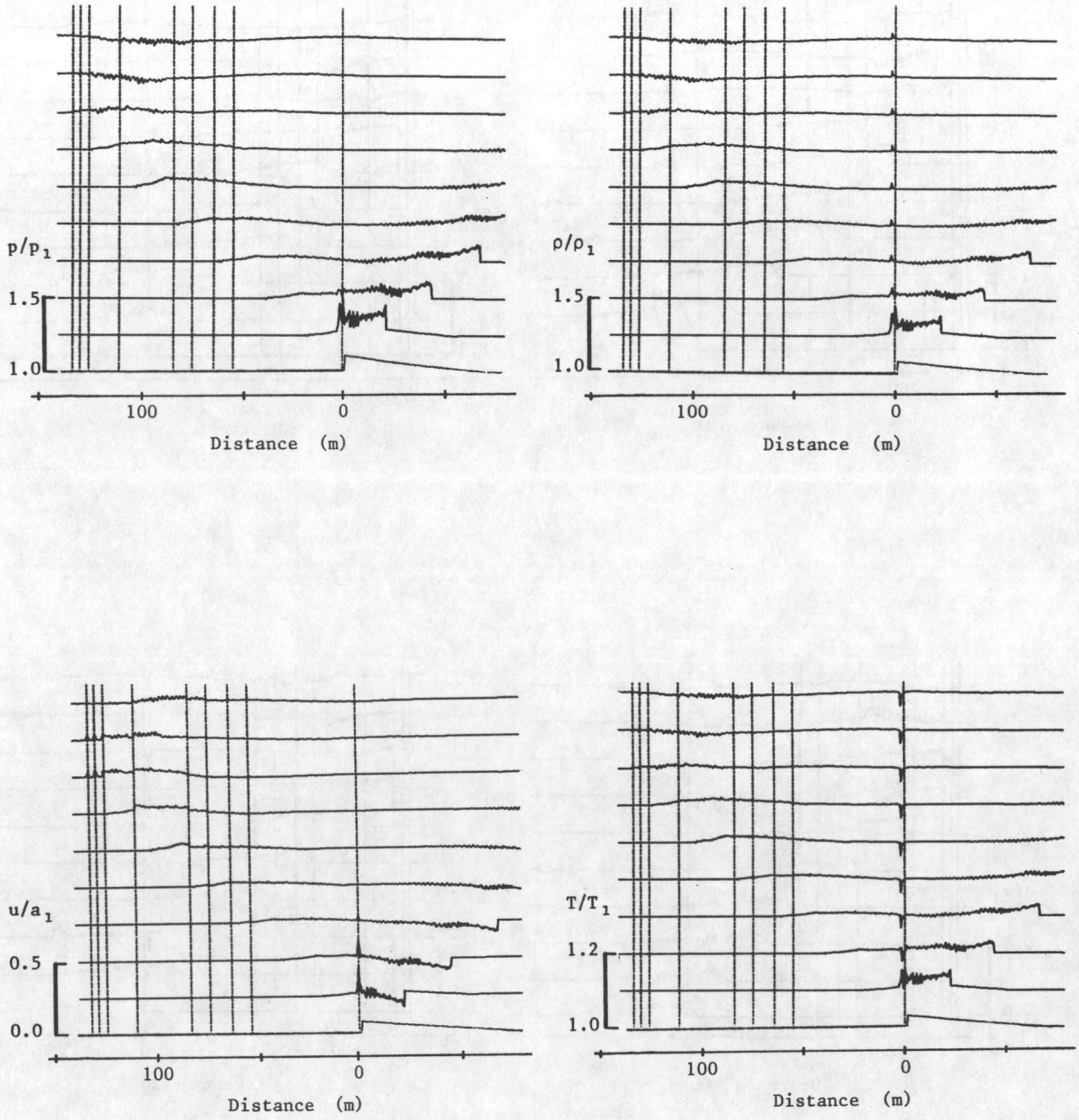

Fig. 30c. Spatial distributions of pressure, density, flow velocity and temperature for the blast-wave flow field inside the power house.

Geometrical configuration: D
Blow-out panel opening time: 500 ms

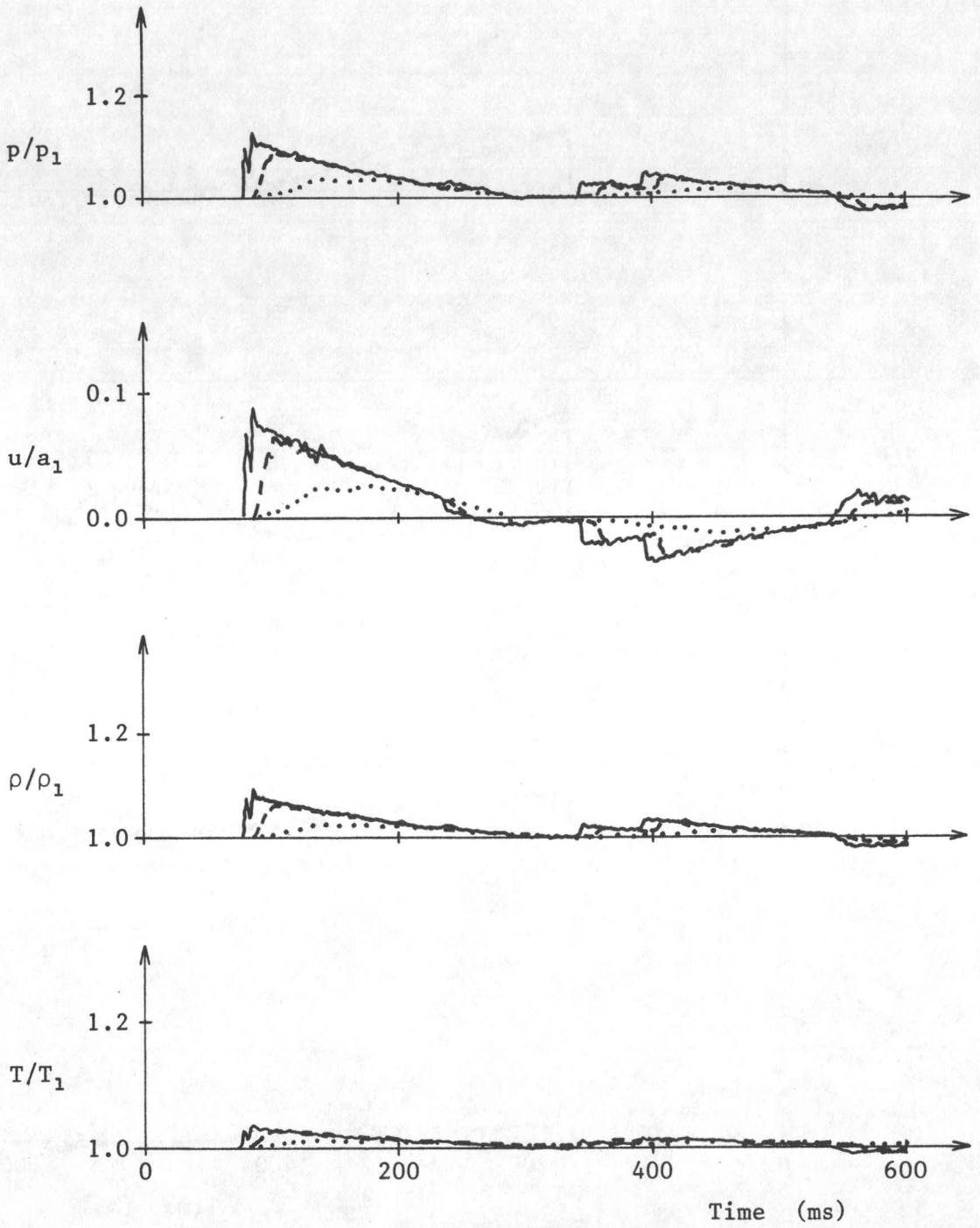

Fig. 30d. Temporal distributions of pressure, density, flow velocity and temperature for the blast-wave flow field inside the power house.

Geometrical configuration:	D
Blow-out panel opening time:	0 ms ———
	100 ms — — — —
	500 ms . . . . .
Location and room number:	1

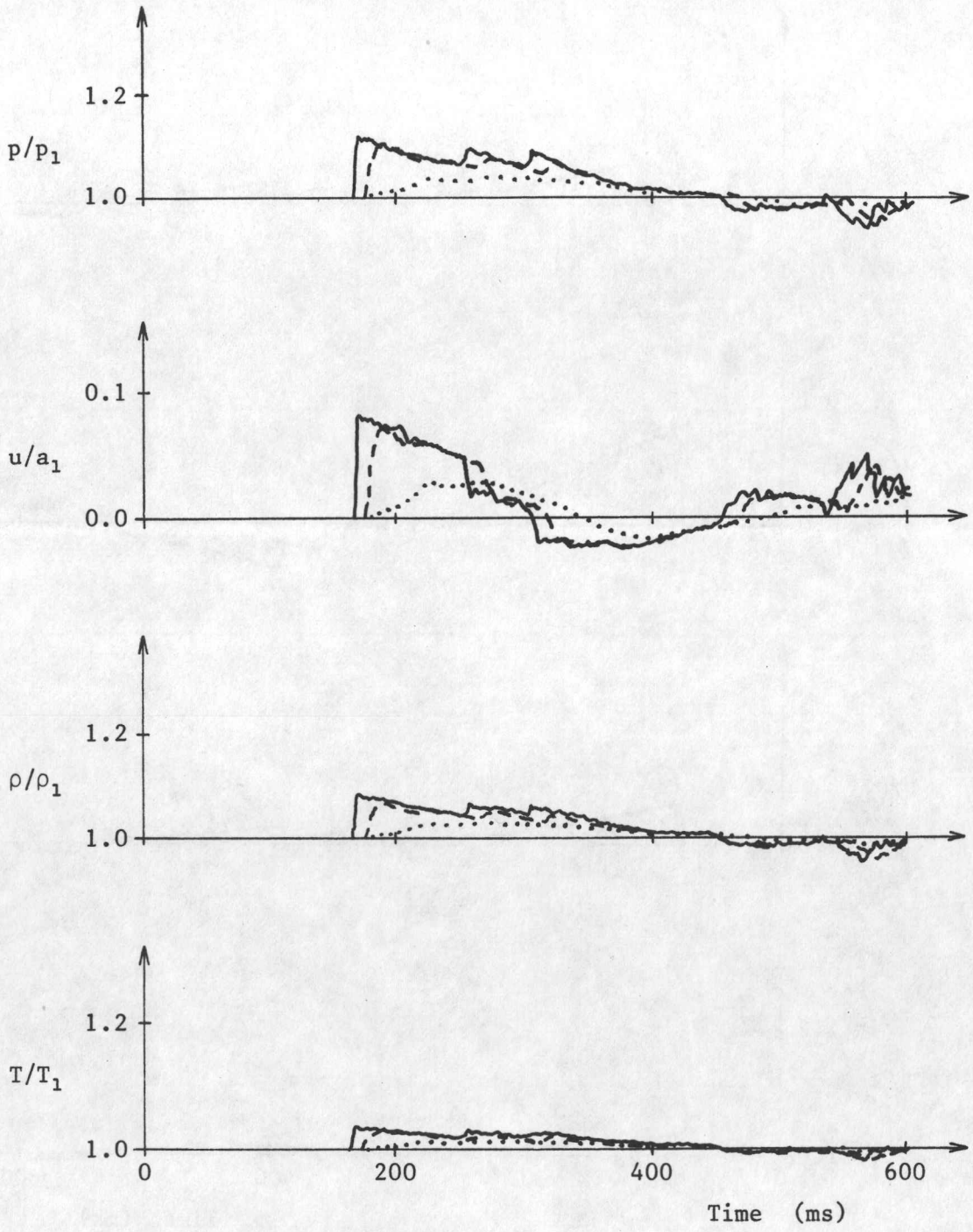

Fig. 30e. Temporal distributions of pressure, density, flow velocity and temperature for the blast-wave flow field inside the power house.

Geometrical configuration:	D
Blow-out panel opening time:	0 ms ———
	100 ms – – – –
	500 ms · · · · ·
Location and room number:	2

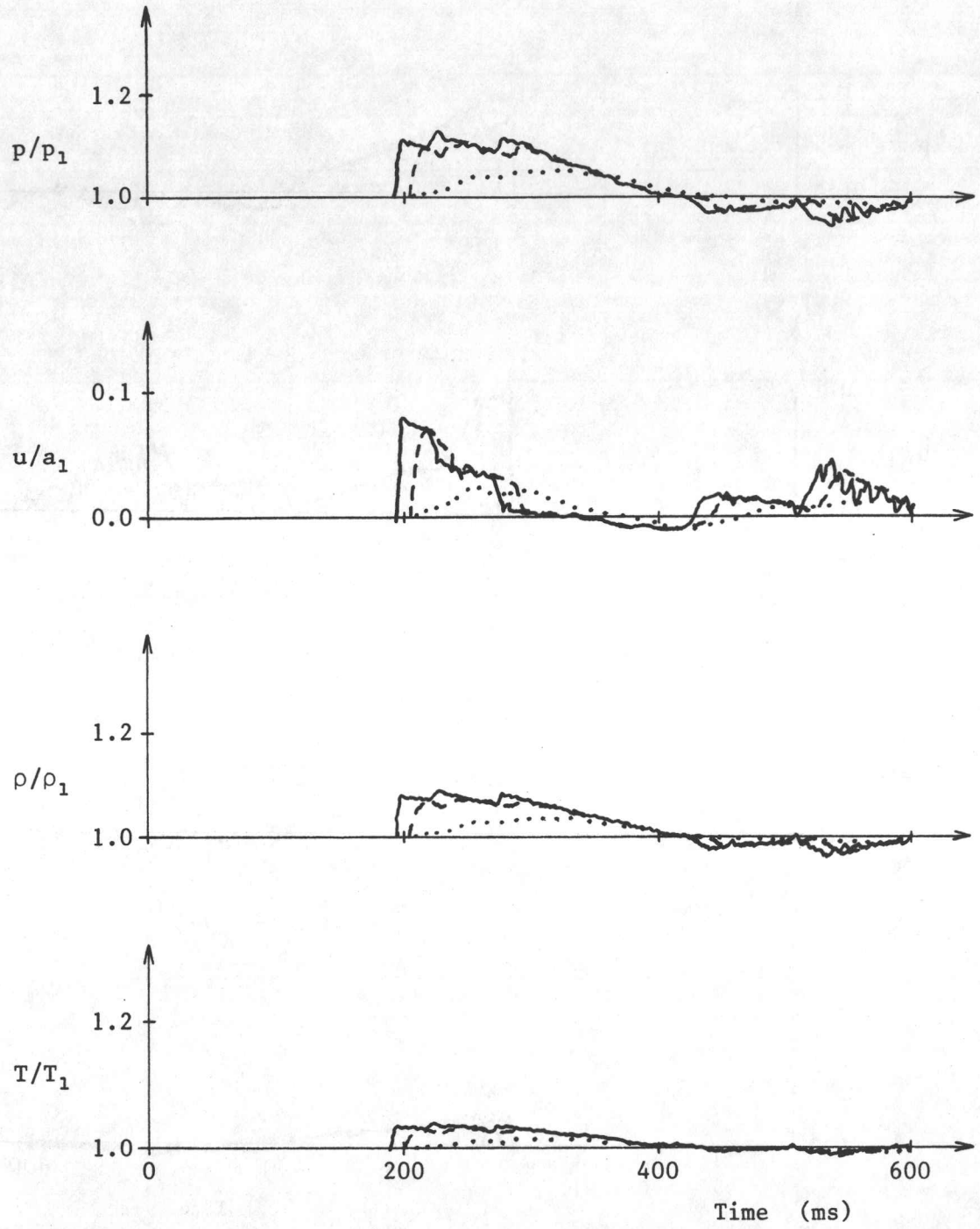

Fig. 30f. Temporal distributions of pressure, density, flow velocity and temperature for the blast-wave flow field inside the power house.

Geometrical configuration:	D
B w-out panel opening time:	0 ms ———
	100 ms - - - -
	500 ms . . . . .
Location and room number:	3

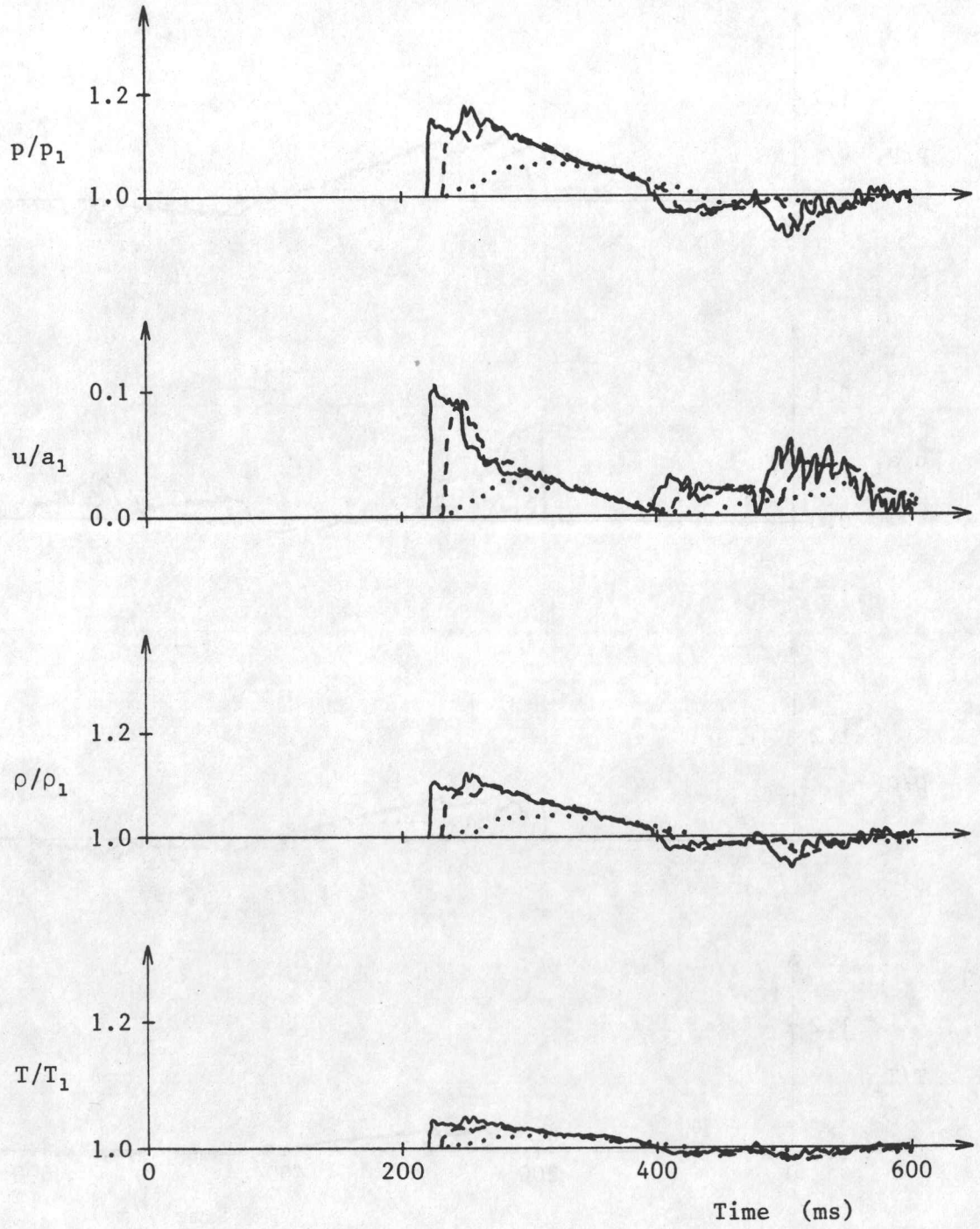

Fig. 30g. Temporal distributions of pressure, density, flow velocity and temperature for the blast-wave flow field inside the power house.

Geometrical configuration:	D
Blow-out panel opening time:	0 ms ———
	100 ms – – – –
	500 ms . . . . .
Location and room number:	4

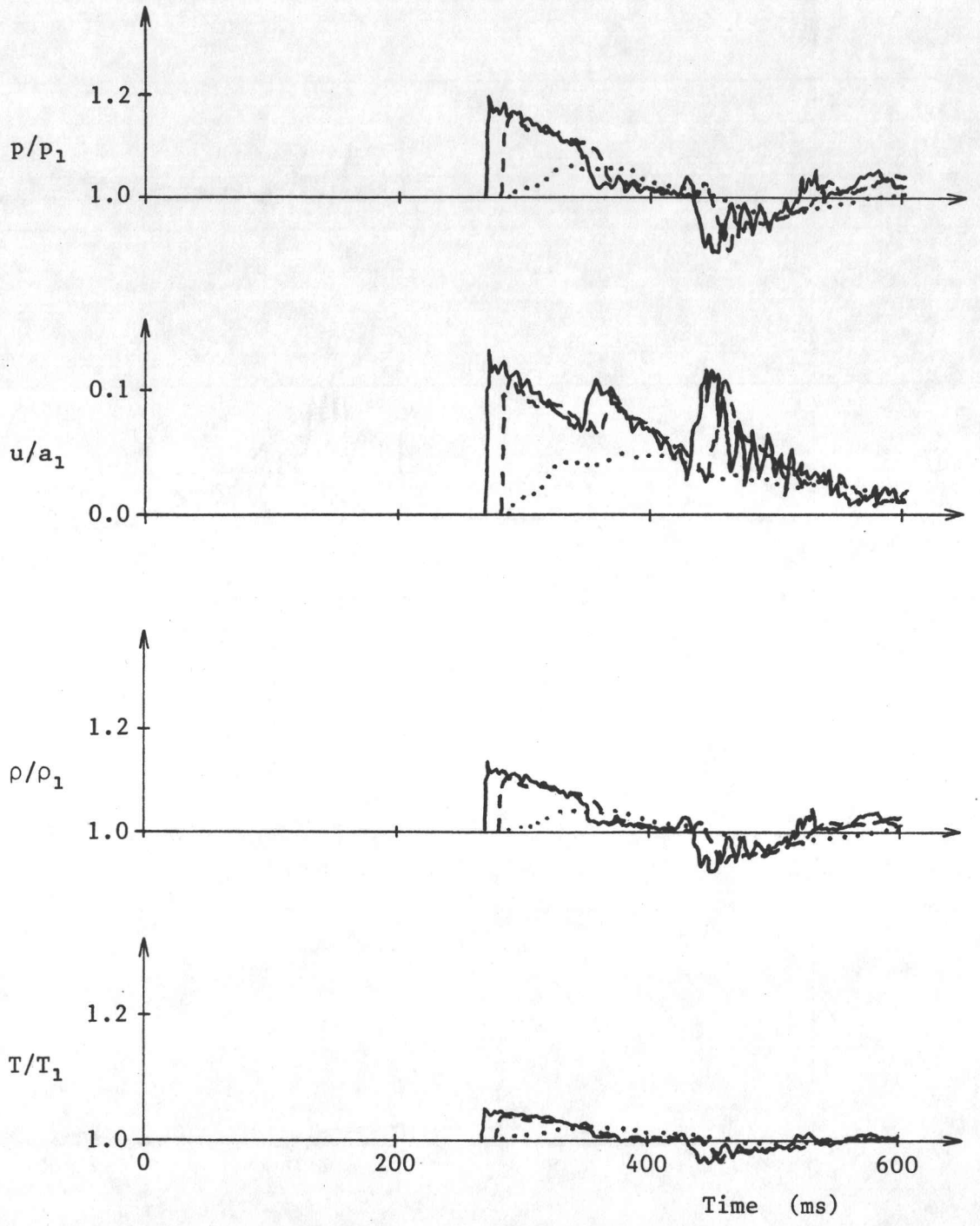

Fig. 30h. Temporal distributions of pressure, density, flow velocity and temperature for the blast-wave flow field inside the power house.

Geometrical configuration:	D
Blow-out panel opening time:	0 ms ———
	100 ms - - - -
	500 ms . . . . .
Location and room number:	5

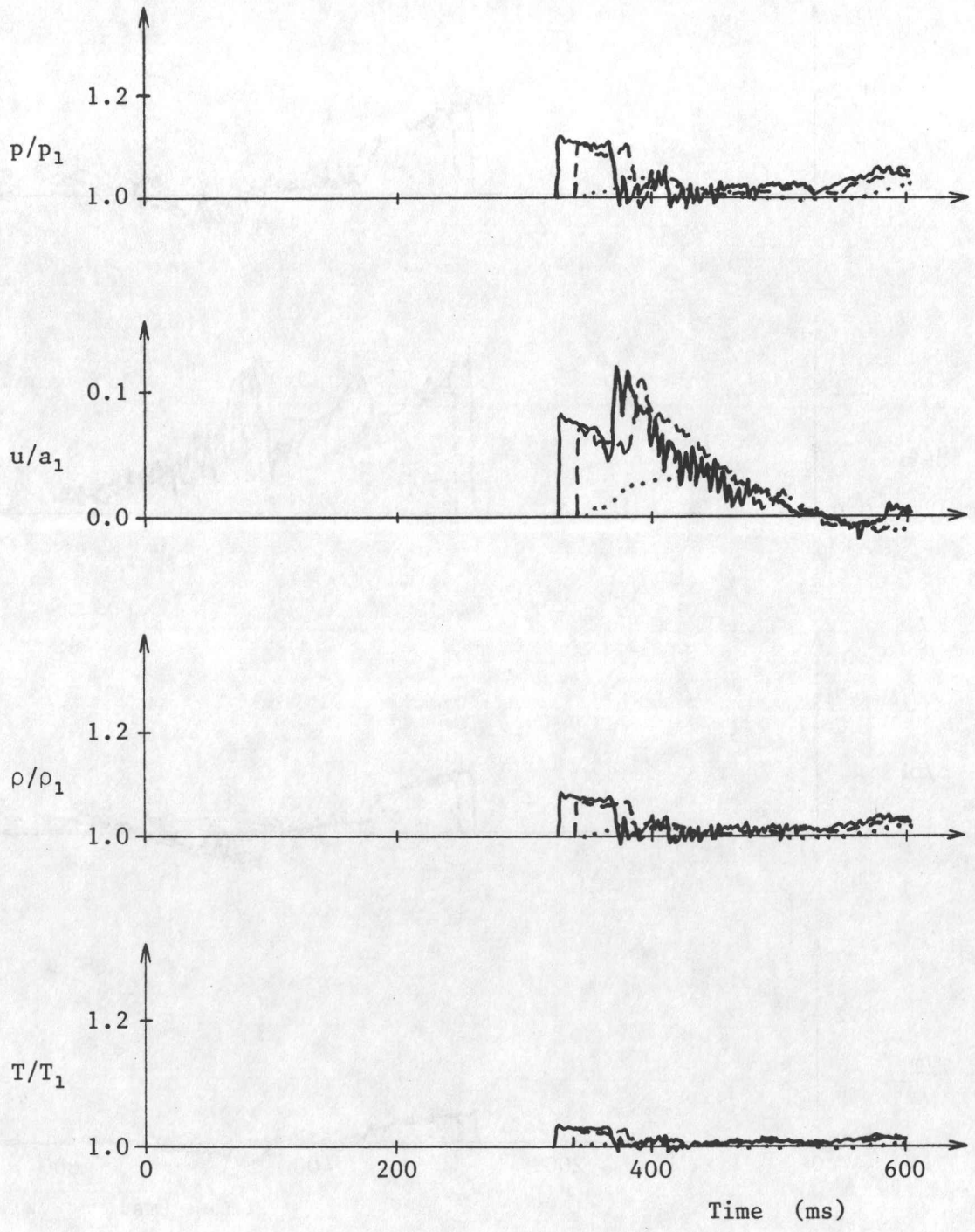

Fig. 30i. Temporal distributions of pressure, density, flow velocity and temperature for the blast-wave flow field inside the power house.

Geometrical configuration:	D
Blow-out panel opening time:	0 ms ———
	100 ms – – – –
	500 ms · · · · ·
Location and room number:	6

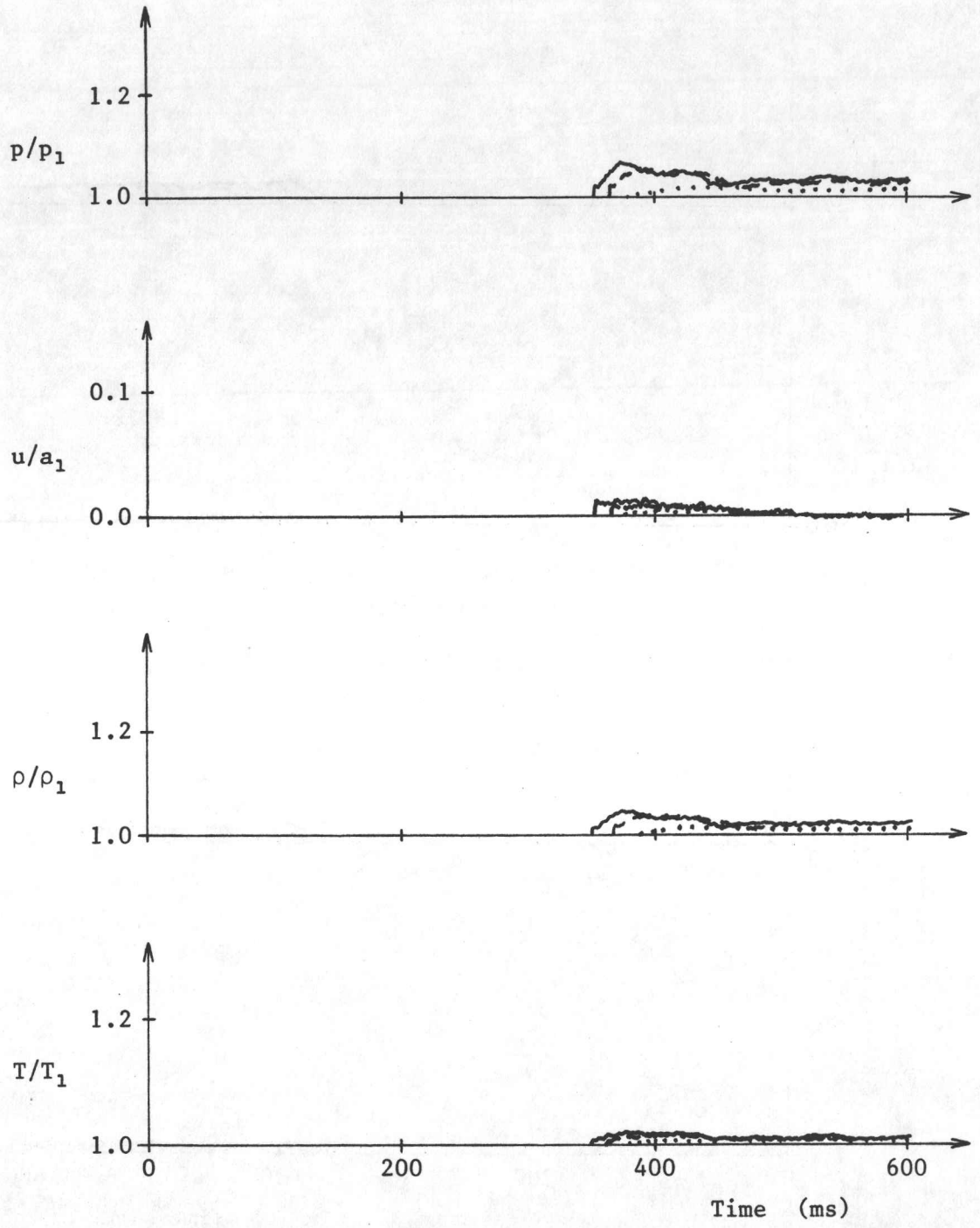

Fig. 30j. Temporal distributions of pressure, density, flow velocity and temperature for the blast-wave flow field inside the power house.

Geometrical configuration: D
Blow-out panel opening time: 0 ms ——————
100 ms — — — —
500 ms . . . . .
Location and room number: 7

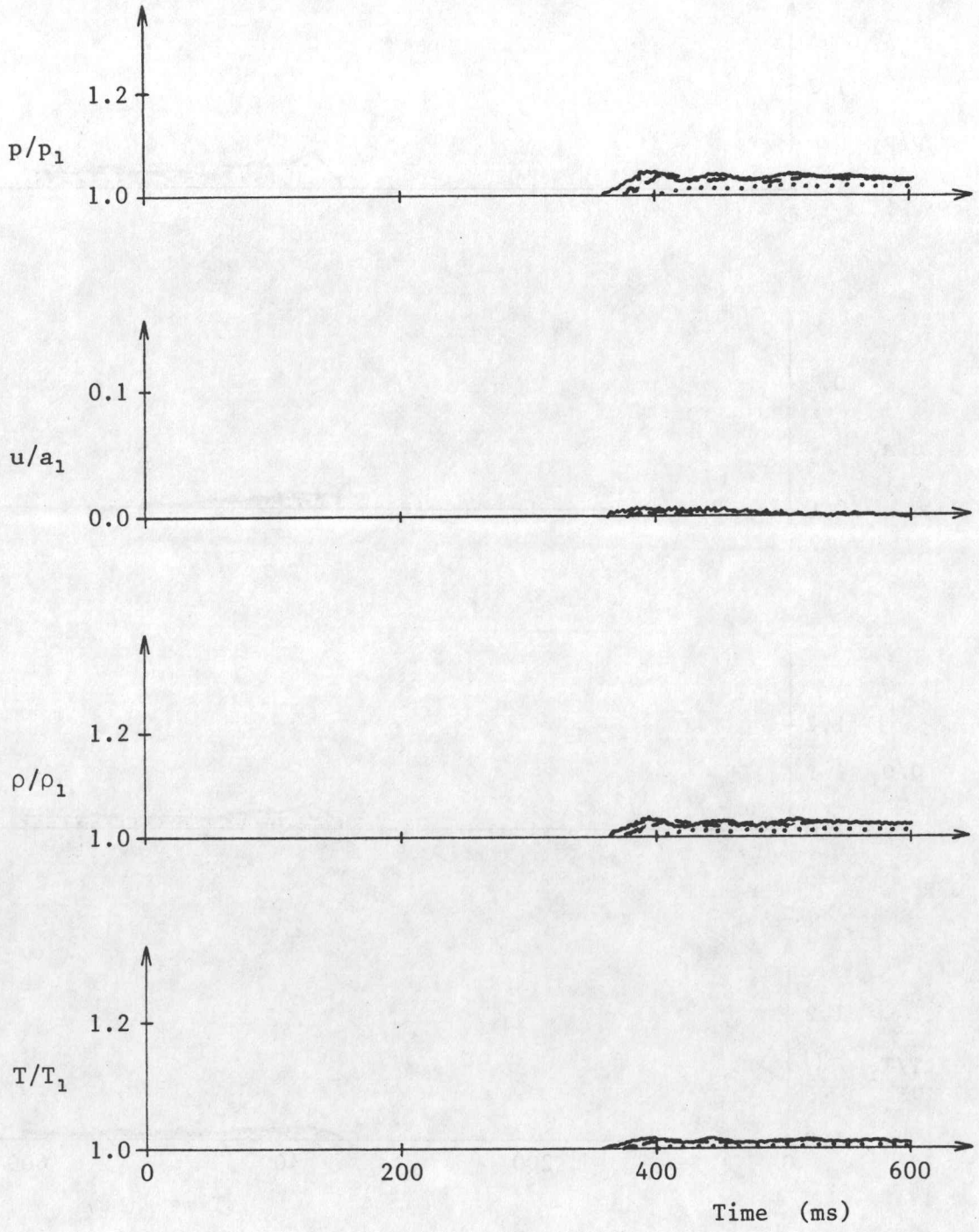

Fig. 30k. Temporal distributions of pressure, density, flow velocity and temperature for the blast-wave flow field inside the power house.

Geometrical configuration:	D
Blow-out panel opening time:	0 ms ———
	100 ms – – – –
	500 ms . . . . .
Location and room number:	8

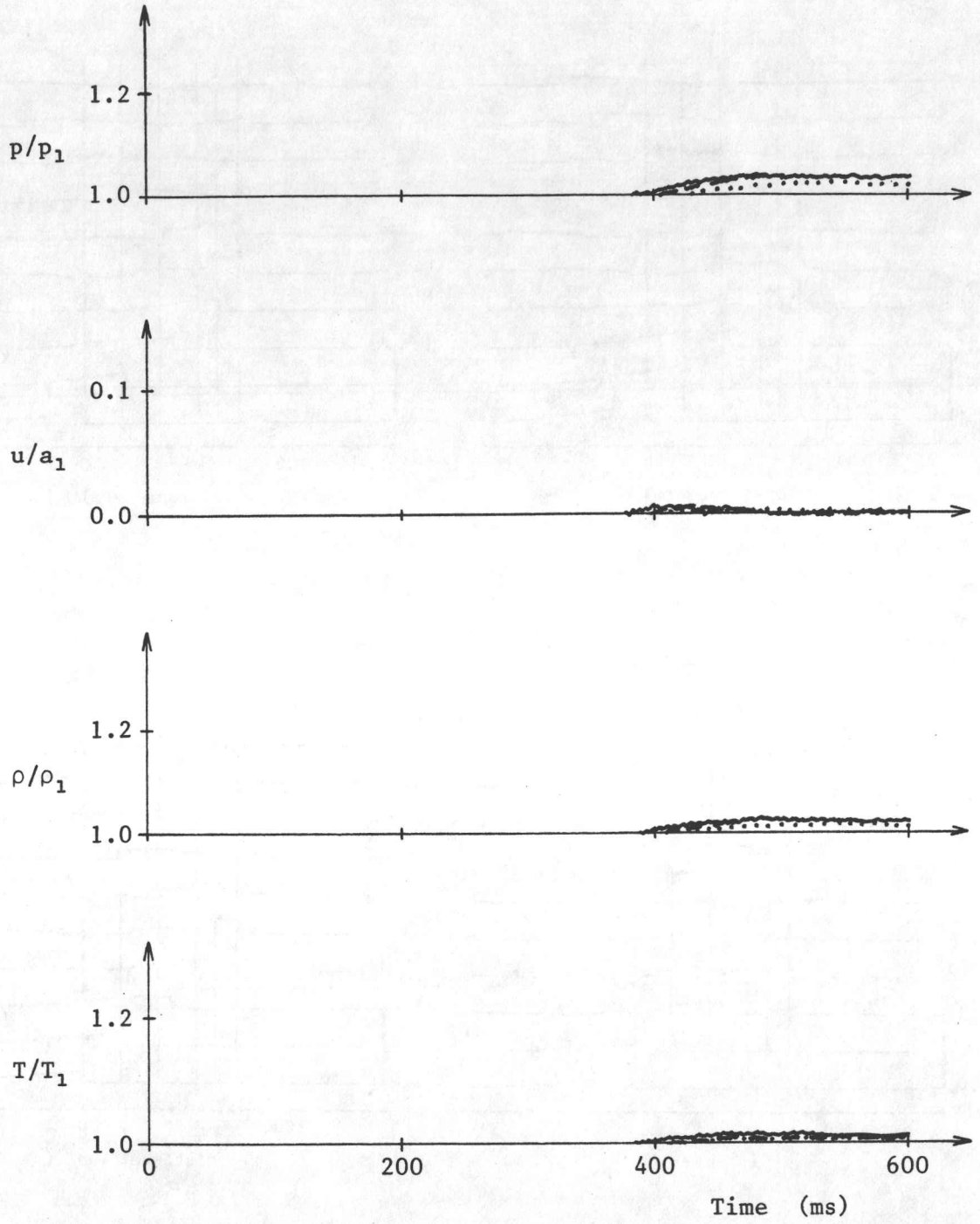

Fig. 301. Temporal distributions of pressure, density, flow velocity and temperature for the blast-wave flow field inside the power house.

Geometrical configuration:	D
Blow-out panel opening time:	0 ms ———
	100 ms – – – –
	500 ms . . . . .
Location and room number:	9

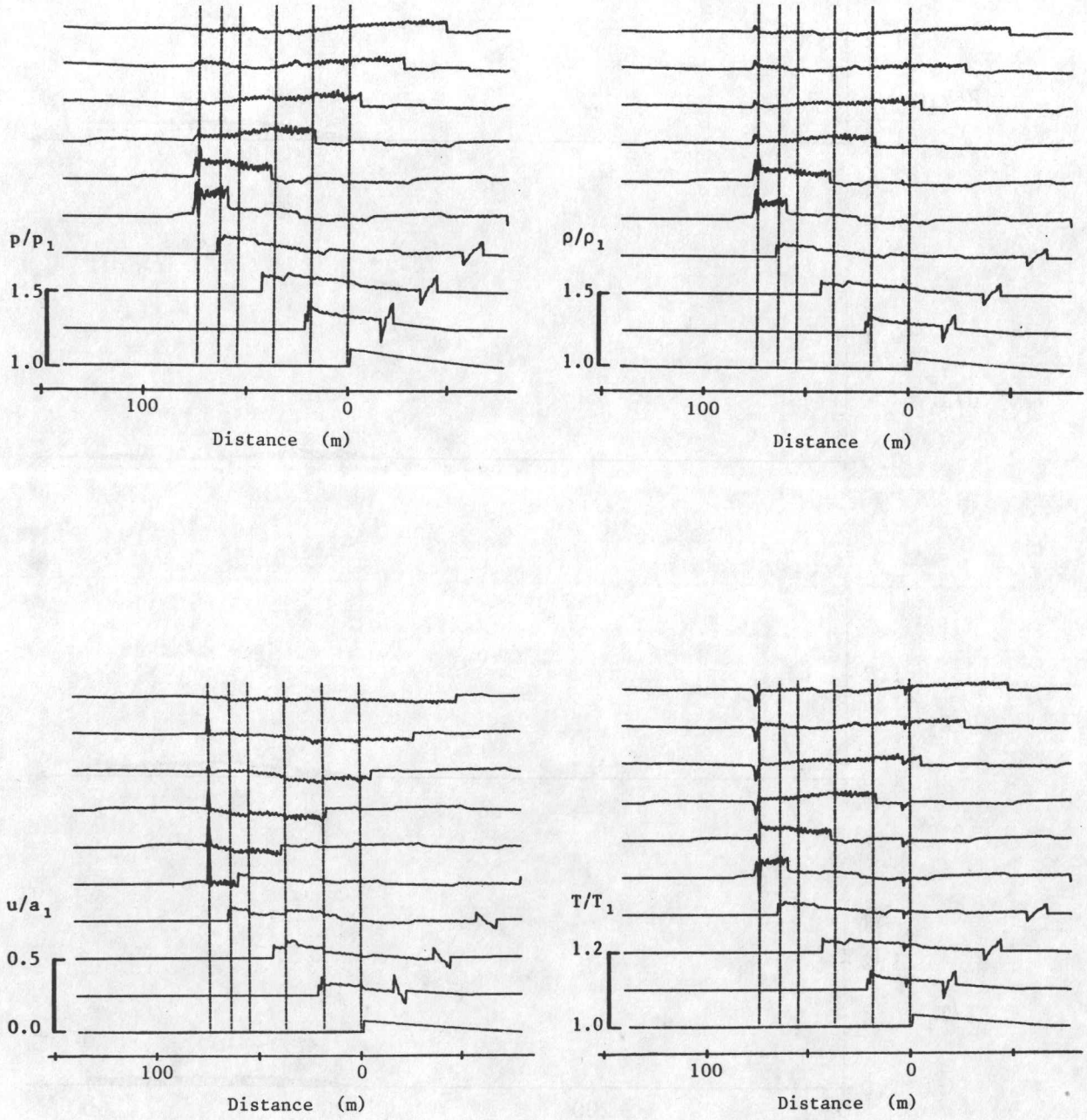

Fig. 3la. Spatial distributions of pressure, density, flow velocity and temperature for the blast-wave flow field inside the power house.

Geometrical configuration: E
Blow-out panel opening time: 0 ms

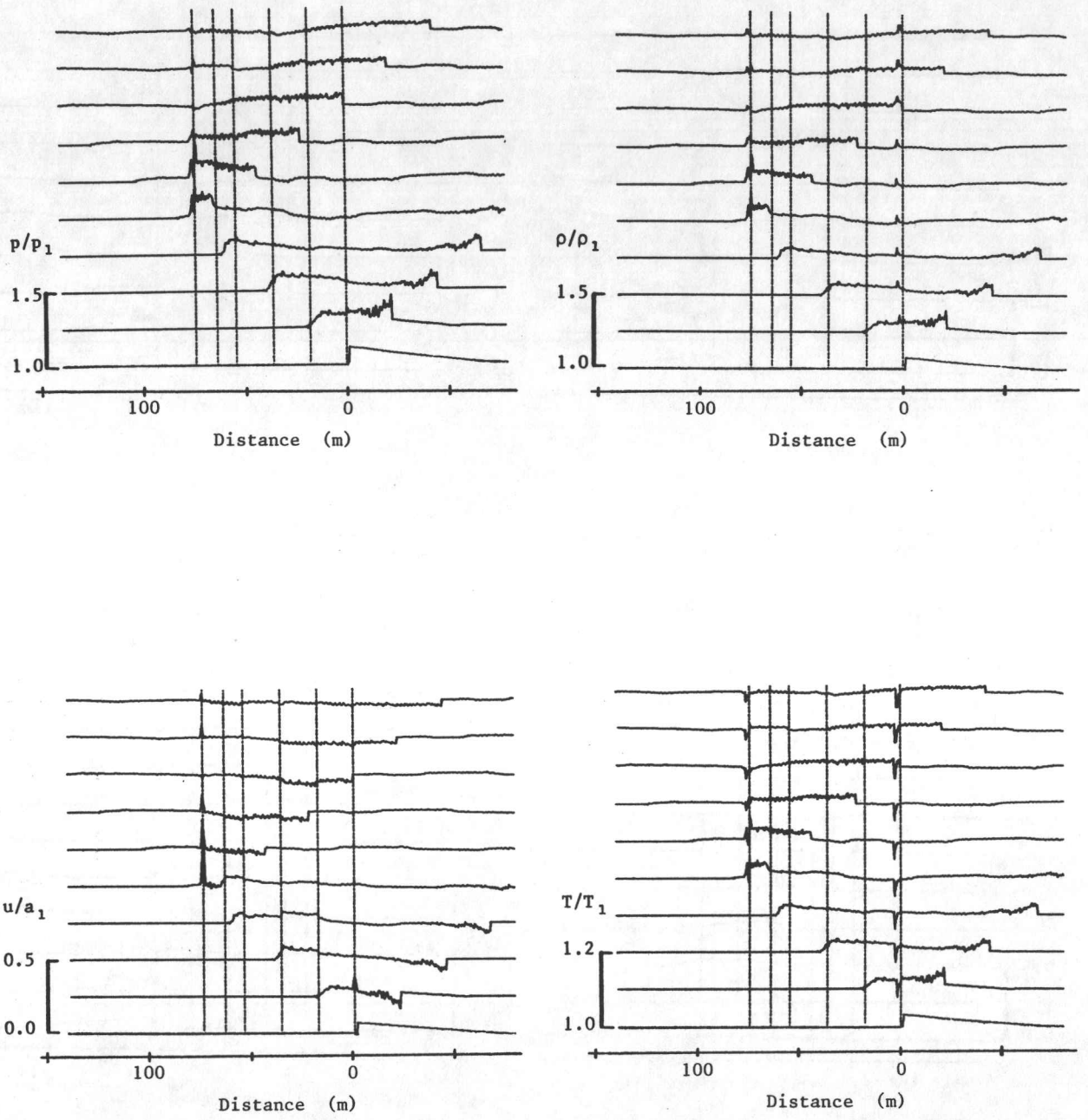

Fig. 31b. Spatial distributions of pressure, density, flow velocity and temperature for the blast-wave flow field inside the power house.

Geometrical configuration: E
Blow-out panel opening time: 100 ms

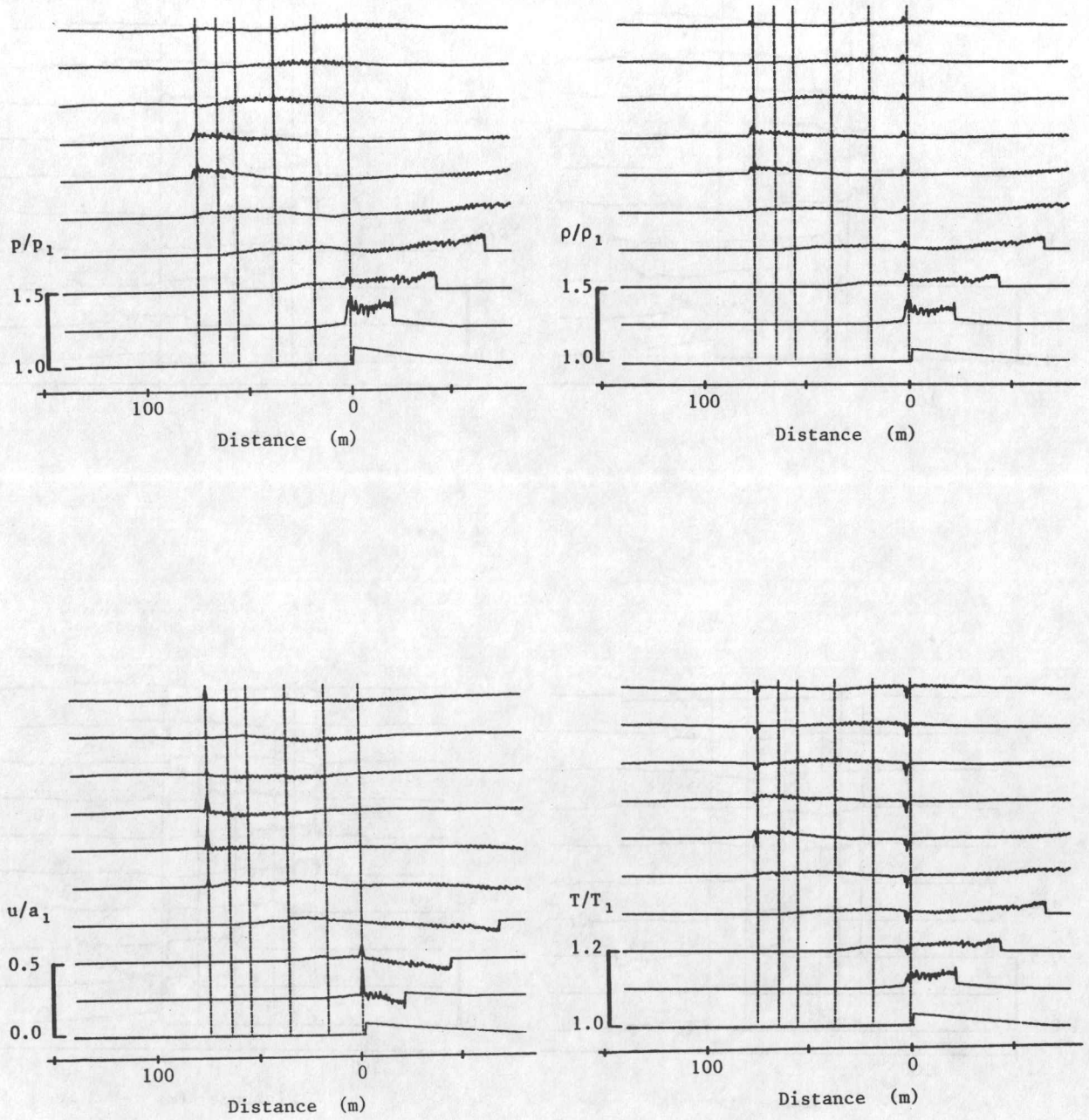

Fig. 31c. Spatial distributions of pressure, density, flow velocity and temperature for the blast-wave flow field inside the power house.

Geometrical configuration: E
Blow-out panel opening time: 500 ms

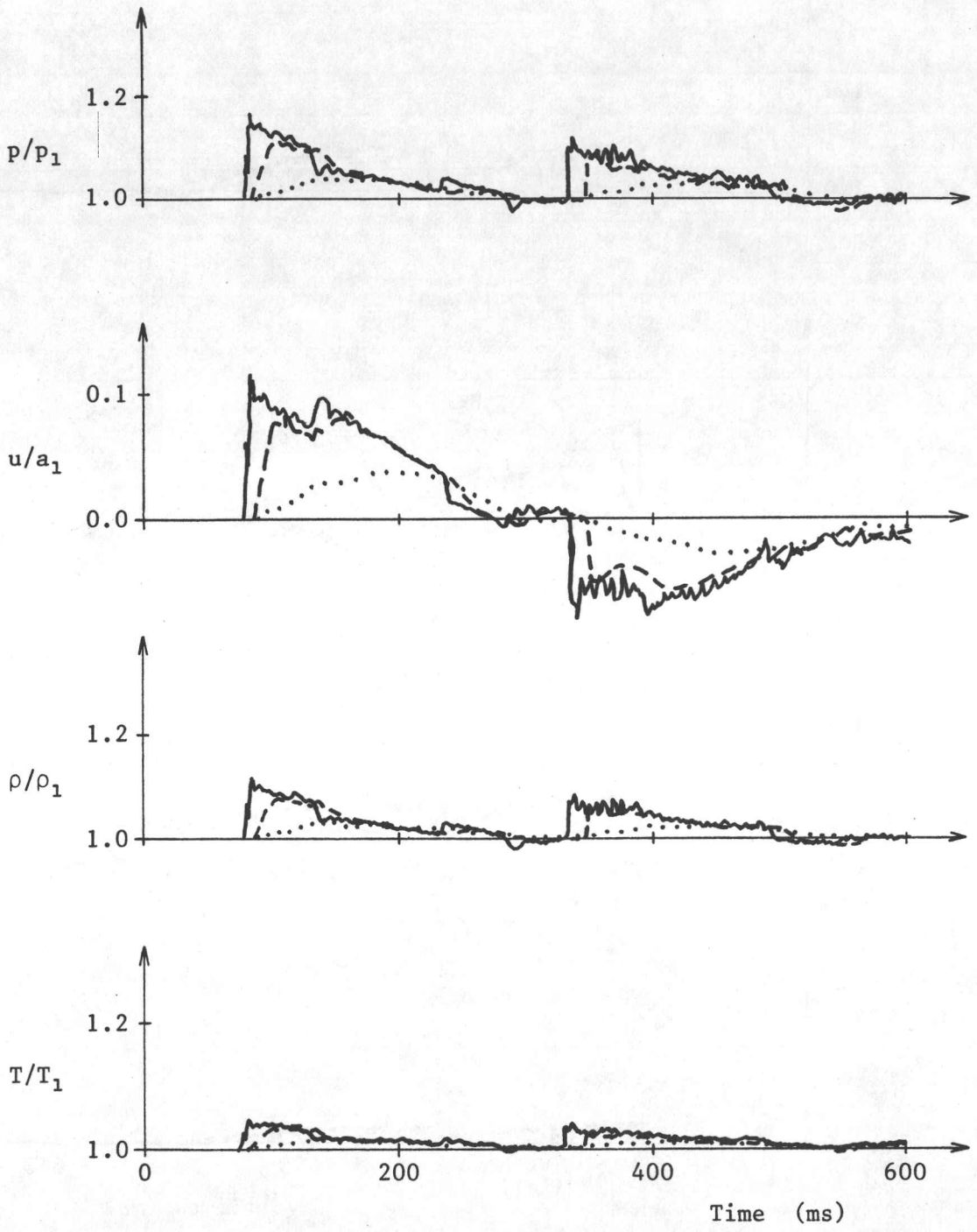

Fig. 31d. Temporal distributions of pressure, density, flow velocity and temperature for the blast-wave flow field inside the power house.

Geometrical configuration:	E
Blow-out panel opening time:	0 ms ———
	100 ms – – – –
	500 ms . . . . .
Location and room number:	2

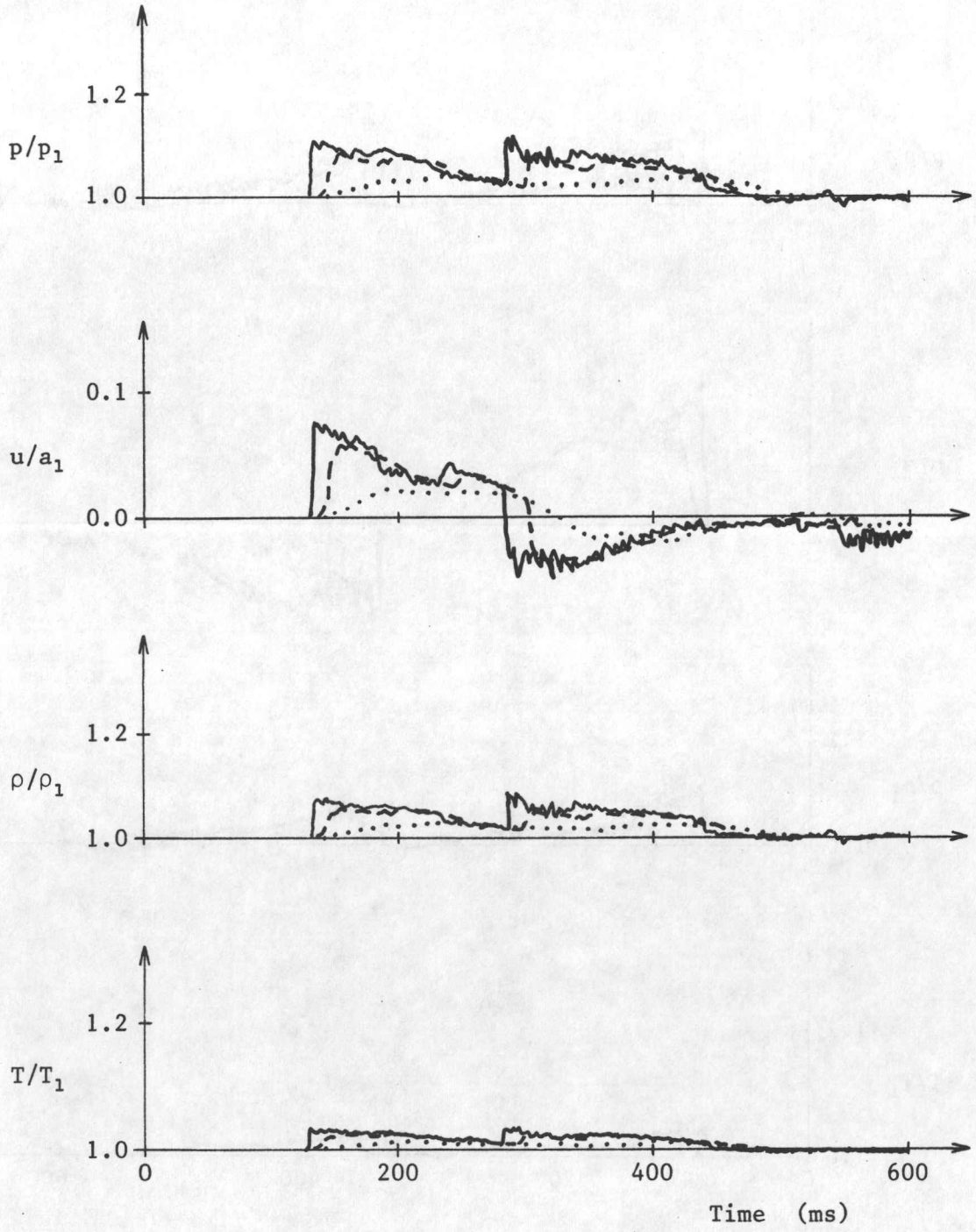

Fig. 3le. Temporal distributions of pressure, density, flow velocity and temperature for the blast-wave flow field inside the power house.

Geometrical configuration:	E
Blow-out panel opening time:	0 ms ———
	100 ms - - - - -
	500 ms . . . . .
Location and room number:	3

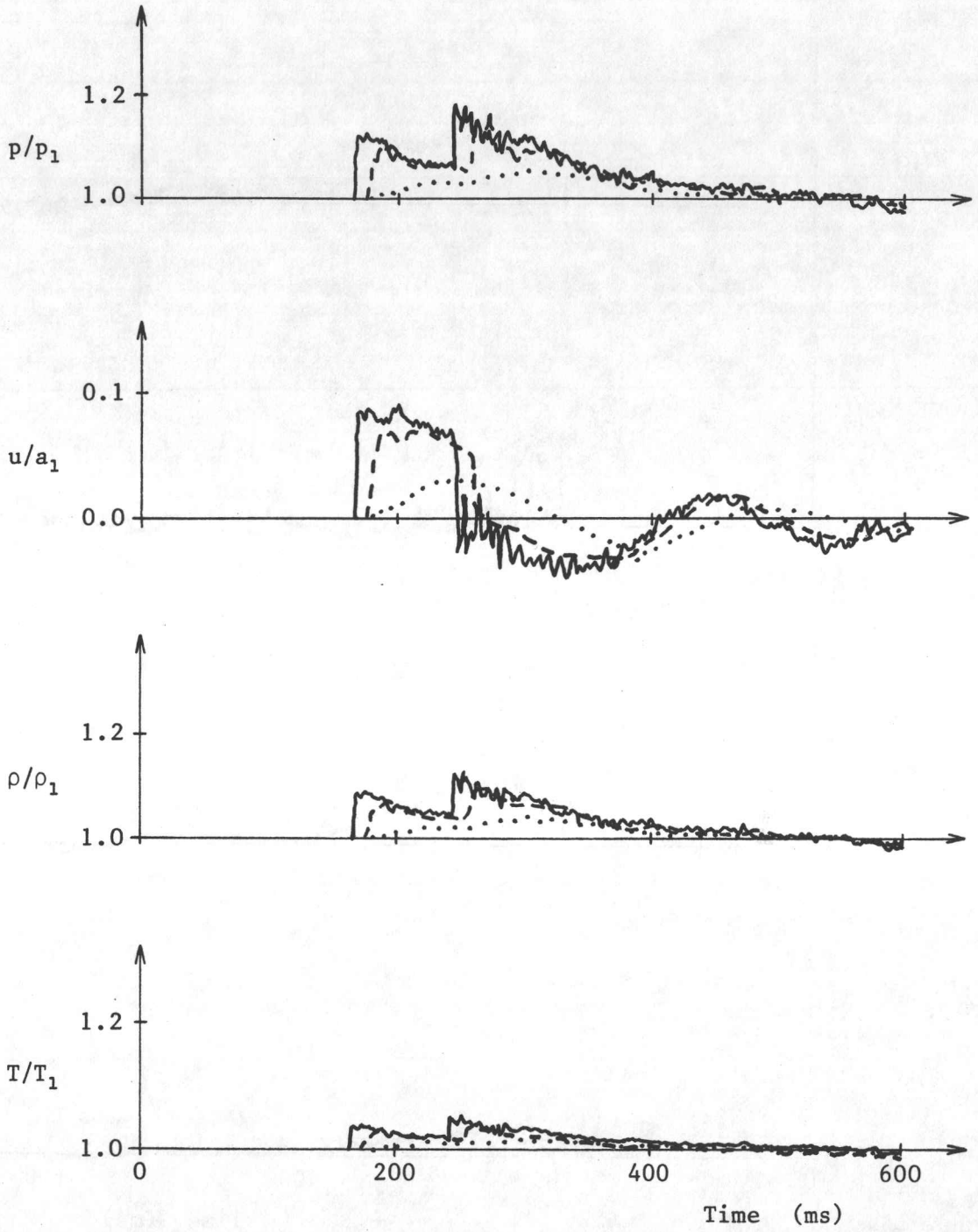

Fig. 31f. Temporal distributions of pressure, density, flow velocity and temperature for the blast-wave flow field inside the power house.

Geometrical configuration:	E
Blow-out panel opening time:	0 ms ———
	100 ms - - - -
	500 ms .....
Location and room number:	4

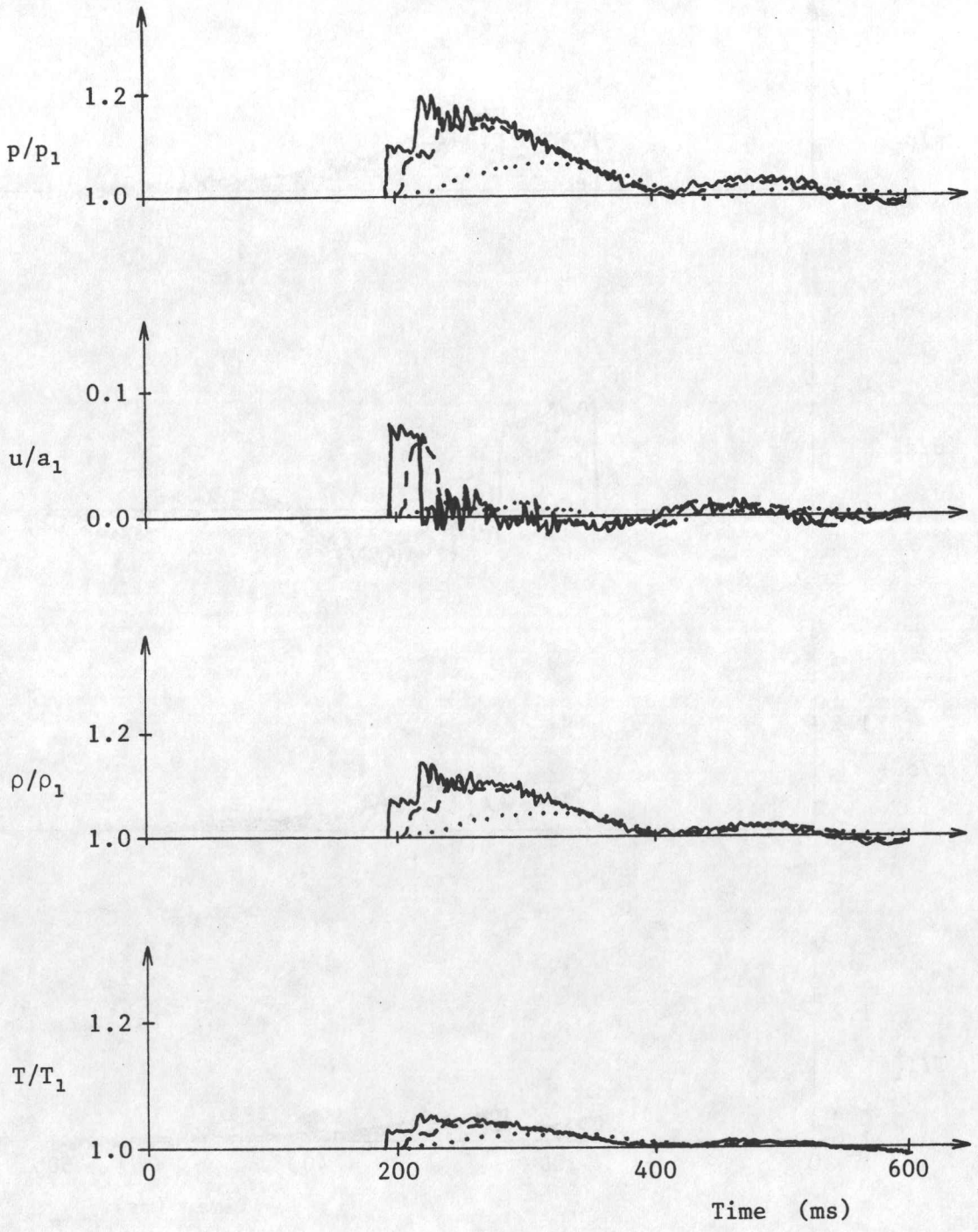

Fig. 31g. Temporal distributions of pressure, density, flow velocity and temperature for the blast-wave flow field inside the power house.

Geometrical configuration:	E
Blow-out panel opening time:	0 ms ———
	100 ms – – – –
	500 ms . . . . .
Location and room number:	5

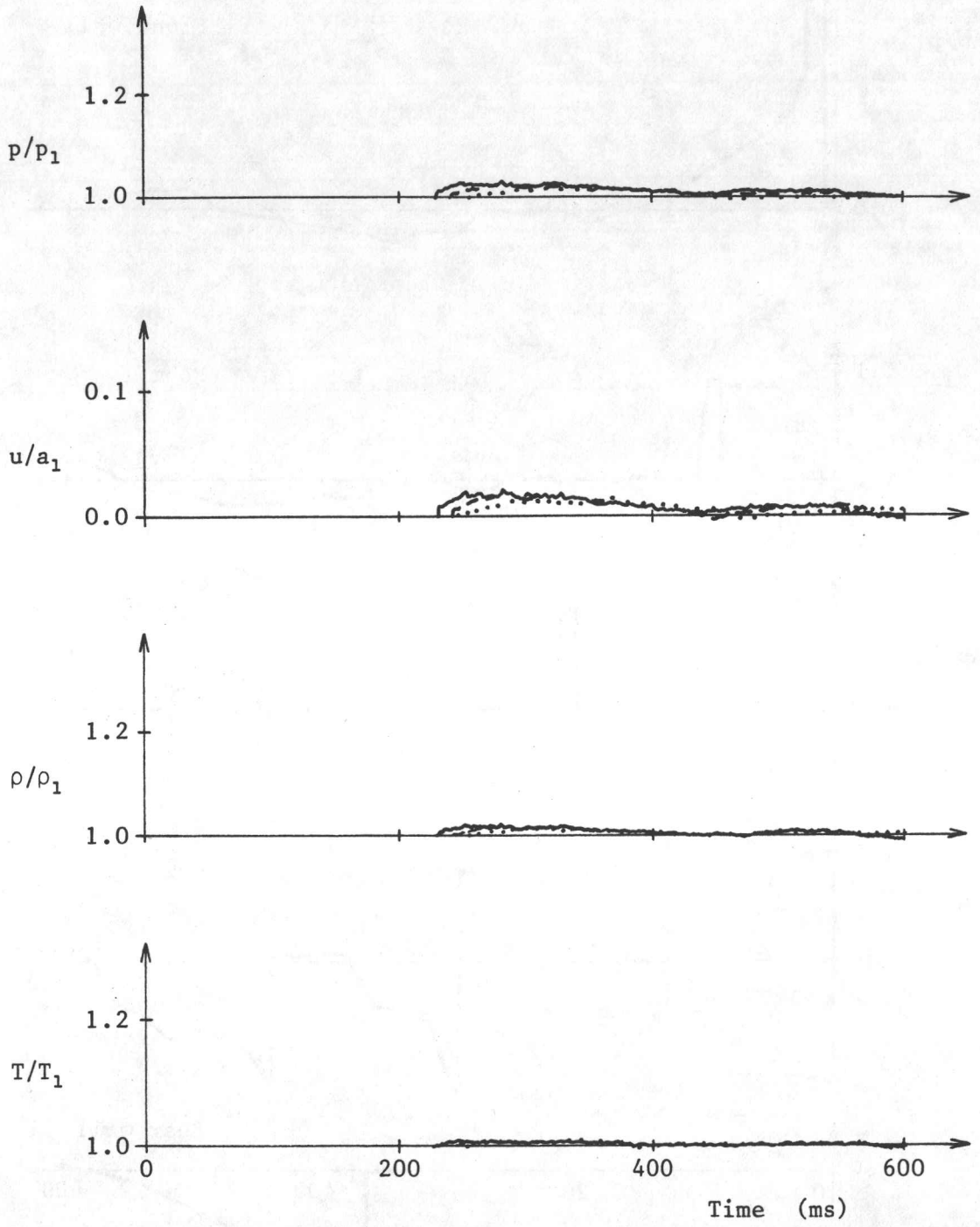

Fig. 31h. Temporal distributions of pressure, density, flow velocity and temperature for the blast-wave flow field inside the power house.

Geometrical configuration: E
Blow-out panel opening time: 0 ms ——————
100 ms — — — —
500 ms · · · · ·
Location and room number: 6

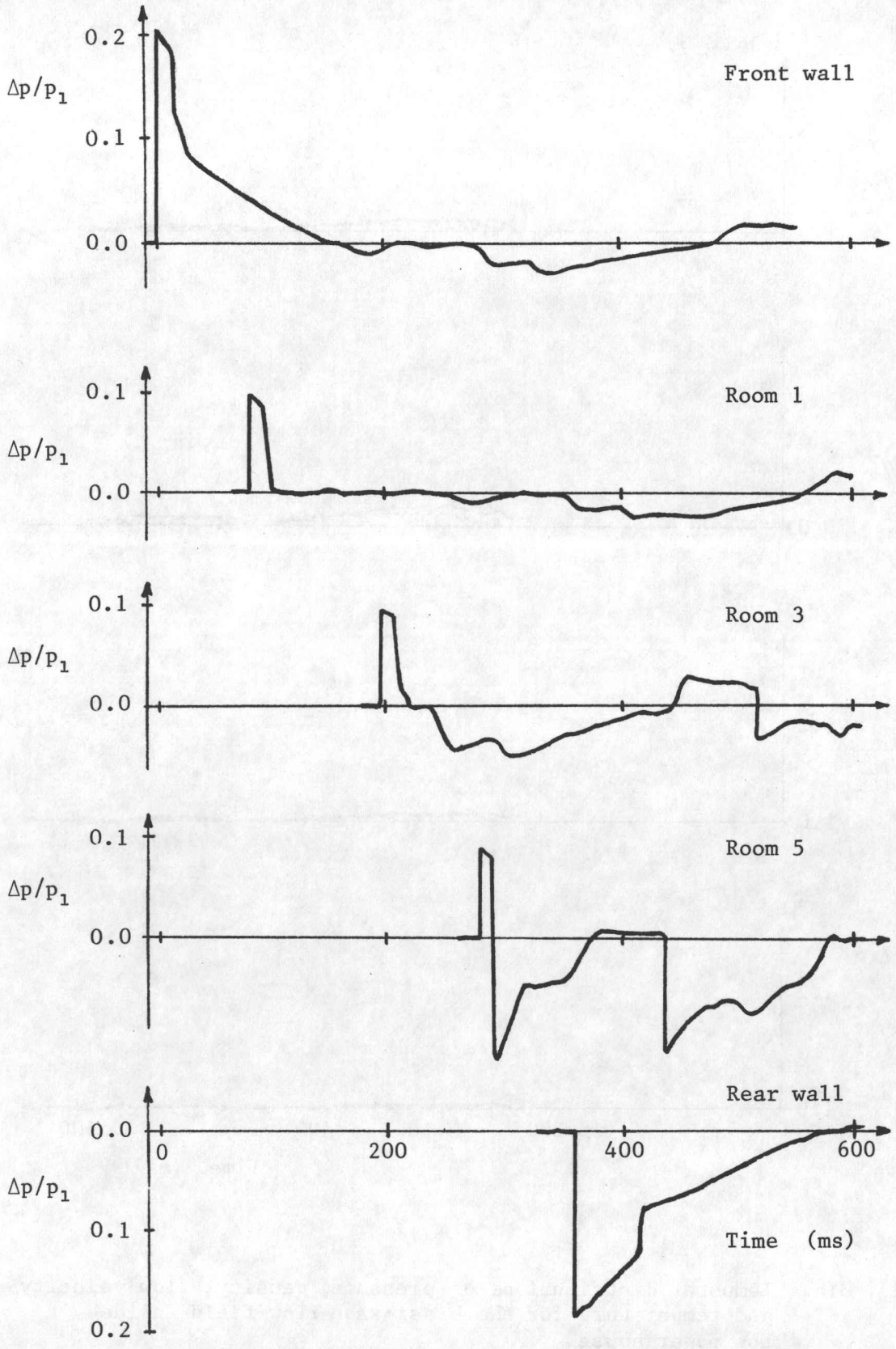

Fig. 32. Pressure difference across the power-house walls for geometrical configuration A.

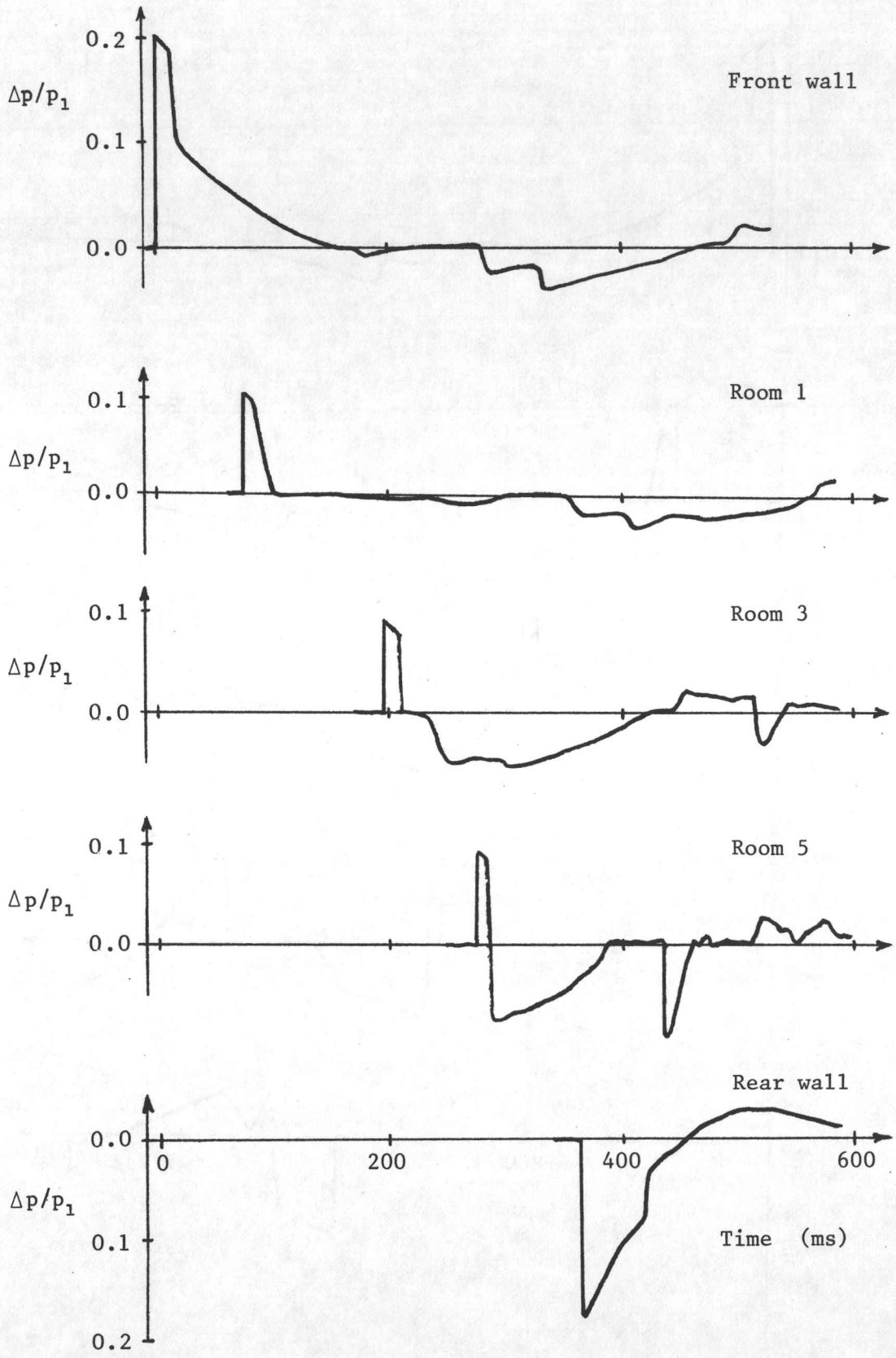

Fig. 33. Pressure difference across the power-house walls for geometrical configuration B.

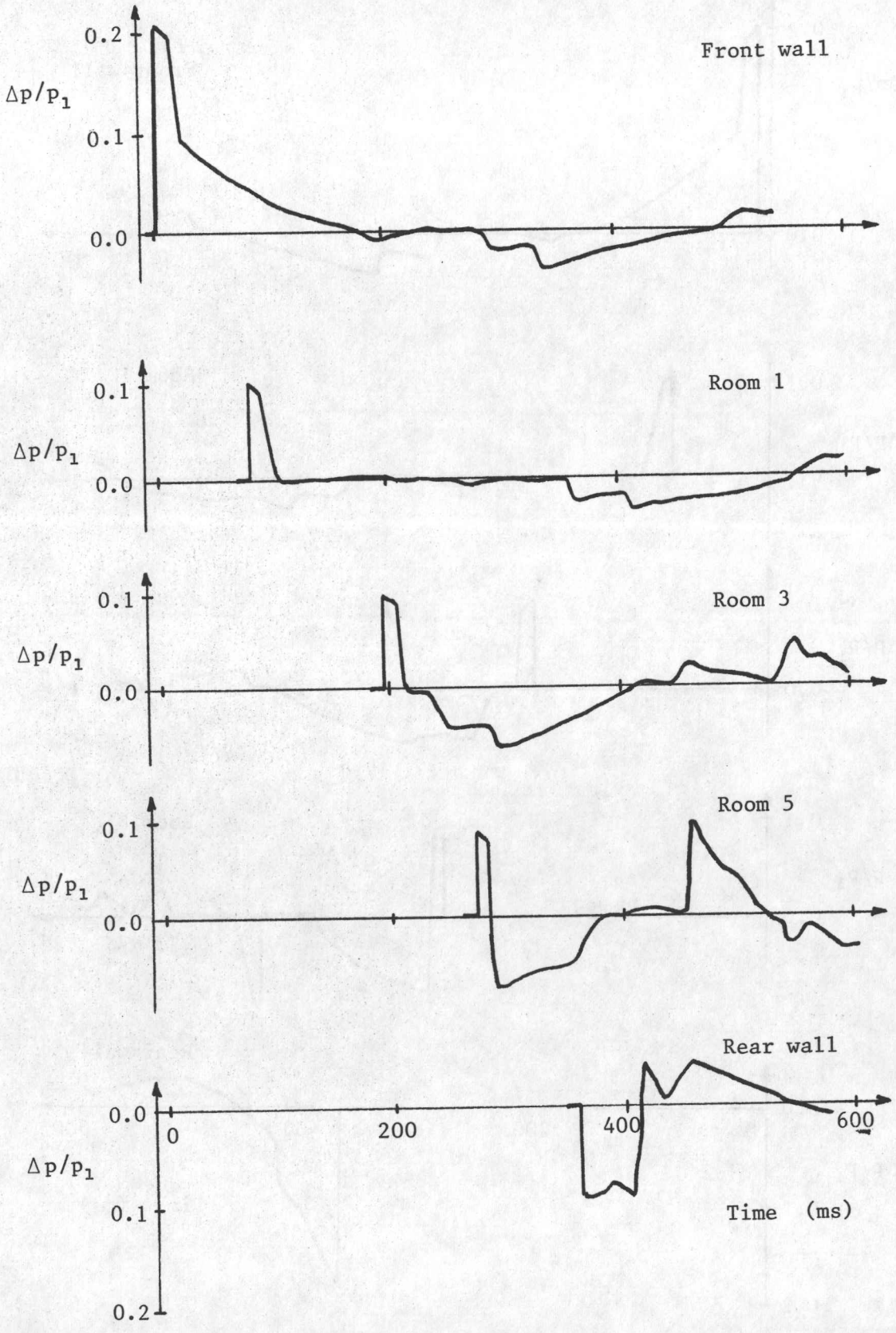

Fig. 34. Pressure difference across the power-house walls for geometrical configuration D.

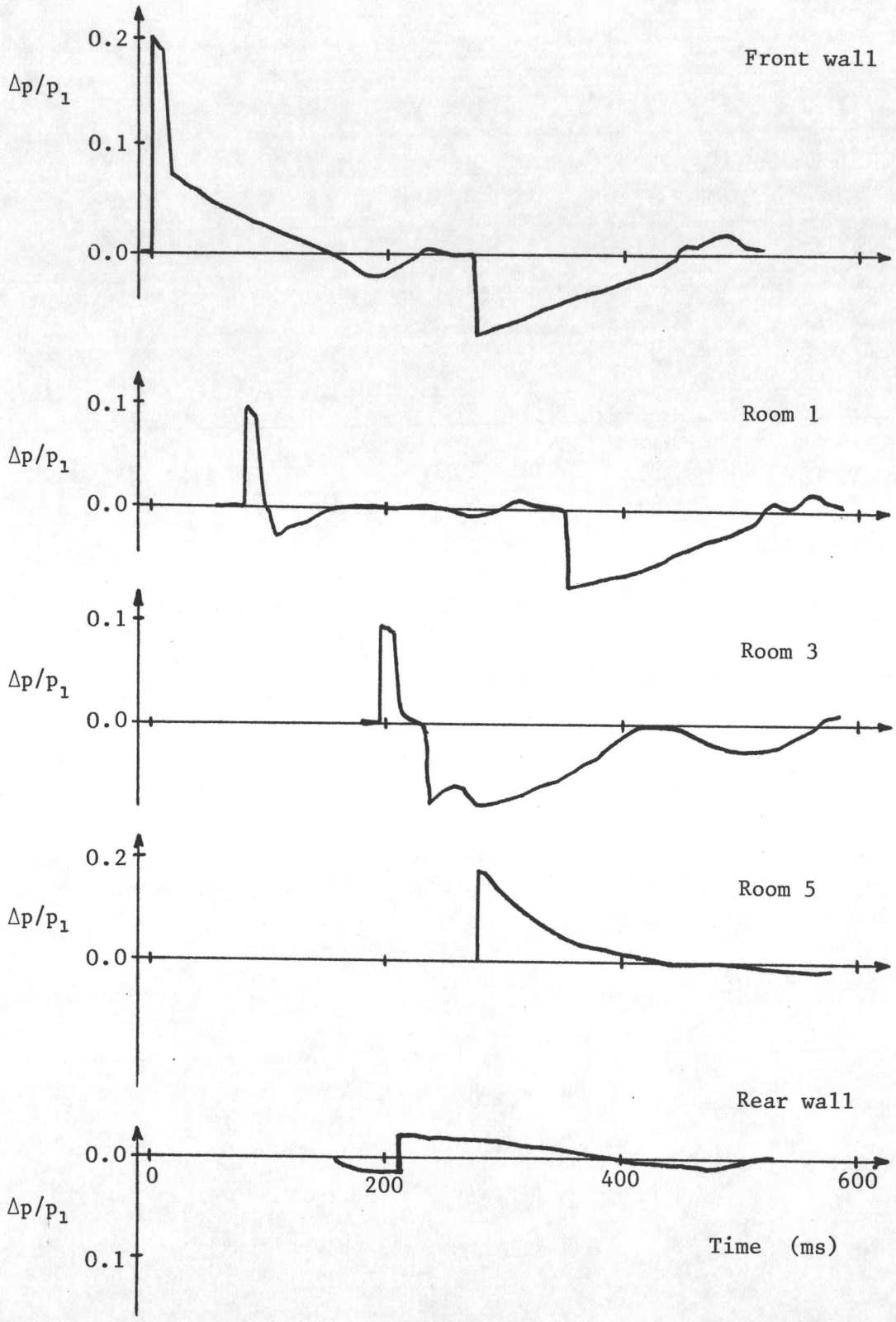

Fig. 35. Pressure difference across the power-house walls for geometrical configuration E.

UTIAS Technical Note No. 239

University of Toronto, Institute for Aerospace Studies (UTIAS)
4925 Dufferin Street, Downsview, Ontario, Canada, M3H 5T6

NUMERICAL PREDICTION OF BLAST-WAVE FLOWS OUTSIDE AND INSIDE A POWER HOUSE
OF A NUCLEAR-POWER GENERATING STATION

Gottlieb, J. J., Saito, T., Zhang, K. Y.

1. Unsteady flow 2. Blast-wave flow 3. Nuclear-power plant

I. UTIAS Technical Note No. 239 II. Gottlieb, J. J., Saito, T., Zhang, K. Y.

The blast-wave flows both outside and inside a power house of a nuclear-power generating station, from an accidental explosion of an explosive, like TNT or its equivalent during transportation past the power house by a train, are studied numerically and assessed with an appropriate model. Detailed descriptions of both the prediction model and numerical method of solution are given, as well as an interpretation of numerical results. The blast-wave flow into the power house through blow-out panels in the front wall is investigated, including the resulting flow inside the power house that travels through the turbine hall, through the turbine auxiliary bay, over the reactivity deck, through the reactor building, and, in some cases, down through a hoistway to three small rooms on the next lower level. Breaking blow-out panels in the rear wall of the power house and their effects on the internal blast-wave flow is also investigated. Two different flow paths are considered, one through an upper level of the power house and another through a lower level. Finally, the blast-wave flow over the outside of the power house is studied, with an approximate model, so that the pressure differences from the blast wave between the inside and outside of the roof side walls, front wall, and rear wall can be determined and the resultant blast-wave loading on the building walls thereby obtained.

Available copies of this report are limited. Return this card to UTIAS, if you require a copy.

UTIAS Technical Note No. 239

University of Toronto, Institute for Aerospace Studies (UTIAS)
4925 Dufferin Street, Downsview, Ontario, Canada, M3H 5T6

NUMERICAL PREDICTION OF BLAST-WAVE FLOWS OUTSIDE AND INSIDE A POWER HOUSE
OF A NUCLEAR-POWER GENERATING STATION

Gottlieb, J. J., Saito, T., Zhang, K. Y.

1. Unsteady flow 2. Blast-wave flow 3. Nuclear-power plant

I. UTIAS Technical Note No. 239 II. Gottlieb, J. J., Saito, T., Zhang, K. Y.

The blast-wave flows both outside and inside a power house of a nuclear-power generating station, from an accidental explosion of an explosive, like TNT or its equivalent during transportation past the power house by a train, are studied numerically and assessed with an appropriate model. Detailed descriptions of both the prediction model and numerical method of solution are given, as well as an interpretation of numerical results. The blast-wave flow into the power house through blow-out panels in the front wall is investigated, including the resulting flow inside the power house that travels through the turbine hall, through the turbine auxiliary bay, over the reactivity deck, through the reactor building, and, in some cases, down through a hoistway to three small rooms on the next lower level. Breaking blow-out panels in the rear wall of the power house and their effects on the internal blast-wave flow is also investigated. Two different flow paths are considered, one through an upper level of the power house and another through a lower level. Finally, the blast-wave flow over the outside of the power house is studied, with an approximate model, so that the pressure differences from the blast wave between the inside and outside of the roof side walls, front wall, and rear wall can be determined and the resultant blast-wave loading on the building walls thereby obtained.

Available copies of this report are limited. Return this card to UTIAS, if you require a copy.

UTIAS Technical Note No. 239

University of Toronto, Institute for Aerospace Studies (UTIAS)
4925 Dufferin Street, Downsview, Ontario, Canada, M3H 5T6

NUMERICAL PREDICTION OF BLAST-WAVE FLOWS OUTSIDE AND INSIDE A POWER HOUSE
OF A NUCLEAR-POWER GENERATING STATION

Gottlieb, J. J., Saito, T., Zhang, K. Y.

1. Unsteady flow 2. Blast-wave flow 3. Nuclear-power plant

I. UTIAS Technical Note No. 239 II. Gottlieb, J. J., Saito, T., Zhang, K. Y.

The blast-wave flows both outside and inside a power house of a nuclear-power generating station, from an accidental explosion of an explosive, like TNT or its equivalent during transportation past the power house by a train, are studied numerically and assessed with an appropriate model. Detailed descriptions of both the prediction model and numerical method of solution are given, as well as an interpretation of numerical results. The blast-wave flow into the power house through blow-out panels in the front wall is investigated, including the resulting flow inside the power house that travels through the turbine hall, through the turbine auxiliary bay, over the reactivity deck, through the reactor building, and, in some cases, down through a hoistway to three small rooms on the next lower level. Breaking blow-out panels in the rear wall of the power house and their effects on the internal blast-wave flow is also investigated. Two different flow paths are considered, one through an upper level of the power house and another through a lower level. Finally, the blast-wave flow over the outside of the power house is studied, with an approximate model, so that the pressure differences from the blast wave between the inside and outside of the roof side walls, front wall, and rear wall can be determined and the resultant blast-wave loading on the building walls thereby obtained.

Available copies of this report are limited. Return this card to UTIAS, if you require a copy.

UTIAS Technical Note No. 239

University of Toronto, Institute for Aerospace Studies (UTIAS)
4925 Dufferin Street, Downsview, Ontario, Canada, M3H 5T6

NUMERICAL PREDICTION OF BLAST-WAVE FLOWS OUTSIDE AND INSIDE A POWER HOUSE
OF A NUCLEAR-POWER GENERATING STATION

Gottlieb, J. J., Saito, T., Zhang, K. Y.

1. Unsteady flow 2. Blast-wave flow 3. Nuclear-power plant

I. UTIAS Technical Note No. 239 II. Gottlieb, J. J., Saito, T., Zhang, K. Y.

The blast-wave flows both outside and inside a power house of a nuclear-power generating station, from an accidental explosion of an explosive, like TNT or its equivalent during transportation past the power house by a train, are studied numerically and assessed with an appropriate model. Detailed descriptions of both the prediction model and numerical method of solution are given, as well as an interpretation of numerical results. The blast-wave flow into the power house through blow-out panels in the front wall is investigated, including the resulting flow inside the power house that travels through the turbine hall, through the turbine auxiliary bay, over the reactivity deck, through the reactor building, and, in some cases, down through a hoistway to three small rooms on the next lower level. Breaking blow-out panels in the rear wall of the power house and their effects on the internal blast-wave flow is also investigated. Two different flow paths are considered, one through an upper level of the power house and another through a lower level. Finally, the blast-wave flow over the outside of the power house is studied, with an approximate model, so that the pressure differences from the blast wave between the inside and outside of the roof side walls, front wall, and rear wall can be determined and the resultant blast-wave loading on the building walls thereby obtained.

Available copies of this report are limited. Return this card to UTIAS, if you require a copy.

UTIAS Technical Note No. 239

University of Toronto, Institute for Aerospace Studies (UTIAS)
4925 Dufferin Street, Downsview, Ontario, Canada, M3H 5T6

NUMERICAL PREDICTION OF BLAST-WAVE FLOWS OUTSIDE AND INSIDE A POWER HOUSE OF A NUCLEAR-POWER GENERATING STATION

Gottlieb, J. J., Saito, T., Zhang, K. Y.

1. Unsteady flow 2. Blast-wave flow 3. Nuclear-power plant

I. UTIAS Technical Note No. 239 II. Gottlieb, J. J., Saito, T., Zhang, K. Y.

The blast-wave flows both outside and inside a power house of a nuclear-power generating station, from an accidental explosion of an explosive, like TNT or its equivalent during transportation past the power house by a train, are studied numerically and assessed with an appropriate model. Detailed descriptions of both the prediction model and numerical method of solution are given, as well as an interpretation of numerical results. The blast-wave flow into the power house through blow-out panels in the front wall is investigated, including the resulting flow inside the power house that travels through the turbine hall, through the turbine auxiliary bay, over the reactivity deck, through the reactor building, and, in some cases, down through a hoistway to three small rooms on the next lower level. Breaking blow-out panels in the rear wall of the power house and their effects on the internal blast-wave flow is also investigated. Two different flow paths are considered, one through an upper level of the power house and another through a lower level. Finally, the blast-wave flow over the outside of the power house is studied, with an approximate model, so that the pressure differences from the blast wave between the inside and outside of the roof side walls, front wall, and rear wall can be determined and the resultant blast-wave loading on the building walls thereby obtained.

Available copies of this report are limited. Return this card to UTIAS, if you require a copy.

UTIAS Technical Note No. 239

University of Toronto, Institute for Aerospace Studies (UTIAS)
4925 Dufferin Street, Downsview, Ontario, Canada, M3H 5T6

NUMERICAL PREDICTION OF BLAST-WAVE FLOWS OUTSIDE AND INSIDE A POWER HOUSE OF A NUCLEAR-POWER GENERATING STATION

Gottlieb, J. J., Saito, T., Zhang, K. Y.

1. Unsteady flow 2. Blast-wave flow 3. Nuclear-power plant

I. UTIAS Technical Note No. 239 II. Gottlieb, J. J., Saito, T., Zhang, K. Y.

The blast-wave flows both outside and inside a power house of a nuclear-power generating station, from an accidental explosion of an explosive, like TNT or its equivalent during transportation past the power house by a train, are studied numerically and assessed with an appropriate model. Detailed descriptions of both the prediction model and numerical method of solution are given, as well as an interpretation of numerical results. The blast-wave flow into the power house through blow-out panels in the front wall is investigated, including the resulting flow inside the power house that travels through the turbine hall, through the turbine auxiliary bay, over the reactivity deck, through the reactor building, and, in some cases, down through a hoistway to three small rooms on the next lower level. Breaking blow-out panels in the rear wall of the power house and their effects on the internal blast-wave flow is also investigated. Two different flow paths are considered, one through an upper level of the power house and another through a lower level. Finally, the blast-wave flow over the outside of the power house is studied, with an approximate model, so that the pressure differences from the blast wave between the inside and outside of the roof side walls, front wall, and rear wall can be determined and the resultant blast-wave loading on the building walls thereby obtained.

Available copies of this report are limited. Return this card to UTIAS, if you require a copy.

UTIAS Technical Note No. 239

University of Toronto, Institute for Aerospace Studies (UTIAS)
4925 Dufferin Street, Downsview, Ontario, Canada, M3H 5T6

NUMERICAL PREDICTION OF BLAST-WAVE FLOWS OUTSIDE AND INSIDE A POWER HOUSE OF A NUCLEAR-POWER GENERATING STATION

Gottlieb, J. J., Saito, T., Zhang, K. Y.

1. Unsteady flow 2. Blast-wave flow 3. Nuclear-power plant

I. UTIAS Technical Note No. 239 II. Gottlieb, J. J., Saito, T., Zhang, K. Y.

The blast-wave flows both outside and inside a power house of a nuclear-power generating station, from an accidental explosion of an explosive, like TNT or its equivalent during transportation past the power house by a train, are studied numerically and assessed with an appropriate model. Detailed descriptions of both the prediction model and numerical method of solution are given, as well as an interpretation of numerical results. The blast-wave flow into the power house through blow-out panels in the front wall is investigated, including the resulting flow inside the power house that travels through the turbine hall, through the turbine auxiliary bay, over the reactivity deck, through the reactor building, and, in some cases, down through a hoistway to three small rooms on the next lower level. Breaking blow-out panels in the rear wall of the power house and their effects on the internal blast-wave flow is also investigated. Two different flow paths are considered, one through an upper level of the power house and another through a lower level. Finally, the blast-wave flow over the outside of the power house is studied, with an approximate model, so that the pressure differences from the blast wave between the inside and outside of the roof side walls, front wall, and rear wall can be determined and the resultant blast-wave loading on the building walls thereby obtained.

Available copies of this report are limited. Return this card to UTIAS, if you require a copy.

UTIAS Technical Note No. 239

University of Toronto, Institute for Aerospace Studies (UTIAS)
4925 Dufferin Street, Downsview, Ontario, Canada, M3H 5T6

NUMERICAL PREDICTION OF BLAST-WAVE FLOWS OUTSIDE AND INSIDE A POWER HOUSE OF A NUCLEAR-POWER GENERATING STATION

Gottlieb, J. J., Saito, T., Zhang, K. Y.

1. Unsteady flow 2. Blast-wave flow 3. Nuclear-power plant

I. UTIAS Technical Note No. 239 II. Gottlieb, J. J., Saito, T., Zhang, K. Y.

The blast-wave flows both outside and inside a power house of a nuclear-power generating station, from an accidental explosion of an explosive, like TNT or its equivalent during transportation past the power house by a train, are studied numerically and assessed with an appropriate model. Detailed descriptions of both the prediction model and numerical method of solution are given, as well as an interpretation of numerical results. The blast-wave flow into the power house through blow-out panels in the front wall is investigated, including the resulting flow inside the power house that travels through the turbine hall, through the turbine auxiliary bay, over the reactivity deck, through the reactor building, and, in some cases, down through a hoistway to three small rooms on the next lower level. Breaking blow-out panels in the rear wall of the power house and their effects on the internal blast-wave flow is also investigated. Two different flow paths are considered, one through an upper level of the power house and another through a lower level. Finally, the blast-wave flow over the outside of the power house is studied, with an approximate model, so that the pressure differences from the blast wave between the inside and outside of the roof side walls, front wall, and rear wall can be determined and the resultant blast-wave loading on the building walls thereby obtained.

Available copies of this report are limited. Return this card to UTIAS, if you require a copy.